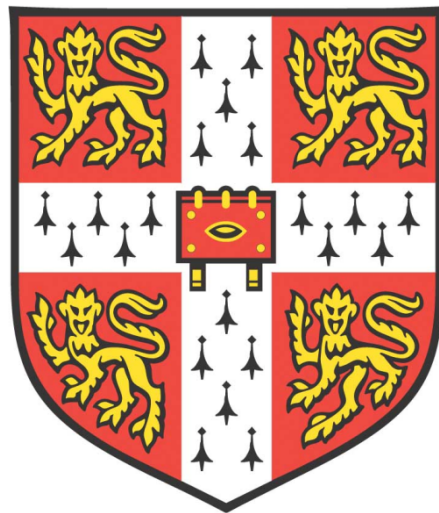


DEFINING THE CELLULAR AND MOLECULAR MECHANISMS OF
MATERNALLY INHERITED HEARING LOSS



Peter Kullar
Corpus Christi College

MRC Mitochondrial Biology Unit
University of Cambridge
October 2017

This dissertation is submitted to the Board of Graduate Studies in partial fulfilment of the requirements for the degree of Doctor of Philosophy

Declaration

This dissertation is the result of my own work and includes nothing, which is the outcome of work done in collaboration except where specifically indicated in the text. It has not been previously submitted, in part or whole, to any university or institution for any degree, diploma, or other qualification. In accordance with the Biology Degree Committee guidelines, this thesis does not exceed 60,000 words.

Signed: _____

Date: _____

Peter Kullar MA MBChir DOHNS MRCS (ENT)

Cambridge

Abstract

Mitochondrial dysfunction causes moderate to profound hearing loss both in isolation and as a feature of multi-systemic mitochondrial disease. The m.1555A>G mitochondrial DNA (mtDNA) variant is associated with a predisposition to aminoglycoside ototoxicity and maternally inherited non-syndromic deafness. However, the reasons for the highly variable penetrance of the associated hearing loss have not yet been fully resolved. Aminoglycosides are a recognised modifier factor of the hearing loss, but cannot account for all hearing impaired carriers in multi-generational pedigrees, implicating additional co-segregating genetic factors. By identifying and characterising the c.3G>A *SSBPI* variant as a nuclear modifier of m.1555A>G the work detailed in this thesis extends our understanding of mitochondrial-nuclear interactions in human disease.

To ascertain the frequency of the m.1555A>G variant in patients with suspected mitochondrial hearing loss we surveyed the laboratories within the United Kingdom that undertake genetic testing for this variant. We determined that the variant was not found more frequently in patients with known hearing impairment providing further evidence that m.1555A>G does not cause hearing loss in isolation. These results strengthened the case for nuclear genetic modifiers as important contributors to m.1555A>G pathogenesis.

We next identified a multi-generational family that transmitted the m.1555A>G variant with variable clinical penetrance of hearing loss. In addition, a cohort of sporadic individuals carrying m.1555A>G was used to test the hypothesis that a conserved genetic mechanism accounted for the phenotype in all carriers. To this effect, we undertook whole exome sequencing in selected familial and sporadic carriers of m.1555A>G, identifying a heterozygous start loss mutation in the core mtDNA replisome protein gene, *SSBPI*, that co-segregated with the m.1555A>G variant and the phenotype in the family. The *SSBPI* variant lead to a perturbation of mtDNA metabolism, and was associated with multiple mtDNA deletions and mtDNA depletion in skeletal muscle. Fibroblasts from these patients also showed mitochondrial network fragmentation and reduced intra-mitochondrial protein synthesis in keeping with the co-existing m.1555A>G variant, leading to reduced proliferation rates under conditions of forced mitochondrial respiration. Our findings provide an explanation for the variable clinical penetrance of the disorder within these m.1555A>G carriers and highlight the importance of trans-acting modifiers in mitochondrial disease.

Acknowledgments

I thank my primary research supervisor, Professor Patrick Chinnery, whose unwavering support, guidance and encouragement throughout all stages of this PhD has been invaluable.

I am indebted to Dr Aurora Gomez-Duran and Dr Marzena Kurzawa-Akanabi for their time and patience in teaching me many of the experimental techniques I needed for this research project. I am sincerely grateful to Dr Payam Gammage, Dr Aurelio Reyes and Dr Michael Keogh for their expert tuition, stimulating discussions and helpful feedback.

I thank my clinical mentors, Professor Janet Wilson and Mr James Tysome who enabled me to continue developing my clinical skills whilst undertaking my research.

Lastly, thank you to my wonderful and caring wife, Kirsty. You've taken every step with me.

Declaration of Contribution

The data presented in this thesis is the result of my own work and does not include any material resulting from collaborative work unless stated in the text.

Primary fibroblast cell lines used in this work were established from individuals either by Professor Kari Majamaa (Oulu University, Finland) or the Newcastle Academic Health Partners Bioresource (Newcastle University, UK). Skeletal muscle biopsies were obtained by Professor Kari Majamaa or the Cambridge BioResource, Cambridge, UK. I solely performed all cell culture, genetic, protein, immunocytochemical and biochemical analysis with the exception of the following:

- 1) Immortalisation of these fibroblast cell lines was performed by Dr Aurelio Reyes (Mitochondrial Biology Unit, Cambridge, UK).
- 2) Mitochondrial histochemical analysis was performed in collaboration with Miss Zoe Golder (Mitochondrial Biology Unit, Cambridge UK).
- 3) Preparation of radiolabelled probes for use in the analysis of mitochondrial 7S DNA were supplied by Dr Payam Gammage (Mitochondrial Biology Unit, Cambridge, UK).
- 4) Generation of exome sequence reads was performed by AROS Applied Biotechnology A/S, Aarhus, Denmark). Read alignment, variant calling and annotation was undertaken by Dr Helen Griffin (Newcastle University, UK). I performed all subsequent variant filtering and prioritisation.

Publications and Presentations

The following publications and presentations have been derived from the work described in this thesis:

Publications

The frequency of the m.1555A>G (*MT-RNR1*) variant in UK patients with suspected mitochondrial deafness. Kullar P, Alston CL, Ball S, Blakely EL, Differ AM, Fratter C, Sweeney MG, Taylor RW, Chinnery PF. *Hearing Balance Communication* 2016; 14(2): 101-102.

Heterozygous SSBP1 start loss mutation co-segregates with hearing loss and the m.1555A>G mtDNA variant in a large multigenerational family. Kullar PJ, Gomex-Duran A, Gammage PA, Garone C, Minczuk M, Golder Z, Wilson J, Montoya J, Hakli S, Karppa M, Horvath R, Majamaa K, Chinnery PF. *Brain* 2018 (currently in press and due to be published January 2018).

Presentations

Heterozygous SSBP1 start loss mutation co-segregates with hearing loss and the m.1555A>G mtDNA variant in a large multigenerational family. ENT UK Annual meeting. September 2017, London. UK.

Defining the cellular and molecular mechanism of maternally inherited hearing loss. The North of England Otolaryngology Society. November 2017, Manchester, UK.

Table of Contents

Abstract	iii
Acknowledgments	iv
Declaration of Contribution	v
Publications and Presentations	vi
List of Figures	xiii
List of Tables	xvii
Nomenclature	xix
Chapter 1 Introduction	1
1.1 Chapter overview	1
1.2 The mitochondrion.....	1
1.3 The origins of mitochondria.....	1
1.4 Structure.....	2
1.5 Mitochondrial function	3
1.5.1 Oxidative phosphorylation (OXPHOS)	3
1.6 Generation of Reactive Oxygen Species.....	5
1.7 Mitochondrial genetics.....	6
1.7.1 Mitochondrial genome	6
1.7.2 Mitochondrial D loop and 7S DNA	8
1.7.3 Mitochondrial DNA inheritance.....	9
1.7.4 Mitochondrial haplogroups	10
1.7.5 Mitochondrial DNA mutations and heteroplasmy	10
1.8 Mitochondrial DNA maintenance and expression.....	11
1.8.1 Mitochondrial nucleoids.....	11
1.8.2 Mitochondrial DNA replication	12
1.8.3 Mitochondrial copy number	16
1.8.4 Mitochondrial transcription.....	17
1.8.5 Mitoribosomes and mitochondrial translation.....	18
1.9 Mitochondrial dynamics	20
1.9.1 Mitochondrial fusion	21

1.9.2	Mitochondrial fission	21
1.9.3	Functions of mitochondrial dynamics	21
1.10	Mitochondrial communication	22
1.10.1	The AMPK signalling pathway	23
1.10.2	Proteostasis	24
1.11	Mitochondrial disease	25
1.11.1	Overview of mitochondrial disease	25
1.11.2	Mitochondrial disease genetics	26
1.11.3	Diagnosis of mitochondrial disease	31
1.12	Overview of the physiology of hearing	32
1.13	Pathophysiology of hearing loss	34
1.13.1	The role of mitochondria in hearing loss	34
1.13.2	Clinical presentation of mitochondrial hearing loss	36
1.13.3	Clinical diagnosis of mitochondrial hearing loss	36
1.13.4	Genetic aetiology of mitochondrial associated hearing loss	39
1.13.5	The role of mitochondrial dysfunction in acquired hearing loss	41
1.13.6	Clinical management of mitochondrial hearing loss	42
1.14	The m.1555A>G variant	42
1.14.1	Aminoglycoside antibiotics	43
1.14.2	Epidemiology of the m.1555A>G variant	43
1.14.3	Clinical features of the m.1555A>G mutation	44
1.14.4	Pathophysiology of the m.1555A>G mutation	45
1.14.5	The role of mtDNA haplogroups in m.1555A>G associated hearing loss	46
1.14.6	Role of heteroplasmy in m.1555A>G associated hearing loss	47
1.14.7	Evidence for nuclear modifiers of the m.1555A>G phenotype	47
1.15	Finding disease genes	51
1.15.1	Next generation sequencing technology	52
1.15.2	The human exome and whole exome sequencing	52
1.15.3	Exome sequencing methodology	53
1.16	Research aims	56
Chapter 2	Materials and Methods	57
2.1	Cell culture methodology	57

2.1.1	Fibroblast and myoblast cell maintenance	57
2.1.2	Cell propagation	57
2.1.3	Cell counting	58
2.1.4	Cryopreservation of cells	58
2.1.5	Immortalisation of primary fibroblasts	58
2.1.6	Analysis of cell growth	59
2.2	Histopathology methodology	59
2.2.1	Mitochondrial histochemistry	59
2.2.2	Haematoxylin and eosin staining	60
2.2.3	COX/SDH dual staining	60
2.3	Genetic analysis methodology	60
2.3.1	Genomic DNA extraction from cultured cells	60
2.3.2	Genomic DNA extraction from muscle homogenate	61
2.3.3	Genomic amplification	62
2.3.4	Polymerase chain reaction (PCR)	62
2.3.5	Agarose gel electrophoresis	62
2.3.6	Agarose gel extraction of PCR amplicons	63
2.3.7	Sequencing of nuclear genes	64
2.3.8	Long-range PCR of mitochondrial DNA	65
2.3.9	Quantification of mitochondrial DNA copy number	66
2.3.10	Gene expression analysis	69
2.3.11	Pyrosequencing	71
2.3.12	Analysis of mitochondrial 7S DNA	75
2.3.13	Mitochondrial repopulation assay	77
2.3.14	Generation of Whole Exome Sequencing data	80
2.4	Protein analysis methodology	84
2.4.1	Preparation of cell lysates	84
2.4.2	Quantification of protein	84
2.4.3	Sample preparation	85
2.4.4	Polyacrylamide gel electrophoresis (SDS-PAGE)	85
2.4.5	Western blotting	85
2.4.6	AMPK-Alpha 1 ELISA	88
2.4.7	Phospho-AMPK pT172 ELISA	88

2.4.8	Optimisation of AMPK pT172 ELISA assay.....	89
2.4.9	Heat shock response assay	90
2.4.10	In vivo mitochondrial translation assay	90
2.5	Immunocytochemistry	91
2.5.1	Mitochondrial network analysis	91
2.5.2	Imaging.....	91
2.5.3	Image processing.....	91
2.5.4	Huygens Essential Software analysis.....	92
2.5.5	Confocal microscopy imaging of mitochondrial nucleoids	92
2.6	Biochemical methodology	93
2.6.1	Measurement of cellular reactive oxygen species (ROS)	93
2.6.2	Oxidative DNA damage analysis	93
2.6.3	Protein carbonylation analysis	94
2.6.4	Assay of cellular respiration by Seahorse XF96 ^e Extracellular Flux Analyser	94
2.7	Statistical analysis.....	95
Chapter 3	A survey of the frequency of the m.1555A>G variant in UK patients with suspected mitochondrial deafness.....	97
3.1	Introduction.....	97
3.2	Materials and Methods.....	98
3.2.1	Survey methodology	98
3.2.2	Statistical analysis	98
3.3	Results.....	98
3.4	Discussion.....	101
Chapter 4	The identification of a nuclear genetic modifier in carriers of m.1555A>G	103
4.1	Introduction.....	103
4.2	Materials and Methods.....	103
4.2.1	A multi-generational Finnish family	103
4.2.2	Sporadic cases	108
4.2.3	Samples	109
4.2.4	Allelic quantification of m.1555A>G by Pyrosequencing.....	109
4.2.5	Exome sequencing.....	109

4.2.6	Analysis of known hearing loss genes	110
4.2.7	Analysis of genes previously suggested as modifiers of the m.1555A>G phenotype.....	112
4.2.8	Analysis of genes associated with mitochondrial replication	113
4.2.9	Genomic amplification and Sanger sequencing validation of candidate genes	113
4.2.10	Sanger sequencing of SSBP1	114
4.3	Results.....	117
4.3.1	Coverage analysis of consensus coding sequence (CCDS) bases and known hearing loss genes	118
4.3.2	Filtering for putative variants acting as modifiers of the m.1555A>G phenotype	121
4.3.3	Mitochondrial variants mediating disease risk.....	136
4.4	Discussion.....	137
Chapter 5 Characterising the functional effect of the SSBP1 variant.....		143
5.1	Introduction.....	143
5.2	Materials and methods	143
5.2.1	Cell lines and skeletal muscle	143
5.2.2	Genomic DNA extraction and Sanger sequencing.....	145
5.2.3	Protein analysis	145
5.2.4	Skeletal muscle analysis.....	146
5.2.5	Long range polymerase chain reaction.....	146
5.2.6	Analysis of mitochondrial 7S DNA	146
5.2.7	Mitochondrial repopulation assay	146
5.2.8	Quantitative real time polymerase chain reaction	147
5.2.9	Analysis of mitochondrial bioenergetics and oxidative stress	147
5.2.10	Mitochondrial network and nucleoid analysis	147
5.2.11	Heat shock response assay	148
5.3	Results.....	148
5.3.1	Confirmatory Sanger sequencing of SSBP1 and m.1555A>G variants....	148
5.3.2	Genetic effect of the c.3G>A SSBP1 variant.....	149
5.3.3	SSBP1 protein expression in fibroblasts	151
5.3.4	SSBP1 gene expression in fibroblasts.....	152

5.3.5	Analysis of SSBP1 skeletal muscle biopsy	153
5.3.6	Analysis of mtDNA copy number analysis in fibroblasts.....	155
5.3.7	Analysis of mtDNA copy number analysis in blood.....	157
5.3.8	Long-range PCR analysis of myoblast and fibroblast DNA	158
5.3.9	Analysis of 7S DNA in fibroblasts.....	158
5.3.10	Mitochondrial repopulation assay	159
5.3.11	Analysis of mitochondrial respiration in fibroblasts	166
5.3.12	Analysis of fibroblast cell growth	168
5.3.13	Analysis of intra-mitochondrial translation in fibroblasts.....	170
5.3.14	Analysis of steady state mitochondrial encoded proteins in fibroblasts ...	171
5.3.15	Analysis of steady state nuclear encoded mitochondrial proteins in fibroblasts.....	172
5.3.16	Analysis of mitochondrial gene expression in fibroblasts	173
5.3.17	Analysis of the mitochondrial network in fibroblasts	174
5.3.18	Analysis of mitochondrial dynamics proteins in fibroblasts.....	177
5.3.19	Analysis of mitochondrial nucleoids in fibroblasts.....	179
5.3.20	Analysis of oxidative stress.....	180
5.3.21	Analysis of retrograde mitonuclear signalling	184
5.4	Discussion.....	191
Chapter 6	Concluding discussion.....	207
Chapter 7	Summary of Conclusions	216
7.1	Conclusions.....	216
7.2	Limitations	216
7.3	Future work.....	217
Appendices.....		218
Appendix 1	Analysis of mitochondrial network.....	218
Appendix 2	Mitochondrial repopulation assay.....	220
Appendix 3	Heat shock response assay	222
References.....		224

List of Figures

Figure 1.1.	The ultrastructure of the mitochondria.	3
Figure 1.2.	The mitochondrial respiratory chain.	5
Figure 1.3.	The human mitochondrial genome.....	7
Figure 1.4.	Structure of the mitochondrial NCR and D-loop.	9
Figure 1.5.	Mitochondrial heteroplasmy and the threshold model of disease.	11
Figure 1.6.	The mtDNA replisome.	13
Figure 1.7.	Mechanisms of mtDNA replication.	15
Figure 1.8.	Structure of the 55S mammalian mitoribosome.....	19
Figure 1.9.	Schematic of mitochondrial translation.....	20
Figure 1.10.	The functions of mitochondrial dynamics.....	22
Figure 1.11.	The AMPK and mTOR signalling pathways.	24
Figure 1.12.	Primary mtDNA mutations linked to human disease.....	27
Figure 1.13	The human auditory system.	33
Figure 1.14.	A cross section through the human cochlea.	35
Figure 1.15.	Audiological assessment for diagnosis of hearing loss.....	39
Figure 1.16.	The structure of human 12S rRNA.	46
Figure 1.17.	Trans-acting modifier effects.	48
Figure 1.18.	Putative nuclear modifiers of m.1555A>G.	51
Figure 1.19.	Illumina exome sequencing methodology.....	53
Figure 2.1.	Analysis of quantitative PCR data.	69
Figure 2.2.	Pyrosequencing for allelic quantification.....	74
Figure 2.3.	Pyrosequencing standard curve.	74
Figure 2.4.	Mitochondrial repopulation optimisation experiment.....	78
Figure 2.5.	Modified mitochondrial repopulation experiment with shorter depopulation phase.	80
Figure 2.6.	A schematic of the bioinformatic pipeline used to analyse exome sequencing data.	82
Figure 2.7.	Bradford assay for protein quantification.....	85
Figure 2.8.	Typical standard curve of AMPK-A SimpleStep ELISA.	88
Figure 2.9.	Typical standard curve of Phospho-AMPK (pT172) ELISA Kit.....	89
Figure 2.10.	Optimisation of Phospho-AMPK (pT172) ELISA.	90

Figure 4.1.	Pedigree of Finnish family transmitting the m.1555A>G variant in 4 generations.	108
Figure 4.2.	Representative pyrograms generated from Pyrosequencing.	117
Figure 4.3.	Hypothesis 1; variant filtering workflow.	123
Figure 4.4.	Confirmatory Sanger sequencing electropherograms of <i>LOXHD1</i> and <i>MYO6</i> variants.	126
Figure 4.5.	Hypothesis 2; variant filtering workflow.	128
Figure 4.6.	Bar graph representing the number of correctly attributed variants in the segregation analysis.	131
Figure 4.7.	Segregation analysis of c.3G>A <i>SSBP1</i> variant within the Finnish family..	132
Figure 4.8.	Sanger sequencing analysis of the c.3G>A <i>SSBP1</i> variant in the children of III-6 (Family D) and III-10 (Family D).	133
Figure 4.9.	Hypothesis 4 variant filtering workflow.	135
Figure 5.1.	Confirmatory Sanger sequencing electropherograms of m.1555A>G and <i>SSBP1</i> variants.	149
Figure 5.2.	Genomic structure of <i>SSBP1</i> gene and multiple sequence alignment of the SSBP1 protein.	150
Figure 5.3.	SSBP1 protein analysis in patient and control fibroblasts.	151
Figure 5.4.	<i>SSBP1</i> mRNA expression in patient and control fibroblasts.	152
Figure 5.5.	Mitochondrial histochemistry of <i>SSBP1</i> skeletal muscle biopsy (patient P5).	153
Figure 5.6.	Long-range PCR analysis for mtDNA deletions in <i>SSBP1</i> and control skeletal muscle biopsies.	154
Figure 5.7.	mtDNA copy number analysis in <i>SSBP1</i> and control skeletal muscle.	155
Figure 5.8.	mtDNA copy number analysis in patient and control fibroblasts.	156
Figure 5.9.	mtDNA copy number analysis in blood from individuals in the Finnish family.	157
Figure 5.10.	Agarose gel of long-range PCR amplified total genomic DNA from myoblasts and fibroblasts.	158
Figure 5.11.	Southern blot analysis of 7S and total mtDNA in patient and control fibroblasts.	159
Figure 5.12.	Quantification of 7S and total mtDNA in patient and control fibroblasts.	159
Figure 5.13.	Optimisation of mitochondrial repopulation assay.	161
Figure 5.14.	Modified mitochondrial repopulation assay.	162
Figure 5.15.	mtDNA repopulation curve for P1 and control.	163
Figure 5.16.	mtDNA repopulation curve for P2 and control.	164

Figure 5.17.	mtDNA repopulation curve for P3 and control.....	165
Figure 5.18.	Calculation of mtDNA repopulation rate.....	166
Figure 5.19.	Example of Seahorse analysis of mitochondrial respiration in patient and control fibroblasts.....	167
Figure 5.20.	Determination of key parameters of mitochondrial respiration in patient and control fibroblasts by Seahorse analysis.	168
Figure 5.21.	Cellular growth curve analysis of patient and control immortalised fibroblasts.....	169
Figure 5.22.	Quantification of doubling time (DT) of patient and control immortalised fibroblasts.....	170
Figure 5.23.	Mitochondrial protein translation analysis in patient and control fibroblasts.....	171
Figure 5.24.	Western blot analysis of mitochondrial encoded proteins in patient and control fibroblasts.....	172
Figure 5.25.	Western blot analysis of nuclear encoded mitochondrial proteins in patient and control fibroblasts.....	173
Figure 5.26.	Analysis of mitochondrial gene expression in patient and control fibroblasts.....	174
Figure 5.27.	Mitochondrial networks in patient and control fibroblasts.....	175
Figure 5.28.	The average length and average number of mitochondrial fragments in patient and control fibroblasts.....	176
Figure 5.29.	Distribution of mitochondrial fragment lengths.....	177
Figure 5.30.	Western blot analysis of mitochondrial dynamics proteins in patient and control fibroblasts.....	178
Figure 5.31.	Quantification of OPA1 levels in patient and control fibroblasts.....	179
Figure 5.32.	Analysis of mitochondrial nucleoids in patient and control fibroblasts.....	180
Figure 5.33.	Measurement of cellular ROS levels in patient and control fibroblasts.....	181
Figure 5.34.	Quantification of 8-hydroxydeoxyguanosine in patient and control fibroblast DNA.....	182
Figure 5.35.	Western blot analysis of glutathione peroxidase 1 in fibroblasts.....	183
Figure 5.36.	Analysis of protein carbonylation in patient and control fibroblasts.....	184
Figure 5.37.	Analysis of cellular AMPK activity in patient and control fibroblasts by ELISA.....	185
Figure 5.38.	Western blot analysis of cellular AMPK activity.....	186
Figure 5.39.	Western blot analysis of total S6K and S6K-pT389.....	187
Figure 5.40.	Analysis of heat shock in fibroblasts.....	188

Figure 5.41. Analysis of heat shock response in patient and control fibroblasts..... 190

List of Tables

Table 2.1.	Details of primers used for Long Range PCR.....	65
Table 2.2.	Details of primer pairs used in qPCR analysis of mtDNA copy number	68
Table 2.3.	Details of the Taqman Gene Expression Assays used in qPCR	71
Table 2.4.	Details of the primers used in Pyrosequencing analysis	72
Table 2.5.	Primer sequences for preparation of radiolabelled dsDNA probes.....	77
Table 2.6.	Primary and secondary antibodies used in Western blotting.	87
Table 3.1.	Summary results of m.1555A>G testing undertaken at UKGTN and mitochondrial diagnostic laboratories	100
Table 4.1.	Clinical characteristics of the 19 children in generation IV.....	105
Table 4.2.	Clinical characteristics and availability of genomic DNA of individuals in generation II and III.	106
Table 4.3.	Clinical characteristics and availability of genomic DNA of children of fathers in generation III.	107
Table 4.4.	Demographic information for nine sporadic Spanish carriers of m.1555A>G ...	109
Table 4.5.	Established genes known to cause monogenic non-syndromic hearing loss classified by inheritance model.....	111
Table 4.6.	Established genes known to cause non-mitochondrial multisystem phenotypes of which hearing loss is a component.	112
Table 4.7.	Nuclear genes associated with mitochondrial disorders of which deafness is a component.....	112
Table 4.8.	Genes previously suggested as modifiers of m.1555A>G hearing loss.....	113
Table 4.9.	Known genes coding for proteins involved in mitochondrial DNA replication.....	113
Table 4.10.	Primer sequences, annealing temperatures and amplicon sizes for candidate genes prioritised from exome sequencing of m.1555A>G carriers.....	115
Table 4.11.	Primer sequences, annealing temperatures and amplicon sizes for all <i>SSBPI</i> coding regions	116
Table 4.12.	Coverage and depth statistics calculated for all Consensus Coding Sequence (CCDS) bases.....	119
Table 4.13.	Coverage and depth statistics calculated for known genes associated with hearing loss in Table 4.5, 4.6 and 4.7	120
Table 4.14.	Summary of variants from all sequenced exomes (n=9) irrespective of MAF in the population or functional impact.....	121
Table 4.15.	Annotation for variants identified in known hearing loss genes.....	125

Table 4.16.	Results of TRMU c.28G>T sequencing.....	127
Table 4.17.	Annotation of all variants seen that were shared between at least 4 of the 5 individuals within the Finnish cohort.....	129
Table 4.18.	Exome sequencing and confirmatory Sanger sequencing results of all patients possessing one of the variants listed in Table 4.17.....	130
Table 4.19.	Results of segregation analysis by Sanger sequencing.	130
Table 4.20.	mtDNA haplogroups of all exome sequenced individuals.....	136
Table 5.1.	Clinical and genetic features of the patient derived fibroblast cell lines. ...	144
Table 5.2.	Details of the control fibroblasts.....	144
Table 5.3.	Clinical and genetic details of skeletal muscle biopsies.....	145
Table 5.4.	Primer sequences, annealing temperatures and mtDNA nucleotide position for targeted analysis of m.1555	145
Table A1.1.	Distribution of mitochondrial fragment length in P1	218
Table A1.2.	Distribution of mitochondrial fragment length in P2	218
Table A1.3.	Distribution of mitochondrial fragment length in P3	218
Table A1.4.	Distribution of mitochondrial fragment length in controls	219
Table A2.1.	Repopulation levels from optimisation experiment.....	220
Table A2.2.	Repopulation levels from modified protocol experiment 1	220
Table A2.3.	Repopulation levels from modified protocol experiment 2	220
Table A2.4.	Repopulation levels from modified protocol experiment 3	221
Table A2.5.	Mean repopulation of the 3 modified protocol experiments.....	221
Table A2.6.	Repopulation rates calculated from the 3 modified protocol experiments.	221
Table A3.1.	Western blot analysis of BiP basal levels (GAPDH loading control).....	222
Table A3.2.	Western blot analysis of HSP60 basal levels (GAPDH loading control) ..	222
Table A3.3.	Western blot analysis of HSP70 basal levels (GAPDH loading control) ..	222
Table A3.4.	Western blot analysis of BiP basal and post heat shock levels (GAPDH loading control)	222
Table A3.5.	Western blot analysis of HSP60 basal and post heat shock levels (GAPDH loading control)	223
Table A3.6.	Western blot analysis of HSP70 basal and post heat shock levels (GAPDH loading control)	223

Nomenclature

Abbreviations used in this thesis are expanded in the following list. Only genes specifically discussed in the text are included. Gene names within tables use standard nomenclature as specified by the HUGO Gene Nomenclature Committee.

-	Unknown
μl	Microlitre
μm	Micrometre
μM	Micromolar
τm ⁵ U	5-taurinomethyluridine
τm ⁵ s ² U	5-taurinomethyl-2-thiouridine
2D-AGE	Two-dimensional agarose gel electrophoresis
4EBP1	Eukaryotic initiation factor 4E binding protein 1
8-OHdG	8-hydroxydeoxyguanosine
A-	Aminoacyl
ABR	Auditory brainstem response
ACMG	American College of Medical Genetics
AD	Autosomal dominant
ADP	Adenosine diphosphate
AMP	Adenosine monophosphate
AMPK	5' adenosine monophosphate-activated protein kinase
ANOVA	Analysis of variance
ANT1	Adenine nucleotide translocator isoform 1
AR	Autosomal recessive
ARHL	Age related hearing loss
ATAD3A	ATPase family AAA domain-containing 3
ATF6	Activating transcription factor 6
ATP	Adenosine triphosphate

ATP5A	ATP synthase subunit alpha
B2M	Beta-2-microglobulin
BCS1L	BCS1 <i>S.Cerevisiae</i> homolog like; BCS1L
BiP	Binding immunoglobulin protein
bp	Base pair
BrdU	Bromodeoxyuridine
BRG1	Transcription activator BRG1
BSA	Bovine serum albumin
cDNA	Complementary DNA
C	Control
°C	degrees Celsius
C10ORF2	Chromosome 10 open reading frame 2
C57BL/6J	C57 Black 6J
C57BL/6N	C57 Black 6N
CI	Confidence interval
CCD	Charged coupled device
CCDS	Consensus Coding Sequence Project
CMV	Cytomegalovirus
CNV	Copy number variation
CO ₂	Carbon dioxide
CoRR	Co-localisation for redox regulation
COX	Cytochrome <i>c</i> oxidase
COX10	Cytochrome <i>c</i> oxidase assembly factor COX10
CPEO	Chronic progressive external ophthalmoplegia
CRISPR/Cas9	Clustered regularly interspaced short palindromic repeats/CRISPR associated protein 9
CSB	Conserved sequence block

Ct	Threshold cycle
CT	Computed tomography
CTP	Cytidine triphosphate
D-loop	Displacement loop
DAPI	4'6'-diamidino-2-phenylindole
dbSNP	Single nucleotide polymorphism database
DCFH	2'7' dichlorofluorescein
DEFA3	Defensin alpha 3
DIABLO	Diablo IAP-Binding mitochondrial protein
DGUOK	Deoxyguanosine kinase
DMEM	Dulbecco's Modified Eagle Medium
DMSO	Dimethyl sulphoxide
DNA	Deoxyribonucleic acid
DNPH	Dinitrophenylhydrazine
dNTP	Deoxyribonucleotide triphosphate
DOA	Dominant optic atrophy
DPOAE	Distortion product otoacoustic emissions
DRP1	Dynamin-related protein 1
E-	Exit
E2F1	Transcription factor E2F1
ECAR	Extracellular acidification rate
ECL	Enhanced chemiluminescence
EDTA	Ethylenediaminetetraacetic acid
Eif2 α	Eukaryotic Translation Initiation Factor 2A
ELISA	Enzyme linked immunosorbent assay
EQTL	Expression quantitative trait loci
ER	Endoplasmic reticulum

EtBr	Ethidium bromide
ExAC	Exome Aggregation Cohort
fMet	N-formylmethionine
FADH ₂	Flavin adenine dinucleotide
FCCP	Carbonylcyanide-p- trifluoromethoxyphenylhydrazone
FCS	Fetal calf serum
Fe/S	Iron-sulphur
FIS1	Fission protein 1
FM	Frequency modulation
FRET	Fluorescence resonance energy transfer
G	Relative centrifugal force
GAPDH	Glyceraldehyde 3-phosphate dehydrogenase
GATK	Genome Analysis Toolkit
GJB2	Gap junction beta 2
GOSH	Great Ormond Street Hospital
GpC	Gapped Circle
GPx	Glutathione peroxidase
GPx1	Glutathione peroxidase 1
Grp78	Glucose-regulated protein 78 kDa
GSSG	Oxidized glutathione
GSH	Reduced glutathione
GTP	Guanosine triphosphate
GTPBP3	GTP binding protein 3
H ⁺	Proton
H-strand	Heavy strand
H&E	Haematoxylin and eosin
H ₂ DCFDA	2', 7'-dichlorodihydrofluorescein diacetate

H ₂ O	Water
H ₂ O ₂	Hydrogen peroxide
HCL	Hydrochloric acid
HEPES	2-(4-(2-hydroxyethyl)piperazin-1-yl) ethanesulphonic acid
Hg19	Human genome version 19
HRP	Horseradish peroxidase
HSF1	Heat shock factor 1
HSP	Heavy strand promoter
HSP10	Heat shock 10 kDa protein
HSP40	Heat shock 40 kDa protein
HSP60	Heat shock 60 kDa protein
HSP70	Heat shock 70 kDa protein
HSP90	Heat shock 90 kDa protein
HSR	Heat shock response
IHC	Inner hair cell
IMM	Inner mitochondrial membrane
Indel	Insertion/deletion
iPSC	Induced pluripotent stem cells
IRE1	Inositol requiring enzyme 1
IVA	Ingenuity Variant Analysis
Kb	Kilobase
kDa	Kilo Daltons
KSS	Kearns-Sayre Syndrome
LC3	Microtubule associated protein 1A/1B light chain 3
LHON	Leber's hereditary optic neuropathy
LKB1	Liver kinase B1
LOXHD1	Lipoxygenase Homology Domains 1

LSP	Light strand promoter
LRT	Likelihood ratio test
l-OPA1	Long OPA1
L-strand	Light strand
M	Molar
mM	Milimolar
MAF	Minor allele frequency
MAPK	Mitogen-activated protein kinase
MDS	Mitochondrial depletion syndrome
MELAS	Mitochondrial myopathy, encephalopathy, lactic acidosis and stroke-like episodes
MERRF	Myoclonic epilepsy and ragged red fibres
MET	Mechanotransducer
MFF	Mitochondrial fission factor
MFN1	Mitofusin-1
MFN2	Mitofusin-2
mg	Milligram
MGAM	Maltase glucoamylase
MGME1	Mitochondrial genome maintenance exonuclease 1
Mid49	Mitochondrial dynamics protein of 49 kDa
Mid51	Mitochondrial dynamics protein of 51 kDa
MIDD	Maternally inherited diabetes and deafness
Min	Minute
ml	Millilitre
mm	Millimetre
MNGIE	Mitochondrial neurogastrointestinal encephalopathy
MOTS-c	Mitochondrial open reading frame of the12S rRNA-c

MPV17	Mitochondrial inner membrane protein MPV17
MRG	Mitochondrial RNA granules
MRI	Magnetic resonance imaging
mRNA	Messenger RNA
MRP	Mitochondrial ribosomal protein
MRPS12	Mitochondrial Ribosomal Protein S12
MRPS16	Mitochondrial Ribosomal Protein S16
MRPS18CP2	Mitochondrial Ribosomal Protein S18C Pseudogene 2
MRPS22	Mitochondrial Ribosomal Protein S22
MT-CO1	Mitochondrially encoded cytochrome c oxidase I
MT-CO2	Mitochondrially encoded cytochrome c oxidase II
MT-CO3	Mitochondrially encoded cytochrome c oxidase III
MT-CYB	Mitochondrially encoded cytochrome b
MT-L1	Mitochondrially encoded tRNA leucine 1 (UUA/G)
MT-LSU	Mitochondrial large ribosomal subunit
MT-ND1	Mitochondrial nicotamide adenine dinucleotide dehydrogenase subunit 1
MT-ND2	Mitochondrial nicotamide adenine dinucleotide dehydrogenase subunit 2
MT-ND4	Mitochondrial nicotamide adenine dinucleotide dehydrogenase subunit 4
MT-ND6	Mitochondrial nicotamide adenine dinucleotide dehydrogenase subunit 6
MtRI	Mitochondrial replication intermediate
MT-RNR1	Mitochondrial 12S ribosomal RNA
MT-TK	Mitochondrially encoded tRNA lysine
MT-TS1	Mitochondrially encoded tRNA serine 1 (UCN)
MT-SSU	Mitochondrial small ribosomal subunit
MT-TE	Mitochondrially encoded tRNA glutamic acid
mtDNA	Mitochondrial DNA
mtEFTU	Mitochondrial translation elongation factor Tu

mtEFTs	Mitochondrial translation elongation factor Ts
mtEFG1	Mitochondrial translation elongation factor G1
mTERF1	Mitochondrial transcription termination factor 1
MTO1	Mitochondrial tRNA translation optimisation 1
mTOR	Mechanistic target of rapamycin
mTORC1	Mechanistic target of rapamycin complex I
mTORC2	Mechanistic target of rapamycin complex II
MTRRF1	Mitochondrial ribosomal recycling factor 1
MTS	Mitochondrial targeting sequence
MYO6	Myosin VI
n.a	Not applicable
n.d	Not determined
NaCl	Sodium chloride
NaOH	Sodium hydroxide
NAD ⁺	Oxidised nicotinamide dinucleotide
NADH	Nicotinamide adenine dinucleotide
NADPH	nicotinamide adenine dinucleotide phosphate
NCBI	National Centre for Biotechnology Information
NCR	Non-coding region
NFκB	Nuclear factor kappa-light-chain enhancer of activated B cells
NHLBIESP	National Heart Lung and Blood Institute Exome Sequencing Project
NGS	Next-generation sequencing
NUMT	Nuclear mitochondrial DNA
O ₂	Oxygen
O ₂ ⁻	Superoxide
O _H	Origin of heavy strand replication
O _L	Origin of light strand replication

OAEs	Otoacoustic emissions
OCR	Oxygen consumption rate
OCT	Optimum cutting temperature
OHC	Outer hair cell
OLB	Oligonucleotide labelling buffer
OMA1	Mitochondrial metalloendopeptidase OMA1
OMIM	Online Mendelian Inheritance in Man
OMM	Outer mitochondrial membrane
OPA1	Optic atrophy 1
ORF	Open reading frame
OriZ	Single zone of replication initiation
OXA1	Mitochondrial oxidase assembly protein
OXPHOS	Oxidative phosphorylation
P	Patient
P-	Peptidyl
pMole	Picomole
pS:pHS	Densitometric quantification steady state: heat shock
PBS	Phosphate buffered saline
PCR	Polymerase chain reaction
PERK	Protein kinase RNA (PKR)-like kinase
PEO	Progressive external ophthalmoplegia
Pi	Inorganic phosphate
PI3K-AKT	Phosphoinositide 3-kinase –AKT (protein kinase B)
PIKK	Phosphatidylinositol 3-kinase related kinases
PMF	Proton motive force
PMSF	Phenylmethylsulphonyl fluoride
POLG	Polymerase DNA gamma

POLG2	Polymerase DNA gamma 2
POLRMT	Mitochondrial RNA polymerase
Pol	DNA polymerase
PS	Pearson syndrome
PTA	Pure tone audiogram
PVDF	Polyvinylidene difluoride
qPCR	Quantitative polymerase chain reaction
R ²	Coefficient of determination
rCRS	Revised Cambridge Reference Sequence
RFU	Relative fluorescent units
RITOLS	Ribonucleotide incorporation throughout the lagging strand
RL	Repopulation level
RNA	Ribonucleic acid
RNAi	RNA interference
RNAseH1	Ribonuclease H1
RNAse P	Ribonuclease P
RNAse Z	Ribonuclease Z
ROS	Reactive oxygen species
RPM	Revolutions per minute
RRM2B	p53 inducible ribonucleotide reductase M2 B
rRNA	Ribosomal RNA
S	Sulphur
s-OPA1	Short OPA1
sORF	Short open reading frame
S6K	p70-S6 kinase
SANDO	Sensory ataxia neuropathy dysarthria and ophthalmoparesis
SD	Standard deviation

SDH	Succinate dehydrogenase
SDS	Sodium dodecyl sulphate
SIFT	Sorting tolerant from intolerant
SMAC	Second mitochondrial derived activator of caspases
SNP	Single nucleotide polymorphism
SNV	Single nucleotide variant
SOD	Superoxide dismutase
SSBP1	Single stranded binding protein
SSC	Saline-sodium citrate
SUCLA2	Succinate-coA ligase
SUMO	Small ubiquitin like modifier
TAE	Tris-acetate EDTA
TAS	Termination associated sequence
TBST	Tris Buffer Saline Tween 20
TBq	Terabecquerel
TCA	Tricarboxylic acid
TE	Tris-EDTA
TEFM	Transcription elongation factor
TFAM	Mitochondrial transcription factor A
TFB1M	Transcription factor B1
TFB2M	Transcription factor B2
TIC	Translation initiation codon
TIFF	Tagged image file format
TOAEs	Transient otoacoustic emissions
TOMM20	Translocase of outer mitochondrial membrane 20
TOP1MT	DNA topoisomerase I mitochondrial precursor
TOP3A	DNA topoisomerase 3-alpha

TP	Thymidine phosphorylase
TRMU	tRNA 5-methylaminomethyl-2-thiouridylate methyltransferase
TRMT61B	tRNA (adenine(58)-N(1))-methyltransferase
tRNA	Transfer RNA
TSC	Tuberous sclerosis complex
TSC1	Tuberous sclerosis complex 1
TSC2	Tuberous sclerosis complex 2
TTP	Thymidine triphosphate
TWINK	Twinkle mtDNA helicase
UCLH	University College London Hospitals
UK	United Kingdom
UPR	Unfolded protein response
USB	Universal Serial Bus
V	Voltage
VCF	Variant call format
VDAC	Voltage dependent anion channels
v/v	Volume/volume
WES	Whole exome sequencing
WGS	Whole genome sequencing
w/v	Weight/volume
YME1L1	ATP-dependent metalloprotease YME1L1

Chapter 1

Introduction

1.1 Chapter overview

This chapter reviews and contextualises the central concepts of this thesis. Firstly, it provides an overview of current mitochondrial biology, focussing primarily on the contribution of dysfunctional mitochondrial DNA (mtDNA) maintenance and expression to human disease. Following this, there is an exploration of the role of mitochondria in hearing loss, a symptom that causes a significant reduction in the quality of life of patients with mitochondrial disease. Next, the mtDNA variant, m.1555A>G, is presented together with the current evidence for the mechanisms underpinning the associated hearing loss. The introduction then concludes with a synopsis of next generation sequencing technologies detailed as justification for the approach adopted in this thesis aiming to identify and characterise novel nuclear modifier genes underlying the variable penetrance of the m.1555A>G variant.

1.2 The mitochondrion

Mitochondria are subcellular organelles that form a dynamic reticular network in eukaryotic cells (Sukhorukov, Dikov et al. 2012). Although characterised by their role in the generation of cellular energy, throughout their evolutionary history mitochondria have acquired numerous additional cellular functions (Huynen, Duarte et al. 2013). Mitochondrial dysfunction therefore compromises many aspects of cellular physiology and leads to a range of human diseases, including hearing loss, that to date remain largely untreatable (Scarpelli, Todeschini et al. 2014).

1.3 The origins of mitochondria

Until the characterisation of the flagellate *Excavata Monocercomonodites*, mitochondria had been identified in every studied eukaryotic organism (Karnkowska, Vacek et al. 2016). Mitochondria are believed to have arisen approximately two billion years ago from the endosymbiotic integration of an aerobic α -proteobacterium into the proto-eukaryotic host

(Margulis 1971, Karnkowska, Vacek et al. 2016). Phylogenetic studies, comparing the sequence of human mtDNA and the genome of the α -proteobacteria *Rickettsia prowazekii* have provided evidence of a common origin for mitochondria and the α -proteobacteria lineages (Andersson, Zomorodipour et al. 1998, Emelyanov 2001, Gray 2012). The origin of the host cell, however, remains more controversial. Currently, the most accepted theory, the ‘hydrogen hypothesis’ posits the host cell was a prokaryotic, hydrogen dependent archaeon possibly resembling modern methanogenic archaea (Martin and Muller 1998).

1.4 Structure

Mitochondria, resembling their bacteria predecessors, are bound by two phospholipid membranes; the inner and outer mitochondrial membrane (IMM; OMM respectively). These membranes establish two distinct organellar sub-compartments; the intermembrane space and the matrix contained by the IMM (**Figure 1.1**). The mitochondrial matrix is the site of numerous metabolic processes (discussed in **Section 1.5**) and houses multiple copies of the mtDNA and mitochondrial ribosomes and hence contains the site of mtDNA replication, transcription and translation (discussed in **Section 1.8**) (Frey and Mannella 2000). The OMM encloses the organelle and consists of a phospholipid bilayer punctuated by voltage dependent anion channels (VDAC). These channels result in the OMM being highly permeable to molecules smaller than 10 kDa (Guo and Mannella 1993, Bayrhuber, Meins et al. 2008). The OMM also functions to engage other cellular components including the endoplasmic reticulum (ER), ribosomes and the nucleus facilitating mitochondrial functional integration into cellular physiologic processes (Pernas and Scorrano 2016).

The IMM is divided into two functionally distinct zones: the inner boundary membrane and the cristae membrane that are linked by cristae junctions (Pernas and Scorrano 2016). The inner boundary membrane lies parallel with the OMM, forming interaction sites containing specific machinery for protein import (Reichert and Neupert 2002). The cristae membrane forms folds into the matrix and contains the majority of the electron transport chain responsible for oxidative phosphorylation (OXPHOS). The IMM is rich in protein, specifically cardiolipin, that necessitates the active transport of molecules from the intermembrane space into the matrix by interaction with a number of mitochondrial carrier proteins (Paradies, Paradies et al. 2014). This lack of permeability enables the creation of a

transmembrane electrochemical gradient, a key requirement for OXPHOS (discussed in **Section 1.5.1**).

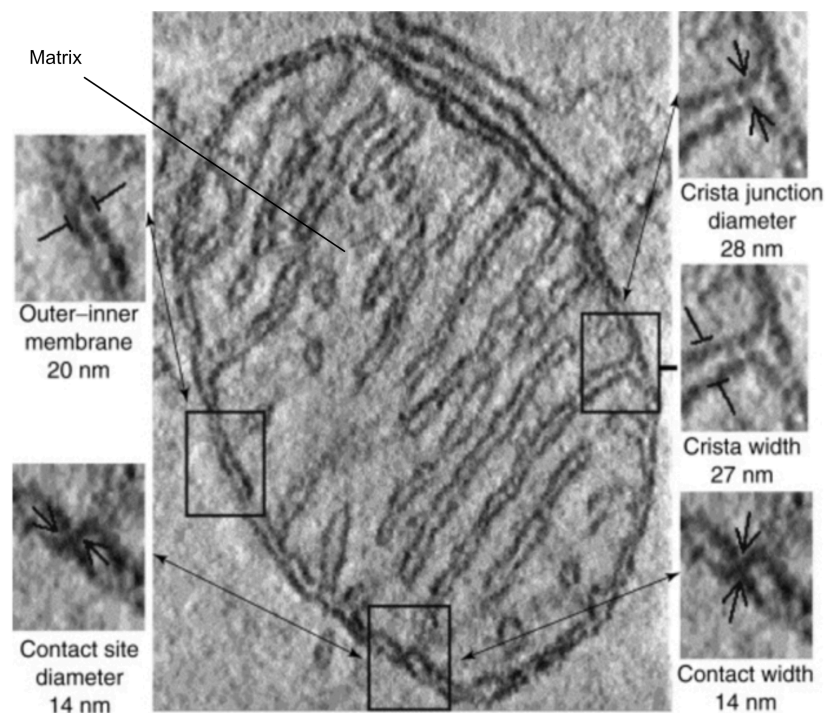


Figure 1.1. The ultrastructure of the mitochondria. A 3D tomogram of a mitochondrion with structural features and dimensions. Adapted from Frey and Mannella 2000.

1.5 Mitochondrial function

Mitochondria are responsible for a number of metabolic processes including the tricarboxylic acid (TCA) cycle, biosynthesis of cellular pyrimidines, steroids and heme and the β -oxidation of fatty acids (Voet 2011). Mitochondria also play a fundamental role in the regulation of cellular calcium, the regulation of apoptosis, adaptive thermogenesis and the generation of reactive oxygen species (ROS) and reactive nitrogen species (Wallace 2005). However, the most recognised role of mitochondria is the use of a transmembrane electrochemical gradient to convert adenosine diphosphate (ADP) and inorganic phosphate (P_i) into adenosine triphosphate (ATP) through the process of OXPHOS (Kadenbach 2012).

1.5.1 Oxidative phosphorylation (OXPHOS)

The OXPHOS respiratory chain consists of four structurally distinct multi-subunit complexes (Complex I-IV), ATP synthase (Complex V) and two electron carriers:

coenzyme Q₁₀ and cytochrome *c* located in the cristal membrane (Smeitink, van den Heuvel et al. 2001) (**Figure 1.2**).

Complex I (nicotinamide adenine dinucleotide (NADH)-ubiquinone oxidoreductase) contains 45 subunits, seven of which are encoded by the mtDNA (Zhu, Vinothkumar et al. 2016). Complex II (succinate dehydrogenase, SDH) by comparison comprises four subunits (A-D) all of which are nuclear encoded. Complex II is unique amongst the respiratory chain complexes, functioning both in OXPHOS and the TCA cycle where it oxidises succinate to fumarate (Sun, Huo et al. 2005). Complex III (ubiquinol-cytochrome *c* oxidoreductase) is composed of ten nuclear encoded subunits and one mitochondrial encoded subunit (cytochrome *b*) whilst Complex IV (cytochrome *c* oxidase, COX) consists of 14 subunits, three of which are encoded by the mtDNA (mitochondrially encoded cytochrome *c* oxidase I-III, MT-COI, MT-CO II, MT-CO III) (Tsukihara, Aoyama et al. 1995, Iwata, Lee et al. 1998). Finally, Complex V (ATP synthase) consists of 19 subunits; two of which (ATP6 and ATP8) are encoded by the mitochondria (Jonckheere, Smeitink et al. 2012).

A prerequisite for OXPHOS is the availability of coenzyme NADH and flavin adenine dinucleotide (FADH₂) produced during glycolysis, the TCA cycle and β -oxidation of fatty acids. Electrons from these cofactors are transferred into the respiratory chain to drive OXPHOS. Initially, Complex I oxidizes NADH to NAD⁺ whilst FADH₂ is reduced to FAD by Complex II. Both Complex I and Complex II reduce ubiquinone (Coenzyme Q₁₀) to ubiquinol that is then transferred to Complex III (ubiquinol-cytochrome *c* oxidoreductase) via the IMM (Kim, Khalimonchuk et al. 2012). Complex III is responsible for the Q cycle that results in the oxidation of ubiquinol with the concurrent reduction of cytochrome *c* (Mitchell and Moyle 1967). Complex IV then accepts an electron from each of the four-cytochrome *c* molecules reduced by Complex III. These electrons are then transferred to a molecule of oxygen that binds four protons to form two molecules of H₂O. The reactions of Complex I, III and IV all couple the transfer of elections to the transport of protons into the intermembrane space thus creating the proton-motive force (PMF) (Mitchell and Moyle 1967). Complex V subsequently can use this electrochemical gradient to produce ATP from ADP and P_i by a process of rotary catalysis (Stock, Gibbons et al. 2000).

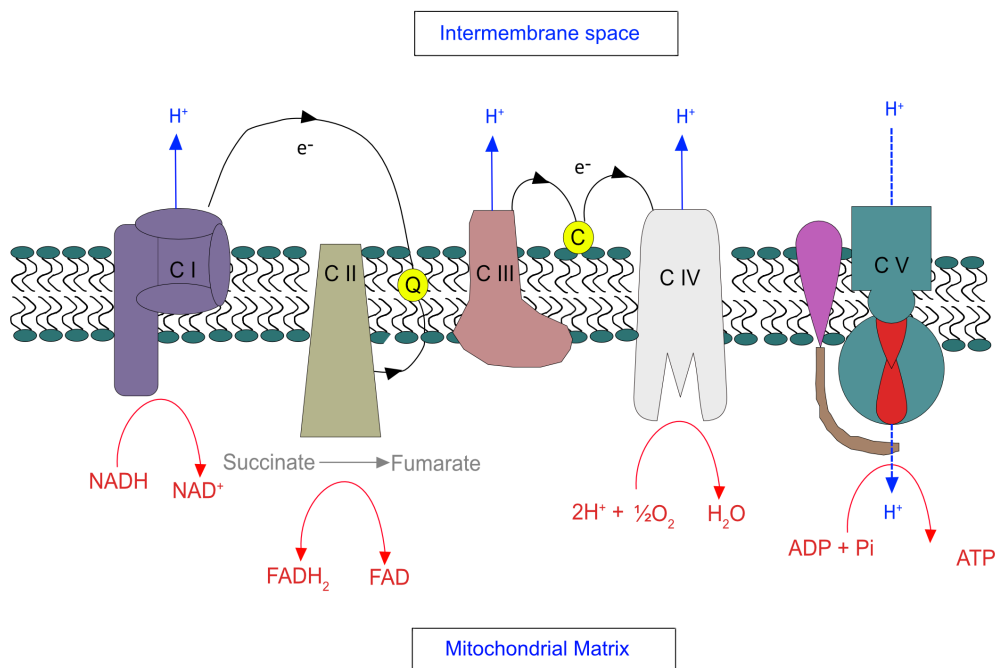


Figure 1.2. The mitochondrial respiratory chain. Electrons enter the respiratory chain through the oxidation of NADH to NAD⁺ by Complex I and via the oxidation of succinate to fumarate with the reduction of FADH₂ to FAD by Complex II. Electrons are transferred by coenzyme Q₁₀(Q) and cytochrome *c* (C) to Complex IV, the final electron acceptor, that converts oxygen to water. The electron transfer of Complex I, III and IV is coupled to translocation of protons into the intermembrane space. This establishes a proton gradient that drives ATP synthesis by Complex V.

1.6 Generation of Reactive Oxygen Species

ROS play an essential role in cellular redox signalling, however, in excess they are responsible for oxidative damage to the cell. ROS are formed by one-electron transfer from a redox donor to oxygen and the majority of cellular ROS, particularly superoxide (O₂⁻) is produced by Complex I and III (Murphy 2009, Bleier and Drose 2013). However, recent studies indicate that numerous other mitochondrial enzymes also contribute to ROS generation, including complex II, nicotinamide adenine dinucleotide phosphate (NADPH)-oxidase and monoaminoxidases (Zhang, Yu et al. 1998, Zorov, Juhaszova et al. 2014). O₂⁻ is subsequently metabolised to hydrogen peroxide, H₂O₂, by dismutation in a reaction catalysed by superoxide dismutases (SOD). H₂O₂ is then able to modulate cellular signalling by altering cell signalling molecules by orchestrating redox dependent modification of thiol groups on cysteine residues (Go, Chandler et al. 2015). There is also evidence that ROS stimulate several intracellular signalling pathways including mitogen-

activated protein kinase (MAPK), NF κ B and the PI3K-Akt pathway (Schoonbroodt, Ferreira et al. 2000, Lee, Yang et al. 2002, McCubrey, Lahair et al. 2006). Cellular ROS are therefore vital for organismal homeostasis and play a fundamental role in numerous cellular processes including metabolism, energy expenditure and the immune system (Shadel and Horvath 2015).

Importantly, however, excessive ROS act as primary mediators of oxidative damage to cellular DNA, lipids and proteins. Oxidative damage to DNA is mediated by single and double strand DNA breaks and modifications of purine and pyrimidine bases to DNA (Bohr 2002). Lipids can also react with ROS to form lipid hydroperoxides and numerous other secondary products including propanal, hexanal and 4-hydroxynonenal (Marrocco, Altieri et al. 2017). Oxidative modifications of proteins include carbonylation, s-nitrosylation and disulphide formation (Gao, Laude et al. 2008, Cai and Yan 2013). Given these important cellular effects of ROS, mitochondria possess a complex ROS defence network consisting of enzymatic and non-enzymatic antioxidants. These include SODs, catalase, peroxiredoxin and most importantly, glutathione (GSH) (Ott, Gogvadze et al. 2007, Sena and Chandel 2012). GSH serves as the major scavenger of cellular hydroxyl radicals by reducing hydrogen and organic peroxides in the presence of glutathione peroxidase (GPx) (Gao, Laude et al. 2008).

1.7 Mitochondrial genetics

1.7.1 Mitochondrial genome

As a product of their evolutionary heritage, mitochondria have retained their own genome, the mtDNA, which exists separately from the nuclear DNA. Human mtDNA is a 16,569 base pair (bp) double stranded circular molecule that is packed into DNA-protein complexes termed nucleoids (discussed in **Section 1.8.1**) (Bogenhagen, Rousseau et al. 2008). mtDNA was first sequenced in 1981 and later corrected and published as the ‘revised Cambridge Reference Sequence (rCRS)’ in 1999 (Anderson, Bankier et al. 1981, Andrews, Kubacka et al. 1999, Bandelt, Kloss-Brandstatter et al. 2014).

During evolution, the vast majority of mitochondrial genes have been transferred to the nucleus; evidenced by the presence of NUMTs (nuclear sequence of mitochondrial origin) (Hazkani-Covo, Zeller et al. 2010). Two main theories attempt to explain the reason the cell maintains a separate mtDNA at energetic expense despite this mass transfer of

mitochondrial genes. Firstly, it has been suggested that hydrophobic membrane proteins may be difficult to import into mitochondria or be targeted to the ER if expressed in the cytoplasm (Claros, Perea et al. 1995, Bjorkholm, Ernst et al. 2017). Alternatively, the co-location for redox regulation (CoRR) hypothesis proposes that mtDNA is essential to provide a sufficiently sensitive redox regulatory system that could not be provided by a nuclear transcription signal (Allen 2015).

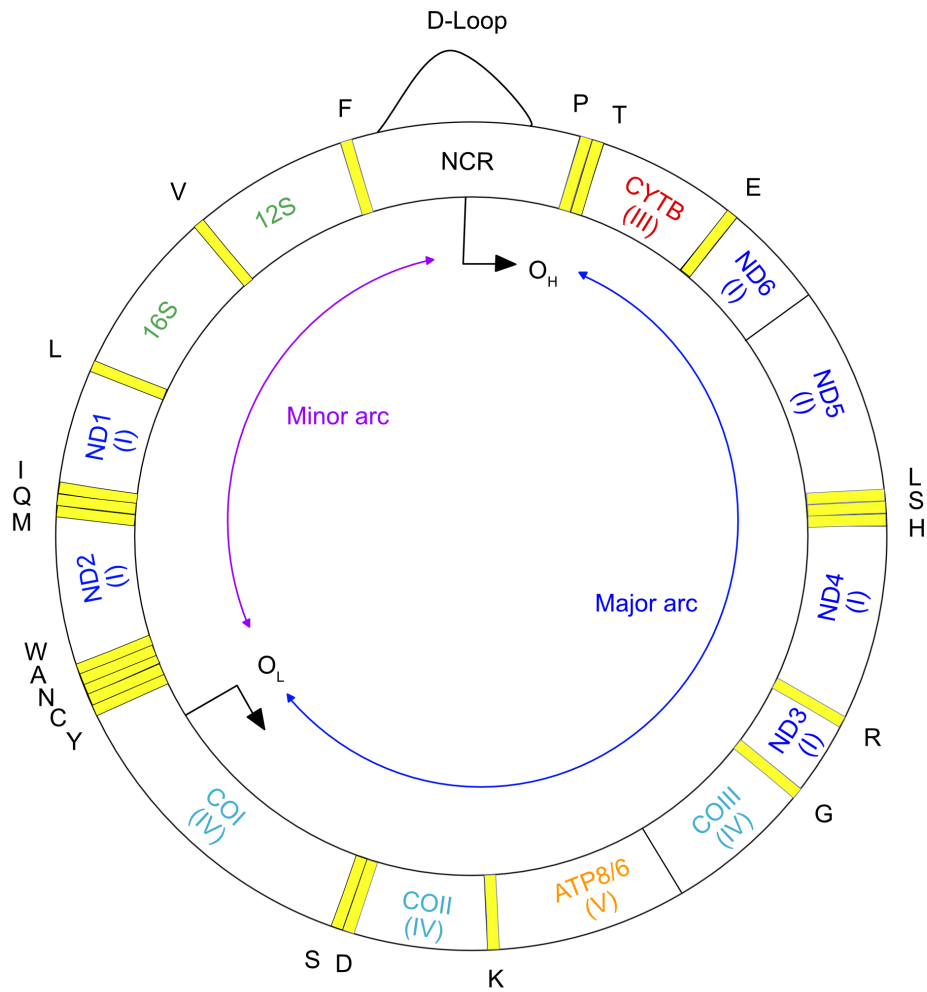


Figure 1.3. The human mitochondrial genome. The human mitochondrial genome is a circular 16,569 bp molecule that encodes 13 protein-coding genes (Genes encoding Complex I proteins in dark blue, Complex III in red, Complex IV in light blue and Complex V in orange), two ribosomal RNAs (12S and 16S in green) and 22 transfer RNAs (marked in yellow identified by their respective amino acid abbreviation). The mtDNA also contains a non-coding region (NCR) that incorporates a third strand, named the D-loop (discussed in **Section 1.7.2**).

The mtDNA consists of a purine-rich heavy (H-) strand and a pyrimidine-rich light (L-) strand. Each cell contains multiple copies of mtDNA and depending on bioenergetic

demand each cell can contain hundreds to thousands of copies of mtDNA (Chinnery and Hudson 2013). mtDNA is densely packed with 37 coding genes: 13 protein coding, 22 transfer ribonucleic acids (tRNAs) and 2 ribosomal ribonucleic acids (rRNA) genes, the 12S and 16S (**Figure 1.3**). The 13 encoded proteins are components of the OXPHOS system and the rRNA products are core components of mitochondrial translation. The majority of mtDNA proteins coding genes are found on the H- strand whereas the L-strand only codes for the ND6 (nicotinamide adenine dinucleotide dehydrogenase subunit 6) component of Complex I and 8 tRNA genes. The mtDNA is remarkably compact, with none of the genes containing introns and only one non coding region (NCR) that extends between the mt-tRNA phenylalanine (F) and proline (P) genes and contains the transcriptional promoters of both the light and heavy strands (LSP and HSP) as well as the origin of heavy strand replication (O_H), three conserved sequence blocks (CSB1, CSB2, CSB3) and a termination associated sequence (TAS) (discussed further in **Section 1.7.2**) (Sbisa, Tanzariello et al. 1997, Andrews, Kubacka et al. 1999). The L-strand origin (O_L) is located in a cluster of five tRNAs and the intervening section between O_H and O_L defines the ‘major arc’ whilst the remaining section of the molecule is classed the ‘minor arc’.

1.7.2 Mitochondrial D loop and 7S DNA

The NCR incorporates a third strand, the 7S DNA, that forms a displacement loop (D-loop) structure of approximately 650 nucleotides from O_H at the variable 5’ end of 7S DNA to the TAS at the 3’ end of 7S DNA (**Figure 1.4**) (Doda, Wright et al. 1981). 7S DNA is primed by 7S RNA transcribed from the LSP and although this transition from RNA to DNA is incompletely understood it has been suggested it occurs in CSB2 (Kang, Miyako et al. 1997). A number of studies have shown 7S DNA synthesis is promoted by various factors, including transcription factor A (TFAM), single stranded binding protein (SSBP1) and Twinkle helicase (discussed in **Section 1.8.2**) (Gensler, Weber et al. 2001, Ruhanen, Borrie et al. 2010, Milenkovic, Matic et al. 2013).

The exact function of the D-loop however, that exists at an energetic expense to the mitochondria, is not yet fully characterised. It has been proposed that it serves to organise the mtDNA into nucleoids (discussed in **Section 1.8.1**), maintain deoxynucleotide (dNTP) pools during the cell cycle and play a critical role in mtDNA replication. It is proposed that the D-loop represents a product of aborted replication of the H- strand according to the

strand displacement model of mtDNA replication (see **Section 1.8.2.5.1**) (Clayton 1982, He, Mao et al. 2007, Antes, Tappin et al. 2010). In this model H- strand replication is initiated using 7S DNA as a primer or by synthesising a 7S DNA that is not terminated at the TAS. It has also been suggested that the D-loop triple strand structure may act to inhibit replication fork progression and hence prevent replication fork collisions that would be detrimental to genome stability (Rudolph, Upton et al. 2013, Nicholls and Minczuk 2014).

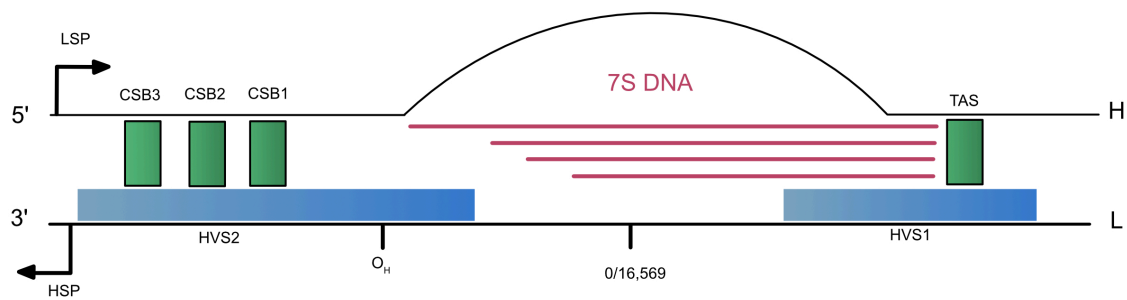


Figure 1.4. Structure of the mitochondrial NCR and D-loop. The NCR contains the LSP and HSP required for mitochondrial transcription, three conserved sequence blocks (CSB 1-3) between HSP/LSP and the origin of heavy strand replication O_H , two hypervariable segments (HVS) and 7S DNA extending from O_H to the termination associated sequence (TAS). Figure adapted from Nicholls and Minczuk 2014.

1.7.3 Mitochondrial DNA inheritance

A central dogma of mitochondrial biology is the exclusive maternal inheritance of mtDNA (Pyle, Hudson et al. 2015). It is thought two major processes account for the lack of transmission of sperm mtDNA. Firstly, mtDNA copy number is greatly down-regulated in spermatogenesis (Larsson, Oldfors et al. 1997). Secondly, the paternal mtDNA is tagged with ubiquitin and degraded early in embryonic development (Hutchison, Newbold et al. 1974, Sutovsky, Moreno et al. 2000). Interestingly, there has been an isolated description of patient with a 2 bp deletion within *MT-ND2* (mitochondrial nicotinamide adenine dinucleotide dehydrogenase subunit 2, Complex I) in skeletal muscle inherited from the father. This suggests dual parental inheritance of mtDNA is possible, although it is likely to be an exceptionally rare occurrence (Schwartz and Vissing 2002).

1.7.4 Mitochondrial haplogroups

Human mtDNA has a mutation rate estimated to be 45 times that of the autosomes largely due to the proximity to free radical production from the OXPHOS respiratory chain, the continuous nature of mtDNA replication and the reduced capacity for mtDNA repair (Lagouge and Larsson 2013, Fu, Li et al. 2014). Given this greater mutation rate, a number of non-pathogenic protein altering variants have arisen that can then be stably transmitted down the maternal lineage. Sequence analysis has allowed the phylogenetic grouping of common single nucleotide polymorphisms (SNPs) into regionally and ethnically specific haplogroups. For example, analysis of European populations has identified 10 major haplogroups (H, I, J, K, M, T, U, V, W and X) (Torroni, Huoponen et al. 1996). Haplogroups can be used to map worldwide population distributions and may alter mitochondrial function and hence modify the risk of various diseases (Gomez-Duran, Pacheu-Grau et al. 2010, Hudson, Gomez-Duran et al. 2014, Stewart and Chinnery 2015).

1.7.5 Mitochondrial DNA mutations and heteroplasmy

Cells contain multiple copies of mtDNA, a proportion of which may contain polymorphic or pathogenic variants (Lightowlers, Chinnery et al. 1997). In a state of homoplasmy the cell contains mtDNA of a single genotype. Heteroplasmy occurs when there exists a subpopulation of mtDNA defined by a variance in mtDNA sequence, either caused by point mutations or deletions. The level of heteroplasmy is defined relative to the level of wild type molecules present in the cell (**Figure 1.5 A**). In the case of a pathological variant, there is a threshold effect where at lower heteroplasmy levels the wild type mitochondria can compensate and no functional deficit results (Hayashi, Ohta et al. 1991). Once the threshold level is reached, there is failure of compensation and subsequent OXPHOS dysfunction (**Figure 1.5 B**). Threshold levels vary among mutations with tRNA mutations requiring high levels of mutant DNA (>80%) although the m.14723 T>C substitution in tRNA^{Glu} has been reported to be pathogenic at only 7% heteroplasmy (Alston, Lowe et al. 2010). Heteroplasmy levels can vary among tissue types, which may account for tissue specific phenotypes observed in some mitochondrial diseases (Chinnery, Zwiijnenburg et al. 1999).

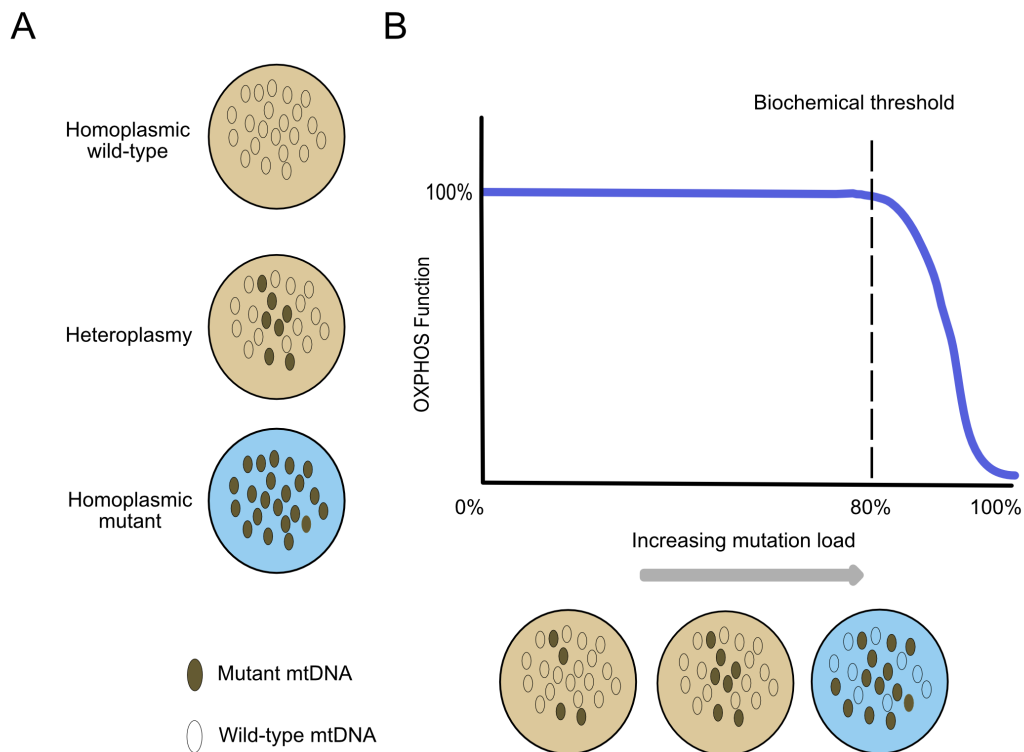


Figure 1.5. Mitochondrial heteroplasmy and the threshold model of disease. (A) A homoplasmic wild type cell consists of 100% wild type mtDNA (unfilled circles), increasing mtDNA mutation load leads to heteroplasmy and finally to a state of homoplasmy when mtDNA is 100% mutant (filled circles) (B) The threshold model of mitochondrial disease. Depicted are 3 cells and corresponding OXPHOS function. Each cell contains mitochondria carrying either mutant mtDNA (filled circles) or wild type (unfilled circles). As mtDNA mutation load increases above a threshold (e.g. >80% for tRNA point mutations) wild type mtDNA fails to compensate and respiratory chain function declines.

1.8 Mitochondrial DNA maintenance and expression

mtDNA expression is a multistage process with numerous control points (Shadel 2008). These include the maintenance of stable mtDNA (mtDNA replication and repair, termed mtDNA maintenance), mtDNA transcription including post-transcriptional regulation and finally, mitochondrial translation by the mitochondrial ribosome (mitoribosome).

1.8.1 Mitochondrial nucleoids

mtDNA is packaged into protein-DNA complexes termed nucleoids containing essential proteins for mtDNA replication and transcription akin to the packaging of nuclear DNA by histones into the structural units called nucleosomes (Kornberg 1974, Brown, Tkachuk et al. 2011). Fluorescence microscopy reveals nucleoids as compact scattered foci localised primarily at the cristae junctions but also throughout the mitochondrial network (Satoh and

Kuroiwa 1991). TFAM is the most comprehensively characterised component of the nucleoid and has been shown to induce negative supercoiling and compaction of the genome (Kaufman, Durisic et al. 2007).

Microscopy studies have revealed most nucleoids have an irregular ellipsoidal shape and contain a single molecule of mtDNA coated with approximately 1000 copies of TFAM (Kukat, Wurm et al. 2011, Kukat, Davies et al. 2015). Numerous additional proteins have been identified that co-purify with mtDNA or TFAM. These include mtDNA polymerase gamma (poly), Twinkle helicase, transcription factor B1M (TFB1M), transcription factor B2M (TFB2M), mitochondrial transcription termination factor 1 (mTERF1) and SSBP1 (Bogenhagen, Rousseau et al. 2008, Gilkerson, Bravo et al. 2013). As well as these interactions with mitochondrial transcription and replication proteins, a number of studies have revealed interactions with molecular chaperones, proteases, lipid metabolic enzymes, mitochondrial ribosomal proteins and cytoskeletal proteins (Bogenhagen 2012). A layered structure of the nucleoid has been proposed where mtDNA replication and transcription occur in the central core whereas complex assembly and translation are peripherally located (Bogenhagen, Rousseau et al. 2008).

1.8.2 Mitochondrial DNA replication

mtDNA replication is a vital process in maintaining mtDNA copy number throughout cell division and occurs independently of the cell cycle (Bogenhagen and Clayton 1977). The minimal constituents of the mtDNA replisome have been reconstituted *in vitro* and consist of poly, Twinkle helicase and SSBP1 (**Figure 1.6**) (Korhonen, Pham et al. 2004).

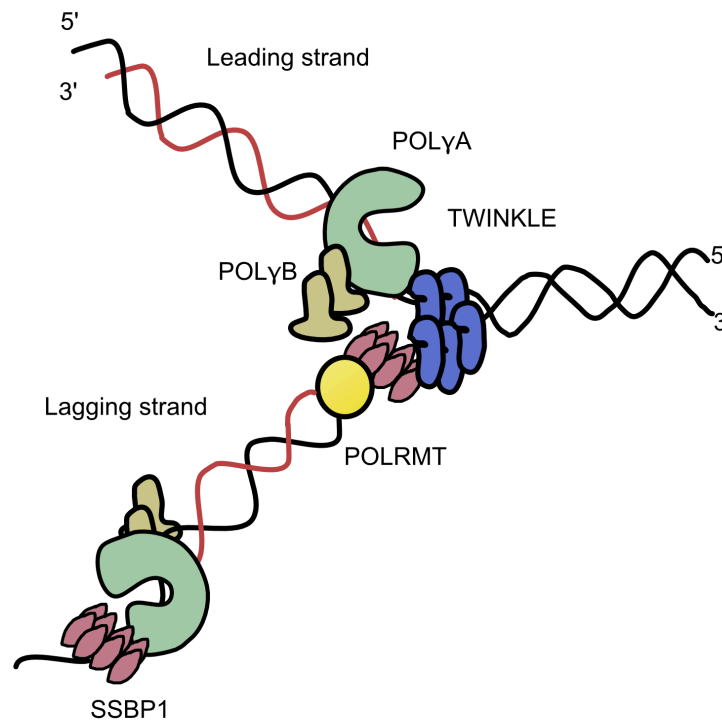


Figure 1.6. The mtDNA replisome. mtDNA replication proceeds in a 5' to 3' direction. Twinkle helicase unwinds double stranded DNA and SSBP1 stabilises the single stranded DNA whilst stimulating the processivity of poly. POLRMT synthesises the RNA primer that primes DNA synthesis. Adapted from Wanrooij and Falkenberg 2010.

1.8.2.1 DNA polymerase gamma

Mammalian mitochondria contain a single DNA polymerase, poly γ , that functions as a heterotrimer with a catalytic subunit (poly γ A) encoded by *POLG* and two accessory poly γ B subunits encoded by *POLG2* (Ropp and Copeland 1996). Poly γ A primarily functions to facilitate 5'→3' DNA polymerisation with the poly γ B subunits increasing the polymerisation processivity and substrate binding (Johnson, Tsai et al. 2000). Poly γ is unable to use dsDNA as a template and hence requires the unwinding of DNA to provide a single stranded template before replication can begin (Korhonen, Pham et al. 2004).

1.8.2.2 Twinkle DNA helicase

Twinkle, encoded by the nuclear *TWINK* gene is the only replicative DNA helicase in mammalian mitochondria and shares homology with the helicase domain of the T7 phage gp4 protein (Spelbrink, Li et al. 2001, Korhonen, Gaspari et al. 2003). Twinkle catalyses 5'→3' unwinding of DNA *in vitro*, forming the single stranded template for poly mediated DNA polymerisation.

1.8.2.3 Mitochondrial single stranded binding protein (SSBP1)

In humans the 7 exon *SSBP1* gene is located on chromosome 7q34 and codes for the 148 amino acid SSBP1, a mitochondrial targeted protein that functions to maintain mtDNA stability (Tiranti, Rossi et al. 1995). SSBP1 shares structural homology with the *Escherichia coli* ssDNA-binding protein and crystal structural studies reveal mtDNA wraps around the protein in electropositive channels (Lohman and Ferrari 1994, Yang, Curth et al. 1997). Functioning as a homotetramer of 16kDa subunits, SSBP1 binds single stranded DNA to prevent the formation of stable secondary structures after unwinding by Twinkle. SSBP1 also stimulates the activity of poly thus increasing the processivity of the poly/Twinkle complex from 2kb to 16kb and facilitating the complete replication of the mitochondrial genome (Korhonen, Pham et al. 2004). Mutational analysis reveals SSBP1 uses exclusive structural elements to interact with other replisome proteins and these variants correlate with defects in mtDNA replication (Oliveira and Kaguni 2011). The significance of SSBP1 to mtDNA maintenance has been demonstrated by the deletion of the yeast *SSBP1* homolog, *RIM1*, resulting in complete loss of mtDNA (Van Dyck, Foury et al. 1992). Similarly, RNAi knockdown of *SSBP1* in *Drosophila* S2 cells also resulted in a severe depletion of mtDNA (Farr, Matsushima et al. 2004). Recent work has also demonstrated SSBP1 plays an important role in the cellular heat shock response (Tan, Fujimoto et al. 2015) (discussed in **Sections 1.10.2 and 5.3.21.4**).

1.8.2.4 Other mitochondrial replication proteins

Although poly, Twinkle and SSBP1 represent the minimal replisome *in vitro*, *in vivo* an expanding number of other proteins have been shown to be required for mtDNA replication. These include, but are not limited to, the topoisomerases, *TOP1MT* (Zhang, Meng et al. 2007) and *TOP3A* (Wang, Lyu et al. 2002), the RNA polymerase *POLRMT* (Tiranti, Savoia et al. 1997) and *RNASEH1* (Cerritelli, Frolova et al. 2003). Additionally, mtDNA replication requires the availability of balanced pool of dNTPs that must be maintained by mitochondrial salvage pathways (discussed further in **Section 1.11.2.3**).

1.8.2.5 Models of replication

Currently there is no consensus on the mechanism of mtDNA replication. Three models have been described (i) strand displacement model, (ii) strand coupled replication (iii) ribonucleotide incorporation throughout the lagging strand (RITOLS) (**Figure 1.7**).

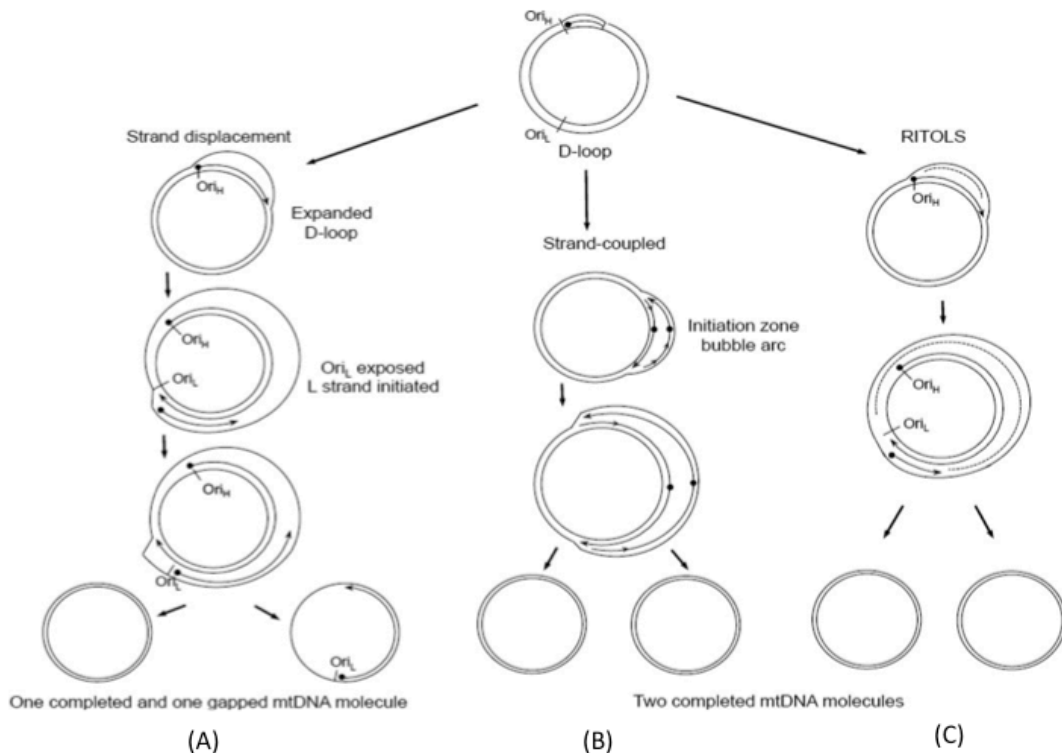


Figure 1.7. Mechanisms of mtDNA replication. (A) Strand displacement model (B) Strand coupled model (C) RITOLS model. A detailed description of the models is presented in the text below. Adapted from Kasiviswanathan, Collins et al. 2012.

1.8.2.5.1 *Strand displacement model*

According to the strand displacement model, mtDNA replication is initiated at O_H and proceeds around the major arc until O_L is exposed as a stretch of single-stranded DNA that is then coated in SSBP1. Second strand synthesis is then initiated back towards O_H (Clayton 1982). The exposed O_L sequence then forms a hairpin structure that can be used by POLRMT to create a primer for poly to commence second strand synthesis (Wanrooij, Miralles Fuste et al. 2012). This delay in second strand synthesis means that one daughter molecule will complete replication before the other molecule has completed L- strand synthesis. This results in two open circle molecules, one complete and one with a single stranded gap on the minor arc (gapped circle, GpC) that requires completion after replication.

1.8.2.5.2 *Ribonucleotide incorporation throughout the lagging strand (RITOLS)*

The RITOLS model can be considered a modification of the strand displacement model and is based on the observation that mitochondrial replication intermediates seen by two-dimensional agarose gel electrophoresis (2D-AGE) are likely to be RNA/DNA hybrid structures that are degraded by RNASEH1 (Holt and Reyes 2012). The RITOLS model is

largely analogous with the strand displacement model with both models predicting asynchronous initiation of strand replication. However, the RITOLS model predicts the lagging strand is not single stranded and coated with SSBP1 as stipulated by the strand displacement model. Instead, the lagging strand is coated in RNA derived from processed mitochondrial transcripts that are later converted to DNA (Reyes, Kazak et al. 2013).

1.8.2.5.3 *Strand coupled replication*

The model of strand coupled replication is predicated on the detection of classical features of synchronous strand coupled replication detected by 2D-AGE that cannot be accounted for by the strand displacement model (Holt, Lorimer et al. 2000). In this model bidirectional replication initiates downstream of O_H in a region termed OriZ. This model predicts continuous leading strand synthesis, coupled with discontinuous synthesis of the lagging strand. This necessitates the generation of Okazaki fragments on the lagging strand, although these have currently not been detected in living mitochondria. However, mitochondria do contain specialised flap endonucleases and helicases that are homologous to the nuclear Okazaki fragment processing machinery, implying the possible relevance of this replication model (Zheng and Shen 2011).

1.8.3 Mitochondrial copy number

The maintenance of mitochondrial copy number is vital for cellular homeostasis and maintaining cellular energy requirements. mtDNA copy number is highly tissue specific with high energy consuming tissues such as muscle and neurons acquiring high copy number compared to less energy demanding tissue such as kidney (Miller, Rosenfeldt et al. 2003, D'Erchia, Atlante et al. 2015). This implies there must exist a mechanism that balances mtDNA synthesis with degradation (Berk and Clayton 1974). Currently, there is no consensus on the cellular mechanism underlying copy number regulation, however one proposed theory is the 'copy number threshold hypothesis' (Clay Montier, Deng et al. 2009). This postulates that copy number is regulated by feedback loops where synthesis or degradation of mtDNA is stimulated as copy approaches respectively a lower or upper threshold limit. A number of mechanisms have been proposed to orchestrate mtDNA copy number changes, including mtDNA compaction, control of primer transcription from LSP and abortion of replication in the TAS with the creation of

7S DNA (Falkenberg, Gaspari et al. 2002, Pohjoismaki, Wanrooij et al. 2006, Jemt, Persson et al. 2015).

A number of studies have shown that maintenance of mtDNA copy number is dependent on the availability of the minimal replisome proteins SSBP1, Twinkle and poly γ (Van Dyck, Foury et al. 1992, Tyynismaa, Sembongi et al. 2004, Stewart, Schoeler et al. 2011, Ikeda, Ide et al. 2015). Further studies have shown mtDNA maintenance is dependent on a host of diverse proteins including, RNASEH1, the DNA-binding AAA protein, TFAM, mitochondrial dynamics proteins and exonucleases (Ekstrand, Falkenberg et al. 2004, He, Mao et al. 2007, Kornblum, Nicholls et al. 2013, Vielhaber, Debska-Vielhaber et al. 2013). Furthermore, recent work using a comprehensive RNA interference (RNAi) screen in *Drosophila* has identified almost a hundred proteins that are required to maintain mtDNA copy number, implying the mechanism of mtDNA copy number regulation is highly complex and requires further investigation (Fukuoh, Cannino et al. 2014).

1.8.4 Mitochondrial transcription

Mitochondrial transcription is initiated from three promoters located in the NCR. Transcription of the L- strand initiates from the LSP, whereas transcription of the H- strand begins from HSP1 and HSP2 (Montoya, Christianson et al. 1982). The HSP-1 initiated transcript contains tRNA^{Phe} tRNA^{Val}, 16S and 12S rRNA whereas the HSP-2 initiated transcript produces large polycistronic transcripts covering almost the entire coding strand. The majority of transcripts from LSP terminate at the guanine tract of CSB2 and this RNA is used as the primer for D-loop synthesis (Zheng, Wu et al. 2014, Tan, Wellesley et al. 2016) (**Section 1.7.2**).

The core mitochondrial transcription machinery consists of POLRMT, TFAM and TFB2M (Masters, Stohl et al. 1987, Litonin, Sologub et al. 2010, Shi, Dierckx et al. 2012). Initially, TFAM binds upstream of the transcription start site where it bends and unwinds DNA (Falkenberg, Larsson et al. 2007). TFAM then recruits POLRMT followed by TFB2M to the promoter via its C-terminal domain (Rubio-Cosials, Sidow et al. 2011). Additional proteins are then required for control of the transcription process including the transcription elongation factor (TEFM) and the termination factors mTERF1-4 (Linder, Park et al. 2005, Posse, Shahzad et al. 2015).

Following transcription, the polycistronic transcripts are processed by RNase P and RNase Z to release the individual RNAs (Puranam and Attardi 2001, Brzezniak, Bijata et

al. 2011). mRNAs are then 3' polyadenylated by the mitochondrial poly (A) polymerase (Tomecki, Dmochowska et al. 2004). The rRNAs, 12S and 16S also require post-transcriptional modification to enable the assembly of the mitoribosome. Modifications of the 16S subunit are not well characterised, although include the recently identified m¹A modification at position m.947, catalysed by the mitochondrial methyltransferase TRMT61B (Bar-Yaacov, Frumkin et al. 2016). There are currently five identified post-transcriptional modifications of the 12S rRNA. These include dimethylation of adenine m.1584 and m.1583 (N6, N6- dimethyladenosine (m⁶2A)) by TFB1M and TFB2M (Cotney and Shadel 2006) (**Figure 1.16**). It has been shown that TFB1M functions as the main 12S rRNA methyltransferase and ablation of TFB1M decreases steady state levels of 12S rRNA resulting in impaired mitochondrial translation (further discussed in **Section 1.8.5**) (Metodieva, Lesko et al. 2009). The function of m⁶2A and 12S rRNA modifications including m⁴C⁸⁴⁶, m⁵U⁴²⁹ is currently unresolved but may play a role in mitoribosomal assembly and stability (Rorbach and Minczuk 2012).

tRNAs must also undergo post-transcriptional modifications including methylation, taurination and pseudouridylation and these modifications have been shown to increase tRNA stability and folding (Suzuki and Suzuki 2014). Following this, the tRNAs must be charged with their cognate amino acid in a process catalysed by the appropriate aminoacyl-tRNA synthase (Chalioy, Vlastaridis et al. 2016). Recent work has demonstrated that these post-transcriptional events occur in mitochondrial RNA granules (MRGs). These specialised sub-compartments of the mitochondrion provide a defined focus for the spatiotemporal regulation required for mitochondrial gene expression (Antonicka and Shoubridge 2015, Jourdain, Koppen et al. 2015).

1.8.5 Mitoribosomes and mitochondrial translation

Mitochondria possess a complete gene expression machinery required to translate the mitochondrial mRNAs of the 13 protein coding genes.

Human mitochondrial mRNAs are translated by the mitoribosome, 55S, consisting of small (mt-SSU, 28S) and a large (mt-LSU, 39S) subunits (**Figure 1.8**) (O'Brien 1971). The mitoribosome contains three rRNAs (12S and 16S and mt-tRNA^{Val}) and 80 mitochondrial ribosomal proteins (MRPs) encoded by the nucleus (Amunts, Brown et al. 2015). The mitoribosome contains three RNA binding sites, named aminoacyl (A), peptidyl (P) and

exit (E). The A-site binds the aminoacylated tRNA, the P-site binds the peptide linked tRNA and the E-site harbours the deacylated tRNA exiting the ribosome.

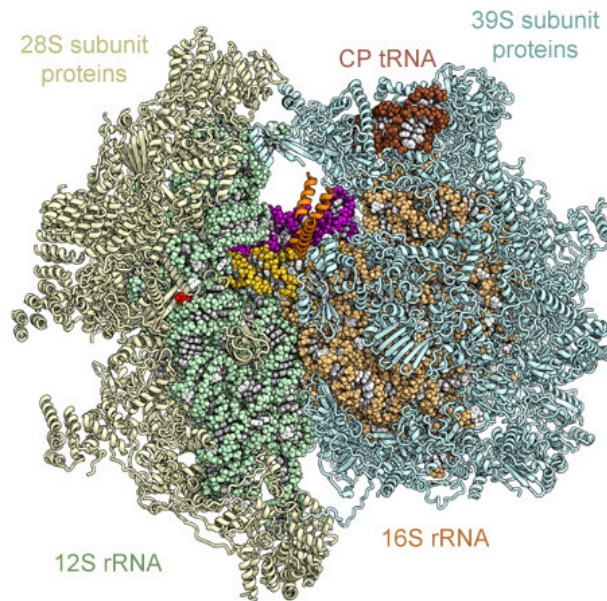


Figure 1.8. Structure of the 55S mammalian mitoribosome. The 55S mitoribosome consists of the large 39S and small 28S subunits. The 28S subunit is represented in yellow, 12S rRNA in green, 16S rRNA in orange, 39S subunit in blue, central protuberance (CP) tRNA in brown. Reproduced from Greber, Bieri et al. 2015.

Mitochondrial translation occurs by a conserved series of stages divided into (i) initiation (ii) elongation (iii) termination and (iv) mitoribosome recycling (Christian and Spremulli 2012) (**Figure 1.9**). Initiation occurs by the selection of an mRNA start codon by the SSU in complex with initiation factors (mtIF2 and mtIF3) and the initiator tRNA (fMet-tRNA^{Met}) paired to the start codon in the ribosomal P-site (Christian and Spremulli 2009, Kuzmenko, Atkinson et al. 2014). Elongation is facilitated by three elongation factors: mtEFTu, mtEFTs and mtEFG1. Firstly, mtEFTu binds an aminoacylated tRNA in conjunction with guanosine triphosphate (GTP) recruiting it to the mitoribosomal A-site. A codon-anticodon interaction causes GTP hydrolysis and peptide bond formation between the amino acid occupying the P- site and the amino acid in the A-site thus extending the polypeptide chain. mtEFG1 facilitates the removal of the deacylated tRNA form the P-site and translocates the peptidyl tRNA to the P-site. Elongation continues with sequential addition of amino acids until a stop codon is encountered (UAA, AGA, UAG or AGG) in the A-site. This triggers the binding of the mitochondrial release factor, mtRF1, the hydrolysis of the peptidyl-tRNA bond in the A-

site and the release of the nascent polypeptide (Lind, Sund et al. 2013). Following termination and release of the polypeptide, the mitoribosome is recycled by the action of the mitochondrial ribosomal recycling factors, mtRRF1 and mtEFG2 (Rorbach, Richter et al. 2008, Tsuboi, Morita et al. 2009). Interestingly, the mitoribosome has been shown to interact directly with the IMM facilitating the co-translational insertion of proteins into the membrane aided by a number of proteins including the mitochondrial oxidase assembly protein, Oxa1 (Ott and Herrmann 2010, Kruger, Deckers et al. 2012).

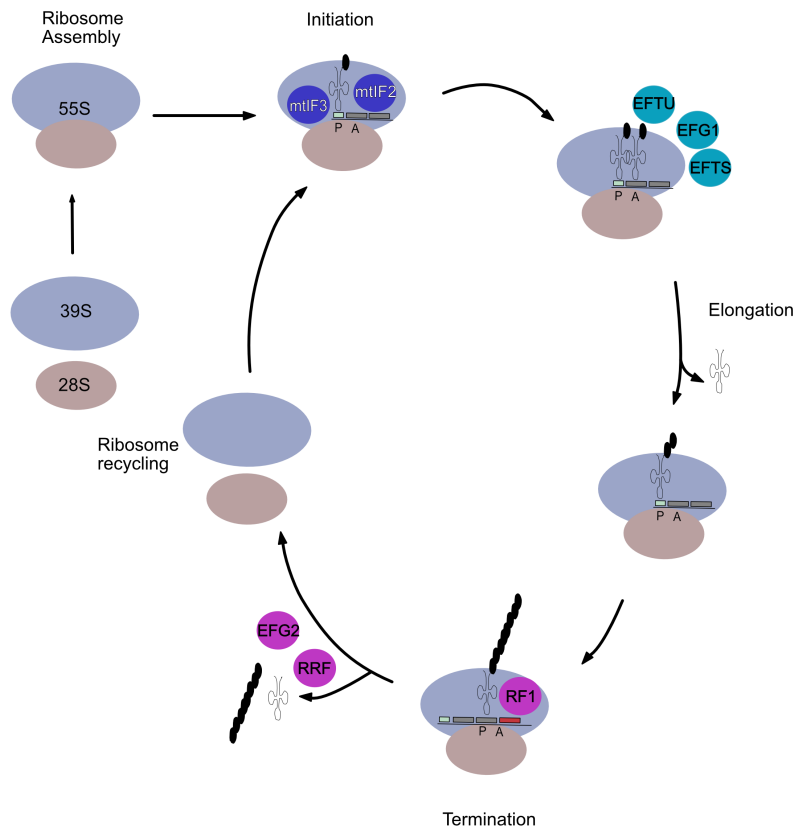


Figure 1.9. Schematic of mitochondrial translation. The mitoribosomal subunits are depicted as blue (39S) and brown (28S) ovals. Mitochondrial translation is divided into initiation requiring mtIF2 and mtIF3 (blue circles), mRNA transcript (grey rectangles, start codon in green) and initiator tRNA fMet-tRNA^{Met}; elongation by addition of amino acids (black circles) requires mtEFTu, mtEFTs and mtEFG1 (green circles) and termination/mitoribosome recycling by mtRF1a and mtRRF/mtEFG2 (pink circles) respectively.

1.9 Mitochondrial dynamics

Mitochondria are dynamic organelles that exist in complex networks undergoing morphological changes through the processes of fusion, fission, movement and mitophagy (Archer 2013, Wai and Langer 2016). The ability of mitochondria to respond by these

mechanisms is vital for cellular function and perturbations in mitochondrial dynamics are thus both a cause and consequence of mitochondrial disease (discussed in **Section 1.11**).

1.9.1 Mitochondrial fusion

Mitochondrial fusion is governed by the dynamin GTPases mitofusin 1 and 2 (MFN1 and MFN2) and optic-atrophy 1, OPA1 (Westermann 2010). The mitofusins synchronise to appose adjacent mitochondria enabling GTP dependent fusion of the OMM, followed by the fusion of the IMM mediated by OPA1 (Mishra, Carelli et al. 2014). Alternative splicing and proteolytic cleavage of OPA1 by the metalloendopeptidases, OMA1 and YME1L have recently been shown to give rise to long (l-OPA1) and short (s-OPA1) isoforms (Anand, Wai et al. 2014). Interestingly, l-OPA1 has been shown to be sufficient for mitochondrial fusion whereas s-OPA1 plays an important role in fission (Wai and Langer 2016).

1.9.2 Mitochondrial fission

Mitochondrial fission is primarily orchestrated by the dynamin like GTPase, dynamin related protein 1 (DRP1). In response to cellular signals including phosphorylation, ubiquitylation and SUMOylation DRP1 translocates from the cytosol to the OMM where it interacts with a number of binding partners including mitochondrial fission protein 1 (FIS1), mitochondrial fission factor (MFF) and mitochondrial dynamics proteins of 49 and 51kDa (MiD49 and MiD51) (van der Bliek, Shen et al. 2013, Wai and Langer 2016). At the OMM, DRP1 forms ring-like structures with FIS1 at division sites where it hydrolyses GTP, promoting membrane constriction (Mears, Lackner et al. 2011).

1.9.3 Functions of mitochondrial dynamics

Mitochondrial fusion and fission permit the adaptation of the mitochondrial network to changing cellular conditions and facilitate the removal of dysfunctional organelles. Mitochondrial fusion is important for complementation of mtDNA products in heteroplasmic cells, whilst fission plays a vital role in cell division, apoptosis, network distribution and mitochondrial quality control, also termed mitophagy (Westermann 2010). Fusion is correlated with increased ATP generation and may act to counter the effects of decreased nutrient availability, whilst fragmentation of the mitochondrial network, when

fission outweighs fusion events, is associated with dysfunctional OXPHOS and cellular stress (**Figure 1.10**) (Liesa and Shirihai 2013).

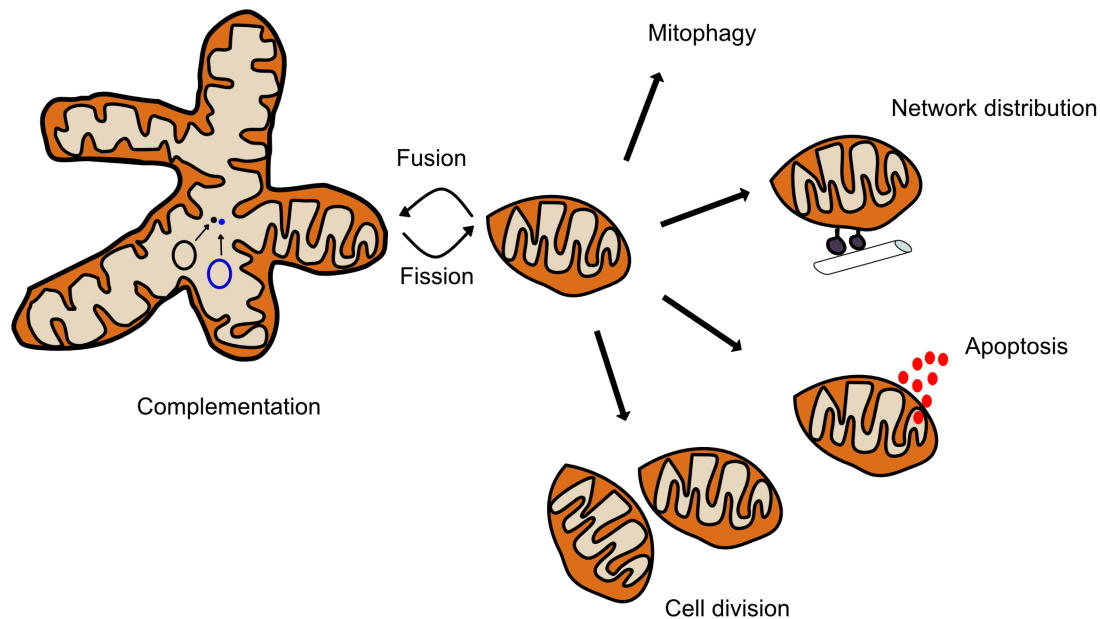


Figure 1.10. The functions of mitochondrial dynamics. Mitochondrial fission is important for mitochondrial quality control (mitophagy), the release of cytochrome *c* in the initiation of apoptosis (depicted by red circles), distribution by cytoskeletal transport and for the segregation of mitochondria during cell division. Mitochondrial fusion is of primary importance in complementing mtDNA products in heteroplasmic cells. Adapted from Westermann 2010.

1.10 Mitonuclear communication

In addition to their crucial function in cellular energy generation, mitochondria fulfil a range of other cellular functions (as discussed in **Section 1.5**). To maintain cellular homeostasis, mitochondria require tight control by the nucleus, so-called ‘antegrade regulation’. Additionally, mitochondria illicit a ‘retrograde response’ that can reprogramme cellular metabolism in response to cellular demand (Quiros, Mottis et al. 2016).

Mitochondrial dysfunction can directly affect the cytosolic milieu, including increasing cytosolic calcium flux, adenosine monophosphate (AMP) levels and ROS (Quiros, Mottis et al. 2016). These perturbations can then directly activate retrograde signalling pathways from the mitochondria to the nucleus. These pathways lead to a plethora of downstream consequences including cell cycle control, cell growth, apoptosis and mitochondrial biogenesis; placing the mitochondrion as a central node in cellular energy control

(Wallace, Fan et al. 2010). The following section highlights two important elements of mitonuclear communication that are further explored in **Chapter 5**: the 5' adenosine monophosphate activated protein kinase (AMPK) signalling pathway and the regulation of cellular protein homeostasis, termed proteostasis.

1.10.1 The AMPK signalling pathway

A key sensor of cellular metabolic status, AMPK is a heterotrimeric serine/threonine kinase consisting of an α catalytic subunit ($\alpha 1$ or $\alpha 2$), a β regulatory subunit ($\beta 1$ or $\beta 2$) and γ adenosine monophosphate (AMP) binding subunits ($\gamma 1$, $\gamma 2$ or $\gamma 3$) (Gowans and Hardie 2014). AMPK is activated via phosphorylation of threonine 172 (pT172) by upstream AMPK kinases, including liver kinase B1 (LKB1) (Hawley, Boudeau et al. 2003) (**Figure 1.11**). High cellular AMP causes allosteric activation of AMPK by increasing pT172, a process that is reversed by higher levels of ATP (Xiao, Sanders et al. 2011). Impaired energy generation in cells with suboptimal respiratory chain function leads to inefficient generation of ATP and over production of ROS, including H_2O_2 , hydroxyl groups and superoxide anions. These species are known to directly activate AMPK in human cell lines (Choi, Song et al. 2008) and excess cellular ROS levels have been shown to lead to AMPK activation in fibroblasts from a patient with myoclonic epilepsy with ragged red fibres (MERRF) (Wu and Wei 2012).

AMPK acts as a central signalling node to detect whole cell bioenergetics and as such the downstream signalling pathways that it activates are complex and context dependent. There has been burgeoning interest in AMPK and its cellular effects in recent years and it has been the subject of a number of excellent reviews (Mihaylova and Shaw 2011, Hardie, Ross et al. 2012, Hardie, Schaffer et al. 2016). Ultimately, in times of energy deficiency, AMPK acts to increase catabolic processes whilst inhibiting energy demand to restore cellular ATP balance. AMPK achieves this by modulating a host of cellular functions including glucose and fatty acid metabolism (Marcinko and Steinberg 2014). Importantly, protein synthesis constitutes the most energy demanding cellular process (Lane and Martin 2010). When nutrients are scarce, AMPK signals via suppression of the mechanistic target of rapamycin (mTOR) pathway to inhibit the production of proteins (Xu, Ji et al. 2012). mTOR is a member of the phosphatidylinositol 3-kinase related kinases (PIKK) superfamily that serves as a central regulator of cellular metabolism, growth and survival (Laplante and Sabatini 2012). mTOR is present in the cell in two distinct complexes, mechanistic target of

rapamycin complex 1 (mTORC1) and complex 2 (mTORC2). AMPK primarily controls the activity of the mTORC1 complex by activation of the tuberous sclerosis complex (TSC) proteins (TSC1 and TSC2) that subsequently inactivate the GTP binding protein, Ras homolog enriched in brain (Rheb), an important upstream activator of mTORC1 (Avruch, Long et al. 2009). This inhibits mTORC1 mediated phosphorylation of p70-S6 kinase (S6K) and eukaryotic initiation factor 4E binding protein 1 (4EBP1), important potentiators of protein synthesis and cellular proliferation (Showkat, Beigh et al. 2014).

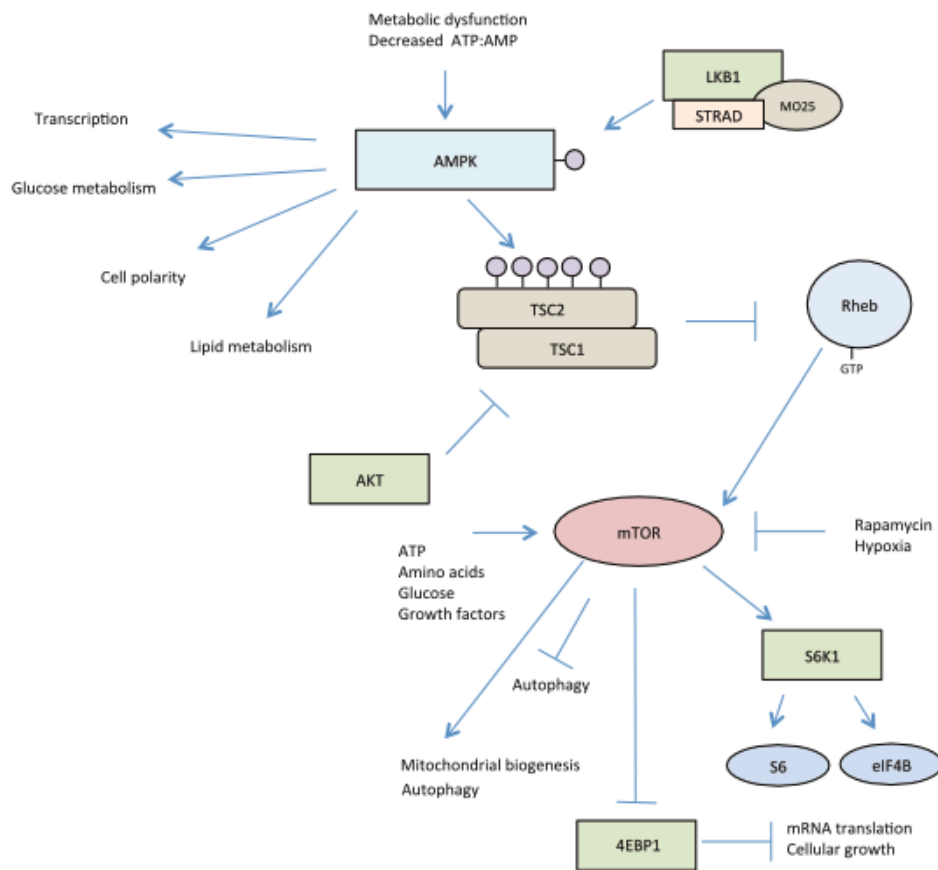


Figure 1.11. The AMPK and mTOR signalling pathways. AMPK is activated by increased cellular levels of AMP and ADP owing to a variety of physiological stresses and the activity of the upstream kinase, LKB1. Once activated AMPK directly phosphorylates a number of substrates to acutely affect cellular metabolism and growth, including inhibiting the mTOR pathway via phosphorylation of TSC1/2. Decreased activity of the mTOR pathway results in a reduction in the phosphorylation of 4E-BP1 and S6K1, reducing protein synthesis and cell proliferation.

1.10.2 Proteostasis

Proteostasis is an integrated cellular response to maintain the integrity of the proteome whilst minimising protein aggregation (Sala, Bott et al. 2017). Unfolded proteins compromise cellular function and therefore cells have evolved pathways to protect against

this potentially toxic insult. These pathways include the unfolded protein response (UPR) in the mitochondria and ER and heat shock response (HSR) in the nucleus and cytoplasm (Hetz, Chevet et al. 2015). The UPR in the ER (UPR_{ER}) is triggered by a number of factors including toxins and altered calcium homeostasis leading to the activation of inositol-requiring 1 (IRE-1), the activating transcription factor 6 (ATF6) and protein-like endoplasmic reticulum kinase (PERK). This results in the induction of binding immunoglobulin protein (BiP, Grp78), a molecular chaperone that actively refolds proteins (Bravo, Parra et al. 2013).

The HSR, a conserved cellular mechanism, maintains cytosolic proteostasis by regulating the transcription factor Heat Shock Factor 1 (HSF1) (Trinklein, Chen et al. 2004). In an unstressed cell, HSF1 associates with cytosolic chaperones HSP70 and HSP90 (Zou, Guo et al. 1998). With cellular stress, unfolded proteins increase and HSF1 dissociates allowing it to trimerize and interact with the promoters of HSR genes, particularly HSP70 (Liu and Thiele 1999). Mitochondria depend on the nucleus to reduce the effect of proteotoxic stressors such as heat shock by eliciting the mitochondrial UPR (UPR_{mt}) (Haynes and Ron 2010). This process has recently been shown to be dependent on SSBP1. Work by *Tan et al* demonstrated that heat shock triggers the nuclear translocation of SSBP1 where it forms a complex with HSF1. This complex can then recruit the chromatin remodelling factor BRG1 that subsequently upregulates transcription of mitochondrial chaperones including HSP60 and HSP10 (Tan, Fujimoto et al. 2015).

1.11 Mitochondrial disease

1.11.1 Overview of mitochondrial disease

Mitochondrial dysfunction is an established contributor to human disease, both in the form of primary mitochondrial disorders but also in a range of complex diseases including neurodegeneration and cancer (Wallace 2011, Keogh and Chinnery 2015, Zong, Rabinowitz et al. 2016). Mitochondrial disorders often manifest as multisystem disease causing significant morbidity and mortality by affecting tissues with high metabolic demand, for example, skeletal muscle, the heart and the central nervous system including the auditory system (discussed in **Section 1.13.1**).

Mitochondrial disease can be classified as (i) primary mtDNA disease caused by point mutations or large-scale mtDNA rearrangements or (ii) nuclear mitochondrial disorders

caused by mutations in nuclear genes that code for mitochondrial proteins. As of May 2017, there are 666 reported mtDNA mutations and 89 nuclear genes associated with mitochondrial disease (Mitomap 2017). This genetic heterogeneity means mitochondrial diseases can follow any pattern of inheritance including autosomal dominant (AD), autosomal recessive (AR) and X-linked for nuclear mutations and maternal inheritance for mutations of the mtDNA (Gorman, Chinnery et al. 2016).

The complexity of mitochondrial genetics together with variable genotype-phenotype relationships mean the prevalence of mitochondrial disease has historically been difficult to define. However, a number of recent genetic and epidemiologic studies have demonstrated that pathological mitochondrial mutations are common in the general population and mitochondrial diseases are among the most prevalent neuromuscular diseases affecting up to 1 in 5000 (Elliott, Samuels et al. 2008, Schaefer, McFarland et al. 2008, Gorman, Schaefer et al. 2015).

1.11.2 Mitochondrial disease genetics

1.11.2.1 Mitochondrial DNA point mutations

Pathological mtDNA point mutations can occur within protein coding, tRNA, rRNA or the NCR regions (**Figure 1.12**) (Tuppen, Blakely et al. 2010, Connor, Hoer et al. 2017). However, over half of disease related point mutations are found in the mt-tRNA genes, for example m.8344A>G tRNA^{Lys} associated with MERRF and m.3243A>G tRNA^{Leu} the major cause of mitochondrial encephalomyopathy with lactic acidosis and stroke like episodes (MELAS). Mutations localised to genes coding for all of the respiratory chain complexes have been identified to cause a range of phenotypes including MELAS, Leigh syndrome and Leber's hereditary optic neuropathy (LHON). In contradistinction, mutations affecting mitochondrial tRNAs and rRNAs affect the expression of all mitochondrial proteins through compromising mitochondrial translation (Holt, Harding et al. 1990, Kirino, Yasukawa et al. 2004).

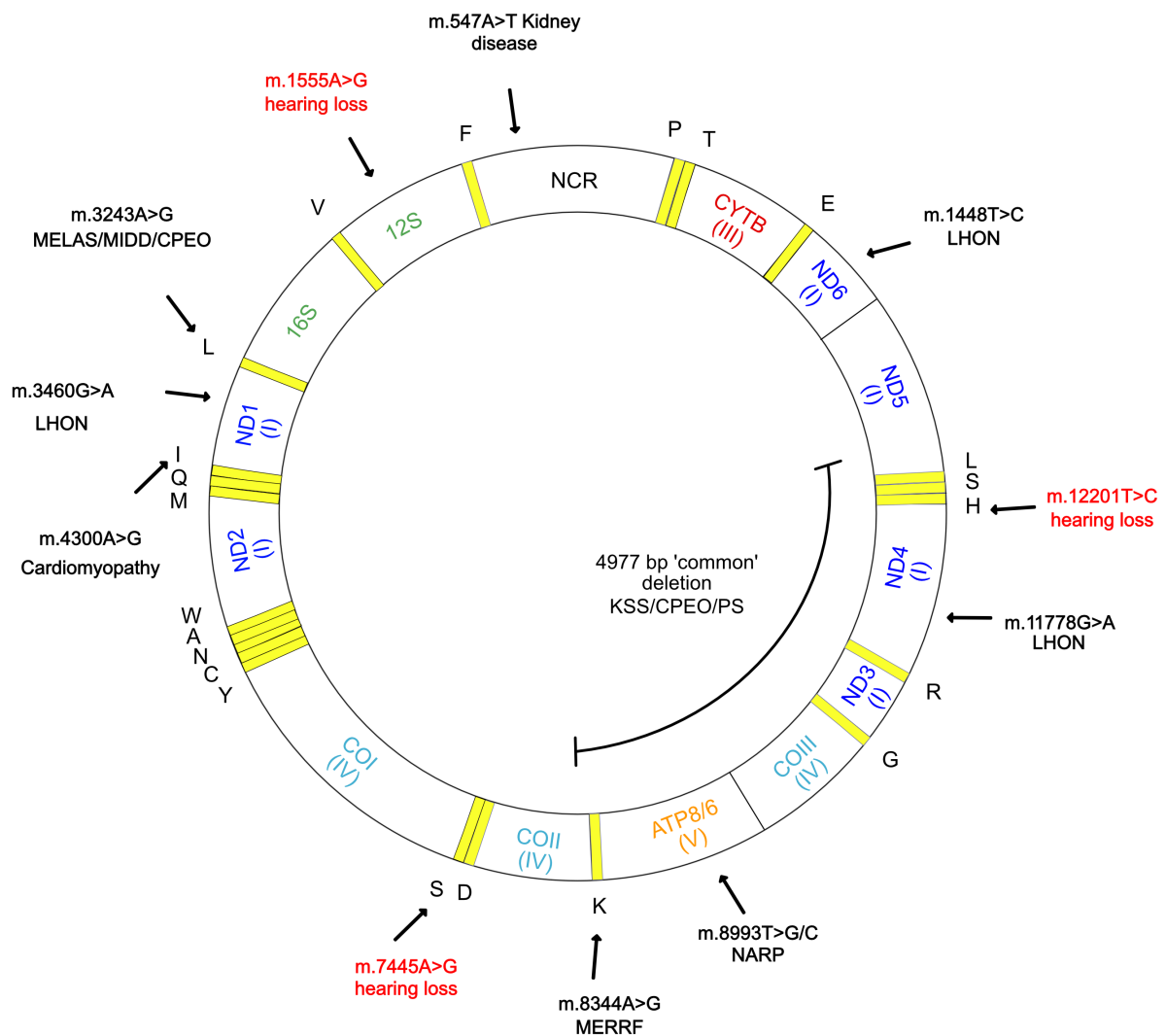


Figure 1.12. Primary mtDNA mutations linked to human disease. A selection of clinically relevant primary mtDNA mutations linked to mitochondrial disease with their associated phenotypes. LHON – Leber’s hereditary optic neuropathy, NARP – neurogenic weakness, ataxia and retinitis pigmentosa, KSS – Kearns-Sayre Syndrome, CPEO – chronic progressive external ophthalmoplegia, MERRF – myoclonic epilepsy and ragged red fibres, MELAS – mitochondrial myopathy lactic acidosis and stroke like episodes, MIDD – maternally inherited diabetes and deafness.

The majority of disease causing mutations are heteroplasmic, although homoplasmic mutations constitute an important subset of mitochondrial disease. It is likely that the severity of the biochemical insult mediated by some homoplasmic mutations mean they are a relatively rare occurrence in the population (Tiranti, Corona et al. 2000, McFarland, Clark et al. 2002, Limongelli, Schaefer et al. 2004). Interestingly, a number of identified homoplasmic

mutations share a common feature of limited tissue expression and incomplete penetrance, for example:

(i) m.4300A>G in tRNA^{ile} causing hypertrophic cardiomyopathy (Taylor, Giordano et al. 2003)

(ii) m.547A>T in the mtDNA control region causing tubulointerstitial kidney disease (Connor, Hoer et al. 2017)

(iii) m.3640G>A in *MT-ND1*, m.11778G>A in *MT-ND4*, m.14484T>C in *MT-ND6* that account for up to 95% of cases of LHON (a maternally inherited blinding disease) (Hudson, Yu-Wai-Man et al. 2008)

(iv) m.1555A>G in *MT-RNR1* (causing hearing loss) (Prezant, Agapian et al. 1993) (discussed in **Section 1.13**).

The tissue-specificity of mitochondrial disease is an important, yet currently unresolved issue. However, it is believed pathogenic mechanisms causing tissue specific effects may depend on cell specific mitochondrial dysfunction and differential cell specific metabolic requirements (Nunnari and Suomalainen 2012).

1.11.2.2 Mitochondrial deletions

Mitochondrial deletions are an important cause of mitochondrial disease and occur in three distinct clinical settings (i) mtDNA deletions can be present at birth and be distributed throughout all somatic tissues (ii) mtDNA deletions can be associated with a defect in mtDNA maintenance proteins leading to the development of deletions in post mitotic tissues such as muscle and brain (iii) mtDNA deletions can be associated with aged post mitotic tissue and neurodegenerative disease (Chen, Prosser et al. 1995, Bender, Krishnan et al. 2006).

As with point mutations, there exists a threshold effect whereby low levels of mtDNA deletions can be compensated for by the effect of wild type mtDNA but with accumulating levels of mtDNA deletion an OXPHOS defect will become apparent (Wallace and Chalkia 2013). This process of accumulating a single mtDNA species that comes to predominate within the cell is known as clonal expansion.

A number of mechanisms have been proposed to explain the clonal expansion of mtDNA mutations. Firstly, it has been postulated that mtDNA molecules with mitochondrial deletions are able to replicate faster than wild type molecules and hence accumulate in the cell due to this replicative advantage (Fukui and Moraes 2009). Secondly, it has been proposed that reduced free radical production by dysfunctional mitochondria reduces natural turnover and hence accumulation of mutant mtDNA species (Campbell, Krishnan et al. 2014). A third hypothesis proposes that relaxed replication of mtDNA and genetic drift leads to the clonal expansion of a single mutant mtDNA species (Elson, Samuels et al. 2001). Further insights into the cellular mechanisms of clonal expansion have been provided by recent work demonstrating the expansion of mtDNA deletions may involve the up-regulation of UPR_{mt} by increasing mtDNA copy number and reducing mitochondrial quality control mechanisms specifically, mitophagy (discussed in **Section 1.9**) (Gitschlag, Kirby et al. 2016).

The majority of mtDNA deletions occur in the major arc between the origins of replication, O_H and O_L and most are flanked by short direct repeats (Samuels, Schon et al. 2004). Initially, it was proposed that mtDNA deletions are a product of faulty replication through a slipped strand mechanism (Shoffner, Lott et al. 1989). This hypothesis assumes the strand displacement model of replication, as it requires large regions of single stranded DNA that are not predicted the RITOLS model. This model also predicts that mitotic cells, where replication is a frequent event should accrue deletions at a greater rate than post mitotic cells (Krishnan, Reeve et al. 2008). An alternative hypothesis proposes that mtDNA deletions are generated through exonuclease activity at double strand breaks resulting in single strands that can misanneal with homologous sequences ultimately resulting in the formation of deleted mtDNA species (Krishnan, Reeve et al. 2008). Multiple deletions arise from mutations in genes coding for mtDNA maintenance proteins whereas single deletions tend to arise as *de novo* events that undergo clonal expansion in post mitotic tissue (Tuppen, Blakely et al. 2010). A clinically important deletion, named the ‘common deletion’ removes 4977 bp of mtDNA between two 13 bp direct repeats at m.13447-13459 and m.8470-8482. This deletes a number of tRNA and protein coding genes resulting in impairment of OXPHOS and a range of phenotypes including, chronic progressive external ophthalmoplegia (CPEO), Kearns-Sayre syndrome (KSS) and Pearson syndrome (PS) (**Figure 1.12**) (Fischel-Ghodsian, Bohlman et al. 1992, Superti-Furga, Schoenle et al. 1993, Meissner, Bruse et al. 2008).

1.11.2.3 Nuclear mitochondrial diseases

Given over 99% of mitochondrial proteins (1395 of 1408 proteins in the mitochondrial proteome) are encoded in the nucleus (Integrated Mitochondrial Protein Index 2016), it is unsurprising that mutations in nuclear genes encoding mitochondrial proteins are an important cause of human disease (Gorman, Chinnery et al. 2016). Broadly, these can be divided into (i) genes encoding structures of the respiratory chain (ii) genes encoding non-structural proteins involved in a range of mitochondrial processes that include mtDNA maintenance, protein synthesis and import, complex assembly, mitochondrial dynamics and iron homeostasis (Mitomap 2017).

The commonest mutations in the nuclear encoded respiratory chain are found in genes coding for subunits of Complex I that primarily cause Leigh syndrome (Benit, Chretien et al. 2001, Benit, Slama et al. 2004). However, mutations in all nuclear encoded subunits of Complex II, III, IV and V have also been identified (Bourgeron, Rustin et al. 1995, Haut, Brivet et al. 2003, Massa, Fernandez-Vizarra et al. 2008, Mayr, Havlickova et al. 2010). Similarly, disease causing mutations have been identified in assembly factors of each respiratory chain complex (Ghezzi and Zeviani 2012).

As discussed in **Section 1.8**, maintenance of stable mtDNA that can be both expressed and replicated requires numerous nuclear encoded proteins. Mutations in these genes cause disease through both qualitative (point mutations and deletions) and quantitative (alteration in mtDNA copy number) mechanisms. The first nuclear gene underlying mitochondrial disease, *POLG*, was identified in 2001 in families with autosomal-dominant CPEO (Van Goethem, Dermaut et al. 2001). Since this time, numerous other nuclear genes underlying mitochondrial mtDNA maintenance have been identified, including *POLG2* (the poly accessory subunit) (Longley, Clark et al. 2006), the replicative helicase Twinkle (Spelbrink, Li et al. 2001) and adenine nucleotide translocator isoform 1 (*ANT1*) that transports ATP across the IMM (Kaukonen, Juselius et al. 2000). mtDNA replication is uncoupled from the replication of the nuclear genome and thus requires a steady supply of dNTPs to maintain genome integrity. Reflecting this, there are several genes regulating dNTP pools that have been shown to be causative for mitochondrial disease. These include thymidine phosphorylase (*TP*) (Nishino, Spinazzola et al. 1999) deoxyguanosine kinase (*DGUOK*) (Mandel, Szargel et al. 2001), p53 inducible ribonucleotide reductase (*RRM2B*) (Spinazzola, Viscomi et al. 2006) and mitochondrial inner membrane protein MPV17

(*MPV17*) (Bourdon, Minai et al. 2007). Mutations in these genes have all been linked to mitochondrial depletion syndrome (MDS) presenting with myopathic, hepatopathic and encephalomyopathic symptoms (Elpeleg 2003).

A number of mutations in the mitochondrial translation machinery, causing a combined OXPHOS deficiency that presents as early onset multi-system disease, have also been identified. These include the small ribosomal subunit components, mitochondrial ribosomal proteins S16 and S22 (MRPS16 and MRPS22) and translation elongation factors mtEFTu and mtEFTS (Miller, Saada et al. 2004, Saada, Shaag et al. 2007, Valente, Tiranti et al. 2007). Similarly, mutations in genes responsible for the post-transcriptional modifications of tRNA have been isolated as important causes of human disease. These include a number of mutations in the aminoacyl-tRNA synthetases that are responsible for the attachment of tRNAs to the correct amino acid (Yao and Fox 2013).

As discussed in **Section 1.9** the regulation of mitochondrial dynamics is integral to optimal cellular function and it hence follows mutations in proteins controlling mitochondrial dynamics are responsible for a subset of mitochondrial disease. Specifically, mutations in *MFN2* are associated with Charcot-Marie-Tooth disease type 2A while *OPA1* mutations are causative for Dominant Optic Atrophy (DOA) (Burte, Carelli et al. 2015).

1.11.3 Diagnosis of mitochondrial disease

The diagnosis of mitochondrial disease is primarily made by a combination of (i) biochemical assessments including the measurement of individual respiratory chain complex activities and analysis of mitochondrial biomarkers in urine, blood, or cerebral spinal fluid and (ii) molecular genetic tests including mtDNA sequencing, whole genome or whole exome sequencing (WGS and WES respectively) (in cases of suspected nuclear mitochondrial disease) and the assessment of mtDNA rearrangements using long-range polymerase chain reaction (PCR), Southern blotting or quantitative real time PCR (qPCR) (Parikh, Goldstein et al. 2015).

Additionally, histochemical analysis of skeletal muscle is a reliable method for the detection of OXPHOS dysfunction. Common diagnostic practice includes staining with haematoxylin & eosin (H&E) to assess overall muscle histology and sequential staining to determine the activity of SDH (Complex II) and COX (Complex IV). SDH is entirely nuclear encoded whereas COX contains both nuclear and mtDNA encoded subunits,

therefore in the case of mtDNA point mutations or deletions COX activity may decrease however SDH will remain unaffected. Following sequential COX/SDH staining, COX-negative fibres are revealed as blue whereas COX positive fibres remain brown. In patients with disorders of mitochondrial maintenance, secondary mtDNA depletion or deletions can result in a mosaic pattern of enzyme deficiency, displaying both COX-positive and COX-negative fibres in the same muscle biopsy (Murphy, Ratnaike et al. 2012)

1.12 Overview of the physiology of hearing

Hearing is the ability to perceive sound by the detection of vibrations. In humans, the hearing mechanism can be subdivided into three components: the outer ear, the middle ear and the inner ear (**Figure 1.13**). The outer ear serves to focus sound energy to the tympanic membrane whose vibrations transfer energy to the middle ear ossicles (malleus, incus and stapes). These function to overcome the impedance mismatch between the air/fluid interface of the middle and inner ear. The stapes then transmits sound energy via the oval window to the inner ear. The inner ear houses the spiral shaped cochlea, the organ of hearing, as well as the vestibular system, responsible for balance. The cochlea is divided into the scala vestibuli, scala tympani and scala media, containing the Organ of Corti that is responsible for the mechanotransduction of sound by its constituent inner and outer hair cells (IHC and OHC respectively) (Purves 2008). The OHC and IHC are the auditory sensory receptors serving distinct roles within the auditory system as a consequence of spatial segregation and morphological variation (Dallos, Billone et al. 1972).

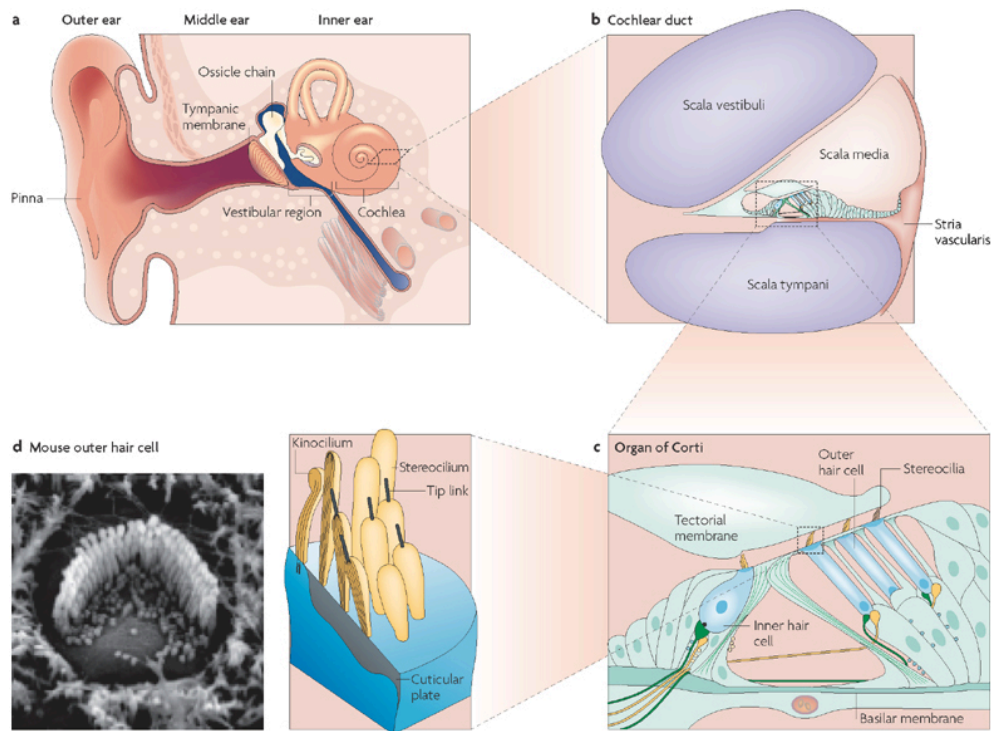


Figure 1.13 The human auditory system. (A) Sound is collected by the pinna and transmitted to the middle ear ossicles via vibration of the tympanic membrane (B) The cochlear duct is divided into the scala vestibuli, scala media and scala tympani. (C) The Organ of Corti containing the inner and outer hair cells and supporting cells. (D) The hair cells project stereocilia attached by tip links that mechanically gate mechanotransducer (MET) channels responsible for the generation of auditory nerve activity. Reproduced from Brown, Hardisty-Hughes et al. 2008.

OHCs contain contractile proteins, such as prestin, that can convert changes in membrane potential into rapid shifts in cell length through the process of electromotility (Zheng, Shen et al. 2000). This phenomenon drives the cochlear amplifier, the process whereby the sensitivity and frequency selectivity of hearing is enhanced (Ashmore, Avan et al. 2010). On the other hand, IHC are the primary transducers of the inner ear that convert the vibration of the basilar membrane into neural signals encoded in the auditory nerve. This occurs via the deflection of stereocilia that project from the surface of the hair cells causing the opening and closing of mechanotransducer (MET) channels (Arnadottir and Chalfie 2010). The opening of the MET channels causes the influx of potassium and calcium ions and depolarisation of the hair cell causing release of neurotransmitters, primarily L-glutamate, which is converted into specific neural activity of the auditory nerve (Nordang, Cestreich et al. 2000).

1.13 Pathophysiology of hearing loss

Hearing loss is a dynamic, multifactorial process affecting 11 million people in the United Kingdom (UK) with varying degrees of disability (Action on Hearing Loss 2017). Hearing loss can result from any process that interferes with the faithful communication of correctly encoded neural signals from cochlea to the auditory cortex. Broadly, this can be classified into sensorineural loss resulting from dysfunction of the cochlea hair cells and/or auditory nerves or cortex and conductive loss caused by disease of the outer or middle ear which prevents sound transmission to the cochlea. Epidemiological studies have indicated that approximately 1 in 500 at birth and more than 70% of those over the age of 70 are affected by some degree of hearing loss. In those affected at birth it is estimated that over 50% have a genetic aetiology with mutations found in a diverse range of genes associated with the development, structure and function of the auditory system inherited in an AR, AD, X-linked or mitochondrial mode of inheritance (Dror and Avraham 2009).

1.13.1 The role of mitochondria in hearing loss

Mitochondrial mutations contribute significantly to cases of genetic hearing loss and are estimated to be causative in approximately 5% of non-syndromic post lingual hearing loss as well as 1% of pre-lingual cases (Jacobs, Hutchin et al. 2005, Morton and Nance 2006). Additionally, mitochondrial mutations may also contribute to age associated hearing loss (Bai, Seidman et al. 1997).

Anecdotally, hearing loss is a well-recognised feature of mitochondrial disease although ascertaining its prevalence in patients with confirmed mitochondrial disease is complicated by both clinical and genetic heterogeneity. Moreover, the true burden of disease may be further disguised by under diagnosis, particularly in patients with complex neuromuscular phenotypes. In one study of 23 patients with mitochondrial disease, including 10 with the m.3243 A>G variant, 74% were found to have hearing loss (Chinnery, Elliott et al. 2000). Additional studies investigating patients with a range of mitochondrial diseases have further confirmed the high rate of hearing impairment in patients with mitochondrial disease (Sue, Lipsett et al. 1998, Kuzmenko, Atkinson et al. 2014).

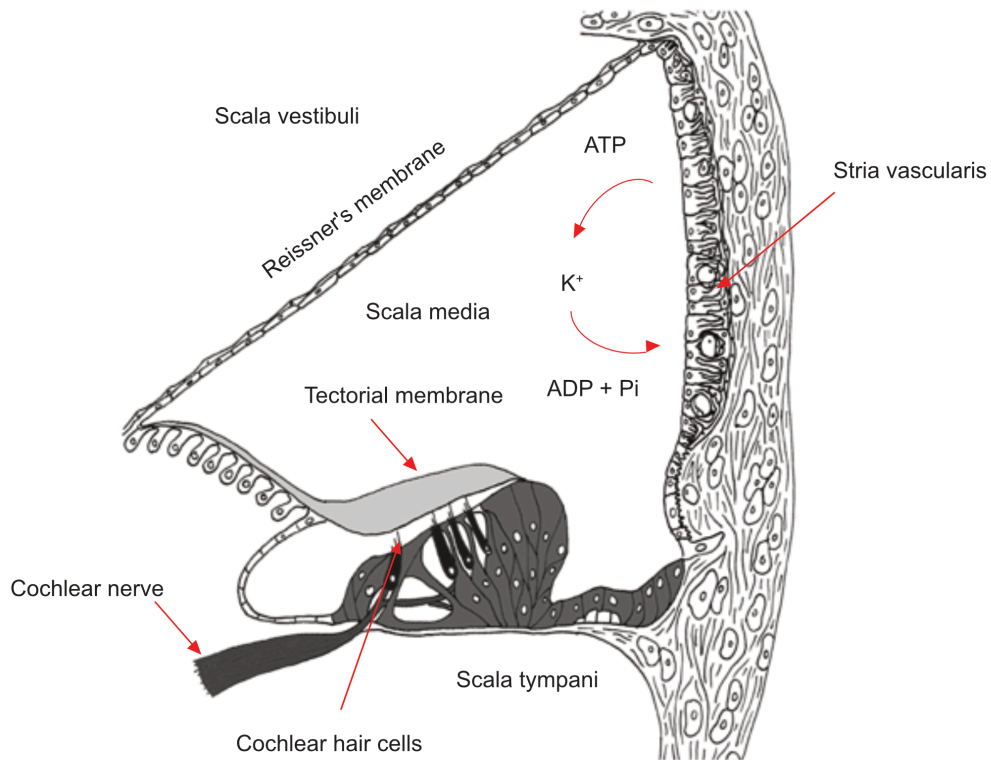


Figure 1.14. A cross-section through the human cochlea. The stria vascularis is responsible for the production of the potassium rich endolymph in the scala media. Reduction in ATP generation resulting from mitochondrial dysfunction causes both a loss of the endocochlear potential, compromising hair cell function and a degradation of auditory neural signalling. Together, these are thought to account for the hearing loss associated with mitochondrial disease. Figure adapted from Rahman, Ecob et al. 2012.

Mitochondrial dysfunction can be causative for hearing loss both in isolation (non-syndromic) and as a feature of systemic mitochondrial disease (syndromic). A number of studies have implicated the cochlea as the primary origin of disease with a corresponding loss of both outer and inner hair cells (Chinnery, Elliott et al. 2000, Sue, Lipsett et al. 1998). However, auditory neuropathy (i.e. dysfunction of the auditory nerve with preserved cochlear function) has also been recognised as an important factor in a subset of mitochondrial diseases (Ceranic and Luxon 2004, Santarelli, Rossi et al. 2015). It has been shown that the cells of the auditory sensory axis, including the cochlea hair cells, stria vascularis (primarily responsible for maintaining the endocochlear potential) and auditory neurones are highly metabolically active and therefore contain an abundance of mitochondria (Karnes, Scaletty et al. 2010). Therefore, the sensitivity of the auditory pathway to mitochondrial dysfunction may result from inadequate mitochondrial oxidative phosphorylation in these metabolically active tissues however detailed histological analyses

of cochlear tissue from patients with mitochondrial disease have not yet been performed (Xing, Chen et al. 2007) (**Figure 1.14**). The initiation of apoptosis by ROS activated caspases may partially explain the link between mitochondrial mis-translation and subsequent cochlea hair cell death (Priuska and Schacht 1997). Although to date, the underlying molecular mechanisms, including those governing tissue specificity, remain unresolved.

1.13.2 Clinical presentation of mitochondrial hearing loss

The hearing loss of mitochondrial disease is sensorineural, symmetrical and primarily affects the higher frequencies although progressive disease can lead to pan-frequency hearing loss (Kokotas, Petersen et al. 2007). The incidence of conductive hearing loss, where sound conduction to the cochlea is reduced by disease of the middle or outer ear, for example in otitis media with effusion, has been shown to be comparable to the general population (Edmonds, Kirse et al. 2002).

Hearing loss onset tends to be in early life and be gradually progressive, although sudden hearing loss has been described in stroke like episodes in patients carrying the m.3243 A>G variant (Chen, Tsai et al. 2007). Predominantly, hearing loss occurs in later childhood or adulthood after the acquisition of speech, however, broad phenotypic variation means there is often a range of hearing loss onset and severity even in family members carrying the same genetic variants. It has also been shown that hearing thresholds decline at a faster rate in m.3243A>G carriers compared to the general population. Therefore, patients with mitochondrial hearing loss should receive regular audiology assessment (Uimonen, Moilanen et al. 2001).

1.13.3 Clinical diagnosis of mitochondrial hearing loss

A mitochondrial cause for hearing loss may be suspected in cases that appear to show maternal transmission or where hearing loss is a known association of systemic mitochondrial disease. There are two main groups of patients presenting with potential mitochondrial associated deafness: (i) children with hearing loss of unknown origin (who may or may not have passed Newborn Hearing Screening due to the variability in onset of hearing loss) (ii) adults with progressive hearing loss with or without a known background of mitochondrial disease.

Although management of the hearing loss is the primary focus of clinicians, fully understanding the aetiology is important to determine (i) the risk of recurrence in future offspring, (ii) the risk of progression and (iii) to exclude syndromic forms of deafness where associated symptoms may require further management.

In both children and adults a detailed history should be undertaken to determine the onset, progression and impact of symptoms on quality of life. A specific enquiry should be made about family history, ethnicity and consanguinity. A general medical history should also be obtained (e.g. visual symptoms, diabetes, renal and cardiovascular disease that may indicate a syndromic cause) and exposure to aminoglycosides should be noted. In paediatric cases it is important to cover the pregnancy and perinatal period and to exclude other important causes of hearing loss by enquiring specifically about toxoplasmosis, rubella, cytomegalovirus (CMV), herpes and syphilis infections (Graham 2008). General developmental progression should be charted against milestones as delays may indicate global or specific language or motor delays indicative of syndromic mitochondrial disease.

In children, clinical examination should include inspection of the craniofacial region including physical measurements, to exclude a number of non-mitochondrial hearing loss syndromes that are associated with defects in craniofacial development. A computed tomography (CT) scan of the petrous temporal bones may be performed to rule out congenital abnormalities of the cochlea, particularly in cases where cochlear implantation is being considered (Graham 2008).

Examination of the peripheral (outer/middle ear and cochlear) and central (auditory nerve and auditory cortex) auditory sensory axis is undertaken using both age-appropriate behavioural tests and physiologic tests that can be undertaken at any age (**Figure 1.15**). Combining information from these tests can both quantify the degree of hearing loss and differentiate between sensory and neural components.

1.13.3.1 Behavioural audiology tests

Pure tone audiometry (PTA), the cornerstone of diagnostic audiology, is a subjective behavioural test of a patient's ability to detect a pure tone signal presented over a range of frequencies (typically 0.25 KHz-8 KHz). This allows the examination of the whole auditory axis from cochlea to brain. Hearing thresholds are presented as an audiogram, a graphical representation of threshold intensity as a function of tone frequency (**Figure 1.15**

ii (b)). PTA tests both air and bone conduction enabling the differentiation between sensorineural and conductive hearing losses (bone conduction bypasses the outer and middle ear and hence mitigates the effect of conductive losses). Typically mitochondrial hearing loss produces isolated high frequency loss (down sloping audiogram) or in more severe cases a pan-frequency loss with no difference between the air and bone thresholds consistent with a sensorineural hearing loss (**Figure 1.15 ii (b)**).

1.13.3.2 Physiological audiology tests

Otoacoustic emissions (OAEs) are cochlea generated sound waves resulting from the mechanical frequency selectivity of the outer hair cells (Kemp 1978). These can be either spontaneous or evoked (by a signal frequency applied by an earphone) and are measured using a flexible indwelling ear probe (**Figure 1.15 i**). In clinical practice, evoked emissions (either transient, TEOAEs, or distortion product, DPOAEs) are routinely used to determine cochlear auditory function. The presence of OAEs confirms that the cochlear sensitivity in the relevant region is 20-40 dB HL or better (normal hearing thresholds are classified as between -10 and +20 dB HL) (Manley 2010).

Auditory brainstem response (ABR) is an evoked electrophysiological response generated by an auditory stimulus, usually a tone pip or broadband click, which can be used to measure the resulting neural activity of the cochlea-brain axis (Watson, McClelland et al. 1996). The amplitude of the response is measured through surface electrodes placed at the vertex and ear lobe. Responses are then plotted against time, giving five morphologically characteristic waveforms (I-V) representing sequential stimulation of the components of the central auditory pathway (**Figure 1.15 ii (a)**). The resulting waveforms can be examined for amplitude, inter-peak latency, absolute latency and inter-aural latency difference. The diagnosis of an auditory neuropathy depends on increased inter-peak latencies in the presence of OAEs with increased thresholds on pure tone audiometry (Berlin, Hood et al. 2003).

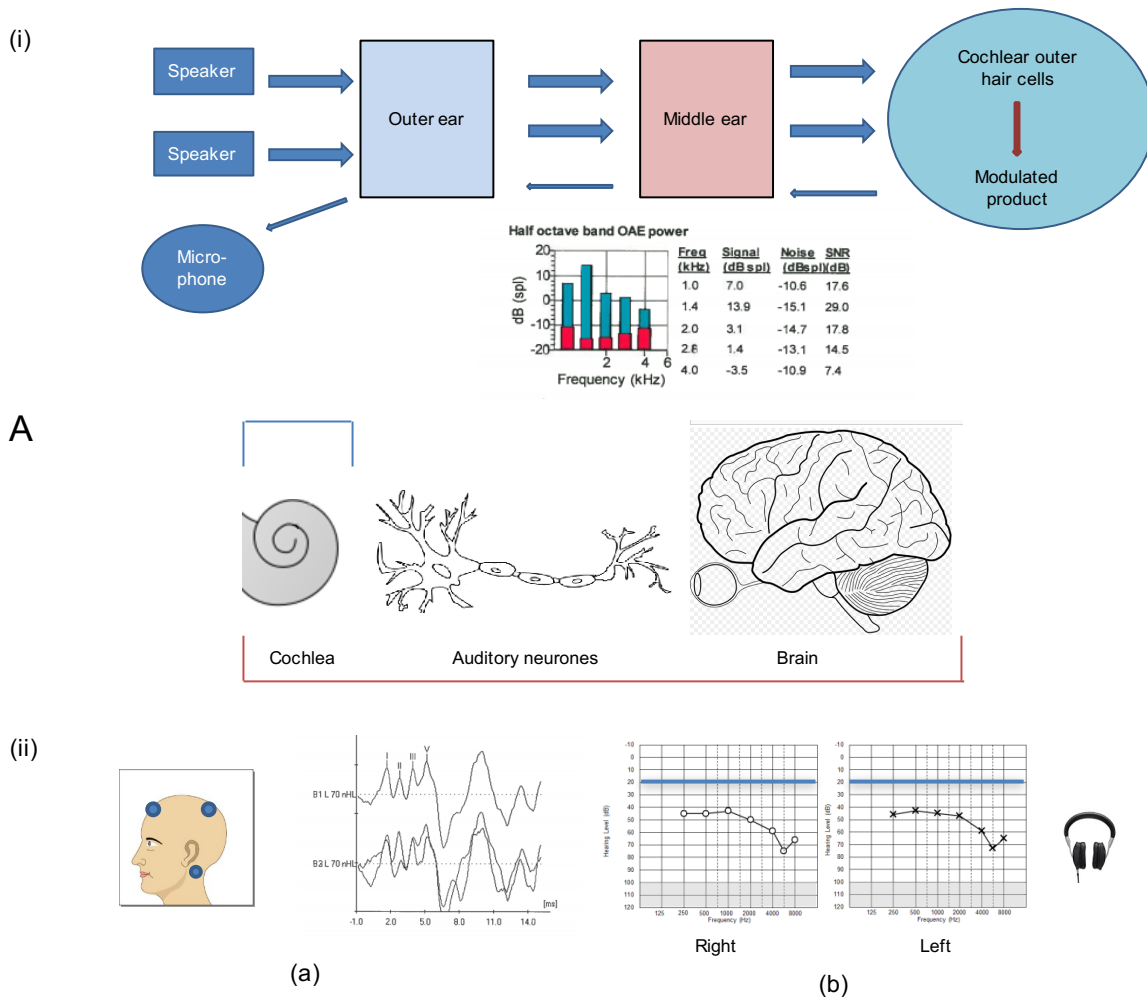


Figure 1.15. Audiological assessment for diagnosis of hearing loss. (A) Schematic representation of the auditory conduction pathway from the cochlea via neuronal auditory brain structures to the auditory cortex. (i) OAEs: A speaker generated tone is delivered to the ear by an indwelling ear probe which also measures the modulated product (in the case of DPOAEs) generated by the stimulated cochlear outer hair cells. Cochlea function is specifically measured (represented by blue diagrammatic brackets in Panel A). (ii) (a) Auditory brainstem response (ABR): position of skull electrodes and representation of electrophysiological response of auditory pathway (waves I-V marked). (ii) (b) PTA: Audiograms of the right and left ears showing pan-frequency hearing loss with raised thresholds at high frequencies (lower limit of normal hearing marked with horizontal blue line). Subject responds to different frequency tones presented by headphones. (ii) Both ABR and PTA measure response of the entire auditory pathway (represented by red diagrammatic brackets in Panel A).

1.13.4 Genetic aetiology of mitochondrial associated hearing loss

Mitochondrial associated hearing loss results from mutation in nuclear genes encoding mitochondrial proteins or from mutation of mtDNA (Kokotas, Petersen et al. 2007).

Subsequently, mitochondrial hearing loss can be inherited following either a Mendelian or maternal inheritance pattern.

1.13.4.1 *mtDNA mutations associated with non-syndromic hearing loss*

Mutations causing non-syndromic hearing loss are found in genes encoding components of the mitochondrial translation machinery including *MT-RNR1*, encoding the mitochondrial 12S rRNA and the *MT-TSI* gene encoding the tRNA for Ser^(UCN). Variants in the mitochondrial *MT-RNR1* gene have been linked to both maternally transmitted non-syndromic and aminoglycoside associated deafness (Estivill, Govea et al. 1998). These variants include m.1555A>G (discussed in **Section 1.14**), m.1095T>C, m.1494C>T and variants at position 961 (Guan 2011). Several mutations in the *MT-TSI* gene encoding tRNA Ser^(UCN), including m.7445A>G, 7472insC, m.7510T>C and m.7445G>A have also been associated with non-syndromic mitochondrial hearing loss. These variants are proposed to lead to a reduction in tRNA processing and a decline in cellular oxidative phosphorylation (Bykhovskaya, Shohat et al. 1998). Variants in *MT-TSI* have also been associated with syndromic cases, for example the m.7445A>G variant causes hearing loss combined with palmoplantar keratoderma whilst m.7512A>G has also been associated with forms of MERRF (Nakamura, Nakano et al. 1995, Seviour, Hatamochi et al. 1998).

1.13.4.2 *mtDNA mutations associated with syndromic hearing loss*

The commonest forms of mitochondrial syndromic hearing loss are associated with the complex neuromuscular syndromes KSS, MELAS and MERRF that are caused by large mtDNA rearrangements and variants in mitochondrial tRNA genes including *MT-TL1* (tRNA^{Leu(UUR)}), *MT-TK* (tRNA^{Lys}), and *MT-TE* (tRNA^{Glu}) respectively. The common MELAS variant, m.3243A>G, is also associated with maternally inherited diabetes and deafness (MIDD) consisting of a triad of maternally inherited diabetes with a normal body mass index, hearing impairment and retinal dystrophy. MIDD can also be associated with mutations in *MT-TK* and *MT-TE* genes (Naing, Kenchaiah et al. 2014).

1.13.4.3 *Nuclear genes associated with mitochondrial hearing loss*

Given that the majority of mitochondrial proteins are encoded by the nuclear genome it follows that nuclear encoded mitochondrial proteins may act to modify the phenotype of primary mtDNA mutations (discussed in **Section 1.11.2**) or cause hearing loss directly.

Most commonly, nuclear gene mutations cause hearing loss as a feature of syndromic mitochondrial disease by dysregulating mtDNA replication or repair (mtDNA maintenance).

Mutations in *OPA1* (discussed in **Section 1.9.1** and **1.11.2.3**) are associated with DOA, a selective degeneration of retinal ganglion cells, however a subset of missense mutations cause a DOA-plus phenotype presenting with optic atrophy in conjunction with myopathic features, progressive external ophthalmoplegia (PEO) and hearing impairment (Yu-Wai-Man, Griffiths et al. 2010). Interestingly, it has been shown that different mutations within the gene result in hearing loss through divergent mechanisms with haploinsufficiency mutations primarily causing a cochlear loss whereas missense mutations cause primarily an auditory neuropathy (Santarelli, Rossi et al. 2015). Mutations in *POLG*, that encodes the unique replicative mtDNA polymerase (discussed in **Section 1.8.2.1** and **Section 1.11.2.2**) cause hearing loss in the context of complex neurological phenotypes including PEO, Alper's disease and Sensory Ataxic Neuropathy, Dysarthria and Ophthalmoparesis (SANDO) (Chan and Copeland 2009). Other mtDNA maintenance genes associated with mitochondrial deafness include *MPV17*, *SUCLA2* (succinate-CoA ligase), *RRM2B* and *TWNK* (Luo, Hou et al. 2013). Similarly, mutations in genes involved in apoptosis SMAC (second mitochondrial activator of caspases) and *DIABLO* (Diablo IAP-Binding mitochondrial protein) and OXPHOS complex assembly, *BCSIL* (BCS1 *S.Cerevisiae* homolog like) and COX10 (Cytochrome *c* oxidase assembly factor 10) have also been implicated (Antonicka, Leary et al. 2003, Fernandez-Vizarra, Bugiani et al. 2007, Cheng, Zhu et al. 2011).

1.13.5 The role of mitochondrial dysfunction in acquired hearing loss

Mitochondria are an important source of cellular ROS generated as a by-product of OXPHOS (discussed in **Section 1.5.1**). Noise exposure has been demonstrated to drive increased mitochondrial ROS production that may exceed the buffering capacity of cellular antioxidants leading to oxidative stress (Henderson, Bielefeld et al. 2006). Subsequent cochlea hair cell death is then driven in part by mitochondrial mediated activation of cellular apoptosis (Le Prell, Yamashita et al. 2007). Interestingly, there is some evidence that treatment with antioxidants is able to attenuate hair cell death and subsequent threshold shifts (Wong and Ryan 2015).

In addition, given the vulnerability of the mitochondrial genome to mutation, genetic changes are known to accumulate throughout life and hence mitochondria have been suggested to play a fundamental role in human ageing (Payne and Chinnery 2015). However, dissecting which of these genetic changes is specific to age induced hearing loss has proved challenging. The common 4977bp deletion (discussed in **Section 1.11.2.3**) has been seen to be over represented in temporal bone material from patients with age onset hearing loss as compared to aged-matched controls (Bai, Seidman et al. 1997). This work has paralleled studies in several mouse models that suggest accumulation of mtDNA mutations and increased oxidative stress in the cochlea contribute to age related hearing loss (ARHL) (Crawley and Keithley 2011). However, a recent larger analysis of the mitochondrial genome in 400 individuals (200 with normal hearing and 200 with poor hearing) found no association between mtDNA mutation load and ARHL (Bonneux, Fransen et al. 2011).

1.13.6 Clinical management of mitochondrial hearing loss

There is currently no specific medical treatment for sensorineural hearing loss. Amplification by hearing aids used with or without hearing assistive technology systems (e.g. infrared/FM systems, induction loop systems) are the mainstay of treatment (Action on Hearing Loss 2017). In cases of severe hearing loss, cochlear implantation may be indicated and has been used effectively in patients carrying the m.3243A>G variant and individuals with DOA, KSS and mitochondrial neurogastrointestinal encephalopathy (MNGIE) syndrome (Yamaguchi, Himi et al. 1997, Li, Han et al. 2011, Scarpelli, Zappini et al. 2012, Santarelli, Rossi et al. 2015).

1.14 The m.1555A>G variant

The homoplasmic m.1555A>G mutation in the mitochondrial *MT-RNR1* gene that codes for the 12S rRNA component of the mitoribosome has been linked to both maternally transmitted non-syndromic and aminoglycoside associated deafness (Prezant, Agapian et al. 1993, Guan 2011). The variant was first identified in three Chinese families with maternally inherited aminoglycoside associated hearing loss and a large Arab-Israeli kindred with maternally inherited non-syndromic deafness (Prezant, Agapian et al. 1993). Subsequently, m.1555A>G has been found in populations throughout the world including Asia, Africa and Europe (Matthijs, Claes et al. 1996, Pandya, Xia et al. 1997, Jacobs, Hutchin et al. 2005).

1.14.1 Aminoglycoside antibiotics

Aminoglycoside antibiotics such as gentamicin, streptomycin and kanamycin are bactericidal antibiotics used in the treatment of a broad range of diseases including genito-urinary and respiratory tract infections (Avent, Rogers et al. 2011). Although in recent decades the use of aminoglycosides in the developed world has fallen, in part due to the development of other broad spectrum antibiotics such as cephalosporins and fluoroquinolones, there has been renewed clinical interest in these drugs due to the emergence of multi-drug resistant bacteria (Xie, Talaska et al. 2011). Administration of aminoglycosides must be considered with regard to the prominent associated adverse effects, notably nephrotoxicity and ototoxicity. Importantly, it has been demonstrated that up to 10% of patients receiving aminoglycosides develop a clinically significant hearing loss that is likely mediated via the generation of intra-hair cell ROS (Ariano, Zelenitsky et al. 2008, Huth, Ricci et al. 2011). Aminoglycosides mediate their therapeutic action via interaction of their 2-deoxystreptamine moiety with the A-site of the 16S rRNA (at m.1409-1491) (Purohit and Stern 1994) in the 30S subunit of the mitoribosome (Purohit and Stern 1994, Recht, Fourmy et al. 1996). Once bound, they affect all 3 stages of protein synthesis; impairing initiation, elongation and translational proofreading. This leads to mRNA misreading and premature termination of translation (Lambert 2012). The subsequent disruption to protein synthesis causes global cellular dysfunction and ultimately results in bacterial cell death (Mingeot-Leclercq, Glupczynski et al. 1999).

1.14.2 Epidemiology of the m.1555A>G variant

Understanding the epidemiology of m.1555A>G requires an appreciation that the frequency of the variant differs depending on the population sampled i.e. depending on whether the individuals under test have hearing loss or a prior exposure to aminoglycosides with subsequent hearing loss. Genotyping of individuals from the general population, unbiased by hearing status, have estimated the frequency of m.1555A>G at between 0.21 and 0.26% (Bitner-Glindzicz, Pembrey et al. 2009, Vandebona, Mitchell et al. 2009). Whereas, with regard to individuals with confirmed aminoglycoside ototoxicity, the incidence of the mutation ranged between 5% and 33% in Chinese and Spanish cohorts, possibly reflecting the increased use of aminoglycosides in these populations (Estivill, Govea et al. 1998, Lu, Li et al. 2010). Alternatively, in cohorts of individuals

with non-syndromic deafness the incidence has been reported to range from 0.6% to 2.9% (Li, Li et al. 2005, Bae, Lee et al. 2008, Kullar, Alston et al. 2016). In one study the penetrance of the hearing loss associated with m.1555A>G was shown to be 50% by 30 years and 88% by 65 years (Estivill, Govea et al. 1998). Interestingly, in this study only 17.7% of the patients with hearing loss and m.1555A>G had received aminoglycosides. On the other hand, in ten families from Taiwan the penetrance of hearing loss ranged from 13 to 78% (Wu, Chiu et al. 2007), while a lower penetrance between 4 and 18% has been reported in Chinese families (Dai, Yuan et al. 2006). Additionally, recent work in a British cohort has demonstrated that hearing in m.1555A>G carriers is not significantly different from the general population and preserved to at least the age of 44-45 years (Rahman, Ecob et al. 2012). Taken together, this variability in the expression of the phenotype strongly suggests that environmental or genetic factors are important determinants of hearing loss associated with m.1555A>G.

1.14.3 Clinical features of the m.1555A>G mutation

The hearing loss associated with m.1555A>G is bilateral, sensorineural loss at high frequencies without vestibular dysfunction (Noguchi, Yashima et al. 2004, Lu, Li et al. 2010). Predominantly, hearing loss is the sole presenting phenotype. However, there are documented incidences of associated symptoms including pigmentary abnormalities and cardiomyopathy (Santorelli, Tanji et al. 1999, Nye, Hayes et al. 2000). It is possible, however, the broader phenotypes demonstrated in these studies could be accounted for by nuclear alleles co-segregating within the families. Hearing loss with aminoglycoside administration is believed to be 100% penetrant in carriers with more profound loss occurring in patients receiving aminoglycosides under 10 years of age, however there have been accounts of carriers receiving multiple dose of aminoglycosides with normal hearing (Al-Malky, Suri et al. 2014).

The penetrance and age of onset of hearing loss in carriers of m.1555A>G not exposed to aminoglycosides is variable with reports of a range of hearing levels from profound loss to normal hearing. For example, in a Spanish cohort of m.1555A>G carriers naïve to aminoglycosides, hearing loss was diagnosed with a median age of 20 years (Estivill, Govea et al. 1998). Whereas, in a large Arab-Israeli family the majority of patients developed profound hearing loss in infancy (Prezant, Agapian et al. 1993).

1.14.4 Pathophysiology of the m.1555A>G mutation

The pathological mechanism of m.1555A>G is incompletely understood but two main hypotheses have been proposed: mRNA misreading and 12S hypermethylation (Hutchin, Haworth et al. 1993, Seidel-Rogol, McCulloch et al. 2003, Hobbie, Bruell et al. 2008). A long-standing and widely accepted hypothesis centres on the effect of mRNA misreading reducing mitochondrial translation below a minimum threshold compatible with normal cochlear physiology (Hobbie, Bruell et al. 2008). Further work has demonstrated the m.1555A>G leads to a 7-fold increase in mRNA misreading and that this deficit can be further exacerbated by aminoglycosides (Hobbie, Akshay et al. 2008). However, in 2012, *Raimundo et al* provided an intriguing insight into the mechanistic link between m.1555A>G and hearing loss (Raimundo, Song et al. 2012). This study built on the observation that m.1555A>G transmitochondrial cybrids (cells constructed to carry mtDNA variants on a constant nuclear background) are hypermethylated at the 12S rRNA stem loop by TFB1M at m.1583 and m.1584A (m⁶2A) (**Figure 1.16**) (Cotney, McKay et al. 2009). The authors report that this modification disrupts efficient mitochondrial respiration; leading to the generation of excess ROS that then activate AMPK triggering E2F1 mediated cellular apoptosis. In this and a further study, a transgenic mouse strain overexpressing TFB1M on a C57BL/6J background demonstrated 12S rRNA hypermethylation in multiple tissues causing a progressive hearing loss mediated by E2F1 induced apoptosis of stria vascularis and spiral ganglion neurones of the inner ear (McKay, Yan et al. 2015).

The current prevailing view holds that mRNA misreading is the most physiologically relevant model accounting for m.1555A>G associated hearing loss, but the role of AMPK in the pathophysiology of m.1555A>G clearly merits further study.

The mechanism of m.1555A>G mediated aminoglycoside ototoxicity depends on the novel G-C base pair created between m.1555G and m.1494C, that decreases the flexibility of the ribosomal decoding centre and causes the rRNA to parallel the bacterial 16S rRNA. (**Figure 1.16**) (Bottger 2010, Amunts, Brown et al. 2015). Ultimately, this leads to increased binding of aminoglycosides to the mitoribosome with subsequent effect on mitochondrial translation (Qian and Guan 2009). It has been proposed that the reduction in protein synthesis in the stria vascularis of the cochlea leads to an energetic crisis resulting in loss of the endocochlear potential (**Figure 1.14**) (Rahman, Ecob et al. 2012). Positively charged aminoglycosides then become concentrated in the endolymph, where they can

dysfunction primarily caused by m.1555A>G and account for some of the phenotypic variation (Wang, Lu et al. 2008). However, other studies have shown m.1555A>G arises on a number of haplotype backgrounds, caused by independent mutations, and the severity of disease varies irrespective of the haplotype background (Torrioni, Cruciani et al. 1999, Otaegui, Irizar et al. 2008, Rahman, Ecob et al. 2012).

1.14.6 Role of heteroplasmy in m.1555A>G associated hearing loss

The m.1555A>G variant is classically described as homoplasmic, however some studies report families with varying levels of heteroplasmy. These studies have proposed that heteroplasmy levels may influence disease manifestation and have proposed a threshold mechanism where increasing levels of heteroplasmy worsen the phenotype (del Castillo, Rodriguez-Ballesteros et al. 2003, Zhu, Huang et al. 2014). These studies present a range of heteroplasmy levels (3.75% – 96.6%) with a threshold for hearing loss of 50%. However, within these and other studies there are patients homoplasmic for the mutation without hearing loss and it is therefore unlikely that heteroplasmy can account for all of the phenotypic variation (Otaegui, Irizar et al. 2008).

1.14.7 Evidence for nuclear modifiers of the m.1555A>G phenotype

Epistasis, whereby the phenotypic effect of an allele is dependent on the allelic status of another gene, is emerging as an important contributor to human health and disease (Phillips 2008, Moore and Williams 2009). In considering the role of nuclear modifiers of m.1555A>G it is useful to review the evidence for their contribution in LHON, another tissue specific mitochondrial disease caused by a homoplasmic mtDNA variant. As described in **Section 1.11.2.1**, LHON is a maternally inherited cause of vision loss where the mtDNA variants m.11778G>A, m.3460G>A and m.14484T>C are necessary but not sufficient to develop optic neuropathy. The majority of carriers remain asymptomatic, with males more likely than females to convert to the disease state (Carelli, d'Adamo et al. 2016). This male predominance and incomplete penetrance suggest the role of additional environmental or genetic factors. Tobacco smoking and alcohol intake are established triggers of disease (Tsao, Aitken et al. 1999, Newman 2009), however the role of genetic factors remains an area of intense investigation. mtDNA haplogroups, specifically haplogroup J, have been shown to increase the risk of visual failure in carriers of the mtDNA variants (Hudson, Carelli et al. 2007). There has also been a substantial amount of

effort in recent years to isolate nuclear susceptibility alleles for LHON. However, despite strong statistical evidence of linkage of a number of genetic regions with the disease there has been limited success in identifying causative mutations (Hudson, Keers et al. 2005, Shankar, Fingert et al. 2008, Phasukkijwatana, Kunhapan et al. 2010, Jiang, Jin et al. 2016).

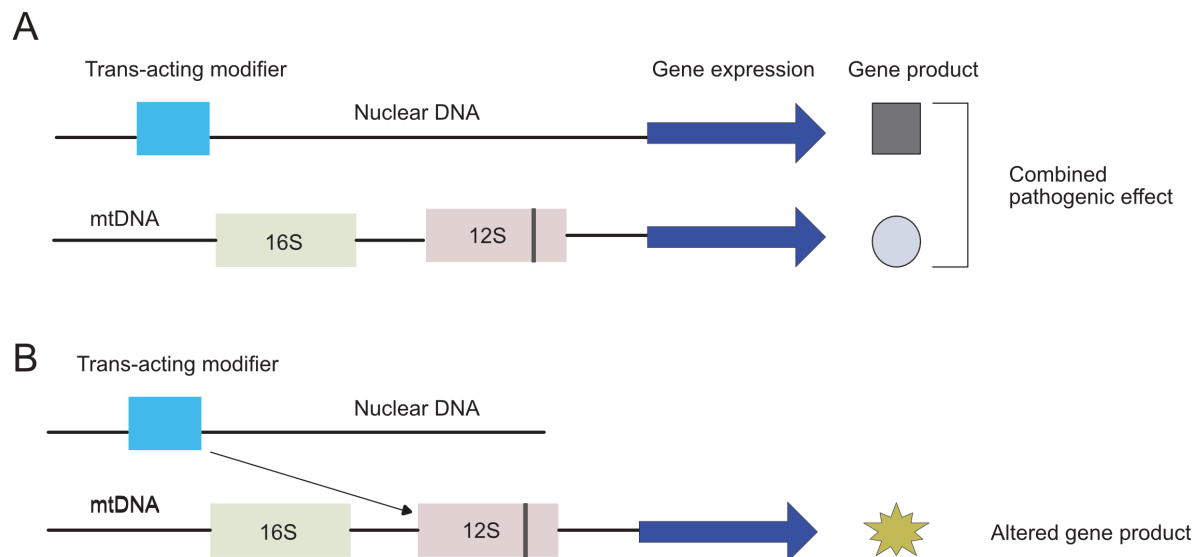


Figure 1.17. Trans-acting modifier effects. The mtDNA genes encoding 16S rRNA (green) and 12S rRNA (pink) and a nuclear trans-acting modifier (blue) are shown. Two potential mechanisms for the effect of a trans-acting modifier can be envisaged: (A) The trans-acting modifier encodes a separate gene product that in conjunction with the m.1555A>G (represented by black line in 12S rRNA gene) causes a pathogenic effect (B) The trans-acting modifier directly modulates the gene expression of 12S rRNA leading to an altered gene product and manifestation of the phenotype.

The incomplete penetrance and mild biochemical dysfunction associated with the m.1555A>G variant implies it is a necessary but not sufficient cause of maternally inherited hearing loss. Aminoglycosides are causative for hearing loss in some carriers, however the presence of hearing loss in carriers unexposed to aminoglycosides suggests the possible importance of epistatic mechanisms. Specifically, trans-acting nuclear modifiers acting in conjunction with m.1555A>G to cause disease (**Figure 1.17**) (Estivill, Govea et al. 1998, Hakli, Luotonen et al. 2013).

The first report of a putative nuclear modifier of m.1555A>G was based on a segregation analysis in a large Arab-Israeli kindred that suggested an undefined autosomal recessive locus may interact with the primary mtDNA variant in determining disease manifestation (Bu, Shohat et al. 1993).

Thus far, work to define nuclear modifiers of m.1555A>G has largely been inconclusive. An initial study using a genome-wide linkage approach suggested the variable phenotype of m.1555A>G may be attributable to a complex interaction of nuclear genes (Bykhovskaya, Shohat et al. 1998). A follow up study employing non-parametric linkage analysis suggested chromosome 8p23.1 may contain a possible modifier gene (Bykhovskaya, Estivill et al. 2000). From this gene dense region, *MRPS18CP2* (mitochondrial ribosomal protein S18V pseudogene 2) and *DEFA3* (defensin alpha 3) were initially prioritised based on their position within the linkage region and their predicted biological function (Bykhovskaya, Estivill et al. 2000, Ballana, Mercader et al. 2007); however no mutations have been found within these or any other genes in this region (Finnila and Majamaa 2003, Otaegui, Irizar et al. 2008). To date, five nuclear genes have been suggested as potential modifiers of m.1555A>G (**Figure 1.18**).

1.14.7.1 *TFB1M*

TFB1M, as discussed in **Section 1.8.4**, encodes the primary 12S rRNA methyltransferase. Non-parametric linkage analysis in 214 individuals from 41 families highlighted *TFB1M* as a potential modifier gene, however no causative mutation was found (Bykhovskaya, Mengesha et al. 2004).

1.14.7.2 *MTO1 and GTPBP3*

A further linkage study in the same families identified *MTO1* (mitochondrial tRNA translation optimisation 1) and *GTPBP3* (GTP binding protein 3), encoding proteins that function as a heterodimer responsible for the 5-taurinomethyluridine ($\tau\text{m}^5\text{U}$) modification found at position 34 (U34) of mt-tRNA^{LeuUUR}, mt-tRNA^{Lys}, mt-tRNA^{Glu}, mt-tRNA^{Gln} and mt-tRNA^{Trp} (Bykhovskaya, Mengesha et al. 2004). The potential importance of the *MTO1* and *GTPBP3* was extended by work with *Saccharomyces cerevisiae* carrying null alleles of these proteins. These strains only manifested reduced growth when coupled with a homolog of the m.1555A>G (*Saccharomyces cerevisiae* 15S rRNA 1409C>G), which could be corrected by introduction of human *MTO1* or *GTPBP3* cDNA (Li, Li et al. 2002). However, presently no causative mutations have been found in *MTO1* or *GTPBP3* in m.1555A>G carriers.

1.14.7.3 *TRMU*

TRMU encodes a highly conserved 5-methylaminomethyl-2-thiouridylate-methyltransferase responsible for the 5-taurinomethyl-2-thiouridine ($\tau\text{m}5\text{s}2\text{U}$) modification of mt-tRNA^{Lys}, mt-tRNA^{Glu}, mt-tRNA^{Gln} in the wobble position that results in an increased functional stability of the tRNAs (Guan, Yan et al. 2006). A homozygous c.28G>T transversion altering an invariant amino acid (p.A10S) has been suggested to cause profound deafness in 18 of 210 Spanish families carrying m.1555A>G (Guan, Yan et al. 2006, Yan, Bykhovskaya et al. 2006). This mutation did not affect importing of *TRMU* precursors into the mitochondria but was demonstrated to lead to a marked failure in mitochondrial tRNA metabolism resulting in a reduction in mitochondrial protein synthesis (Guan, Yan et al. 2006). However, it is noteworthy that this mutation is also found in 20% of controls and was not present in 31 Chinese pedigrees in the same study or a cohort of 281 Korean m.1555A>G carriers (Bae, Kim et al. 2012). In a further Spanish study of 38 hearing impaired individuals carrying m.1555A>G, 14 were heterozygous for the *TRMU* mutation and 1 carried the homozygous variant. However, the authors conclude that *TRMU* is not modulating the expression of the phenotype in these individuals given the presence of heterozygotes with and without hearing loss and symptomatic individuals carrying wild type *TRMU* (Otaegui, Irizar et al. 2008).

1.14.7.4 *MRPS12*

The primate family *Cercopithecoidea* (old world monkeys) carry the 12S rRNA variant m.1494C>T but are known to have normal hearing. *Emperador et al* determined the R68L variant in *MRPS12* (mitochondrial ribosomal protein S16), that encodes a 28S mitochondrial ribosomal subunit, protects primary fibroblasts derived from a *Cercopithecoidea* species from aminoglycoside mediated compromise of complex IV and a reduction of mitochondrial protein synthesis (Emperador, Pacheu-Grau et al. 2014). The authors then confirm this protective effect by overexpressing the variant in human transmitochondrial cybrids carrying the m.1494C>T or m.1555A>G variants thus mitigating the cellular effect of aminoglycosides. These data demonstrate that nuclear alleles may also play a protective role in carriers of 12S rRNA variants.

It is also important to consider the possibility that hearing loss in m.1555A>G carriers may be caused by a second mutation in a gene known to be associated with hearing function whereby the m.1555A>G variant can be regarded as a 'bystander' mutation. For example,

deleterious mutations in gap junction beta 2, *GJB2*, the commonest cause of AR deafness, have been previously identified as causative for hearing loss in m.1555A>G carriers (Abe, Kelley et al. 2001).

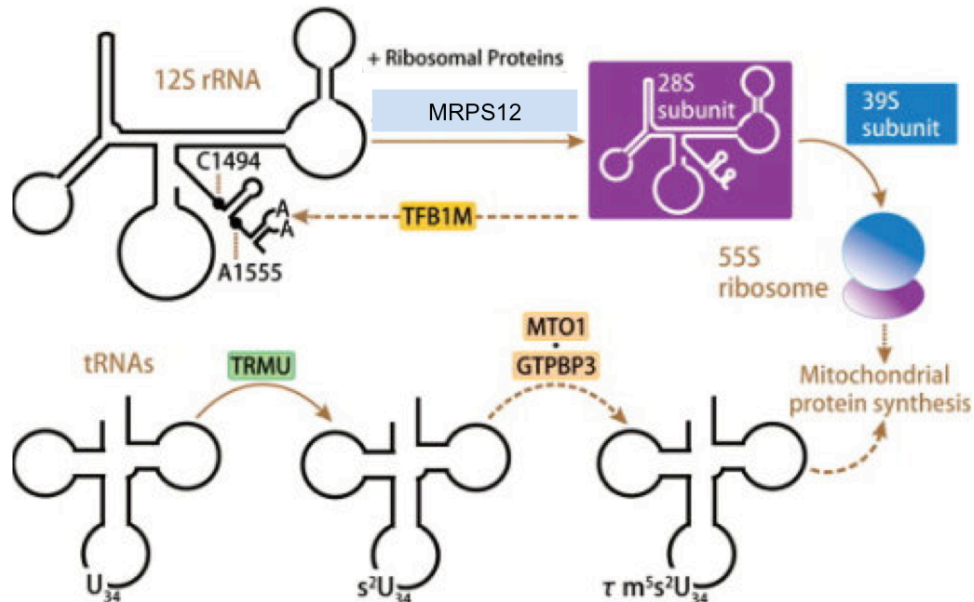


Figure 1.18. Putative nuclear modifiers of m.1555A>G. The protein products of five suggested nuclear modifiers of m.1555A>G are shown with their respective functions in mitochondrial protein synthesis as described in Section 1.14.7. Adapted from Luo, Hou et al. 2013.

1.15 Finding disease genes

Until the advent of next generation sequencing (discussed in Section 1.15.1) the identification of causal pathogenic variants in monogenic diseases, including hearing loss, was focussed on two Sanger (‘first generation’) sequencing approaches (i) genetic linkage analysis and (ii) candidate gene analysis. Genetic linkage analysis capitalises on the phenomenon of linkage disequilibrium, defined as the non-random association of alleles at different chromosomal loci (Slatkin 2008). By genotyping polymorphic markers in affected and unaffected members in large multi-generational pedigrees, it is possible to identify a chromosomal region that segregates with the disease. This strategy is often hampered by the size of the region isolated, given that they are often very large and contain numerous genes, making the subsequent prioritisation of candidate genes unfeasible. This is particularly true in consanguineous families that share large genetic regions identical by descent (Woods, Cox et al. 2006).

Candidate gene analysis relies on the prior knowledge of disease causing mutations associated with the relevant phenotype. Suitable genes can also be selected based on putative functional or biological relevance to the disease. However, this requirement for *a priori* knowledge can seriously hinder the selection of causative alleles that could be identified by a hypothesis-free approach (Zhu and Zhao 2007). Since 2005, the advent of next generation sequencing technology (NGS) has to a large extent circumvented the methodological limitations of these approaches ushering in the post-genomic era (Goodwin, McPherson et al. 2016).

1.15.1 Next generation sequencing technology

NGS refers to high throughput technologies that allow massively parallel DNA sequencing (Shendure and Ji 2008). For large scale genome analyses these technologies have supplanted traditional chain terminating dideoxynucleotide sequencing first described by Frederick Sanger (Sanger, Nicklen et al. 1977). A number of different NGS platforms currently exist with the most widely used being Illumina HiSeq 2000 (Illumina[®]), Roche 454 sequencing (Roche Applied Science) and Ion torrent: Proton/Personal Genome Machine sequencing (Thermo Fisher Scientific).

1.15.2 The human exome and whole exome sequencing

The exome is the part of the genome that is formed by the exons. These sequences once transcribed, form the mature mRNA after removal of the introns by RNA splicing (Voet 2011). The human exome consists of 180,000 exons constituting approximately 1% of the genome, however, it is estimated that 85% of disease causing mutations are exonic (Ng, Turner et al. 2009, Gilissen, Hoischen et al. 2012). A mandatory prerequisite for isolating pathogenic variants by exome sequencing is a clear definition of the exome, however presently; delineating which sequences are protein-coding remains problematic (Kellis, Wold et al. 2014). To maximise exome coverage, current commercially available exome capture kits use exon lists defined by the CCDS (Consensus Coding Sequence Project), RefSeq and GENCODE databases and target up to 64 Mb of coding sequence (Chilamakuri, Lorenz et al. 2014).

Exome sequencing employs NGS technologies to simultaneously couple targeted exon capture with massively parallel DNA sequencing that can be used to isolate candidate variants in a hypothesis free approach (Yang, Muzny et al. 2013). This allows the

identification of disease causing variants without prior knowledge of gene function, hence overcoming some of the difficulties of finding causal alleles in conditions where pathophysiology is incompletely understood (Rabbani, Tekin et al. 2014).

1.15.3 Exome sequencing methodology

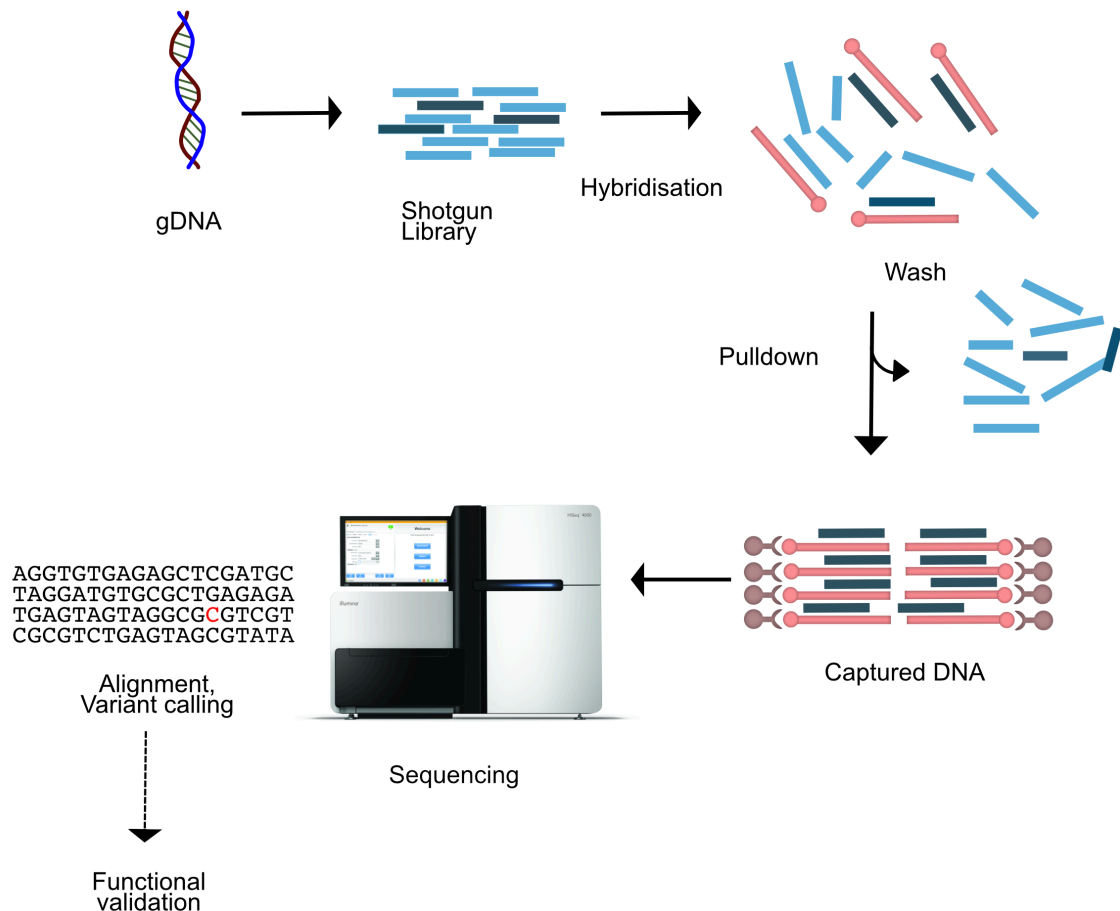


Figure 1.19. Illumina exome sequencing methodology. Genomic DNA (gDNA) is sheared and prepared into a shotgun library. The library is then enriched in exonic sequences (dark blue fragments). After washing the exons are captured by biotinylated DNA (orange fragments). The hybridized fragments are recovered by biotin-streptavidin pulldown, amplified and sequenced (HiSeq 2000 Sequencing System depicted). Sequence reads are mapped and variants called. Biologically plausible candidate variants can then be prioritised for functional validation. Adapted from (Bamshad, Ng et al. 2011).

Although there are specific technical differences between the individual NGS platforms, exome sequencing largely follows a common workflow of (i) sample preparation, (ii) exon capture by hybridisation to biotinylated bait probes, (iii) enrichment by biotin-streptavidin pull down, sequencing, alignment followed by variant detection and identification of causal alleles (Metzker 2010) (**Figure 1.19**).

1.15.3.1 Illumina HiSeq Sequencing

In this study exome sequencing was performed using Illumina HiSeq 2000 technology (Illumina 2016) (**Figure 1.19**). Illumina technology employs bridge amplification PCR to create clonal clusters on the surface of a glass flow cell that can then be subjected to massively parallel sequencing. Firstly, DNA is fragmented into 200-300 bp lengths that are ligated to adapters creating a sequencing library. These adapters contain universal priming sites, which following the loading of the linked fragments on to a flow cell, can be used to amplify the fragments using common PCR primers. The Illumina platform then utilises a sequencing-by-synthesis approach to sequence the clusters. Sequences are then aligned to the reference sequence for variant detection (Metzker 2010).

1.15.3.2 Approaches to filtering

The primary challenge in the analysis of exome sequencing data is distinguishing novel disease causing variants from a vast background of sequencing errors and non-pathogenic polymorphisms. The exome sequence of a typical individual consists of 5-9 gigabases and approximately 20,000- 25,000 variants (Bamshad, Ng et al. 2011, Cherukuri, Maduro et al. 2015). The principle of filtering this data is to find rare (minor allele frequency, (MAF) $\leq 1\%$) or novel variants shared between affected individuals. This is undertaken by exome sequencing a defined number of affected individuals and comparing isolated variants to sets of polymorphisms available in public datasets such as 1000 Genomes project, dbSNP 137 and ExaC databases (Exome Aggregation Cohort) (National Center for Biotechnology Information, Genomes Project, Auton et al. 2015, Lek, Karczewski et al. 2016). This approach assumes that variants found in these databases at a MAF above the defined threshold are not causative, a justified assumption given that only approximately 2% of single nucleotide variants (SNVs) identified in an individual are novel (Bamshad, Ng et al. 2011). This approach therefore allows the prioritisation of a manageable number of variants that can be taken forward for further analysis.

1.15.3.3 Use of inheritance mode in filtering

The inheritance pattern of the disease in question must be considered both in the experimental design, but also in the subsequent analysis of the sequencing data. For example, recessive conditions necessitate the sequencing of fewer individuals than dominant conditions, given the genome of any individual has approximately 50-fold fewer

genes with two, rather than one deleterious variant per allele (Bamshad, Ng et al. 2011). For AD diseases only single heterozygous variants shared between affected and absent in unaffected individuals should be considered. On the other hand, for AR conditions homozygous or compound heterozygous variants are considered (Farwell, Shahmirzadi et al. 2015).

1.15.3.4 Identification of deleterious variants

Candidate variants are further prioritised as recommended by the ‘MacArthur criteria’ to determine predicted pathogenicity (MacArthur, Manolio et al. 2014). These widely accepted guidelines provide a robust framework for establishing causality of sequence variants. For example, variants causing nonsense or frameshift mutations alter protein function and hence are prioritised over synonymous mutations that are not directly protein altering. Variants can also be analysed by bioinformatic tools designed to predict pathogenicity, e.g. Sorting Intolerant from Tolerant (SIFT), Polymorphism Phenotyping (Polyphen2), Likelihood ratio test (LRT) and MutationTaster (Kumar, Henikoff et al. 2009, Adzhubei, Schmidt et al. 2010, Schwarz, Rodelsperger et al. 2010). These tools attempt to assign a pathogenicity prediction by computing evolutionary sequence constraints across species as well as predicting the effect of amino acid changes on overall protein function. Subsequently, candidate genes can be prioritised for further analysis based on their known biological characteristics and function, for example in establishing variants potentially causative for mitochondrial associated hearing loss, known deafness genes would be initially prioritised before pursuing genes with defined mechanistic links to either mitochondrial function or the auditory system.

1.16 Research aims

This research project was undertaken to define nuclear genetic variants that account for the variable penetrance of hearing loss associated with the m.1555A>G variant. Specifically, there were three aims:

- To ascertain the frequency of the m.1555A>G variant in patients in the UK with suspected mitochondrial deafness by undertaking a survey of the UK laboratories performing genetic testing for the m.1555A>G variant.
- To define nuclear gene variants that co-segregate with hearing loss and the m.1555A>G variant by using a whole exome sequencing approach followed by iterative filtering and prioritisation of selected variants.
- To functionally assess the pathogenic effect of the m.1555A>G variant on mtDNA translation and interrogate identified novel nuclear modifier genes focussing on their known biological function. This will be performed using a number of experimental techniques including genetic, protein, immunocytochemical, histochemical, and biochemical analyses.

Chapter 2

Materials and Methods

2.1 Cell culture methodology

2.1.1 Fibroblast and myoblast cell maintenance

Fibroblasts and myoblasts were maintained in high glucose Dulbecco Minimal Essential Medium (DMEM) (Gibco, Thermo Fisher Scientific, MA. USA) supplemented with 10% (v/v) heat inactivated Fetal Calf Serum (FCS, Sigma-Aldrich, MO. USA), 2 mM L-glutamine, 1 × MEM vitamin solution, 1 mM sodium pyruvate (Thermo Fisher Scientific); and 50 µg/ml uridine (Sigma-Aldrich). This medium is referred to as 'supplemented high glucose DMEM' throughout this thesis. Cells were grown in either T25 or T75 cell culture vessels (VWR, Lutterworth, UK) in a humidified incubator at 37°C and 5% CO₂. Cells were examined using an inverted Leica DM IL LED microscope (Leica, Wetzlar, Germany).

2.1.2 Cell propagation

Cells were frequently examined and media refreshed approximately every 4 days. Cells were passaged once they reached 90% confluency. To passage cells the medium was aspirated and the cells were rinsed in 1X Phosphate Buffered Saline (PBS, Thermo Fisher Scientific) until the medium was completely removed. The cells were then treated with 0.05% Trypsin ethylenediaminetetraacetic acid (EDTA) (Gibco, Thermo Fisher Scientific) and replaced into the culture incubator for 5 minutes. The culture vessel was examined under the microscope and once all cells had detached a double volume of fresh medium was added to inactive the trypsin. This mixture was then collected using a serological pipette, transferred into a 15 ml Falcon Conical Centrifuge Tube (Thermo Fisher Scientific) and centrifuged at 1300 × g for 3.5 minutes in a bench top centrifuge (Heraeus Megafuge 16, Thermo Fisher Scientific). After centrifugation the supernatant was poured off and the pellet of cells was dissolved in fresh medium. This cell solution was then split between 1 in 2 and 1 in 4 into fresh culture vessels depending on the number of cells obtained.

2.1.3 Cell counting

Cells were either counted using a haemocytometer (AC1000 Improved Neubauer, HawksleyVet, Lancing, UK) or Countess II FL Automated Cell Counter (Thermo Fisher Scientific). For both methods, cells were collected as described in **Section 2.1.2** and re-suspended in fresh medium. For the haemocytometer method, 10 μ l of the cell suspension was applied to the haemocytometer chamber and covered with a glass coverslip. Cells were counted in the large four corner squares and an average number of cells per square was calculated. This value was multiplied by 1×10^4 to calculate the total number of cells in the original suspension. For the automated method, 10 μ L of the cell suspension was combined with 10 μ l of 0.4% Trypan Blue (Thermo Fisher Scientific); 10 μ l of this solution was loaded into a Countess Cell Counting Chamber Slide and placed into the Countess II FL Automated Cell Counter to derive the number of cells per ml in the original suspension.

2.1.4 Cryopreservation of cells

A bank of cells was created for future experiments by cryopreservation in liquid nitrogen. Cells were first harvested as described in **Section 2.1.2**. The pelleted cells were then re-dissolved in pre-made freezing medium (90% FCS and 5% dimethyl sulfoxide (DMSO; Sigma-Aldrich) at a concentration of 1×10^6 cells per ml of freezing medium. The cell suspension was added to a cryovial pre-labelled with cell line details, passage number and freezing date. The cryovial was then placed in a 'Mr Frosty' Freezing Container (Thermo Fisher Scientific) filled with 100% isopropyl alcohol to the fill line. This procedure ensures the cells are cooled at approximately 1°C/minute. The 'Mr Frosty' was placed in the -80°C freezer and after a minimum of 24 hours the cryovial was removed from the 'Mr Frosty' and transferred to liquid nitrogen for extended storage. To thaw cells a cryovial was taken from liquid nitrogen and rapidly warmed under running warm water. The thawed cells were then transferred into a 15 ml Falcon tube Conical Centrifuge Tube containing 5 ml of medium. The suspension was centrifuged for 4 minutes at $1300 \times g$ in a bench top centrifuge (Heraeus Megafuge 16). The supernatant was removed and the pellet was re-suspended in fresh medium that was then transferred into a fresh culture vessel.

2.1.5 Immortalisation of primary fibroblasts

Primary fibroblasts were immortalised by Dr Aurelio Reyes (Mitochondrial Biology Unit, Cambridge, UK) using lentiviral transduction of pLOX-Ttag-iresTK (Addgene #12246,

Tronolab, Lausanne, Switzerland). For the generation of lentiviral particles, human 293T cells (2.5×10^6) were plated 24 hours before co-transfection with 10 μ g of transfer vector (pLOX-Ttag-iresTK), 7.5 μ g of second-generation packaging plasmid (pCMVdR8.74) and 3 μ g of envelope plasmid (pMD2.VSVG) (Naldini, Blomer et al. 1996). FuGENE 6 Transfection Reagent (Roche, Basel, Switzerland) was used as transfectant reagent. Infectious particles were collected 24 and 48 hours after transfection. Transduced fibroblasts were grown for at least six passages in order to make sure immortalized cells were selected. Changes in cell shape and doubling time were observed as part of the normal process of immortalization.

2.1.6 Analysis of cell growth

Fibroblast cells were plated in 24 well plates (Corning Costar®, Sigma-Aldrich) at 2.5×10^4 cells/well in high glucose DMEM including 2 mM L-glutamine, 1 mM sodium pyruvate and supplemented with 10% (v/v) FCS (Sigma-Aldrich) or glucose free DMEM including 2 mM L-glutamine, 1 mM sodium pyruvate and supplemented with 5mM galactose (Sigma-Aldrich). The IncuCyte® Live Cell Imager (Essen Bioscience, MI, USA) was used to generate growth curves using IncuCyte® ZOOM software (Essen Bioscience).

2.2 Histopathology methodology

2.2.1 Mitochondrial histochemistry

Skeletal muscle biopsies were snap frozen in liquid nitrogen and maintained at -80°C by Kari Majamaa (Oulu University, Finland). The sectioning and staining of muscle biopsies was performed in collaboration with Miss Zoe Golder (Mitochondrial Biology Unit, Cambridge, UK). The tissue was mounted in optimum cutting temperature medium (OCT) and adjusted to -20°C in the cryostat chamber. Sections were cut with Microm HM 560 Cryostat (Thermo Fisher Scientific) at 10 μ m and collected on Single Frost microscope slides (VWR Polysine™ Microscope Adhesion slides, Thermo Fisher Scientific) were then used to attach the section. Sections were then dried for 1 hour to minimise freezing artefacts.

2.2.2 Haematoxylin and eosin staining

Slides were fixed in Formol Calcium solution (40% Formaldehyde, 10% CaCl₂, both Sigma-Aldrich) for 10 minutes and then were washed for 2 minutes in running tap water. Slides were then placed in Mayers Haemalum (LAMB/170-D, Raymond Lamb, Thermo Fisher Scientific) solution for 1 minute. Slides were washed again for 2 minutes in running tap water and placed in 1% aqueous eosin solution for 1 minute (LAMB/100-D, Raymond Lamb). Slides were washed for 2 minutes in dH₂O before being dehydrated in graded alcohol: 70% ethanol for 30 seconds, 95% ethanol for 30 seconds, 100% ethanol for 2 minutes. Sections were covered in D.P.X. solution (VWR, Product 360294H) and a glass coverslip was placed on top.

2.2.3 COX/SDH dual staining

COX activity staining was undertaken by incubating sections for 35 minutes at 37°C in medium containing 20% (v/v) 500 µM cytochrome c (Sigma-Aldrich), 80% (v/v) 3,3'-diaminobenzidine tetrahydrochloride (Sigma-Aldrich) and a few grains of catalase (Sigma-Aldrich). Following incubation, sections were washed twice for 1 minute in PBS. Staining for SDH was undertaken by incubation for 45 minutes at 37°C in medium containing 80% (v/v) 1.875mM nitroblue tetrazolium (Sigma-Aldrich), 10% (v/v) 1.3 M sodium succinate (Sigma-Aldrich), 10% (v/v) 2 mM, phenazine methosulphate (Sigma-Aldrich) and 0.01% (v/v) 100 mM sodium azide (Sigma-Aldrich). Following this, the sections were washed twice for 1 minute in PBS.

2.3 Genetic analysis methodology

2.3.1 Genomic DNA extraction from cultured cells

Total genomic DNA was extracted from a pellet of cultured fibroblast or myoblast cells (maximum 5×10^6 cells per pellet) using the DNeasy® Blood & Tissue Kit (Qiagen, Hilden, Germany). All reagents used were provided with the kit. Firstly, the pellet was re-suspended in 200 µl PBS. Following this, 20 µl of Proteinase K and 200 µl of Buffer AL was added and the whole mixture was vortexed and incubated at 56°C for 10 minutes. The sample was then precipitated by the addition of 200 µl of 100% ethanol. This mixture was vortexed to ensure a homogenous solution and added to a DNeasy® Mini spin column in a 2 ml collection tube. The sample was centrifuged at $6797 \times g$ at room temperature. The flow through was discarded and the spin column was placed in a new collection tube. The

sample was washed with 500 μl of Buffer AW1 and centrifuged for 1 minute at $6797 \times g$ rpm at room temperature. The flow through was discarded and the column was placed in a fresh collection tube. The sample was then washed in 500 μl of Buffer AW2 and centrifuged at $20817 \times g$ for 3 minutes to dry the DNeasy® membrane. The spin column was then placed in a 1.5 ml Eppendorf microcentrifuge tube (Eppendorf, Hamburg, Germany) and eluted with the AE elution buffer. The volume of elution used was determined by the amount of starting material (range 35 μl -100 μl). The concentration and purity (determined by the A260/A280 ratio) of the eluate DNA was determined by the NanoDrop 2000 UV-Vis spectrophotometer (Thermo Fisher Scientific). DNA was placed at 4°C for short-term or -20°C for long-term storage.

2.3.2 Genomic DNA extraction from muscle homogenate

The extraction of total genomic DNA from muscle homogenate was performed using the DNeasy® Blood & Tissue Kit (Qiagen). All reagents used were provided with the kit. Muscle biopsy tissue was sectioned at 10 μm thickness using the Microm HM 560 Cryostat (Thermo Fisher Scientific). Approximately 10 sections were placed in a 1.5 ml Eppendorf microcentrifuge tube and 180 μl Buffer ATL was added. Following this, 20 μl of Proteinase K and was added and the whole mixture was vortexed and incubated at 56°C for 5 hours until the tissue was completely lysed. Next, 200 μl of Buffer AL was added and the whole mixture was vortexed followed by the addition of 200 μl of 100% ethanol. This mixture was vortexed to ensure a homogenous solution and added to a DNeasy® Mini spin column in a 2 ml collection tube. The sample was centrifuged at $6797 \times g$ at room temperature. The flow through was discarded and the spin column was placed in a new collection tube. The sample was washed with 500 μl of Buffer AW1 and then centrifuged for 1 minute at $6797 \times g$ rpm at room temperature. The flow through was discarded and the column was placed in a fresh collection tube. The sample was then washed in 500 μl of Buffer AW2 and centrifuged at $20817 \times g$ for 3 minutes to dry the DNeasy® membrane. The spin column was then placed in a 1.5 ml Eppendorf microcentrifuge and eluted with 35 μl AE elution buffer. The concentration and purity (determined by the A260/A280 ratio) of the eluate DNA was determined by the NanoDrop 2000 UV-Vis spectrophotometer (Thermo Fisher Scientific). DNA was placed at 4°C for short-term or -20°C for long-term storage.

2.3.3 Genomic amplification

When required for DNA sequencing reactions, total genomic DNA was amplified using the REPLI-g Ultrafast Mini Kit (Qiagen). All reagents were supplied with the kit. Firstly, Buffer D1 was prepared by adding 5 μL of Buffer DLB to 35 μL nuclease free water and 1 μL of Buffer D1 was combined with 1 μL template DNA in a PCR tube (Bio-Rad, Hemel Hempstead, UK). This solution was vortexed and incubated at room temperature for 3 minutes. Buffer N1 was prepared by combining 8 μL Stop solution to 72 μL nuclease free water and 2 μL of this was added to the incubated solution. A master mix of 15:1 Ultrafast Reaction Buffer and Ultrafast DNA polymerase was prepared and 16 μL was added to the 4 μL of denatured DNA. This solution was incubated at 30°C for 1.5 hours and the reaction was then inactivated by heating for 5 minutes at 65°C in a Veriti® 96-well Thermocycler (Thermo Fisher Scientific). DNA was stored as in **Section 2.3.1**.

2.3.4 Polymerase chain reaction (PCR)

All PCR reactions were performed in a Veriti® 96-well Thermocycler in 96 well plates (Star Lab, Hamburg, Germany) or PCR tubes (Bio-Rad). PCR reactions were performed in a final reaction volume of 25 μL containing 1 μL MyTaq™ DNA Polymerase (Bioline, London, UK), 10 μL 5x MyTaq Reaction Buffer (Bioline), 1 μL of specific forward and reverse primers (10 μM , Integrated DNA Technologies, IA, USA) and 2-4 μL of total genomic DNA extract containing on average 50 ng DNA. The sample was made up to 25 μL by the addition of dH₂O. The product was amplified using the following conditions: 95°C for 1 minute, followed by 30 cycles of denaturation at 95°C for 15 seconds, annealing at the appropriate primer annealing temperature for 15 seconds and then extension at 72°C for 10 seconds. The final extension step was performed at 72°C for 10 minutes. The PCR reactions were cooled to 4°C and stored at -20°C. The optimal annealing temperature was determined by running a gradient PCR with temperatures ranging from 58°C to 62°C at 2°C intervals for each primer pair.

2.3.5 Agarose gel electrophoresis

Amplified DNA fragments were separated using electrophoresis on an agarose gel. Depending on the product size a 0.6-2% (w/v) agarose gel was used. Agarose (0.6-2g) (Helena Biosciences Europe, Gateshead, UK) was dissolved in 100 ml 1X TAE buffer (0.04M Tris acetate, 0.001M EDTA; Sigma-Aldrich). The mixture was boiled in an 800 W

microwave for approximately 1.5 minutes and then cooled under running water. Once cooled, 0.4 µg/ml of ethidium bromide (Sigma-Aldrich) or 100 µl Safeview Nucleic Acid Stain (NBS Biologicals, Huntingdon, UK) was added for visualisation of the resolved products. The mixture was then poured into a gel-casting tray with an inserted gel comb and allowed to solidify for 30 minutes at room temperature. For gel loading, 5 µl of PCR product was mixed with 5 µl of Orange G loading buffer (50% glycerol (Sigma-Aldrich), 50% H₂O, Orange G (Sigma-Aldrich) and loaded along with 5 µl of Hyperladder IV DNA marker (Biolone). These were run in a gel tank (Scie-Plas, Cambridge, UK) in 1X TAE buffer at a voltage of 90 V for 30 minutes. The gel was then imaged using the UV GelDoc-It[®] 2 Imager (UVP, Upland, California, USA).

2.3.6 Agarose gel extraction of PCR amplicons

Standard PCR technique was used to generate DNA amplicons that were then separated on a 1% (w/v) TAE agarose gel as described in **Section 2.3.5**. Under UV illumination the appropriate fluorescent band was identified by size and excised from the gel with a scalpel, subdivided and placed in a 1.5 ml Eppendorf microcentrifuge tube. Each tube was weighed so that it held a maximum of 200 mg of gel. The QIAquick[®] Gel Extraction Kit (Qiagen) was then used to extract DNA. All reagents were supplied with the kit and all centrifugation steps were undertaken at 10000 x g at room temperature in an Eppendorf Centrifuge 5430R. Initially, 900 µL QG buffer was added to the tube and the mixture was then incubated at 50°C for 10 minutes. The mixture was frequently vortexed to aid dissolving the gel. Following this, 100 µl isopropanol was added to precipitate the DNA. The sample was then added to a QIAquick[®] spin column placed in 2 ml collection tube and centrifuged for 1 minute. The flow through was discarded and 750 µl of buffer PE was added and the mixture was centrifuged at for 1 minute. The spin column was then placed into a fresh collection tube and centrifuged for 1 minute to dry the membrane. The column was then placed in a clean 1.5 ml Eppendorf microcentrifuge tube and 30 µl EB elution buffer was added. The mixture was incubated at room temperature for 1 minute and centrifuged for 1 minute to elute the DNA. The DNA was quantified and stored for future use as described in **Section 2.3.1**.

2.3.7 Sequencing of nuclear genes

PCR products were amplified as described in **Section 2.3.4** using appropriate primer pairs (Integrated DNA Technologies) and then visualised as described in **Section 2.3.5**.

2.3.7.1 *Exonuclease I/FastAP treatment*

Before sequencing, PCR products must be cleaned by the removal of unincorporated primers and nucleotides that would otherwise reduce sequencing fidelity. Firstly, 0.5 μl of Exonuclease I (Thermo Fisher Scientific) and 1 μl of FastAP Thermosensitive Alkaline Phosphatase (Thermo Fisher Scientific) were mixed with approximately 20 ng PCR product per well in a 96 well plate (Star Lab) on ice. The mixture was then incubated at 37°C for 15 minutes and then at 80°C for 15 minutes to inactivate the enzymes. All reactions were performed in a Veriti[®] 96-well Thermal Cycler (Thermo Fisher Scientific).

2.3.7.2 *BigDye™ sequencing*

Sequencing of the PCR amplicons was performed using the BigDye[®] Terminator v3.1 Cycle Sequencing Kit (Thermo Fisher Scientific). After clean up of the PCR product, 1 μl of BigDye[®] Terminator v3.1 Ready Reaction Mix, 2 μl of BigDye[®] Terminator v3.1 5X Sequencing Buffer and 1 μl of appropriate forward or reverse primer (10 μM) was added to 5 μl PCR product and made up to 20 μl with dH₂O. The BigDye[®] Terminator cycle sequencing was performed in a Veriti[®] 96-well Thermal Cycler (Thermo Fisher Scientific). The PCR reaction conditions were an initial denaturing step at 96°C for 1 minute, followed by 25 cycles of 96°C for 10 seconds, 50°C for 5 seconds and 60°C for 4 minutes.

2.3.7.3 *Ethanol precipitation*

Ethanol precipitation was used to remove unincorporated dye-labelled nucleotides and excess salt. 2 μl of 125 mM EDTA (Sigma-Aldrich), 2 μl of 3M sodium acetate (Sigma-Aldrich) and 70 μl of 100% ethanol (Sigma-Aldrich) was added to each sample. These were then mixed and incubated at room temperature for 15 minutes. The plate was then centrifuged at 2060 \times g for 30 minutes. The supernatant was removed by inverting the plate on tissue followed by a brief centrifugation at 100 \times g. Following this, 70 μl of 70% ethanol (Sigma-Aldrich) was added and the sample centrifuged at 1650 \times g for 15 minutes. The supernatant was removed by again inverting the plate on tissue and centrifuging at 100 \times g. The sample was then air dried in the dark for 10 minutes to allow the evaporation of all the ethanol.

2.3.7.4 *Capillary electrophoresis sequencing*

The precipitated DNA pellets were re-suspended in 10 µL Hi-Di™ Formamide (Thermo Fisher Scientific) and incubated for 2 minutes at 95°C in a Veriti® 96-well Thermal Cycler (Thermo Fisher Scientific) followed by rapid cooling on ice. Sequencing was performed on the ABI PRISM® 3100 Genetic Analyser (Thermo Fisher Scientific).

2.3.7.5 *Sequence analysis*

SeqScape® v2.6 Software (Thermo Fisher Scientific) was used to analyse the generated sequencing data. Sequencing results were aligned to the reference GenBank reference sequences available from the Ensembl Genome Browser (<http://www.ensembl.org/index.html>).

2.3.8 **Long-range PCR of mitochondrial DNA**

For the investigation of mitochondrial DNA deletions an approximately 16 kB fragment encompassing almost the complete mitochondrial genome was amplified. Each sample was amplified in a 20 µl PCR master mix containing 5 µl TaKaRa PrimerSTAR GXL buffer (Takara, Saint Germaine-en-Laye, France), 2 µl dNTP mixture (Takara), 0.5 µl of 10 µM forward or reverse primers (see **Table 2.1**), 0.5 µL TaKaRa PrimerSTAR GXL DNA Polymerase (Takara) and 15.5 µl water. DNA was amplified in a Veriti® 96-well Thermal Cycler under the following conditions: 94°C for 1 minute, then 30 cycles of 98°C for 10 seconds and 68°C for 13 minutes and then followed by 72°C for 10 minutes. The mixture was then cooled to 4°C. For gel loading, 5 µL of the PCR amplicons were mixed with 5 µL Orange G loading buffer (Sigma-Aldrich) and were separated by electrophoresis on a 0.7% (w/v) agarose gel at 40 V for 90 minutes as described in **Section 2.3.5**. In parallel, 5 µL of GeneRuler 1Kb Plus DNA Ladder premixed with 6X loading buffer (Thermo Fisher Scientific) was run to aid sizing of the DNA amplicons. The PCR products were then visualised as described in **Section 2.3.1**.

Table 2.1. Details of primers used for Long Range PCR

Name	Sequence	Size	mtDNA position
16kb mtDNA_1	D2F - TTAAAACTCAAAGGACCTGGC D1R- AGGGTGATAGACCTGTGATC	15432 bp	m.1650-1671 m.19-1
16kb mtDNA_2	16F- CTCAAAGGACCTGGCGGTGCTTC 16R- GTAGTGTCTGGCGAGCAGTTTTG	16552 bp	m.1163-1185 m.1123-1146

2.3.9 Quantification of mitochondrial DNA copy number

Quantification of mtDNA copy number in fibroblasts and blood was performed in a duplex qPCR assay with primers specific to the mtDNA gene, *MT-ND1* and the nuclear housekeeping genes, *B2M*. mtDNA copy number in muscle samples used the mtDNA gene *MT-CO3* and the nuclear gene, *RNaseP*. The assay was performed on the CFX96 C1000 Touch Thermocycler (Bio-Rad). The assay employs the use of TaqMan probes (Applied Biosystems, CA, USA) designed to bind a specific region of a gene of interest. Target probes specific to a region of the gene of interest are designed with an attached fluorescent reporter dye at the 5' end and a non-fluorescent quencher dye on the 3' end. When the reporter and quencher are in proximity the fluorescence of the reporter is quenched by Förster resonance energy transfer (FRET). As the PCR product extends the fluorescent reporter is cleaved by Taq exonuclease and ceases to be quenched. The signal generated is proportional to the amount of target DNA present in the sample. The in-built detector of the CFX96 detects the signal and the CFX manager software (Bio-Rad) is able to determine the level of fluorescence exceeding the background fluorescence. The threshold cycle (Ct) is defined as the number of cycles in which the fluorescence exceeds the background noise. This occurs when there was a linear increase in the amplification curve that corresponds to exponential increase in the PCR product. All qPCR reactions were set up was performed in a UV-sterilised Aura PCR workstation (Bioair Instruments, Milan, Italy).

To assess technical reliability and efficiency standard curves were generated by serial dilution of *MT-ND1* and *B2M* (or *MT-CO3* and *RNaseP*) (**Figure 2.1**). These PCR products were generated by a standard PCR technique and extracted from agarose gel and quantified as described in **Section 2.3.5**. Primer pairs used to generate the templates are shown in **Table 2.2**. This DNA concentration was then used to calculate the DNA copy number from the formula:

$$\text{Copies}/\mu\text{l} = \frac{C}{Mw} \cdot A$$

Where C is the concentration g/ μl , Mw is the molecular weight given by product length in bp x 2 x 330 and A is Avogadro's constant ($6.02 \times 10^{23} \text{ mol}^{-1}$).

Each DNA sample for quantification was initially diluted to produce a starting concentration of 10 ng/ μL . A 20 μL reaction mix was set up as follows: 0.6 μL of each

primer (*MT-ND1/B2M* or *MT-CO3/RNaseP* forward and reverse primers), 0.4 µL of each probe (*MT-ND1-HEX*, *B2M-FAM* or *MT-CO3-FAM*, *RNaseP-HEX*), 10 µL iTaq SuperMix reaction buffer (Bio-Rad), 1 µL of sample DNA and 4.2 µL nuclease free water. Primer pairs for the qPCR reaction are shown in **Table 2.2**. Cycling conditions were as follows: 95°C for 3 minutes, then 40 cycles of 62.5°C for 1 minute and 95°C for 10 seconds and then followed by 95°C for 1 minute. For each DNA sample the Ct values of each gene were assayed in triplicate and a mean was calculated (**Figure 2.1**). A maximum of 0.5 Ct value was set as the acceptable threshold difference between replicates. Relative mtDNA copy number values were calculated with the delta Ct method where:

$$\text{Delta Ct} = \text{Ct } MT-ND1 - \text{Ct } B2M$$

Or

$$\text{Delta Ct} = \text{Ct } MT-CO3 - \text{Ct } RNaseP$$

and

$$\text{Copy number} = 2^{(2-\text{delta Ct})}$$

Table 2.2. Details of primer pairs used in qPCR analysis of mtDNA copy number

Template	Forward Sequence	Reverse Sequence	Size
<i>MT-ND1</i>	AGGAACTCGGCAAATCTTACC	GTCATGTGAGAAGAAGCAGG	1092 bp
<i>B2M</i>	CGCAATCTCCAGTGACAGAA	GCAGAATAGGCTGCTGTTCC	1040 bp

qPCR	Dye	Forward Sequence	Reverse Sequence	Probe
<i>MT-ND1</i>	HEX	ACGCCATAAACTCTTCA CCAAAG	GGGTTCATAGTAGAAGAGCGATGG	CCGTGGAACCATGTGACTTTGTC
<i>MT-CO3</i>	FAM	ATGACCCACCAATCACATG	ATCACATGGCTAGGCCGGAG	ACCCAGCCCATGACCCCTAAC
<i>MT-CYB</i>	HEX	ATGACCCCAATACGCAAAA	CGAAGTTTCATCATGCGGAG	CATTCATCGACCTCCCCACCC
<i>B2M</i>	FAM	CACTGAAAAAGATGAGTA TGCC	AACATTCCCTGACAATCCC	ACCCGCCACATCTACCATCACCTC
<i>RNAseP</i>	HEX	AGATTTGGACCTGCGAGCG	GAGCGGCTGTCTCCACAAGT	TTCTGACCTGAAGGCTCTGCGCG

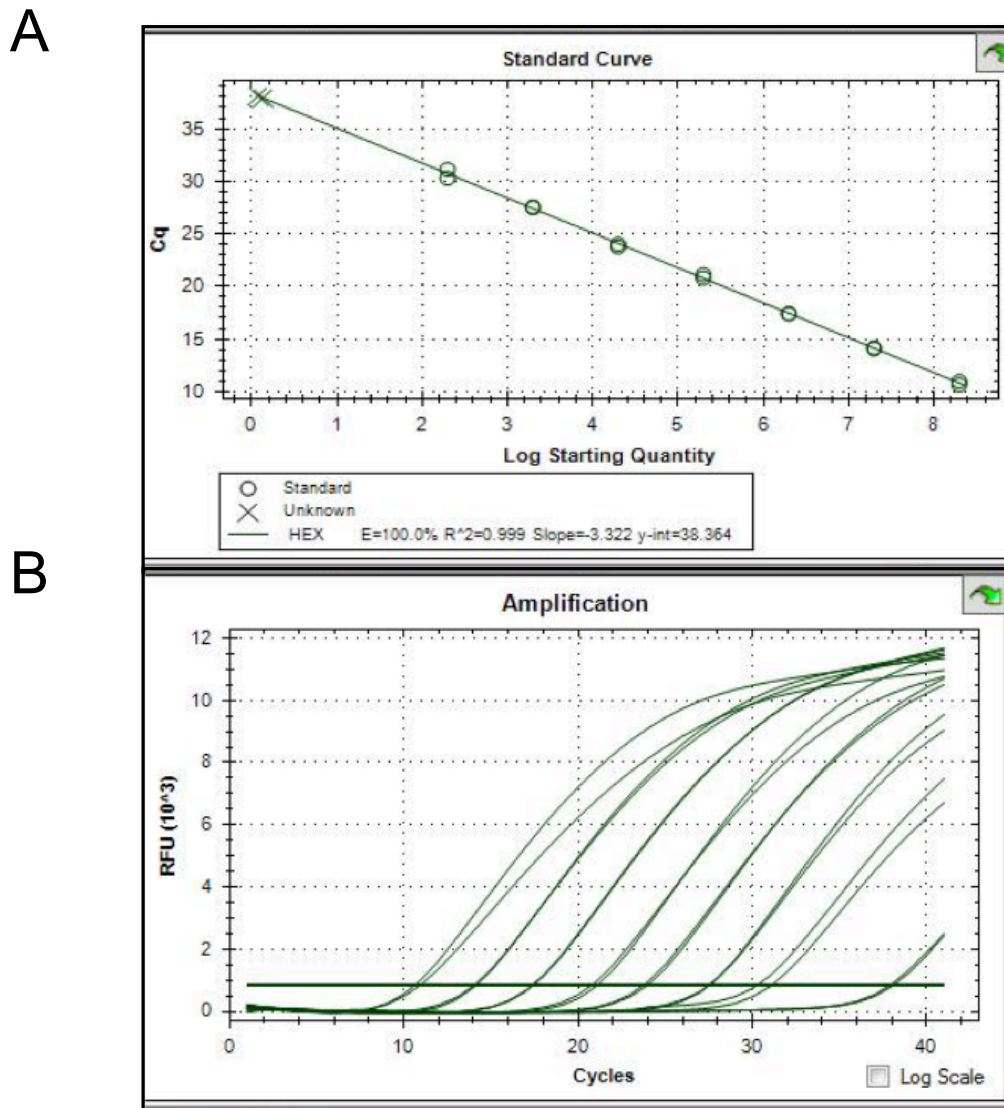


Figure 2.1. Analysis of quantitative PCR data. (A) Standard curve and (B) amplification plots generated by CFX Manager Software using serial dilutions of MT-ND1 template (E= Reaction efficiency, R^2 = coefficient of determination)

2.3.10 Gene expression analysis

2.3.10.1 RNA isolation from cultured cells

RNA was isolated from fibroblast cells using RNeasy Mini Kit (Qiagen). All buffers were supplied with the kit. Cells were harvested from culture flasks and pelleted as described in **Section 2.1.2**. Approximately 1×10^6 cells were lysed in 350 μ l of Buffer RLT containing 0.1% β -mercaptoethanol (Sigma). This mixture was then transferred into an Eppendorf microcentrifuge tube and rotated on a tube rotator for 5 minutes. Following this 350 μ l of 70% ethanol was added and the mixture was transferred to an RNeasy spin column in a 2 ml collection tube. After centrifugation for 15 seconds at $8000 \times g$ the flow through was

discarded and 700 μ l of Buffer RW1 was added. This mixture was centrifuged for 15 seconds at $8000 \times g$ and the flow through was discarded and 500 μ l of Buffer RPE was added and the column centrifuged for 2 minutes. The spin column was then placed in a fresh 1.5 ml collection tube and 45 μ l of RNase free water was used to elute the sample by centrifugation at $8000 \times g$ for 1 minute. The RNA concentration was ascertained using the NanoDrop 2000 spectrophotometer (UVP) and the sample was then stored at -80°C for further analysis.

2.3.10.2 Complementary DNA (cDNA) synthesis

cDNA was synthesised from RNA isolated from fibroblast cell lines as described in **Section 2.3.10.1** using High-Capacity cDNA Reverse Transcription Kit (Applied Biosystems). All reagents were supplied with the kit. To denature the RNA 1.8 μ g of sample was made to 14.2 μ l with water and combined with 2 μ l 10X RT buffer, 0.8 μ l 25X dNTP mix (100 mM), 2 μ l 10X RT Random Primers, 1 μ l MultiScribe Reverse Transcriptase and briefly centrifuged. All reactions were performed on ice in a total volume of 20 μ l. The samples were then incubated at 25°C for 10 minutes, 37°C for 120 minutes and 85°C for 5 minutes in a Veriti[®] 96-well Thermal Cycler. The samples were then stored for future analysis as described in **Section 2.3.10.1**.

2.3.10.3 Quantitative Real Time PCR for gene expression

Quantification of the expression of specific genes was carried out with qPCR using the TaqMan gene Expression Assay (Applied Biosystems) as described in **Section 2.3.9**. The assay was performed on the 7500 Fast Real Time PCR System (Thermo Fisher Scientific) using the following mix: 10 μ L 2 x TaqMan Gene Expression Master Mix, 1 μ L 20 X Taqman Gene Expression assay (**Table 2.3**), 7 μ L RNase free water and 2 μ L cDNA. The reaction cycling conditions were as follows, initial incubation at 50°C for 2 minutes, denaturing at 95°C for 20 seconds and 40 cycles annealing at 60°C for 30 seconds and 95°C for 3 seconds. Serial 1:10 dilutions of cDNA in RNase free water were used to ensure linearity and efficiency of the reaction and for standard curve quantification. Each sample was measured in triplicate and a cDNA negative control was used to exclude contamination of reagents. The relative amount of cDNA for each target gene was calculated by comparison with a housekeeping gene (*GAPDH*) whereby:

$$\text{Delta Ct} = \text{Ct Target Gene} - \text{Ct GAPDH}$$

$$\text{Relative RNA transcription} = 2^{-\text{delta Ct}}$$

Table 2.3. Details of the Taqman Gene Expression Assays used in qPCR for gene expression analysis

Gene	Assay ID	Amplicon length (bp)
<i>SSBPI</i>	Hs00995376_g1	80
<i>MT-CYB</i>	Hs02596867_s1	151
<i>GAPDH</i>	Hs02758991_g1	63

2.3.11 Pyrosequencing

Pyrosequencing of extracted DNA was performed to quantify mtDNA heteroplasmy levels at m.1555. Pyrosequencing enables real time DNA sequencing based on the detection of pyrophosphate released during DNA elongation. A specific pair of PCR primers is used to generate a locus specific amplicon (approximately 200 bp) where the reverse primer is biotin labelled. A sequencing primer is then used to amplify the region of interest and quantify heteroplasmy levels.

The procedure firstly converts the double stranded PCR products into single stranded fragments. The biotin labelled strand is then used as the template for Pyrosequencing by the addition of a sequencing primer with specific nucleotide dispensed to a known order. Pyrophosphate molecules are released when the nucleotide is incorporated into the elongating strand and converted by ATP-sulfurylase into ATP. This is used to drive a luciferase dependent light response that can be detected using a charged couple device (CCD) camera. The output is represented in the form of a pyrogram peak providing information on the percentage level of A and G present at the m.1555 nucleotide location. Apyrase eliminates excess nucleotides that would otherwise interfere with subsequent reactions. The cycle was repeated for each dNTP type at each DNA-strand nucleotide.

2.3.11.1 Pyrosequencing assay design

PCR and sequencing primers for the assay were designed using PyroMark Assay Design Software 2.0 (Qiagen). The *MT-RNR1* sequence was visualised in Ensembl

(<http://www.ensembl.org>) and 400 bp surrounding the variant of interest was entered into the software. The Allele Quantification mode was selected and the base change A/G was inserted at the appropriate position. The primers are given a ranking of 0 to 100 based on predicted fidelity of PCR. The highest scoring primer pair was selected. The reverse primer was biotinylated for product identification. The software generated the dispensation order of nucleotides for sequencing (**Table 2.4**).

Table 2.4. Details of the primers used in Pyrosequencing analysis

Primer	Sequence 5'-3'
Forward	GACATTAACTAAAACCCCTACGC
Reverse (5'biotin—3')	TTTGGCTAAGGTTGTCTGGTAGTA
Sequencing	CCCTACGCATTTATATAGAG
Sequence to analyse	GAGA/GCAAGTCGTAACATGGTAAGTGTACT

2.3.11.2 Pyrosequencing procedure

Amplification of the primary PCR product was performed by standard PCR as described in **Section 2.3.4**. The cycling conditions were as follows: denaturation at 95°C for 10 minutes, followed by 30 cycles of 96°C for 30 seconds, annealing at 60°C for 30 seconds and extension at 72°C for 30 seconds, followed by 72°C for 10 minutes. An aliquot of the PCR product was electrophoresed on an agarose gel to check product size as described in **Section 2.3.5**.

Pyrosequencing was performed using a Pyromark Q24 Instrument (Qiagen). To start the assay 10 µl PCR sample was added into an 8 tube PCR strip (Starlab). This was made to 80 µl with 28 µl dH₂O, 40 µl PyroMark Binding Buffer (Qiagen) and 2 µl Streptavidin Sepharose High Performance beads (GE Healthcare, Amersham, UK). The sepharose beads bind to the biotin labelled strand by shaking the plate for 15 minutes on a microplate agitator (Bioshake IQ, Quantifoil Instruments, GmbH, Germany). Once the samples had been agitated they were transferred to the PyroMark Q24 Workstation (Qiagen). The workstation consists of 6 reservoirs that are filled to the marked line. The reservoirs are as follows: 70% ethanol, PyroMark Denaturation Solution (Qiagen), PyroMark 1X washing buffer (Qiagen), parking (unfilled reservoir) and two dH₂O reservoirs.

The samples were taken up by the Workstation vacuum pump tool, to which the sepharose beads adhered. The vacuum pump was then placed in 70% ethanol for 10 seconds with the vacuum pump turned on to remove any contaminants. The vacuum pump was next placed in Denaturation Solution for 5 seconds whilst turned on. This removes the opposite DNA strand leaving only the attached single-stranded DNA with biotin label. The vacuum pump was then placed in Wash Buffer for 10 seconds. After this the pump was switched off and held vertically to remove excess liquid. The pump was then placed into a 24-Well PyroMark Q24 Plate (Qiagen), with each well containing 2.5 μ l PyroMark Sequencing Primers (Qiagen) and 22.25 μ l PyroMark Annealing Buffer (Qiagen), to allow the single-stranded DNA to enter the mixture.

The plate was incubated at 80°C for 2 minutes on a hot block (Digital Dry bath, Accublock, Labnet, NJ, USA) then cooled to room temperature to allow primer binding. The plate was then placed into the Pyromark Q24 Instrument (Qiagen). The PyroMark Q24 Software (Qiagen) was used to create a plate map by loading the designed assay as described in **Section 2.3.11.1**. This generates a pre-run information sheet detailing the volumes of reagents (PyroMark Gold reagents, Qiagen) to be used. The generated run file is saved to a USB drive for use in the Pyrosequencer.

The sequencing cartridge was loaded with the pre-determined volumes of Pyromark Enzyme Mixture (containing DNA polymerase, ATP-sulfurylase, luciferase, and apyrase), PyroMark Substrate Mixture (containing adenosine 5' phosphosulfate and luciferin), and nucleotides (dATP, dTTP, dGTP, and dCTP) (PyroMark Gold reagents, Qiagen) as determined by the Pyromark Q24 Software. Typical loaded volumes were as follows: 116 μ l enzyme, 116 μ l Substrate Mixture and 57 μ l of the 4 separate dNTPs.

The reaction was performed and the sequencing cartridge and reservoirs were thoroughly cleaned. Data, in the form of representative pyrograms were analysed using PyroMark Q24 Software (**Figure 2.2**).

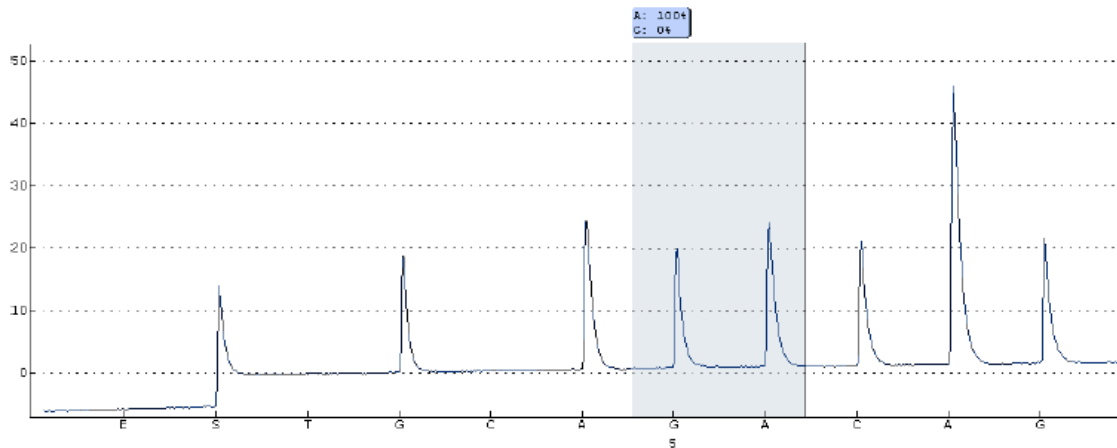


Figure 2.2. Pyrosequencing for allelic quantification. A representative pyrogram from a Pyrosequencing reaction for the allelic quantification of m.1555 using a wild type control (100% A at m.1555).

2.3.11.3 Generation of assay standard curve

In order to assess the accuracy of the Pyrosequencing reaction a standard curve of m.1555A>G heteroplasmy levels was constructed by proportional dilution of a known 100% m.1555 G sample with wild type DNA (100% A at m.1555). The dilutions were as follows: 100% G, 90% G, 75% G, 50% G, 25% G, 10% G and 0% G. The data was plotted as observed to expected heteroplasmy level and represented in **Figure 2.3**.

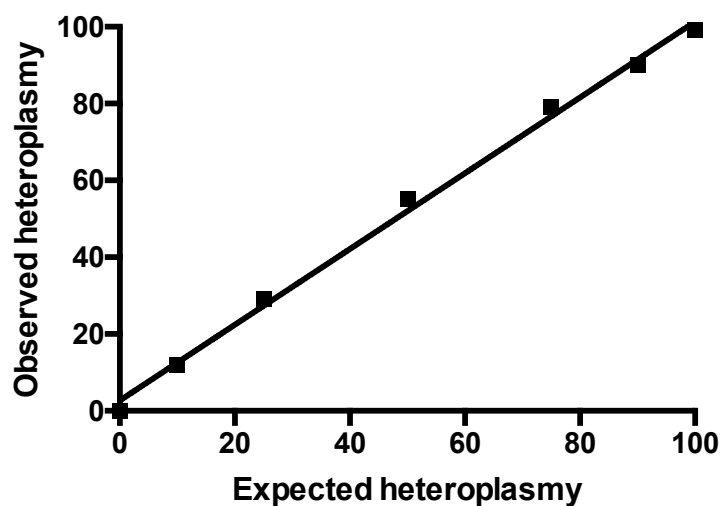


Figure 2.3. Pyrosequencing standard curve. The observed compared to expected heteroplasmy levels at m.1555 are compared by construction of a standard curve (Coefficient of determination $R^2=0.997$)

2.3.12 Analysis of mitochondrial 7S DNA

2.3.12.1 *Smash and grab extraction of total cellular DNA*

Total cellular DNA was isolated by two sequential phenol-chloroform extractions with subsequent precipitation. Phenol-chloroform extraction is a liquid-liquid based extraction method based on the differing solubilities of compounds in two different immiscible liquids. Proteins segregate into the denser organic phase whereas nucleic acids remain in the less dense aqueous phase. Culture vessels of confluent fibroblast cells were harvested as described in **Section 2.1.2** and lysed using 16 ml of ‘Smash and Grab’ lysis buffer (75mM NaCl, 50mM acid EDTA pH 8, 20mM HEPES pH 7.8, 0.5% (w/v) sodium dodecyl sulphate (SDS), 0.2 mg/ml Proteinase K at 37°C, all Thermo Fisher Scientific). To this 16 ml of phenol (Sigma-Aldrich) was added and the mixture was agitated for 15 minutes at room temperature. The mixture was then centrifuged at $5200 \times g$ for 15 minutes at room temperature and the aqueous phase isolated. This was then mixed with an equal volume of chloroform/isoamylalcohol (24:1) (Sigma-Aldrich), and agitated for 15 minutes at room temperature followed by centrifugation at $5200 \times g$ for 15 minutes at 4°C. The aqueous phase was again isolated and a final concentration of 100 mM NaCl was added (using a stock solution of 175 mM NaCl) to precipitate the DNA. This was followed by addition of an equal volume of isopropanol and centrifugation at $5200 \times g$ for 10 minutes at 4°C to pellet the DNA. The pellet was washed with 1 ml of 70% ethanol, transferred to an Eppendorf microcentrifuge tube and centrifuged at $21000 \times g$ for 5 minutes at 4°C. The pellet was air-dried and re-suspended in 415 μ l TE buffer (10mM Tris-HCl pH 7.4, 1mM EDTA) overnight. Following this, 7.5 μ l of 5 M NaCl, 50 μ l of 0.5 M EDTA, 5 μ l of 20 mg/ml proteinase K, 12.5 μ l of 20 % sodium lauroyl sarcosinate (Sigma-Aldrich) and 10 μ l of 1 M HEPES-NaOH pH 7.8 (Thermo Fisher Scientific). The mixture was incubated at 4°C for 30 minutes followed by an addition of an equal volume of phenol before centrifugation at $21000 \times g$ for 5 minutes at room temperature. The aqueous phase was isolated and mixed with an equal volume of chloroform/isoamylalcohol (24:1). This was then centrifuged at $21000 \times g$ for 5 minutes at 4°C. The aqueous phase was isolated and a final concentration of 100 mM NaCl was added (using a stock solution of 175 mM NaCl) followed by an equal volume of isopropanol with gentle mixing. The mixture was incubated at 4°C for 10 minutes and then centrifuged at $21000 \times g$ for 10 minutes at 4°C. The pellet of DNA was air-dried and re-suspended in 150 μ l TE buffer. The concentration and quality of the DNA were determined as described in **Section 2.3.1**.

2.3.12.2 DNA restriction enzyme digestions

Five µg of total DNA was restricted in 25 µl reactions using 10 units of PvuII restriction enzyme (New England Biolabs, MA, USA) and 10X NeBuffer 3.1 (New England Biolabs) for 2.5 hours at 37°C. Each sample was combined with 2.5 µl of 10X DNA loading dye (0.25% (w/v) bromophenol blue, 0.25% (w/v) xylene cyanol, 40% (v/v) glycerol, all Thermo Fisher Scientific) and loaded on to a 0.6% agarose gel as described in **Section 2.3.5**.

2.3.12.3 Southern blotting

Following the separation of restricted DNA fragments by electrophoresis the agarose gel was depurinated in 0.25N HCL (Thermo Fisher Scientific) for 20 minutes with gentle agitation. The gel was then denatured by twice incubating in a buffer consisting of 0.5 M NaOH (Sigma-Aldrich) and 1.5 M NaCl for 10 minutes. This was followed by twice incubating in a buffer consisting of 5M Tris-HCl pH 7.4 and 1.5 M NaCl for 10 minutes. The gel was then dry blotted overnight using weights on to a nylon membrane and then cross-linked by UV exposure (254 nm, 120 mJ/cm²).

2.3.12.4 Preparation of radiolabelled probes

Probes were PCR amplified from total HeLa cell DNA using *Taq* polymerase with specific primers (**Table 2.5**) and purified using a PCR purification kit (performed by Dr Payam Gammage, Mitochondrial Biology Unit, Cambridge, UK). OLB buffer A (2 M HEPES pH 6.6) and OLB buffer B (1.25 M Tris-HCl pH 8, 125 mM MgCl₂ (Thermo Fisher Scientific), 250 mM β-mercaptoethanol (Sigma-Aldrich), 0.5 mM dATP, dGTP and dTTP (Promega, WI, USA)) were mixed in a 5:2 ratio to make 1X OLB buffer. Fifty ng of PCR product was heated at 95°C for 5 minutes and labelled by adding 10 µl 1X OLB buffer, 5 U Klenow polymerase (New England Biolabs), 2 µl 1 mg/ml BSA (Sigma-Aldrich), 1 µl of 50 mM random hexamers (Thermo Fisher Scientific), 13 µl nuclease-free water (Thermo Fisher Scientific) and 3 µl of α-³²P dCTP (111 TBq/mmol, Perkin Elmer, Beaconsfield, UK), at 37°C for 1 hour. The probe was then further purified by adding it to a Sephadex® size exclusion spin column (Sigma-Aldrich) and centrifuging at 8000 × g for 5 minutes to remove excess ³²P. The purified probe was then heated at 95 °C for 5 minutes.

Table 2.5. Primer sequences for preparation of radiolabelled dsDNA probes

Probe		Sequence 5'-3'	mtDNA position
A	Forward	CTAGGATACCAACAAACCTACCC	16270 - 16292
A	Reverse	CTGTTAGGCTGGTGTAGGG	389 – 369
28S	Forward	GCCTAGCAGCCGACTTAGAACTGG	-
28S	Reverse	GAGGTGTAGAATAAGTGGGAGGCC	-

2.3.12.5 Hybridisation with radiolabelled probes

The membrane was blocked by incubation in 25 ml Church's Buffer (0.25 M phosphate buffer, 7% (w/v) SDS) for 1 hour at 65°C in a hybridisation tube. The buffer was then replaced with 15 ml of Church's buffer that included the labelled probe and heated at 65°C for 12 hours. The probe was then removed and stored for future use. The membrane was washed in 50 ml 1X saline-sodium-citrate (SSC) (150 mM NaCl, 15 mM sodium citrate pH 7 (Sigma-Aldrich)) three times for 30 minutes.

2.3.12.6 Imaging of radiolabelled blots

The labelled membrane was exposed to a BAS Storage Phosphor screen (GE Healthcare) for 72 hours, scanned on a Typhoon 9410 scanner (GE Healthcare) and quantified using ImageJ software (National Institutes for Health, Maryland, USA).

2.3.13 Mitochondrial repopulation assay

The mitochondrial repopulation assay determines the rate of mtDNA repopulation after depletion using the intercalating agent ethidium bromide (EtBr).

2.3.13.1 Optimisation of experimental protocol

Fibroblast cells were seeded in T25 flasks at 1.7×10^4 cells per flask in supplemented high glucose DMEM with the addition of uridine to avoid selection against respiratory incompetent cells due to loss of functional dihydroorotate dehydrogenase occurring in mitochondria lacking mtDNA. Alternatively, cells were grown in glucose free DMEM supplemented with 5 mM galactose (Sigma-Aldrich), 2 mM L-glutamine, 1 mM sodium pyruvate, 10% FCS and 50 µg/ml uridine. Mitochondrial DNA depletion was undertaken by supplementing the medium with 50 ng/ml EtBr for 15 days. At this point the cells were

switched to grow in supplemented high glucose DMEM cell culture medium without EtBr for a further 21 days. For each cell line, EtBr treated cells were grown in parallel with untreated controls. At day 0, 3, 6, 15, 23, 29 and 36, treated and untreated cells were pelleted individually and used for independent technical replicates or to reseed T25 flasks in order to continue the experiment (**Figure 2.4**). Genomic DNA isolation from individual pellets was performed as described in **Section 2.3.1**. The mtDNA copy number was determined by performing the *MT-ND1/B2M* qPCR assay as described in **Section 2.3.9**.

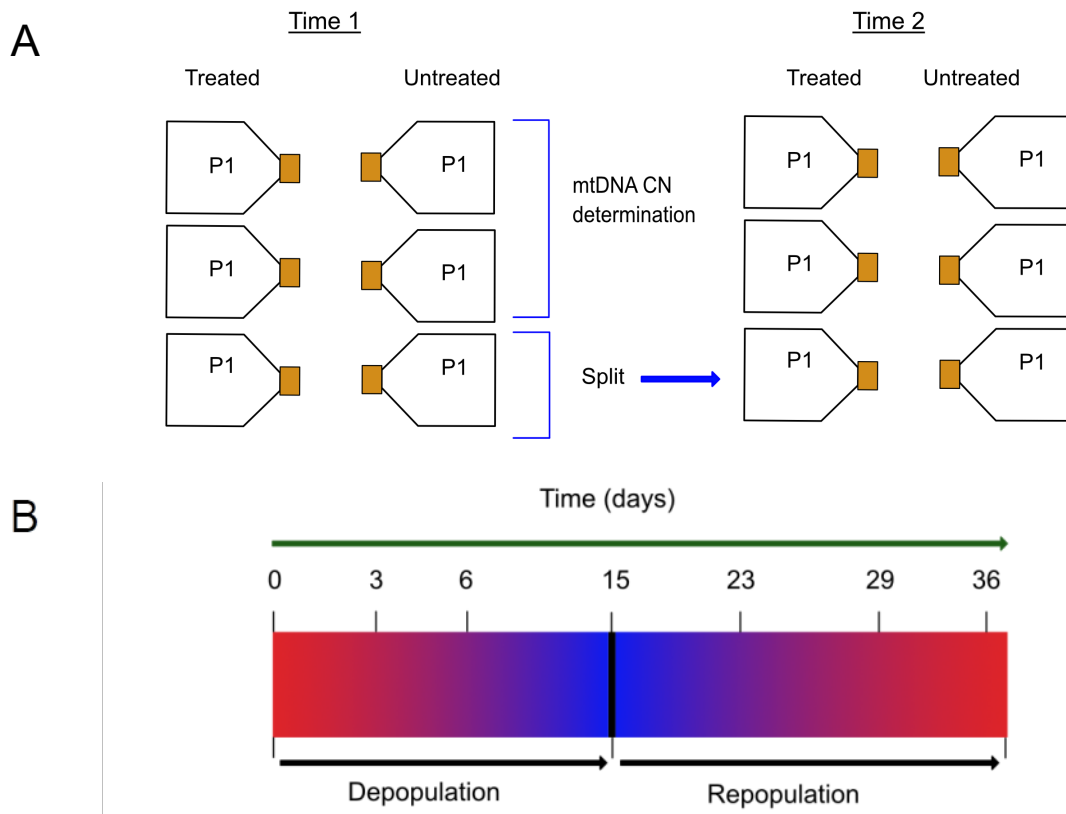


Figure 2.4. Mitochondrial repopulation optimisation experiment. (A) Fibroblast cells treated with EtBr to cause depopulation of mtDNA in parallel with untreated cells were grown in T25 flasks. At each time point indicated in (B) cells were harvested for mtDNA copy number determination.

2.3.13.2 Calculation of mtDNA repopulation level

The repopulation level (RL) was determined at each time point as a ratio of mtDNA copy number of treated cells to mtDNA copy number of untreated cells as follows:

$$RL = \frac{\text{Copy Number Treated}}{\text{Copy Number Untreated}}$$

2.3.13.3 Mitochondrial repopulation assay with shorter depletion phase

Cells were seeded at 3×10^4 cells per well in 6 well plates in either (i) supplemented high glucose DMEM or (ii) glucose free DMEM with 5 mM galactose (Sigma-Aldrich) supplemented as described in **Section 2.3.13.1**. mtDNA depletion was undertaken by supplementation with EtBr at a concentration of 50 ng/ml for 4 days. At this point, the cells were switched to growth in supplemented high glucose DMEM without EtBr for a further 6 days. For each cell line in a 6 well plate, 3 wells of EtBr treated cells were grown in parallel with 3 wells of untreated controls. At day 0, 4, 6, 8 and 10 cells were pelleted individually and used for independent technical replicates or to reseed six well plates in order to continue the experiment as described in **Section 2.3.13.1 (Figure 2.5)**. Genomic DNA isolation from individual pellets was performed as described in **Section 2.3.1**. The mtDNA copy number was determined by performing the *MT-ND1/B2M* qPCR assay as described in **Section 2.3.9**. RL for each time point was determined as described in **Section 2.3.13.1**.

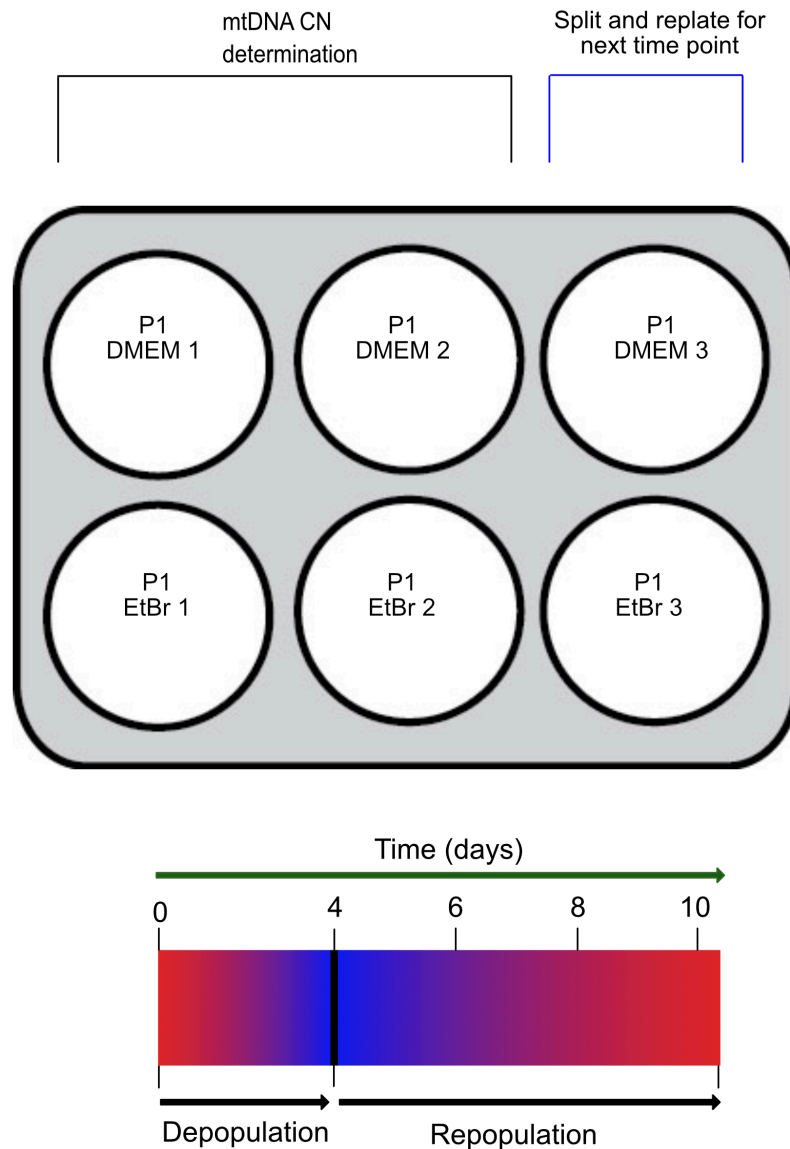


Figure 2.5. Modified mitochondrial repopulation experiment with shorter depopulation phase. (A) Fibroblast cells treated with ethidium bromide to cause depopulation of mtDNA in parallel with untreated cells were grown in six well plates. At each time point indicated in (B) cells were harvested for mtDNA copy number determination.

2.3.14 Generation of Whole Exome Sequencing data

One μg total cellular DNA was fragmented and enriched by TruSeq™ DNA Sample Preparation Kit and TruSeq™ 62 Mb Exome Enrichment Kit (Illumina, CA, USA). Sequencing was performed on an Illumina HiSeq 2000 Sequencing System (Illumina) with 100 bp paired-end reads by AROS (AROS Applied Biotechnology A/S, Aarhus, Denmark)

2.3.14.1 Bioinformatic analysis

Read alignment, variant calling and annotation was undertaken by Dr Helen Griffin (Newcastle University, UK). FASTQ files were initially checked for quality control using FASTQC (Babraham Bioinformatics, UK), a java application that quantifies data quality by analysing a number of parameters including GC content and per base Phred scores quantifying the probability that a nucleotide base is called correctly.

Reads were aligned to UCSC hg19 (<https://genome.ucsc.edu>) using Burrows-Wheeler Aligner (BWA) (Li and Durbin 2010). Subsequently, duplicate DNA sequencing reads were removed with Picard v1.85 (Broad Institute, MA, USA). GATK (Genome Analysis Toolkit) was used to detect single nucleotide variants (SNVs) and insertion/deletions (INDEL) using standard filtering parameters according to GATK Best Practice Recommendations for detection of somatic SNPs in exomes (DePristo, Banks et al. 2011). GATK performs SNV and INDEL calling by comparing the aligned read file against the reference genome producing a Variant Call Format (VCF) file. A single multi-sample VCF, containing data from all sequenced exomes, was created using VCFtools (<http://vcftools.sourceforge.net/>). Read depth and exome coverage was computed using SAMTools (Li, Handsaker et al. 2009).

Interrogation of mtDNA variants was performed using MITOMASTER, an online bioinformatic tool that performs automatic evaluation of inputted mtDNA sequence variation through comparisons against data sets encompassing information such as common mtDNA pathogenic mutations and known haplogroups polymorphisms (Brandon, Ruiz-Pesini et al. 2009). mtDNA variants were subsequently manually cross-referenced using Phylotree (www.phylotree.org), a comprehensive phylogenetic tree of global mtDNA variation (van Oven and Kayser 2009).

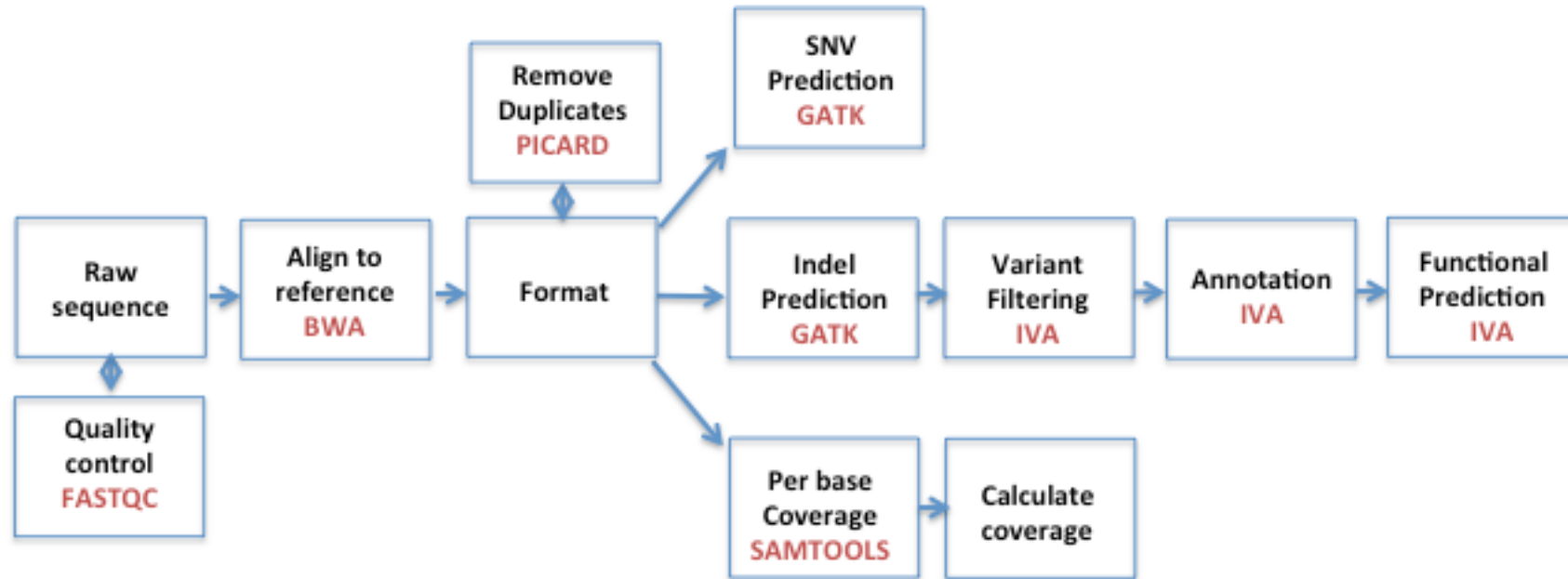


Figure 2.6. A schematic of the bioinformatic pipeline used to analyse exome sequencing data. Bioinformatic programmes as described in Section 2.3.14.1 and 2.3.14.2.

2.3.14.2 *Ingenuity Variant Analysis and in silico prediction tools*

Ingenuity Variant Analysis (IVA) is a cloud-based application that allows the iterative filtering of variants to a manageable number of candidates that can be then prioritised for further analysis. The platform supports the upload of a multi-sample VCF file (e.g. containing cases and controls) before annotation with relevant metadata from the 'Ingenuity Knowledge Base'. Four levels of variant filtration are automatically applied to the data. Firstly, the 'Confidence filter' considers only variants with a Phred score of 20 in at least one case or control and a read depth of 10 to remain within the dataset. The Frequency filter removes variants on the basis of a specified minor allele frequency e.g. >1% in ExAc, 1000 Genomes Project and NHLBI ESP (National Heart Lung and Blood Institute Exome Sequencing Project) (Genomes Project, Auton et al. 2015, Lek, Karczewski et al. 2016). Following this, the 'Predicted Deleterious' filter keeps only variants deemed Pathogenic, Likely Pathogenic or Uncertain Significance in accordance with the American College of Medical Genetics guidelines (ACMG). IVA computationally implements these guidelines in conjunction with clinical evidence from the Ingenuity Knowledge Bank to automatically provide ACMG classifications. This filter also highlights variants that are associated with a gain or loss of function. Loss of function variants includes missense, frameshift, in-frame indel, change to start/stop codon or splice site change. IVA integrates external pathogenicity prediction tools SIFT (Kumar, Henikoff et al. 2009) and PolyPhen-2 (Adzhubei, Jordan et al. 2013). These *in-silico* prediction tools estimate potential pathogenicity on the degree of sequence homology and the degree of conservation across evolutionarily diverse species.

The Genetic Filter allows filtration by zygosity depending on the suspected mode of inheritance e.g. heterozygous changes for autosomal dominant conditions, homozygous or compound heterozygous changes for autosomal recessive conditions. The final gene list can then be prioritised by gene function by either manually searching through the linked Gene Ontology and OMIM Gene Descriptions or by using the in-built Biological Context Filter. This filter highlights genes involved in relevant diseases, processes, pathways or phenotype.

Further pathogenicity prediction was undertaken using MutationTaster (Schwarz, Rodelsperger et al. 2010) and LRT (Chun and Fay 2009). Open reading frame (ORF) prediction was undertaken using ORF Finder (http://www.bioinformatics.org/sms2/orf_find.html). Multiple

sequence alignments were undertaken using the Clustal Omega bioinformatic tool (<http://www.ebi.ac.uk/Tools/msa/clustalo/>).

2.4 Protein analysis methodology

2.4.1 Preparation of cell lysates

Cells were harvested from culture vessels by first washing in PBS followed by trypsinisation and pelleting as described in **Section 2.1.2**. Lysis of the cell pellet was performed either using a lysis buffer (50 mM Tris HCL pH 7.5, 130 mM NaCl, 2 mM magnesium chloride, 0.1% Triton X, all Sigma-Aldrich) and supplemented with a Protease inhibitor (Roche) or a Cell Extraction buffer (FNN0011, Thermo Fisher Scientific) (1 ml per 1×10^8 cells) supplemented with 1 mM phenylmethylsulphonyl fluoride (PMSF) designed to minimise cellular phosphatases. On ice, 50 μ l lysis buffer was added to the cell pellet for 30 minutes, vortexing every 10 minutes. The extract was then centrifuged at $8000 \times g$ for 10 minutes. The supernatant was then aliquoted into fresh microcentrifuge tubes and stored at -80°C .

2.4.2 Quantification of protein

The Bradford assay was used to quantify protein concentration (Bradford 1976). The assay is based on a shift in the maximum absorbance at 595 nm detected by the spectrophotometer when an acidic solution of Coomassie Brilliant Blue G-250 dye binds to proteins within the sample. Samples were diluted depending on amount of starting cellular material. A standard curve was established each time an assay was performed using 0.05 μ g, 0.1 μ g, 0.2 μ g, 0.3 μ g, 0.4 μ g and 0.5 μ g Bovine Serum Albumin (BSA, Sigma-Aldrich) per μ l solution. Ten μ l of the BSA standards and diluted samples were loaded in triplicate on to a 96 well microplate (Thermo Fisher Scientific). A blank was also used to correct for background absorbance. To each of the standards and diluted samples, 200 μ L of 1:5 dilution (in dH₂O) of Bradford solution (BioRad) was added and absorbance was determined by the Multiskan™ Ascent Plate Reader (MTX Lab Systems, FL, USA). The concentration of the test sample was determined relative to its absorbance by interpolation from the standard curve. An example of a standard curve is shown in **Figure 2.7**.

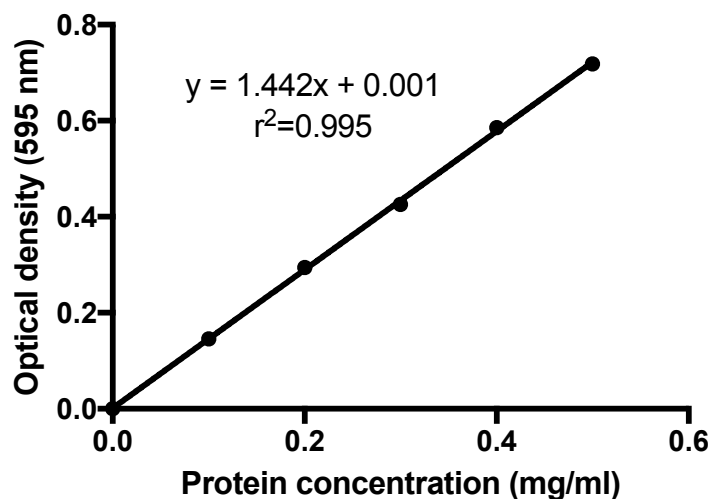


Figure 2.7. Bradford assay for protein quantification. Standard curve with linear regression of protein concentration against absorbance (measured at 595 nm). Coefficient of determination (r^2) >0.99.

2.4.3 Sample preparation

A 20 μ L sample volume was made by adding 2 μ L 10X Sample Reducing Agent, 5 μ L 4X LDS Sample Buffer (both Novex[®], Thermo Fisher Scientific), the appropriate volume of sample lysate based on the protein concentration as determined by the Bradford assay and the remaining volume was made with dH₂O. The samples were boiled at 70°C for 5 minutes in a dry bath incubator and then cooled on ice to allow protein denaturation. Samples were then vortexed and centrifuged at 8000 \times g for 1 minute.

2.4.4 Polyacrylamide gel electrophoresis (SDS-PAGE)

Samples were loaded on to 4-12% polyacrylamide gel (NuPAGE[®] Bis-Tris Precast Gels, Thermo Fisher Scientific) in an XCell SureLock electrophoresis system (Thermo Fisher Scientific). Gels were run for 2 hours at 150 V in 1x MES buffer with 500 μ L antioxidant (both NuPAGE[®], Thermo Fisher Scientific) until the molecular weight dye (SeeBlue Plus 2, Thermo Fisher Scientific) reached the bottom of the gel.

2.4.5 Western blotting

Transfer to a polyvinylidene difluoride (PVDF) membrane was undertaken using the iBlot 2 Semi Dry Transfer System (Thermo Fisher Scientific). The gel was removed from its casing using a plastering spatula and soaked in Tris Buffer Saline with Tween 20[®] (TBST buffer, consisting of 20mM Tris hydrochloride pH 7 (Sigma-Aldrich), 0.5mM NaCl

(VWR, Lutterworth, UK) and 0.1% Tween 20 (Sigma-Aldrich) for 1 minute. IBlot 2 Transfer Stacks were used as instructed by the manufacturer. The supplied filter paper was soaked in dH₂O and the stack assembled as follows; stack-membrane-gel-filter paper-stack. The P0 protocol for mixed molecular weight was used for 7 minutes at a constant 1.3 A.

The membrane was then washed with TBST buffer and then blocked with 5% (w/v) milk in TBST. Following this, the membrane was incubated with the primary antibody at 4°C under the conditions indicated in **Table 2.6**. The membrane was then washed three times for 5 minutes in TBST and incubated with secondary antibody for 2 hours at room temperature. After washing three times for 5 minutes in TBST, protein signal was detected by developing with Clarity Western ECL Western Blotting substrate (Bio-Rad) for 5 minutes in the dark. The membrane was then imaged using the Amersham Imager 600 (GE Healthcare). Densitometric analysis was performed using ImageQuant TL 8.1 software (GE Healthcare). GAPDH, a constitutively expressed protein, was used to normalize the results and the protein of interest : GAPDH ratio was calculated. To facilitate re-probing of membranes with additional primary antibodies, membrane stripping was undertaken by incubating with 20 ml Restore™ Western Blot Stripping Buffer (Thermo Fisher Scientific) for 30 minutes at 37°C. Following this, the membrane was incubated with the appropriate secondary antibody and developed to ensure there was no detectable signal before incubation with additional primary antibodies.

Table 2.6. Primary and secondary antibodies used in Western blotting.

Antibody	Company	Product ID	Host	Size	Conditions
Anti-AMPK alpha	Cell signalling	2532	Rabbit	63kD	1:1000 in TBST and 5% BSA
Anti-pT172 AMPK alpha	Cell signalling	40H9	Rabbit	63kD	1:200-1000 in TBST and 5% BSA
Anti-S6K	Cell signalling	9202	Rabbit	70kD	1:1000 in TBST and 5% BSA
Anti-pT389 S6K	Cell signalling	9205	Rabbit	70kD	1:1000 in TBST and 5% BSA
Anti-MTCO1	Abcam	ab14705	Mouse	40kD	1:1000 in 5% milk
Anti-SDHA	Abcam	ab14715	Mouse	70kD	1:5000 in 5% milk
Anti-MTCO2	Abcam	12C4F12	Mouse	26kD	1:1000 in 5% milk
Anti-TFAM	Source Biosci.	LS-C143233	Mouse	25kD	1:5000 in 5% milk
Anti-HSP60	Gene Tex	GTX110089	Rabbit	61kD	1:5000 in 5% milk
Anti-OXPHOS cocktail	MitoSciences	MS604	Mouse	55kD	1:250 in 5% milk
Anti-BiP	Abnova	PAB2462	Rabbit	78kD	1:4000 in 5% milk
Anti-HSP70	Abcam	ab182844	Rabbit	70kD	1:5000 in 5% milk
Anti-GPx1	Genetex	GTX116040	Rabbit	22kD	1:1000 in 5% milk
Anti-OPA1	Abcam	ab42364	Rabbit	93kD	1:2000 in 5% milk
Anti-TOMM20	Abcam	ab56783	Mouse	16kD	1:1000 in 5% milk
Anti-SSBP1	Proteintech	12212-1-AP	Rabbit	17kD	1:1000 in 5% milk
Anti-DRP1	Cell Signalling	D6C7	Rabbit	82 kD	1:1000 in TBST and 5% BSA
Anti-MFN2	Abcam	ab56889	Mouse	86 kD	1:2000 in 5% milk
Anti-GAPDH	Santa Cruz	sc-25778	Rabbit	38kD	1:1000 in 5% milk
Swine anti-rabbit HRP	DAKO	P0399	Swine	63kD	1:1000 in 5% milk
Rabbit anti-mouse HRP	DAKO	P0260	Rabbit	63kD	1:1000 in 5% milk

2.4.6 AMPK-Alpha 1 ELISA

Total cellular AMPK- α 1 was measured using an *in vitro* SimpleStep ELISA (Enzyme-linked immunosorbent assay) (Abcam, MA, USA. Product, ab181422). This assay uses an affinity tag labelled capture antibody with a reporter conjugated detector antibody that can immune-capture the sample analyte (AMPK- α 1) in solution. This complex is then immobilized by an anti-tag antibody that coats the well of the ELISA plate. The assay was performed following the manufacturer's instructions. Cell lysates were diluted 1:10 with 1X cell extraction buffer and a total of 5 μ g of total protein was loaded for each sample. A standard curve was constructed by reconstitution of the provided AMPK- α 1 standard sample. Absorbance was measured at 450 nm using the MultiSkan Ascent plate reader. The concentration of AMPK- α 1 (ng/ml) in the sample was calculated by interpolating the blank subtracted absorbance values against the standard curve and multiplying by the dilution factor (10X) (**Figure 2.8**).

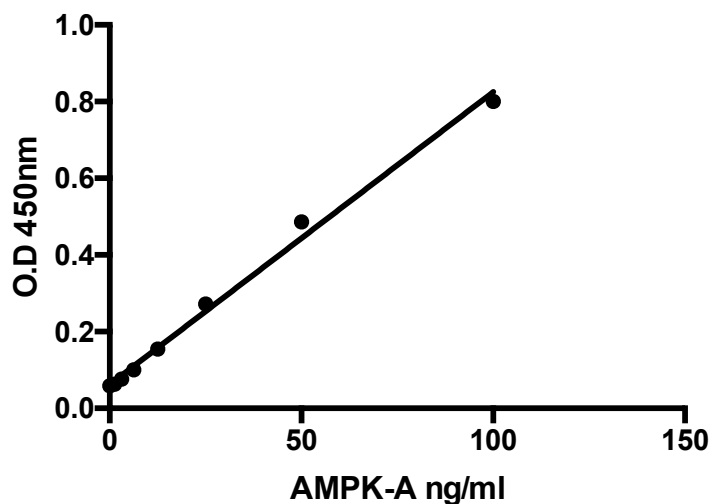


Figure 2.8. Typical standard curve of AMPK-A SimpleStep ELISA

2.4.7 Phospho-AMPK pT172 ELISA

Phosphorylation of AMPK Threonine-172 was measured by the Phospho-AMPK (pT172) ELISA Kit (Thermo Fisher). This assay is a solid phase sandwich ELISA where an AMPK- α 1 specific monoclonal antibody is immobilized in the wells of an ELISA plate. Samples are pipetted into the wells of the ELISA plate and incubated allowing the AMPK- α 1 antigen to bind the immobilized (capture) antibody. After washing a detection antibody specific for AMPK- α 1 phosphorylated at Threonine 172 is added

followed by a horseradish peroxidase (HRP) labelled Anti-Rabbit IgG. The assay was performed in accordance with the manufacturer's guidelines. A standard curve was constructed by reconstitution of the provided phosphorylated recombinant AMPK-alpha 1 phosphorylated standard. Absorbance was read at 450 nm using the MultiSkan™ Ascent plate reader. The activity of Phospho-AMPK (pT172) (AMPK-P) in the sample was calculated by interpolating the blank subtracted absorbance values against the standard curve and expressed as AMPK-P activity units/ml (**Figure 2.9**).

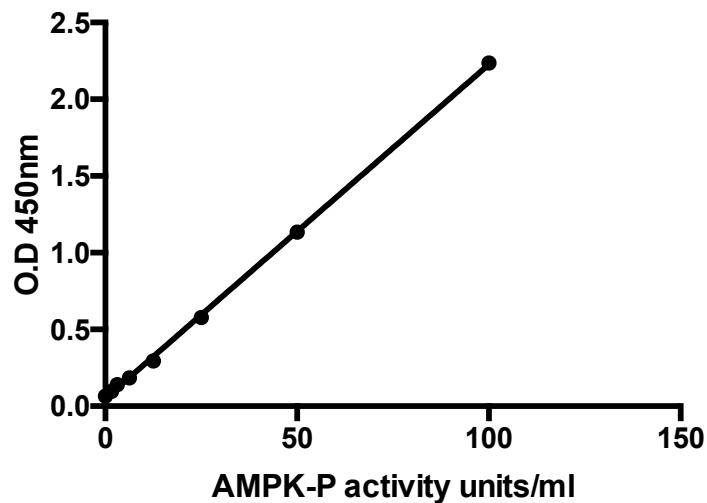


Figure 2.9. Typical standard curve of Phospho-AMPK (pT172) ELISA Kit

2.4.8 Optimisation of AMPK pT172 ELISA assay

Cell extraction from control fibroblasts was performed according to the manufacturer's instructions. To determine the amount of total protein to load into the assay, a standard curve was constructed by loading known quantities of this protein into the ELISA assay. The optimum amount of protein (40 µg) was chosen as the least amount of protein that lay on the linear part of the standard curve (**Figure 2.10**).

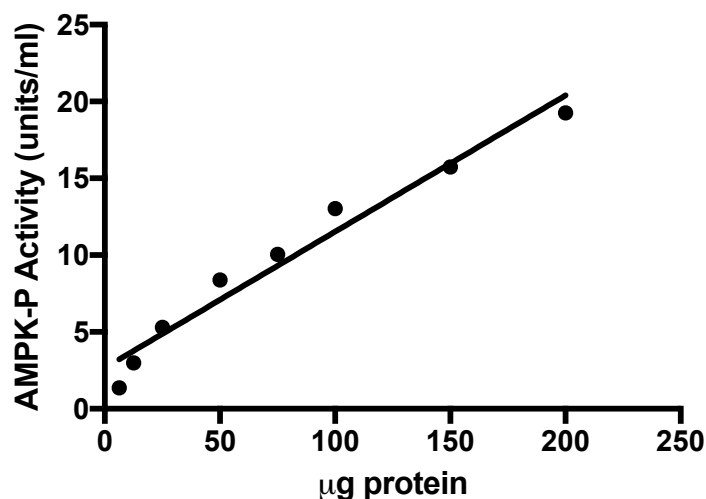


Figure 2.10. Optimisation of Phospho-AMPK (pT172) ELISA

2.4.9 Heat shock response assay

Fibroblast cells were plated in T25 culture vessels at a density of 3×10^5 cells per flask in supplemented high glucose DMEM. For each cell line, cells were either maintained at 37°C or treated with heat shock at 42°C for 1 hour and allowed to recover at 37°C for 4 hours. Cells were then harvested by pelleting as described in **Section 2.1.2**. Cell lysates were prepared as described in **Section 2.4.1**. Samples were then loaded on to 4-12% polyacrylamide gel and Western blot analysis was performed as described in **Section 2.4.5** using antibodies to HSP60, HSP70 and BiP (**Table 2.6**).

2.4.10 *In vivo* mitochondrial translation assay

Fibroblast cells were plated at a density of 3×10^5 cells/well in six well dishes (Corning Costar®, Sigma-Aldrich) and allowed to adhere for 24 hours. Following this, cells were washed twice in supplemented high glucose DMEM medium without methionine and cysteine (Gibco, Thermo Fisher Scientific) for 10 minutes at 37°C. In order to block cytosolic translation the cells were incubated in DMEM without methionine and cysteine supplemented with 10% dialysed FCS, 2 mM L-glutamine, 1 mM sodium pyruvate and a final concentration 100 µg/ml emetine dihydrochloride (Sigma-Aldrich) for 20 minutes at 37°C. Following this, 100 µCi EasyTag™ ³⁵S L-methionine (Perkin Elmer) was added to each well and incubated at 37°C for 1 hour after which the labelling mix was removed. The cells were harvested with 0.05% trypsin/PBS, collected and centrifuged at $500 \times g$ for 5 minutes. Cell pellets were further washed in PBS, re-pelleted and frozen at -80°C. Prior to

electrophoresis, samples were thawed and combined with 100 μ l PBS and incubated on ice for 20 minutes with 50 units Benzonase Nuclease (Novagen, WI, USA) and 0.1% n-Dodecyl β -D-maltoside (Sigma-Aldrich). The protein was then quantified as described in **Section 2.4.2**. For gel loading, 40 μ g protein was combined with 1X loading buffer and separated on a 4-12% (w/v) SDS-PAGE as described in **Section 2.3.5**. Sample loading was assessed by Western blot using TOMM20 as described in **Section 2.4.5**. Gels were then de-stained for 1 hour using de-stain solution (20% methanol, 7% acetic acid, Sigma-Aldrich). Gels were then dried at 80°C for 1 hour using a Bio Rad 583 Electrophoresis Gel Dryer (Bio Rad). Visualisation of proteins was performed as described in **Section 2.3.12.6**.

2.5 Immunocytochemistry

2.5.1 Mitochondrial network analysis

For each fibroblast cell line 1×10^5 cells were seeded in supplemented high glucose DMEM on a glass bottom dish (Willco, Amsterdam, Netherlands) and incubated for 24 hours to allow attachment. Medium was then aspirated and the cells were washed twice in PBS. The medium was replaced with medium containing 75 nM Mitotracker Red CMXRos (Thermo Fisher Scientific). Cells were incubated at 37°C, 5% CO₂ for 30 minutes. The cells were then washed twice in PBS and placed in 1 ml MEM medium without phenol red and supplemented with 25 mM HEPES (Sigma-Aldrich).

2.5.2 Imaging

The mitochondrial network was analysed using live-cell imaging. Individual images were acquired at room temperature with an inverted Nikon A1R confocal microscope (Nikon, Tokyo, Japan) using a 60 \times , 1.40 numerical aperture oil immersion objective. Images were acquired along the Z-axis using a piezo Z stage (69 Z-stacks of 0.12 μ m). These images were then reconstructed to model the mitochondrial network within each individual cell.

2.5.3 Image processing

Raw data files were converted into tagged image file format (TIFF) by NIS elements software (Nikon). A 3-Dimensional reconstruction of the mitochondrial network was then created using ImageJ to stack the 69 image planes acquired from each cell.

2.5.4 Huygens Essential Software analysis

The images were subsequently deconvolved with Huygens Essentials software (SVI, Hilversum, Netherlands) using the batch processor. Huygens Object Analyzer (SVI) was used to analyse the mitochondrial network of individually imaged fibroblasts for each cell line. The software uses a seed-threshold method to label specific objects whilst removing objects with a size below a set 'garbage' volume. The parameters were set as follows: threshold automatically determined, 0% seed and 60 voxels garbage volume. For each fibroblast, the following parameters were analysed: (i) the average length of mitochondrial fragments, and (ii) the total number of mitochondrial fragments. Average values were then generated for each individual cell line and the merged control dataset. The distribution of mitochondrial fragment lengths was determined by sorting mitochondrial fragments into bins defined by their length as follows: <2 μm , 2 to 5 μm , 5 to 10 μm and >10 μm .

2.5.5 Confocal microscopy imaging of mitochondrial nucleoids

Fibroblast cells were plated on to FisherBrand™ Borosilicate Glass Circle Coverslips (Thermo Fisher Scientific) and placed in 6 well tissue culture dish (Corning Costar®, Sigma-Aldrich) and incubated at 37°C, 5% CO₂ overnight. The cover slips were removed from the 6 well plate and rinsed once with 2 ml 1X PBS. Cells were then fixed by adding 1 ml 4% paraformaldehyde (Sigma-Aldrich) in PBS for 15 minutes at 37°C. This was followed by a further three washes with 2 ml PBS for 5 minutes. Cells were then permeabilized with the addition of 1% Triton X-100 (Sigma-Aldrich) in PBS for 5 minutes at room temperature. Cells were then washed again three times with 1 ml PBS for 5 minutes. Cells were then blocked by incubation with 1 ml 5% FCS in PBS at room temperature for 30 minutes. The blocking solution was removed and the cells were rinsed in 2 ml of PBS. The cells were then incubated at 4°C overnight with the primary antibodies, TOMM20 1:300 (Abcam, ab56783) and Anti-DNA 1:150 (Progen Biotechnik GmbH, Heidelberg, Germany) in PBS with 5% FCS. The cells were then washed with 2 ml PBS with 5% FCS for 5 minutes three times. The cells were then incubated with 1:1000 dilution of Alexa Fluor 488 goat anti-mouse IgG and Alexa Fluor 647 goat anti-rabbit IgG (both Thermo Fisher Scientific) in the dark for 1 hour at room temperature. Following this, the cells were washed three times for 5 minutes with 2ml PBS. To visualise the cells 10 μl of ProLong Gold Anti Fade Mountant with DAPI (Thermo Fisher Scientific) was applied to a microscope slide (VWR) and the cover slip was placed cell side down on to the

mountant. The slide was left to dry overnight. Slides were then imaged with the Zeiss Axio Imager (Carl Zeiss, Oberkochen, Germany).

2.6 Biochemical methodology

2.6.1 Measurement of cellular reactive oxygen species (ROS)

Cellular ROS were measured using the fluorescent cell permeant dye 2', 7'-dichlorofluorescein diacetate (H₂DCFDA). H₂DCFDA diffuses into the cell where it is deacetylated by cellular esterases to dichlorofluorescein (DCFH), a non-fluorescent compound that can be oxidized by cellular ROS including hydroxyl radicals, hydrogen peroxide and peroxynitrite to the highly fluorescent compound DCF.

Fibroblast cells were seeded at 3×10^4 cells/well in Nunc [™] Microwell 96- well optical bottom plates (Thermo Fisher Scientific) and allowed to adhere for 24 hours. Cells were then washed twice with PBS and incubated with H₂DCFDA (20 μ M, Thermo Fisher Scientific) in 100 μ l PBS for 30 minutes at 37°C. Following this, the cells were washed twice with PBS and fluorescence was measured on a Fluoroskan Ascent (Thermo Fisher Scientific) by excitation 485 nm followed by emission at 535 nm. The fluorescence signal was normalised to the amount of protein quantified by the Bradford assay as described in **Section 2.4.2**.

2.6.2 Oxidative DNA damage analysis

The Oxiselect [™] Oxidative DNA Damage kit (Cell Biolabs, CA, USA) measures 8-OHdG DNA modification by a competitive ELISA. Firstly, a microplate is conjugated with 8-OHdG/BSA by adding 8-OHdG conjugate overnight at 4°C. DNA was extracted from cell pellets using DNeasy Blood & Tissue Kit (Qiagen) and quantified as described in **Section 2.3.1**. To perform the assay 2.5 μ g of extracted DNA was converted to single-stranded DNA by boiling at 95°C. DNA was digested using 6 units of nuclease P1 (Sigma-Aldrich) for 2 hours at 37°C in a final concentration of 20 mM sodium acetate pH 5.2 (Sigma-Aldrich). This was then treated with 8 units alkaline phosphatase (Sigma-Aldrich) for 1 hour at 37°C in a final concentration of 100 mM Tris pH 7.5 (Sigma-Aldrich). This mixture was then centrifuged for 5 minutes at $6000 \times g$ and the supernatant was used for the ELISA performed in accordance with the manufacturer's instructions. Absorbance was measured at 450 nm on the MultiSkan Ascent plate reader and normalised to μ g of DNA.

2.6.3 Protein carbonylation analysis

Oxyblot™ Protein Oxidation Detection Kit (MerckMillipore, Darmstadt, Germany) was used to detect oxidative modification of the cellular proteome as directed by the manufacturer's instructions. Protein carbonyl groups are common forms of protein oxidation by reactive oxygen species. Cells were trypsinised, pelleted and lysed as described in (**Section 2.1.2 and Section 2.4.2**). Detection of protein carbonyl groups in the cell lysates was performed by derivatization of the carbonyl group to 2,4-dinitrophenylhydrazone using dinitrophenylhydrazine (DNPH). Then 7-9 µg was subjected to electrophoresis and transferred to a PVDF membrane. Following this, immunoblotting with an anti-DNP antibody and HRP-linked secondary antibody (provided with the kit) was performed according to the manufacturer's protocol. For each cellular lysate a second corresponding aliquot was treated with 1X Derivatization-Control Solution that acted as an untreated negative control. GAPDH protein levels in the corresponding negative control lane of the same gel were used as a loading control.

2.6.4 Assay of cellular respiration by Seahorse XF96^e Extracellular Flux Analyser

Cellular respiration was assessed with the Seahorse XF96^e extracellular flux analyser (Agilent Technologies, CA, USA). The Seahorse analyser measures real time oxygen consumption and extracellular acidification rate in intact live cells (OCR and ECAR respectively). A transient microchamber is created above a monolayer of cells plated in a Seahorse 96 well plate. A solid-state sensor probe is then used to measure the rate of change of dissolved oxygen. Different aspects of cellular respiration can be assessed by the use of a variety of chemical inhibitors of respiration. Oligomycin (1 µM, Sigma-Aldrich) blocks ATP synthase (Complex V) and enables determination of the proton leak through the mitochondrial membrane. Carbonyl cyanide 4-trifluoromethoxy phenylhydrazone (FCCP) (0.5 µM/1 µM, Sigma-Aldrich) is an uncoupling agent allowing protons to leak across the mitochondrial membrane. This enables determination of the maximal oxygen consumption and spare respiratory capacity. Rotenone and Antimycin A (1 µM, both Sigma-Aldrich) inhibit Complex I and III to abolish mitochondrial respiration and enable the determination of non-mitochondrial respiration.

Firstly, the sensor cartridge was pre-hydrated in a calibration plate containing 200 µl per well of XF Calibrant Solution at 37°C without CO₂ for 12 hours prior to the start of the assay. Fibroblasts were seeded into a 96 well microplate (Thermo Fisher Scientific) at 3

$\times 10^4$ cells per well in 175 μ l of XF Mito Stress Test Assay Medium containing MEM, 11.1 mM D-Glucose (Sigma-Aldrich) and 2 mM L-Glutamine (Thermo Fisher Scientific) adjusted to pH 7. The plate was then incubated for 1 hour in the non-CO₂ incubator. The chemical inhibitor drugs were then prepared in assay medium and loaded into the 4 injection ports in the sensor cartridge. The calibration plate was then replaced with assay plate containing the plated primary fibroblasts and the assay was started. Sequential addition of the chemical inhibitors allowed the following aspects of cellular respiration to be measured: endogenous respiration, maximal respiration and proton leak respiration. These were determined as follows: endogenous respiration is the difference between basal OCR and non-mitochondrial OCR; maximal respiration is the difference between maximal OCR and non-mitochondrial OCR; proton leak respiration is the difference between post-oligomycin OCR and non-mitochondrial respiration. The recorded OCR data was then normalised to the total protein content per well by using the Bradford assay as described in **Section 2.4.2**.

2.7 Statistical analysis

All data was collected in Microsoft Excel 2013 (Microsoft, Washington, USA). Tests of significance between proportions (Fisher's exact test), calculation of confidence intervals and independent t-tests or one-way analysis of variance (ANOVA) with Tukey's post hoc analysis were performed as appropriate to the data set using Graphpad v7 (Graphpad Software, La Jolla, USA). A p-value of less than 0.05 was considered statistically significant.

Chapter 3

A survey of the frequency of the m.1555A>G variant in UK patients with suspected mitochondrial deafness

3.1 Introduction

The m.1555A>G variant in the mitochondrial 12S rRNA gene, *MT-RNR1*, is a recognised cause of both maternally transmitted aminoglycoside ototoxicity and maternally inherited non-syndromic deafness (Prezant, Agopian et al. 1993). The background frequency of the variant is estimated at 0.21% in the population (95% confidence interval (CI), 0.08–0.46, 6/2856 positive tests) (Vandebona, Mitchell et al. 2009) but the majority of carriers have been shown to have normal hearing well into adult life (Rahman, Ecob et al. 2012). The major modifiable risk for the manifestation of hearing impairment associated with the m.1555A>G mutation is the administration of aminoglycoside antibiotics, as the variant is thought to alter the secondary structure of the 12S rRNA molecule to more closely resemble that of susceptible bacteria (Hobbie, Akshay et al. 2008). This evidence, along with genetic linkage studies in hearing impaired families carrying the m.1555A>G variant unexposed to aminoglycosides suggests hearing loss in carriers depends on both the nuclear genetic background and environmental insults (Bykhovskaya, Estivill et al. 2000). Together, this suggests the variant is a necessary but not sufficient cause of maternally inherited deafness (Guan, Fischel-Ghodsian et al. 2001, Rahman, Ecob et al. 2012).

In the UK, testing for the m.1555A>G variant is performed both in the diagnostic work-up of hearing loss of unknown origin and in cases of prospective aminoglycoside use, for example in the treatment of cystic fibrosis (Veenstra, Harris et al. 2007). Targeted mutation analysis of m.1555A>G in the UK is provided by the UK Genetic Testing Network (UKGTN) in five accredited laboratories: Oxford (Oxford Medical Genetics Laboratories, Oxford University Hospitals NHS Trust), Birmingham (West Midlands Inherited Metabolic Disease unit), London (University College London Hospitals Queen Square, UCLH, and Great Ormond Street Hospital, GOSH) and Newcastle upon Tyne (NHS Highly Specialised Mitochondrial Service). The whole mitochondrial genome,

encompassing the *MT-RNR1* gene, is also sequenced in the diagnosis of suspected mitochondrial disease by the laboratories in Newcastle and UCLH.

3.2 Materials and Methods

3.2.1 Survey methodology

Each of the five laboratories was contacted by e-mail or telephone and asked to provide information on the total number of genetic diagnostic tests performed for the m.1555A>G variant in the previous 5 years (period: November 2009-November 2014). This included both targeted variant tests and whole mitochondrial genome sequencing where appropriate. Each laboratory also supplied information on the clinical indications for each test.

3.2.2 Statistical analysis

Tests of significance between proportions (Fisher's exact test) and confidence intervals were calculated using Graphpad Prism v7 (Graphpad Software, La Jolla, USA). A p-value of less than 0.05 was considered statistically significant.

3.3 Results

A total of 3979 m.1555A>G specific test requests and 1336 complete mitochondrial genomes (including the *MT-RNR1* gene, total=5315 tests) were recorded at the five testing laboratories in the study period. A review of clinical referral data revealed that this included testing in patients with hearing loss of unknown origin, patients for prospective aminoglycoside treatment and patients with undetermined neurological phenotypes suspected to result from a pathogenic mtDNA mutation (**Table 3.1**).

In total 20 positive test results within the 5-year survey period were recorded (20/5315, 0.37%, 95% CI=0.21-0.53). Mitochondrial genome sequencing in patients with suspected mtDNA disease (e.g. neonatal leukodystrophy and lactic acidosis and hence not specifically for hearing impairment) detected 4 positive diagnoses (4/1336, 0.3% 95% CI=0.1-0.59) consistent with the background population frequency (Fisher's exact p=0.735) (Vandebona, Mitchell et al. 2009).

Of the specific tests for m.1555A>G the number of positive tests (16/3979, 0.4% 95% CI=0.2-0.6) appears to be higher than the published background population incidence for the variant within the population, but was not statistically different (Fisher's exact p=0.19)

(Vandebona, Mitchell et al. 2009). All but one of the positive results in the hearing loss group was detected at GOSH (n=12) and the number of positive tests in this group (12/2147, 0.56%, 95% CI=0.24-0.88) was also not significantly higher than the background population frequency (Fisher exact p=0.06). Additionally, it was noteworthy that 15/20 (75%) of the positive tests were recorded at GOSH, although this was not significantly different from the detection rate at other centres (GOSH 15/2957 positive tests vs. other centres 5/2358 positive tests, Fisher's exact p=0.113).

Table 3.1. Summary results of m.1555A>G testing undertaken at UKGTN and mitochondrial diagnostic laboratories

Testing laboratory	m.1555A>G tests for hearing loss (i)	m.1555A>G tests for prospective aminoglycoside use (ii)	Total tests for m.1555A>G (i+ii)	Hearing loss positives (iii)	Non-hearing loss positives (iii)	Complete mitochondrial genomes	Number of positive tests (iv)	Total positive tests (iii+iv)
Oxford	270	83	353	0	0	0	0	0
Newcastle	212	226	438	1	0	713	3	4
London (UCLH)	35	0	35	0	0	623	1	1
London (GOSH)	1434	1523	2957	11	4	0	0	15
Birmingham	196	0	196	0	0	0	0	0
Total	2147	1832	3979	12	4	1336	4	20

3.4 Discussion

We surveyed the 5 laboratories in the UK providing either specific genetic testing for m.1555A>G or whole mitochondrial genome sequencing that incorporates the *MT-RNR1* gene. As expected, the frequency of the variant in patients undergoing mitochondrial genome sequencing i.e. a group not selected on the basis of hearing loss, was no different to the background frequency reported in a previous study (Vandebona, Mitchell et al. 2009). Surprisingly, however, the m.1555A>G variant was not found at a frequency higher than in the background population in patients referred with hearing loss (i.e. a selected group with a relatively greater risk for the variant).

Although there was no statistically significant difference, our results also demonstrate an apparent geographical bias in the detection of m.1555A>G, with the majority of positive tests found at GOSH. It is possible that this is a result of the ethnic heterogeneity of the UK population, reflecting the worldwide variation in the frequency of m.1555A>G in published studies (Estivill, Govea et al. 1998, Usami, Abe et al. 2000, Bitner-Glindzicz, Pembrey et al. 2009). Alternatively, this may reflect the diagnosis of m.1555A>G in numerous individuals within families.

On the basis of our results, we conclude that the m.1555A>G variant is not significantly associated with hearing loss in the UK population. It is therefore possible that m.1555A>G testing could be potentially misleading in patients with hearing loss of unknown origin without a maternal family history or documented aminoglycoside usage. Moreover, our findings are further evidence that the m.1555A>G variant does not confer a strong effect size, but requires the presence of an additional factor either environmental e.g. aminoglycosides or a permissive nuclear background, to cause hearing loss. In view of this, we designed an exome sequencing strategy to identify nuclear genetic modifiers of the m.1555A>G variant which constitutes the body of work presented in **Chapter 4**.

Chapter 4

The identification of a nuclear genetic modifier in carriers of m.1555A>G

4.1 Introduction

The use of aminoglycosides is a known modifier factor for the hearing loss associated with the m.1555A>G variant. However, their use cannot account for all hearing impaired carriers in multi-generational pedigrees (Hakli, Luotonen et al. 2013). Moreover, the severity and age of onset of hearing loss is highly variable amongst individuals in these families carrying the m.1555A>G variant, independent of aminoglycoside usage (Estivill, Govea et al. 1998). Together, this evidence suggests the manifestation of m.1555A>G associated hearing loss may be dependent on additional co-segregating nuclear genetic factors (Bykhovskaya, Shohat et al. 1998, Guan, Yan et al. 2006, Meng, Cang et al. 2017).

Given the suggestion that nuclear modifiers may modulate the risk for hearing loss we aimed to determine protein coding risk factors that may confer this function. Carriers of the m.1555A>G variant were identified from (i) a multigenerational family living in northern Finland by Professor Kari Majamaa (Oulu University, Finland) and (ii) 9 sporadic cases from north-eastern Spain by Professor Julio Montoya (University of Zaragoza, Spain). To address the hypothesis that a nuclear variant accounted for the variable hearing loss associated with m.1555A>G, exome sequencing was undertaken in selected Finnish familial (n=5) and Spanish sporadic cases (n=4).

4.2 Materials and Methods

4.2.1 A multi-generational Finnish family

A large multi-generational family transmitting the m.1555A>G variant along the maternal lineage was previously identified and characterised by Professor Kari Majamaa, Oulu University, Finland (Lehtonen, Uimonen et al. 2000). The family consists of 46 individuals (21 female: 25 male, **Figure 4.1**). Full audiological history and phenotyping of individuals in generation IV has been described previously (Hakli, Luotonen et al. 2013). In this study,

Hakli et al, undertook prospective audiological phenotyping with a combination of TEOAEs and sound field audiometry, with pure tone audiometry when age appropriate. Pure tone thresholds were measured at 0.125, 0.25, 0.5, 1, 2, 3, 4, 6 and 8 kHz. On the basis of these pure tone thresholds, individuals were categorised as having (i) normal hearing, (ii) high frequency hearing loss (iii) moderate progressive pan-frequency hearing loss or (iv) profound pan-frequency hearing loss. There was no documented history of aminoglycoside usage in any family member (Hakli, Luotonen et al. 2013) and neurological examination of all individuals was otherwise normal (Professor Kari Majamaa, personal communication).

Generation IV consists of 19 individuals (9 female: 10 male) forming three families – Family A (n=6), Family B (n=9) and Family C (n=4). Individuals were categorised based on the results of audiological investigations as having normal hearing (n=9) or hearing loss (n=10, either high frequency (n=3), moderate progressive pan-frequency (n=6) or profound pan-frequency hearing loss (n=1)). The mean age of diagnosis of hearing loss was 3.7 years (range 1.6 – 5.4 years) although 13 of the children had passed universal neonatal hearing screening (**Table 4.1**). Phenotypic information, where available, for individuals in generation II and III was provided by personal communication from Professor Kari Majamaa (**Table 4.2**). We subsequently also identified the children of fathers in generation III (Family D, n=9; and Family E, n=6) (discussed in **Section 4.3.2.1.3, Table 4.3**)

Table 4.1. Clinical characteristics of the 19 children in generation IV. n.a = not applicable. P = profound pan-frequency hearing loss, HF = high frequency hearing loss, M = moderate progressive pan-frequency hearing loss, N = normal hearing Adapted from Hakli, Luotonen et al. 2013.

Pedigree I.D	Sex (M/F)	Age at diagnosis (years)	Age at last examination (years)	Hearing phenotype	Genomic DNA available (Yes/No)
Family A					
IV-1 (A)	F	n.a	8.8	N	Yes
IV-2 (A)	F	5.4	9.3	HF	Yes
IV-3 (A)	F	n.a	6.5	N	Yes
IV-4 (A)	M	2.9	7.2	M	Yes
IV-5 (A)	M	2.3	5.5	HF	Yes
IV-6 (A)	M	3.5	3.5	HF	Yes
Family B					
IV-1 (B)	M	n.a	8	N	Yes
IV-2 (B)	F	4.8	13.2	P	Yes
IV-3 (B)	M	5.2	10.9	M	Yes
IV-4 (B)	M	4.7	10.3	M	Yes
IV-5 (B)	M	n.a	6.2	N	No
IV-6 (B)	M	3.8	7.0	M	Yes
IV-7 (B)	M	3.0	5.3	M	Yes
IV-8 (B)	F	n.a	3.6	N	Yes
IV-9 (B)	M	1.6	2.1	M	Yes
Family C					
IV-1 (C)	F	n.a	7.9	N	Yes
IV-2 (C)	F	n.a	5.3	N	Yes
IV-3 (C)	F	n.a	3.9	N	Yes
IV-4 (C)	F	n.a	2.1	N	Yes

Table 4.2. Clinical characteristics and availability of genomic DNA of individuals in generation II and III. n.a = not applicable, -= unknown P = profound pan-frequency hearing loss, HF = high frequency hearing loss, N = normal hearing.

Pedigree I.D	Sex (M/F)	Age at diagnosis (years)	Hearing phenotype	Genomic DNA available (Yes/No)
II-1	F	n.a	N	Yes
II-2	M	20	HF	No
II-3	M	n.a	N	No
II-4	F	n.a	N	No
II-5	F	n.a	N	No
II-6	M	n.a	N	No
II-7	F	n.a	N	Yes
II-8	F	42	HF	Yes
II-9	F	n.a	N	Yes
III-1	F	n.a	N	Yes
III-2	M	-	P	No
III-3	F	n.a	N	Yes
III-4	M	n.a	N	No
III-5	F	8	HF	Yes
III-6	M	4	P	Yes
III-7	M	n.a	N	No
III-8	F	7	HF	Yes
III-9	F	21	HF	Yes
III-10	M	5	P	Yes
III-11	M	-	HF	No
III-12	M	-	N	No

Table 4.3. Clinical characteristics and availability of genomic DNA of children of fathers in generation III. As discussed in Section 4.3.2.1.3. N = normal hearing

Father	Pedigree I.D	Sex (M/F)	Age (Years)	Hearing phenotype	Genomic DNA available (Yes/No)
Family D					
III-6	IV-1 (D)	M	19	N	Yes
III-6	IV-2 (D)	F	15	N	Yes
III-6	IV-3 (D)	M	13	N	Yes
III-6	IV-4 (D)	F	10	N	Yes
III-6	IV-5 (D)	F	7	N	Yes
III-6	IV-6 (D)	F	17	N	Yes
III-6	IV-7 (D)	F	4	N	Yes
III-6	IV-8 (D)	F	12	N	Yes
III-6	IV-9 (D)	F	1	N	Yes
Family E					
III-10	IV-1 (E)	F	14	N	Yes
III-10	IV-2 (E)	M	13	N	Yes
III-10	IV-3 (E)	F	11	N	Yes
III-10	IV-4 (E)	M	6	N	Yes
III-10	IV-5 (E)	M	3	N	Yes
III-10	IV-6 (E)	M	10	N	Yes

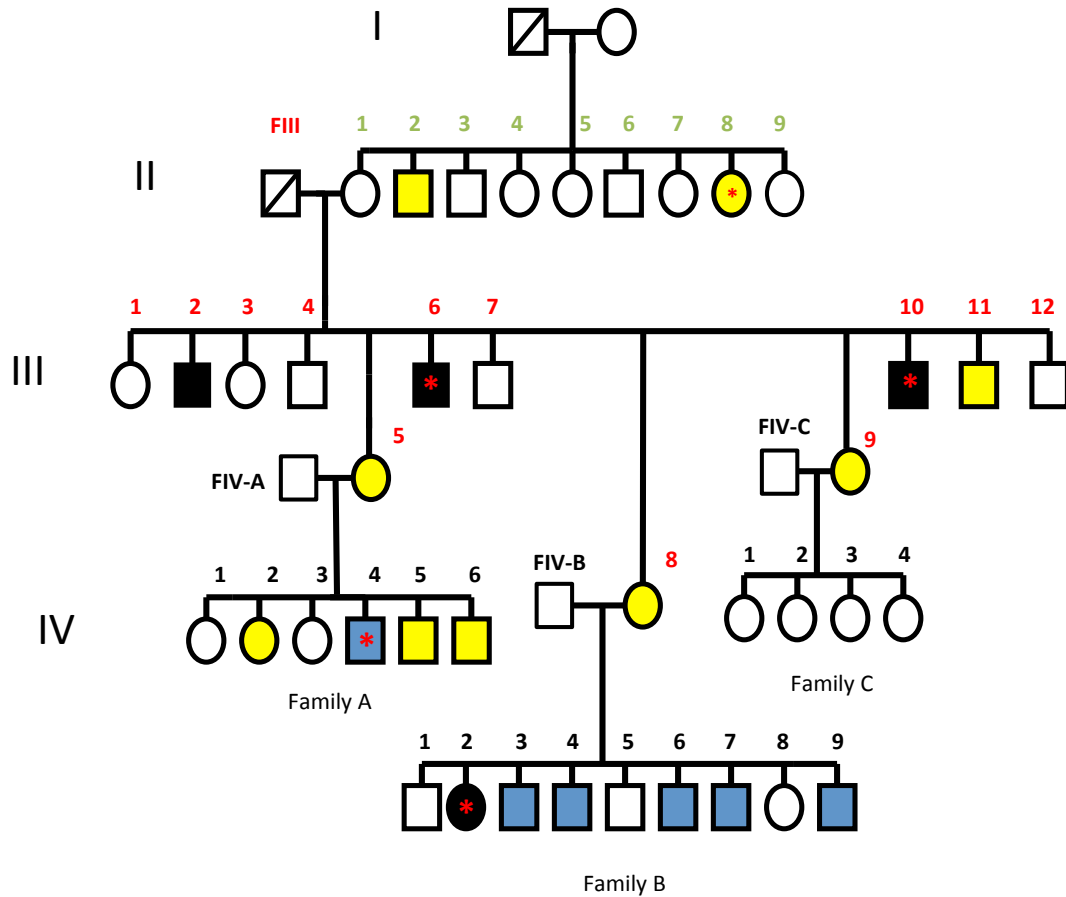


Figure 4.1. Pedigree of Finnish family transmitting the m.1555A>G variant in 4 generations. Individuals numbered sequentially (generation II – green, generation III – red, generation IV- black). Fathers in families A, B, C marked as FIV-A, FIV-B and FIV-C respectively, father of generation III is denoted FIII. Symbols are as follows: yellow filled- high frequency hearing loss; grey filled- moderate progressive pan-frequency hearing loss; black filled- profound pan-frequency hearing loss; unfilled- normal hearing; red star- exome sequenced individual (II-8, III-6, III-10, IV-4 (A), IV-2 (B)).

4.2.2 Sporadic cases

A second cohort of patients was also identified to determine if a conserved genetic mechanism accounted for hearing loss in m.1555A>G carriers. Nine sporadic carriers of m.1555A>G were identified during diagnostic workup for hearing impairment by Professor Julio Montoya (Universidad Zaragoza, Spain). Phenotypic data consisted only of the presence of hearing loss with no additional available information. All patients had received antibiotics in infancy; however, whether this included the administration of aminoglycosides was unknown. Available demographic information is shown in **Table 4.4**.

Table 4.4. Demographic information for nine sporadic Spanish carriers of m.1555A>G

Patient I.D	Sex (M/F)	Age (Years)
DF40	M	51
DF95	F	44
DF39	F	45
DF178	M	8
DF56	F	70
DF195	F	64
DF36	M	48
DF38	M	52
DF206	M	42

4.2.3 Samples

Genomic DNA was extracted from peripheral blood lymphocytes by standard procedures in the laboratories of Professor Kari Majamaa (Finnish samples) and Professor Julio Montoya (Spanish samples). Detection of the m.1555A>G mutation was performed by restriction fragment polymorphism analysis or a direct sequencing approach (Hakli, Luotonen et al. 2013). Genomic DNA was available from 44 Finnish individuals (29 individuals from generations II – IV and 15 individuals from Family D and E) and 9 individuals from the cohort of sporadic Spanish cases (see **Table 4.1, 4.2, 4.3 and 4.4**).

4.2.4 Allelic quantification of m.1555A>G by Pyrosequencing

Pyrosequencing was undertaken to quantify the A: G nucleotide composition at m.1555 (determined between 100% A for wild type to 100% G for homoplasmic mutant) as described in **Section 2.3.11**.

4.2.5 Exome sequencing

Exome sequencing of 1 µg of extracted DNA was undertaken using a Illumina HiSeq 2000 Sequencing System (Illumina, CA, USA) with 100 bp paired-end reads by AROS (AROS Applied Biotechnology A/S, Aarhus, Denmark) as described in **Section 2.3.14**. The following affected patients from the Finnish family were chosen for exome sequencing: II-8, III-6, III-10, IV-4 (A) and IV-2 (B) and selected based upon the maximum number of meioses between the individuals. Individuals III-6, III-10, IV-4 (A), IV-2 (B) had profound

pan-frequency hearing loss, individual II-8 had high frequency hearing loss. In addition, four sporadic cases from the Spanish cohort were selected for exome sequencing: DF95, DF178, DF40, DF39.

4.2.5.1 Exome sequencing bioinformatics analysis

Read alignment, variant calling and annotation were undertaken by Dr Helen Griffin (Newcastle University, UK) as described in **Section 2.3.14.1**. Variant filtering and prioritisation were performed using IVA as described in **Section 2.3.14.2**. Determination of mitochondrial haplogroups was performed using MITOMASTER and Phylotree as described in **Section 2.3.14.2**.

4.2.6 Analysis of known hearing loss genes

In accordance with the recommendations for the interrogation of putative pathogenic variants in human disease, initial analysis focussed on genes that have been previously linked to hearing loss (MacArthur, Manolio et al. 2014). The Hereditary Hearing Loss Homepage (www.hereditaryhearingloss.org) gives an up to date list of all known genes identified to be causative for both syndromic and non-syndromic monogenic hearing impairment. Non-syndromic hearing loss can be further classified based on the respective models of inheritance as; AD, AR and X-linked based. Genes in these lists were screened for putative pathogenic variants that could account for the hearing loss in the patients (**Table 4.5**, **Table 4.6** and Hypothesis 1, **Section 4.3.2.1.1**). Similarly, nuclear genes associated with mitochondrial disorders of which deafness is a component were also prioritised for assessment (**Table 4.7**).

Table 4.5. Established genes known to cause monogenic non-syndromic hearing loss classified by inheritance model. Information obtained from Hereditary Hearing Loss Homepage (October 2016) (www.hereditaryhearingloss.org)

Autosomal dominant		Autosomal recessive		X-linked
<i>CEACAM16</i>	<i>ACTG1</i>	<i>GJB2</i>	<i>BSND</i>	<i>PRPS1</i>
<i>GJB3</i>	<i>SLC17A8</i>	<i>GJB6</i>	<i>TECTA</i>	<i>POU3F4</i>
<i>GJB2</i>	<i>GRHL2</i>	<i>MYO7A</i>	<i>OTOA</i>	<i>SMPX</i>
<i>GJB6</i>	<i>OSBPL2</i>	<i>MYO15A</i>	<i>PCDH15</i>	<i>COL4A6</i>
<i>MYH14</i>	<i>HOMER2</i>	<i>SLC26A4</i>	<i>RDX</i>	
<i>DFNA5</i>	<i>MCM2</i>	<i>TMIE</i>	<i>GRXCR1</i>	
<i>WFS1</i>	<i>KITLG2</i>	<i>TMC1</i>	<i>TRIOBP</i>	
<i>TECTA</i>	<i>COL11A2</i>	<i>MYO15A</i>	<i>CLDN14</i>	
<i>COCH</i>		<i>SLC22A4</i>	<i>MYO3A</i>	
<i>POU4F3</i>		<i>TMICE</i>	<i>WHRN</i>	
<i>MYH9</i>		<i>TMC1</i>	<i>ESRRB</i>	
<i>MYO6</i>		<i>TMPRSS3</i>	<i>ESPN</i>	
<i>SIX1</i>		<i>OTOF</i>	<i>MYO6</i>	
<i>TMC1</i>		<i>CDH23</i>	<i>HGF</i>	
<i>P2RX2</i>		<i>GIPC3</i>	<i>ILDR1</i>	
<i>CCDC50</i>		<i>STRC</i>	<i>ADCY1</i>	
<i>MIRN96</i>		<i>USH1C</i>	<i>CIB2</i>	
<i>TJP2</i>		<i>OTOG</i>	<i>MARVELD2</i>	
<i>TNC</i>		<i>BDP1</i>	<i>CABP2</i>	
<i>SMAC/DIABLO</i>		<i>MSRB3</i>	<i>MET</i>	
<i>TBC1D24</i>		<i>BSND</i>	<i>TSPEAR</i>	
<i>CD164</i>		<i>OTOGL</i>	<i>GRXCR2</i>	
<i>CRYM</i>		<i>TBC1D24</i>	<i>EPS8</i>	
<i>DIAPH1</i>		<i>ELMOD3</i>	<i>CLIC5</i>	
<i>EYA4</i>		<i>KARS</i>	<i>CDC14A</i>	
<i>MYO7A</i>		<i>SERPINB6</i>	<i>FAM65B</i>	
		<i>EPS8L2</i>		
		<i>PJKK</i>		
		<i>DCDC2</i>		
		<i>PNPT1</i>		
		<i>COL11A2</i>		
		<i>COMT</i>		
		<i>LHFPL5</i>		

Table 4.6. Established genes known to cause non-mitochondrial multisystem phenotypes of which hearing loss is a component. Information obtained from Hereditary Hearing Loss Homepage (October 2016) (www.hereditaryhearingloss.org)

Genes associated with syndromic hearing loss				
<i>COL4A5</i>	<i>SEMA3E</i>	<i>FOXI1</i>	<i>COL9A2</i>	<i>CDH23</i>
<i>COL4A3</i>	<i>CHD7</i>	<i>KCNJ10</i>	<i>TCOF1</i>	<i>PCDH15</i>
<i>COL4A4</i>	<i>KCNQ1</i>	<i>COL2A1</i>	<i>POLR1D</i>	<i>SANS</i>
<i>EYA1</i>	<i>KCNE1</i>	<i>COL11A1</i>	<i>POLR1C</i>	<i>CIB2</i>
<i>SIX5</i>	<i>NDP1</i>	<i>COL11A2</i>	<i>MYO7A</i>	<i>USH2A</i>
<i>SIX1</i>	<i>SLC26A4</i>	<i>COL9A1</i>	<i>USH1C</i>	<i>VLGR1</i>

Table 4.7. Nuclear genes associated with mitochondrial disorders of which deafness is a component. Adapted and updated from Luo, Hou et al. 2013.

Nuclear genes associated with mitochondrial deafness	
<i>OPA1</i>	<i>POLG1</i>
<i>MPV17</i>	<i>RRM2B</i>
<i>PDSS1</i>	<i>HARS2</i>
<i>BCS1L</i>	<i>SERAC1</i>
<i>SUCLA2</i>	<i>C21ORF2</i>
<i>C100RF2</i>	<i>WFS1</i>
<i>COX10</i>	<i>TIMM8A</i>

4.2.7 Analysis of genes previously suggested as modifiers of the m.1555A>G phenotype

A number of nuclear genes encoding mitochondrial proteins have previously been described as possible modifiers of the m.1555A>G variant specifically; *TRMU* (Meng, Cang et al. 2017), *GTPBP3* (Bykhovskaya, Mengesha et al. 2004), *MTO1* (Li, Li et al. 2002), *TFB1M* (Bykhovskaya, Mengesha et al. 2004) and *MRPS12* (Emperador, Pacheu-Grau et al. 2014) (**Table 4.8**). The studies deriving the association between m.1555A>G and deafness are described in **Section 1.14.7**.

Table 4.8. Genes previously suggested as modifiers of m.1555A>G hearing loss

Putative nuclear gene modifiers	
<i>GTPBP3</i> (Bykhovskaya, Mengesha et al. 2004)	<i>MTO1</i> (Li and Guan 2002)
<i>TRMU</i> (Guan, Yan et al. 2006, Meng, Cang et al. 2017)	<i>TFB1M</i> (Bykhovskaya, Mengesha et al. 2004)
<i>MRPS12</i> (Emperador, Pacheu-Grau et al. 2014)	

4.2.8 Analysis of genes associated with mitochondrial replication

To determine whether a conserved mechanism accounted for the phenotype in the familial and sporadic cases, genes coding for proteins known to be involved in mtDNA replication were assessed in the sporadic cohort. A list of current known genes associated with mtDNA replication was obtained by performing a Gene Ontology annotation search of MitoCarta, a compendium of all known mitochondrial proteins, via the MitoMiner v3.1 interface (**Table 4.9**) (Calvo, Clauser et al. 2016, Smith and Robinson 2016).

Table 4.9. Known genes coding for proteins involved in mitochondrial DNA replication. Information obtained from Mitocarta via Mitominer v3.1 (October 2016).

Genes coding for proteins involved in mitochondrial DNA replication			
<i>DNAJA3</i>	<i>DNA2</i>	<i>SLC25A33</i>	<i>POLG2</i>
<i>SSBP1</i>	<i>PIF1</i>	<i>RNASEH1</i>	
<i>CI0ORF2</i>	<i>POLG</i>	<i>TEFM</i>	
<i>TFAM</i>	<i>TK2</i>	<i>TOP1MT</i>	
<i>MGME1</i>	<i>DUT</i>	<i>NT5M</i>	

4.2.9 Genomic amplification and Sanger sequencing validation of candidate genes

Total genomic DNA was amplified using the REPLI-g Ultrafast Mini Kit (Qiagen) when required for sequencing reactions as described in **Section 2.3.3**. Confirmation of variants identified by exome sequencing as putative disease modifiers of the m.1555A>G mutation was performed by Sanger sequencing as described in **Section 2.3.7**. Each putative candidate variant was sequenced in 5 affected and 5 unaffected individuals within the family in order to determine whether putative pathogenic mutations segregated with the phenotype. All primer pairs were designed with Primer3 (<http://primer3.ut.ee/>) and primer

specificity was determined using Primer-Blast (Ye, Coulouris et al. 2012). Details of primer pairs are shown in **Table 4.10**.

4.2.10 Sanger sequencing of *SSBP1*

All coding regions (exons 2–9) including at least 10 bp overlap of the exon-intron boundaries of *SSBP1* were Sanger sequenced in DF40, DF95, DF39, DF178, DF56, DF195, DF36, DF38 and DF206 as described in **Section 2.3.7**. Primer pairs for each exon are shown in **Table 4.11**.

Table 4.10. Primer sequences, annealing temperatures and amplicon sizes for candidate genes prioritised from exome sequencing of m.1555A>G carriers.

Gene	Forward primer sequence 5'-3'	Reverse primer sequence 5'-3'	Anneal temp (°C)	PCR product size (bp)
<i>MYO6</i>	GGTGCTGAGATCTTGCCAAG	ACAAATTCACCAAAAAGCCGTG	58	289
<i>LOXHD1</i>	ACCTAAGCTGGAGAAAACACC	TGGGGTAGCCACTGTCTAAC	58	221
<i>SSBP1</i>	TGGTGAGTTGTACTTTTGCCA	AGGTCTTTTGCCCCTGTAGT	58	226
<i>ITIH4</i>	GAGGCTCAGGGACAAAGAGG	CGGGAGAAACATGGAGCAGT	58	240
<i>SMG7</i>	AGCTCTCCTCCAACACACAA	CACCCATGGCTAAGGGATGA	58	247
<i>CCDC136</i>	GGCTGCTTCTCAACTTGACT	GGGGAGTGCAGAGCCTCT	58	500
<i>TRMU</i>	CGCAGAAGAAGAGCAGTGAG	TCCGAACCAAAGTCAGAGGA	58	542
<i>MGAM</i>	GACTCCCTGCTGTTGAATCC	AAGGGAACAGGCGATGCTTA	58	344
<i>GBP5</i>	CTTTGGTGCCATCCCATAACC	AGTACTCTGATCACCCCACT	58	384
<i>VPS33B</i>	ACCCACCTCTAAATGCCAT	CCCCAGTAACAGGCTCTCC	58	230
<i>MMP14</i>	GAACCAGAGACCTAGGCCG	CGCCTCACTCCCAAAGACTA	58	237

Table 4.11. Primer sequences, annealing temperatures and amplicon sizes for all *SSBP1* coding regions

Exon	Forward primer sequence 5'-3'	Reverse primer sequence 5'-3'	Anneal temp (°C)	PCR product size (bp)
2	GGTGCTGAGATCTTGCCAAG	ACAAATTCACCAAAAAGCCGTG	60	300
3	ACCTAAGCTGGAGAAAACACC	TGGGGTAGCCACTGTCTAAC	60	275
4+5	TGGTGAGTTGTACTTTTGCCA	AGGTCTTTTGCCCCTGTAGT	60	557
6	GAGGCTCAGGGACAAAGAGG	CGGGAGAAACATGGAGCAGT	60	243
7	AGCTCTCCTCCAACACACAA	CACCCATGGCTAAGGGATGA	60	252

4.3 Results

Allelic quantification of the m.1555 base was undertaken in all available DNA samples reported to possess the m.1555A>G variant by Pyrosequencing as described in **Section 2.3.11**. The Pyrosequencing assay was performed on the following samples from the Finnish family in duplicate: II-2, II-7, II-8, II-9, III-1, III-3, III-5, III-6, III-8, III-9, III-10, and all individuals from generation IV except IV-5 (B) where no DNA was available. Pyrosequencing was also performed in duplicate on genomic DNA from the sporadic Spanish cases: DF40, DF95, DF39, DF178, DF56, DF195, DF36, DF38 and DF206. Given the known limit of sensitivity of detection of the Pyrosequencing assay (approximately 5%, Qiagen Knowledge Resource) all samples were confirmed to be homoplasmic at m.1555A>G (range 98-100%, see **Figure 4.2**).

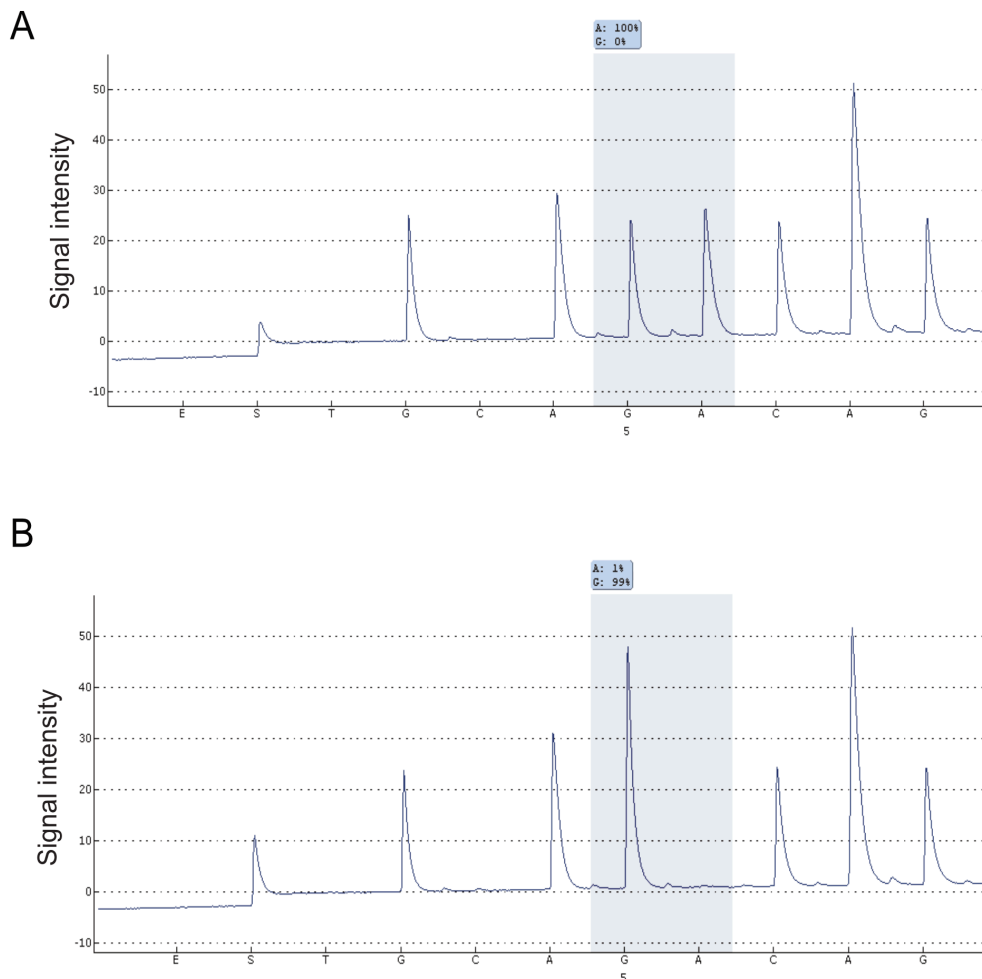


Figure 4.2. Representative pyrograms generated from Pyrosequencing. (A) Pyrogram of positive control demonstrating 100% A at m.1555 and (B) Pyrogram of individual IV-1(B) showing 99% G at m.1555 and hence classified as homoplasmic.

4.3.1 Coverage analysis of consensus coding sequence (CCDS) bases and known hearing loss genes

Read coverage and depth for all CCDS bases for all nine exome sequenced individuals across (a) the whole exome, (b) within known hearing loss genes (**Table 4.12, 4.13**) was performed by Dr Helen Griffin (Newcastle University, UK) using SAMtools (Li, Handsaker et al. 2009). Custom Perl scripts were then used to calculate mean base depth across the exome and within the genes of interest together with the percentage of bases covered above a depth of 30, 10, 5 and 1 read depth.

The mean target base coverage of all CCDS bases for all 9 individuals was 55.2-fold (SD=8.8). On average, 69.0% of all CCDS bases were covered above 30-fold depth, 93.0% of all CCDS bases were covered at greater than 10-fold depth, and 99.4% of all CCDS bases were covered at greater than 5-fold (**Table 4.12**). The mean target base coverage for the CCDS regions within of known hearing loss genes in this study was 42.3-fold (SD=6.6). Within these genes, 59.1% of bases were covered 30-fold, 88.7% of bases were covered 10-fold and 94.9% of bases were covered 5-fold (**Table 4.13**). These metrics indicated that there was adequate coverage of the whole exome and the specific hearing loss genes examined in Hypothesis 1, **Section 4.3.2.1.1**.

Table 4.12. Coverage and depth statistics calculated for all Consensus Coding Sequence (CCDS) bases. Target bases as defined by Illumina Truseq 62Mb enrichment kit.

Patient I.D	Total target bases	Mean target base depth	Number CCDS bases covered 30-fold	% CCDS bases covered 30-fold	Number CCDS bases covered 10-fold	% CCDS bases covered 10-fold	Number CCDS bases covered 5-fold	% CCDS bases covered 5-fold	Number CCDS bases covered 1-fold	% CCDS bases covered 1-fold
IV-4 (A)	31935069	62.5	23870817	74.7	30159703	94.4	31218112	97.8	31798034	99.6
IV-2 (B)	31935069	65.5	24470472	76.6	30296467	94.9	31243217	97.8	31789289	99.5
II-9	31935069	61.7	23798526	74.5	30146737	94.4	31191978	97.7	31782896	99.5
III-6	31935069	42.2	18206224	57.0	28614409	89.6	30606737	95.8	31711023	99.3
III-10	31935069	56.1	22669349	71.0	30018674	94.0	31187756	97.7	31804326	99.6
DF95	31935069	50.1	21342809	66.8	29703723	93.0	30977233	97.0	31714121	99.3
DF178	31935069	42.2	18513570	58.0	28829490	90.3	30613101	95.9	31652856	99.1
DF40	31935069	53.5	21748658	68.1	29528268	92.5	30964339	97.0	31770530	99.5
DF39	31935069	62.8	23736845	74.3	29915314	93.7	31065601	97.3	31755972	99.4
Mean	31935069	55.2	22039697	69.0	29690309	93.0	31007564	97.1	31753227	99.4
SD	0	8.8	2327320	7.2	599952	1.87	247174	0.77	50610	0.16

Table 4.13. Coverage and depth statistics calculated for known genes associated with hearing loss in Table 4.5, 4.6 and 4.7

Patient I.D	Total target bases	Mean target base depth	Number CCDS bases covered 30-fold	% CCDS bases covered 30-fold	Number CCDS bases covered 10-fold	% CCDS bases covered 10-fold	Number CCDS bases covered 5-fold	% CCDS bases covered 5-fold	Number CCDS bases covered 1-fold	% CCDS bases covered 1-fold
IV-4 (A)	29287	47.7	19497	66.6	26433	90.3	28014	95.7	28750	98.2
IV-2 (B)	29287	49.4	19564	66.8	26825	91.6	28076	95.9	28671	97.9
II-9	29287	46.6	18863	64.4	26448	90.3	28038	95.7	28559	97.5
III-6	29287	32.1	13413	45.8	24473	83.6	27170	92.8	28644	97.8
III-10	29287	42.9	17557	59.9	26057	89.0	27981	95.5	28666	97.9
DF95	29287	38.2	16918	57.8	26288	89.8	27890	95.2	28648	97.8
DF178	29287	32.9	14053	48.0	25108	85.7	27504	93.9	28663	97.9
DF40	29287	41.9	16840	57.5	25974	88.7	27896	95.3	28658	97.9
DF39	29287	48.8	19150	65.4	26120	89.2	27690	94.5	28732	98.1
Mean	29287	42.3	17317	59.1	21840	88.7	27806	94.9	28665	97.9
SD	0	6.6	2288	7.8	1502	2.5	301	1.02	54.5	0.18

4.3.2 Filtering for putative variants acting as modifiers of the m.1555A>G phenotype

A multi-sample VCF file containing data from all sequenced exomes (n=5 Finnish family, n=4 Spanish cohort) was uploaded into IVA together with 8 age-matched control individuals. The controls were derived from a cohort of patients investigated for cerebral vascular malformations and did not have any hearing impairment after extensive neurological examinations (personal communication, Dr Michael Keogh, Mitochondrial Biology Unit, Cambridge, UK). All controls were processed on the same exome sequencing run on a Hi-Seq 2000, and were selected to remove run-specific sequencing errors. A total of 120411 variants in 16293 genes were identified in the 9 exomes and further classified by translational impact (see **Table 4.14**).

Table 4.14. Summary of variants from all sequenced exomes (n=9) irrespective of MAF in the population or functional impact.

Translation impact	No. Variants
Non-coding	66346
Synonymous	27017
Missense	25473
In-frame	774
Frameshift	345
Stop gain	293
Unknown	74
Start-loss	63
Stop-loss	26

4.3.2.1 Filtering strategies

Iterative filtering using IVA was used to address four specific hypotheses of the cause of hearing loss within both the Finnish familial and Spanish sporadic cases.

4.3.2.1.1 Hypothesis 1

(1a) *A single rare pathogenic variant in a known hearing loss gene (n=141 genes, **Table 4.5, 4.6 and 4.7**), or in a previously suggested putative nuclear modifier gene of the m.1555A>G variant (n=5 genes, **Table 4.8**) segregates with the phenotype in the Finnish family.*

(1b) *A single rare pathogenic variant(s) in known hearing loss gene(s) or in a putative nuclear modifier gene causes the phenotype in the Spanish sporadic cases.*

Four filters were applied to the complete set of identified variants in the familial and sporadic cases, specifically; (i) confidence filter, (ii) frequency filter, (iii) predicted deleterious filter, (iv) a user defined list of known hearing loss genes (compiled from genes in **Table 4.5**, **4.6** and **4.7** and see **Figure 4.3**). The confidence and predicted deleterious filters were used as described in **Section 2.3.14.2**. The frequency filter was set to remove variants with a MAF >3% in the 1000 Genome Project or ExAC databases. This threshold was selected in order to capture potential monogenic cases of hearing loss (caused by alleles with a MAF of <0.1% (Shearer, Eppsteiner et al. 2014), and also to include alleles that may act as putative risk factors for common diseases (Manolio, Collins et al. 2009). The final stage of the filtering process involved the manual cross-referencing of the remaining variants with a list of genes known to be associated with hearing loss, see **Section 4.2.6**. For hearing loss genes that cause disease through AD inheritance, only heterozygous changes shared between affected individuals were retained. For hearing loss genes associated with AR inheritance only compound heterozygous or homozygous variants were considered.

We first considered genes known to cause disease in a recessive manner, by initially aiming to detect homozygous or compound heterozygous variants in an established hearing loss gene present in all individuals within the Finnish family. No homozygous, compound heterozygous or heterozygous alleles were detected. Relaxing our filtering to detect variants shared by only 4 of the 5 individuals (to account for potential false negatives with variant calling due to poor coverage or pipeline calling error), we again detected no homozygous or compound heterozygous variants shared between individuals, as also expected by the multigenerational phenotype seen within the family. We subsequently therefore considered a dominant model, detecting a heterozygous variant in *MYO6* (c.3755A>G, p.1252C) in 4 of 5 individuals in the family (**Table 4.15**). This variant was then sequenced by Sanger sequencing in affected and unaffected individuals from the Finnish family, but did not segregate with disease (3 affected individuals, IV-7 (B), IV-2 (B) and IV-2 (A), were confirmed have the wild-type allele, **Table 4.15**, **4.17**, **4.18** and see **Figure 4.4**). On this basis, it was concluded that there was no established rare genetically determined form of deafness causing disease within the family.

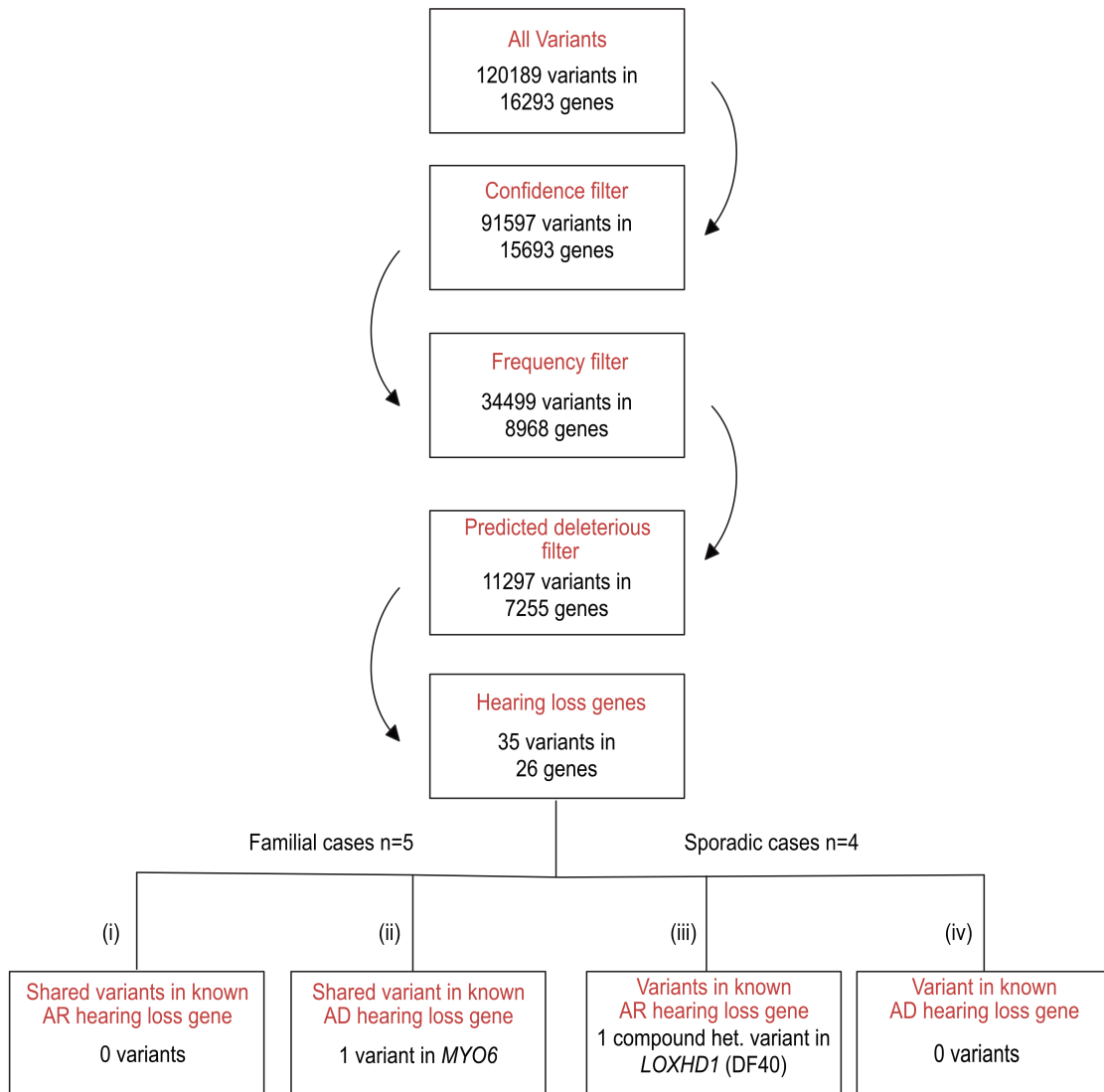


Figure 4.3. Hypothesis 1; variant filtering workflow. All variants were iteratively filtered using defined criteria as discussed in the text above to attempt to identify rare, deleterious variants shared by at least 4 of 5 familial cases in known autosomal recessive (AR) hearing loss genes (ii) variants shared by at least 4 of 5 familial cases in known autosomal dominant (AD) hearing loss genes (iii) variants in known AR hearing loss genes in discrete sporadic cases (iv) variants in known AD hearing loss genes in discrete sporadic cases.

Hypothesis (1b) sought to determine whether any of the sporadic cases also had a previously established genetically determined cause of deafness. Each of the Spanish cases was considered as a discrete case and examined for deleterious heterozygous or homozygous/compound heterozygous variants for AD and AR hearing loss genes respectively. No variants passing the iterative filtering steps were found in genes associated with autosomal dominant hearing loss. In contrast, when assessing genes

associated with an AR inheritance model, one individual (DF40) possessed a compound heterozygous variant *LOXHD1* c.1894 G>T, p.G632C, and *LOXHD1* c.1876G>T p.G626C, **Table 4.15** and **Figure 4.4**. However, on closer analysis these variants were considered ‘likely benign’ under ACMG guidelines due to an allele frequency greater than is expected for the associated hearing loss (ExAC frequency = 2.512% for both variants). In addition, *LOXHD1* variants have only been reported to be causally linked to hearing loss in 4 families worldwide (Grillet, Schwander et al. 2009, Edvardson, Jalas et al. 2011, Mori, Moteki et al. 2015) and have not been detected as a cause of deafness in several other large studies (Bademci, Foster Li et al. 2016, Jung, Lee et al. 2017).

When taken together, these data are consistent with the conclusion that the sporadic cases, as per the familial Finnish cases do not have established nuclear genetic causes of hearing loss.

Table 4.15. Annotation for variants identified in known hearing loss genes in familial and sporadic cases after iterative filtering as shown in **Figure 4.3**. Ch = chromosome, SIFT, PolyPhen2, 1000 genomes project, ExAC – as discussed in **Section 2.3.14**.

Familial cases											
Ch	Position	Ref allele	Alt allele	Gene	Transcript variant	Protein variant	Translation impact	SIFT function prediction	PolyPhen-2 function prediction	1000 Genome freq.	ExAc freq
6	76624695	A	G	<i>MYO6</i>	c.3755A>G	p.Y1252C	Missense	-	Probably Damaging	0.359	0.535
Sporadic cases											
Ch	Position	Ref allele	Alt allele	Gene	Transcript variant	Protein variant	Translation impact	SIFT function prediction	PolyPhen-2 function prediction	1000 Genome freq.	ExAc freq
1	44157764	C	A	<i>LOXHD1</i>	c.1894G>T	p.G632C	Missense	-	Probably Damaging	1.238	2.512
1	44157746	C	A	<i>LOXHD1</i>	c.1876G>T	p.G626C	Missense	-	Probably Damaging	1.278	2.512

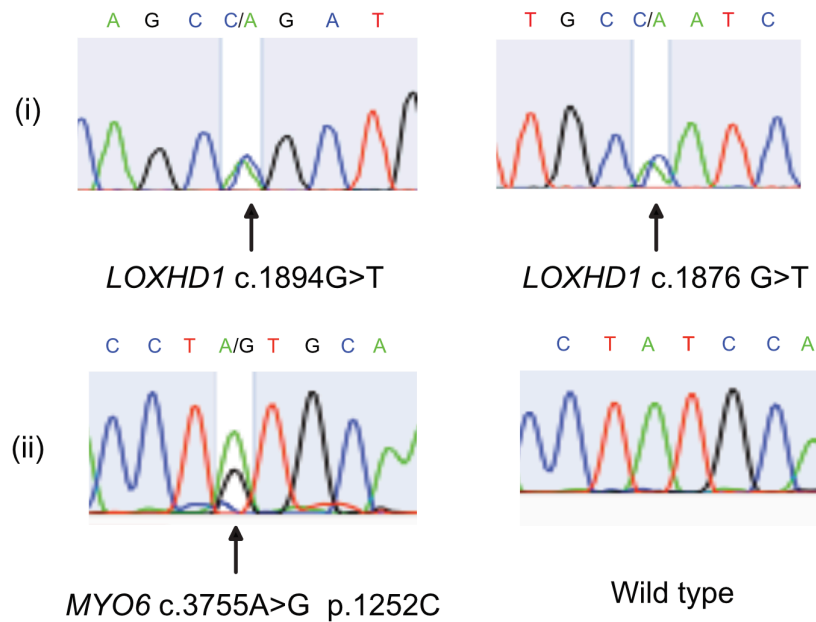


Figure 4.4. Confirmatory Sanger sequencing electropherograms of *LOXHD1* and *MYO6* variants. (i) *LOXHD1* variants present in individual DF40 and (ii) *MYO6* c.3755A>G variant, that did not segregate with the phenotype in the Finnish family (sequencing result of individual III-9 (left panel) and IV-4A (right panel) representing variant and wild type sequence respectively).

An additional analysis to screen the five genes that have previously been suggested as modifiers of the m.1555A>G phenotype (**Table 4.8**) was also undertaken using filters (i)-(iii) as previously defined, followed by manual cross-referencing of the remaining variants using a gene list compiled from genes in **Table 4.8**. This revealed that there were no shared rare, deleterious variants in these genes in either the familial or sporadic cases.

Of note, we specifically searched for a recently characterised variant in *TRMU* c.28G>T p.A10S, that occurs at a MAF significantly in excess of our threshold (ExAC frequency= 19.7%) (Meng, Cang et al. 2017). This allele was present in 2 of 5 exomes from the Finnish family (IV-4 (A) and IV-2 (B), **Table 4.16 (i)**) and one of the exome sequenced Spanish individuals (DF95) but also 2/8 normal hearing controls, consistent with the MAF in reference databases. Further Sanger sequencing of affected and unaffected individuals from the Finnish family confirmed the variant was found in both hearing impaired (4/10, 40%) and normal hearing (2/5, 40%) individuals in the Finnish family and hence cannot account for the variable penetrance of m.1555A>G in our patients (**Table 4.16 (ii)**).

Table 4.16. Results of TRMU c.28G>T sequencing. (i) Exome sequencing and confirmatory Sanger sequencing (ii) segregation analysis by Sanger sequencing in affected and unaffected individuals in the Finnish family.

(i)

Gene	Exome sequencing					Sanger sequencing				
	II-8	III-6	III-10	IV-4 (A)	IV-2 (B)	II-8	III-6	III-10	IV-4 (A)	IV-2 (B)
TRMU	wt	wt	wt	het	het	wt	wt	wt	het	het

(ii)

Gene	Affected					Unaffected				
	IV -5 (A)	II-2	IV-2 (A)	IV-7 (B)	IV-6 (B)	IV-8 (B)	IV-3 (A)	IV-1 (C)	IV-2 (C)	IV-3 (C)
TRMU	wt	het	wt	wt	het	het	wt	wt	het	wt

4.3.2.1.2 Hypothesis 2

A single, rare, nuclear variant within the exome segregates with the phenotype in the Finnish family.

Between all individuals within the Finnish family (n=5), 110875 variants in 15883 genes were detected across the whole exome. Four filters were subsequently applied to this data (i) confidence filter (ii) frequency filter (iii) predicted deleterious filter (iv) genetic filter. The confidence and predicted deleterious filters were used as described in **Section 2.3.14.2**, and variants with a MAF <1% in the 1000 Genome Project or the ExAC databases were selected.

The genetic filter was used to further filter variants on the suspected mode of inheritance, assumed to be AD based on the segregation of hearing impairment across multiple generations within the family. We also considered an X-linked dominant model due to the absence of any male-male transmission in the pedigree. Subsequently, only heterozygous or hemizygous variants present in at least 4 of the 5 patients and absent in control cases (n=8) were included in further analysis. After this filtering strategy, 10 variants in 10 genes were present in all affected individuals in the Finnish family; see **Figure 4.5** and **Table 4.17**. Confirmatory Sanger sequencing was then performed on all variants and the results for each exome sequenced individual are shown in **Table 4.18**.

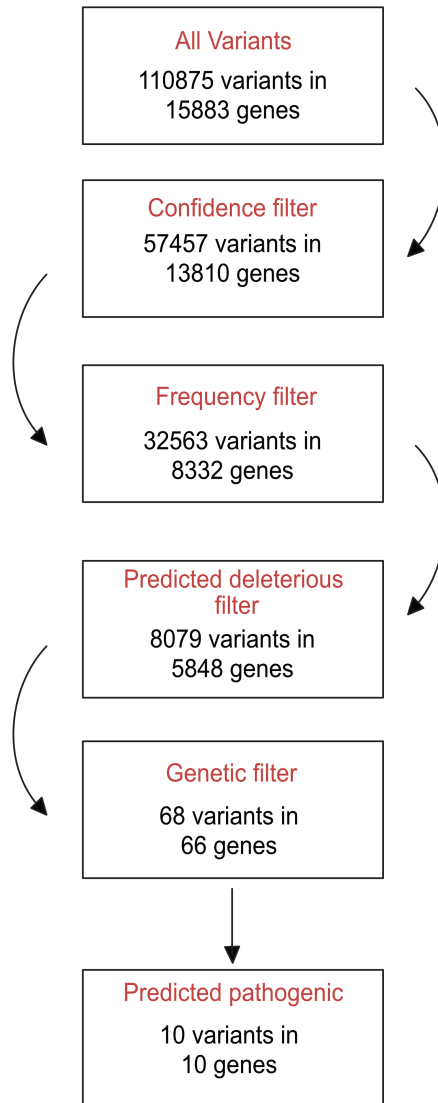


Figure 4.5. Hypothesis 2; variant filtering workflow. All variants were iteratively filtered using defined criteria as discussed above to attempt to identify rare, deleterious variants shared by at least 4 of 5 familial cases.

Table 4.17. Annotation of all variants seen that were shared between at least 4 of the 5 individuals within the Finnish cohort. Iterative filtering was performed as shown in **Figure 4.5**. Ch = chromosome, freq = frequency, SIFT, PolyPhen2, 1000 genomes project, ExAC – as discussed in **Section 2.3.14**.

Ch	Position	Ref allele	Alt allele	Gene	Transcript variant	Protein variant	Translation impact	SIFT function prediction	PolyPhen-2 prediction	1000 Genomes freq	ExAc freq
1	89733172	A	T	<i>GBP5</i>	c.356C>T	p.A119V	Missense	Damaging	Possibly Damaging	0.1	0.36
1	98144726	T	C	<i>DPYD</i>	c.775A>G	p.K259E	Missense	Damaging	Benign	0.439	1.022
3	52860854	C	T	<i>ITIH4</i>	c.472G>A	p.E158K	Missense	Damaging	Probably Damaging	0.02	0.017
7	141438969	G	A	<i>SSBP1</i>	c.3G>A	p.M1?	Start Loss	Damaging	Benign	-	0.003
7	141736753	C	T	<i>MGAM</i>	c.2207C>T	p.T736M	Missense	Damaging	Probably Damaging	-	0.007
14	23313633	G	A	<i>MMP14</i>	c.1065G>A	p.M355I	Missense	Damaging	Benign	0.559	1.811
7	12834498	G	A	<i>CCDC136</i>	c.113G>A, c.263G>A	p.G38D, p.G88D	Missense	Possibly Damaging	Possibly Damaging	0.2	0.375
15	91548307	A	G	<i>VPS33B</i>	c.1067T>C, c.1148T>C, c.875T>C	p.I292T, p.I356T, p.I383T	Missense	Possibly Damaging	Possibly Damaging	0.08	0.116
6	76624695	A	G	<i>MYO6</i>	c.3755A>Gc. 3824A>G	p.Y1252C p.Y1275C	Missense	-	Probably Damaging	0.359	0.535
1	183520048	A	T	<i>SMG7</i>	c.3008A>T, c.3146A>T, c.3158A>T, c.3170A>T	p.D1003V p.D1049V p.D1053V p.D1057V	Missense	Tolerated	Possibly Damaging	0.08	0.217

Table 4.18. Exome sequencing and confirmatory Sanger sequencing results of all patients possessing one of the variants listed in Table 4.17. het = heterozygous, wt = wild type.

Gene	Exome sequencing					Sanger sequencing				
	II-8	III-6	III-10	IV-4 (A)	IV-2 (B)	II-8	III-6	III-10	IV-4 (A)	IV-2 (B)
<i>GBP5</i>	het	het	het	het	wt	het	het	het	het	wt
<i>DPYD</i>	het	het	het	het	wt	het	het	het	het	wt
<i>ITIH4</i>	het	het	het	wt	het	het	het	het	wt	het
<i>SSBP1</i>	wt	het	het	het	het	wt	het	het	het	het
<i>MGAM</i>	wt	het	het	het	het	wt	het	het	het	het
<i>MMP14</i>	het	het	het	het	het	het	het	het	het	het
<i>CCDC13</i>	wt	het	het	het	het	wt	het	het	het	het
<i>VPS33B</i>	wt	het	het	het	het	wt	het	het	het	het
<i>MYO6</i>	het	het	het	het	wt	het	het	het	het	wt
<i>SMG7</i>	het	het	het	het	wt	het	het	het	het	wt

Table 4.19. Results of segregation analysis by Sanger sequencing. *SSBP1* and *MGAM* (highlighted in purple) were heterozygous in those affecteds (except II-8, discussed below) and wild type in all those unaffected. n.d = not determined.

Gene	Affected					Unaffected				
	III-9	IV-7 (B)	IV-2 (A)	IV-6 (B)	IV-5 (A)	IV-8 (B)	IV-3 (A)	IV-3 (C)	IV-2 (C)	IV-1 (C)
<i>GBP5</i>	wt	het	het	wt	wt	wt	wt	het	het	wt
<i>DPYD</i>	wt	wt	het	het	het	het	het	wt	wt	wt
<i>ITIH4</i>	het	wt	wt	het	wt	het	wt	het	wt	het
<i>SSBP1</i>	het	het	het	het	het	wt	wt	wt	wt	wt
<i>MGAM</i>	het	het	het	het	het	wt	wt	wt	wt	wt
<i>MMP14</i>	het	wt	wt	wt	het	wt	het	wt	het	wt
<i>CCDC136</i>	wt	wt	het	wt	het	het	het	wt	wt	het
<i>VPS33B</i>	het	wt	wt	het	wt	wt	wt	n.d	wt	het
<i>MYO6</i>	het	wt	wt	het	het	wt	wt	het	het	n.d
<i>SMG7</i>	het	n.d	wt	n.d	wt	n.d	het	het	n.d	wt

Sanger sequencing confirmed all 50 (100%) of the exome sequence results of the 10 variants of interest (**Table 4.18**) indicating there were no false positives and no false negatives due to missing coverage. To confirm segregation of the variants with hearing loss in the Finnish

family, an additional 5 affected and unaffected individuals were selected and Sanger sequencing of the variants was performed. This revealed that the c.3G>A *SSBP1* and c.2207C>T *MGAM* variants segregated with the phenotype, being heterozygous in the affected individuals (n=5) and wild type in all unaffected individuals (n=5) (**Table 4.19**). The number of correctly attributed variants (either heterozygous for affected individuals or wild type for unaffected individuals, maximum = 10 correct) is represented for each gene in **Figure 4.6**.

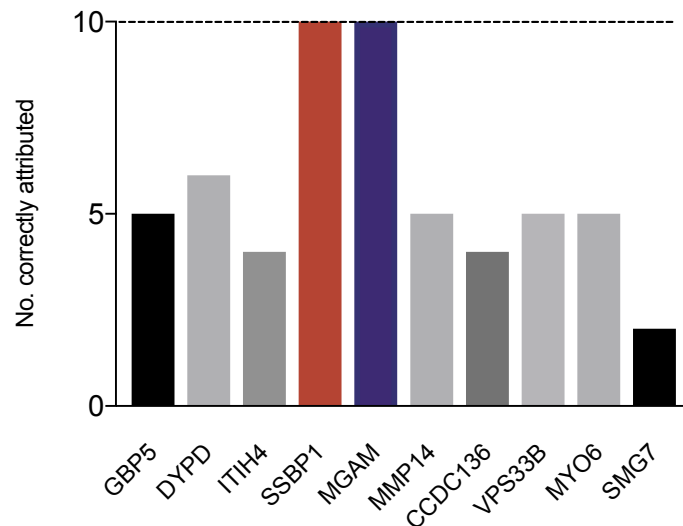


Figure 4.6. Bar graph representing the number of correctly attributed variants in the segregation analysis. c.3G>A *SSBP1* and c.2207C>T *MGAM* variants were correctly attributed with the phenotype in 10/10 Sanger sequenced individuals.

Of the variants in the two genes that segregated with the phenotype, the *SSBP1* variant was considered the more likely candidate as a modifier variant and therefore the *MGAM* variant was not further analysed, but is discussed in **Section 4.4**.

Given that the c.3G>A *SSBP1* variant segregated with the phenotype in the 10 selected cases, further sequencing was performed for all individuals in generations II-IV where DNA was available (n=29). This revealed that the variant segregated with the phenotype within the whole family. As such, 15 of 16 affected individuals (93.8%) were confirmed to be heterozygous for the mutation, and 13/13 unaffected individuals, (100%) were wild type (**Figure 4.7**). Individual II-8 was the only case where the variant was not correctly attributed to the phenotype. Importantly, however, hearing loss in II-8 was diagnosed aged 42 years whereas the remainder of the family were diagnosed with hearing loss in childhood or early adulthood, mean age of diagnosis=6.3±5.7 years. Thus, the age of

hearing loss diagnosis in II-8 is >2 SD greater than mean of rest of family. This individual was removed from further analysis and considered most likely to have another cause for hearing loss.

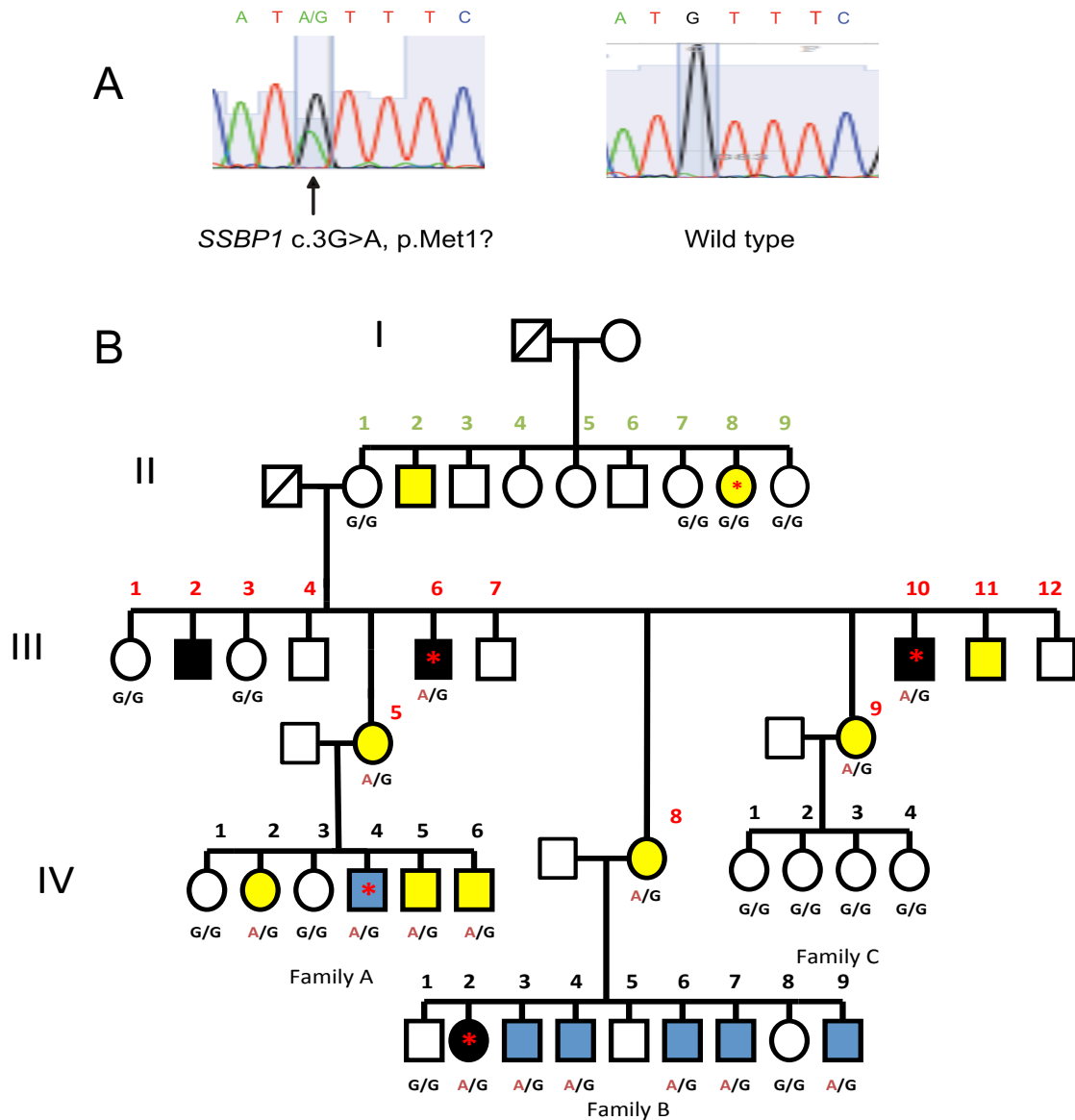


Figure 4.7. Segregation analysis of c.3G>A *SSBP1* variant within the Finnish family. (A) Confirmatory Sanger sequencing electropherograms of *SSBP1* variant. Sequencing of the *SSBP1* variant reveals segregation with the phenotype in the Finnish family (sequencing result of III-9, affected, and IV-3 (A), unaffected, reveals c.3G>A variant and wild type sequence respectively). (B) Finnish pedigree, sequencing result noted below each individual: G/G represents wild type alleles, A/G represents heterozygous variant. Symbols are as follows: yellow filled-, high frequency hearing loss; grey filled-, moderate progressive pan-frequency hearing loss; black filled profound pan-frequency hearing loss; unfilled-, normal hearing, red star- exome sequenced individual (II-8, III-6, III-10, IV-4 (A) and IV-2 (B)).

4.3.2.1.3 Sanger sequencing of *SSBP1* c.3G>A in children of fathers in generation III

The members of the multi-generational Finnish family were originally identified and characterised by Professor Kari Majamaa, Oulu University, Finland (Lehtonen, Uimonen et al. 2000). As a clinical mitochondrial diagnosis, the initial phenotyping study focussed solely on the maternal lineage. Having identified the *SSBP1* c.3G>A variant, we hypothesised that the children of the fathers in generation III would not carry m.1555A>G, given the strict maternal inheritance of mtDNA, but may carry the *SSBP1* variant inherited from their fathers. Sanger sequencing of the *SSBP1* in the children of III-6 (n=9, 2 male: 7 female) and of III-10 (n= 6, 4 male: 2 female) revealed 10/15, (66.7%) were carriers of the *SSBP1* c.3G>A variant but all carried the wild- type m.1555A allele (**Figure 4.8**). An investigation into the clinical history of these children revealed that school hearing tests indicated normal hearing in all individuals (personal communication, Dr Sanna Hakli, Oulu University, Finland).

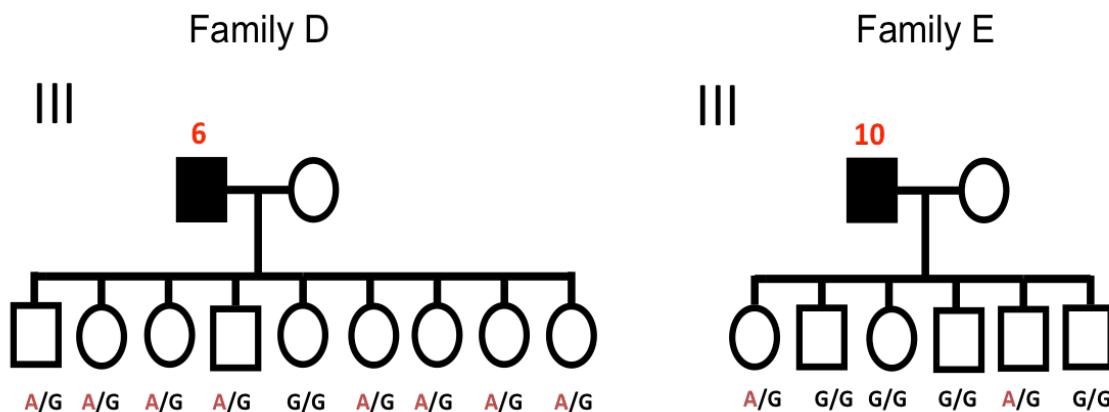


Figure 4.8. Sanger sequencing analysis of the c.3G>A *SSBP1* variant in the children of III-6 (Family D) and III-10 (Family D). Sequencing results noted below each individual: G/G represents wild type alleles, A/G represents heterozygous variant. Symbols are as follows: black filled- profound pan-frequency hearing loss; unfilled-, normal hearing.

4.3.2.1.4 Hypothesis 3

There is a conserved genetic mechanism identified in the Finnish family that also causes disease in the sporadic Spanish cohort.

Having identified the *SSBP1* variant segregating with the phenotype in the Finnish family the read coverage and depth for all CCDS bases in *SSBP1* was performed by Dr Helen Griffin (Newcastle University, UK) using SAMtools (Li, Handsaker et al. 2009). Custom Perl scripts were then used to calculate mean base depth across the exome and within the

genes of interest together with the percentage of bases covered above a depth of 30, 10, 5 and 1 read depth. This revealed that the 100% of CCDS bases in *SSBPI* were covered at 10-fold read depth in all exome sequenced individuals (familial cases n=5, sporadic cases n=4), implying that pathogenic variants within this gene were unlikely to be missed as false negatives. Nevertheless, all coding exons of the *SSBPI* gene (exon 2-7) were also Sanger sequenced in the 9 individuals in the Spanish cohort, confirming that no variants were present in any individual.

Whilst no variants in *SSBPI* were therefore seen in the sporadic cases, we subsequently sought to identify if a single rare, deleterious variant in another established mitochondrial replication protein (**Table 4.9**) was shared between all individuals. Further analysis of 16 genes from the exome sequencing data of these individuals revealed there were no shared variants between all 4 or even 3 individuals within these genes, suggesting that no shared allele within mitochondrial DNA replication proteins was responsible for disease in the sporadic cases.

4.3.2.1.5 Hypothesis 4

A novel genetic variant(s) are responsible for disease within the Spanish sporadic cases.

Having excluded the possibility of either a single variant, or multiple variants in an established hearing loss gene cause disease in the sporadic Spanish cases (Hypothesis 1b), we sought to determine whether a single mutation was present between all four individuals in a novel disease gene, which would be consistent with the hypothesis of a possible conserved single allele causing disease in all four individuals. The same filtering strategy as was used in Hypothesis 2 was employed. However, we did not find any rare, non-synonymous alleles with predicted pathogenicity that were shared between all four, or even three of the Spanish cases suggesting that was no shared genetic variant causing disease (**Figure 4.10**).

An alternative hypothesis that a ‘burden’ of rare variants in a novel gene was responsible for the phenotype in the Spanish cases was also considered. Restricting the analysis to rare heterozygous mutations revealed no genes in which rare, deleterious variants were shared between more than 2 individuals (**Figure 4.9**). In order to generate some power calculations for the number of cases we would therefore require to detect a novel gene that may be associated with deafness in m.1555A>G carriers, we determined that we would require 42 carriers of m.1555A>G (assuming 50% carry a variant) and 42 controls to have

95% power to detect a 100% difference in allele frequency, or 287 affected and unaffected individuals to have a 95% power to detect a 50% difference in allele frequency (Faul, Erdfelder et al. 2009). Given that these cohorts are significantly larger than the samples available in this study, further investigations for a burden of mutations in sporadic cases was not undertaken, but is discussed in **Section 4.4**.

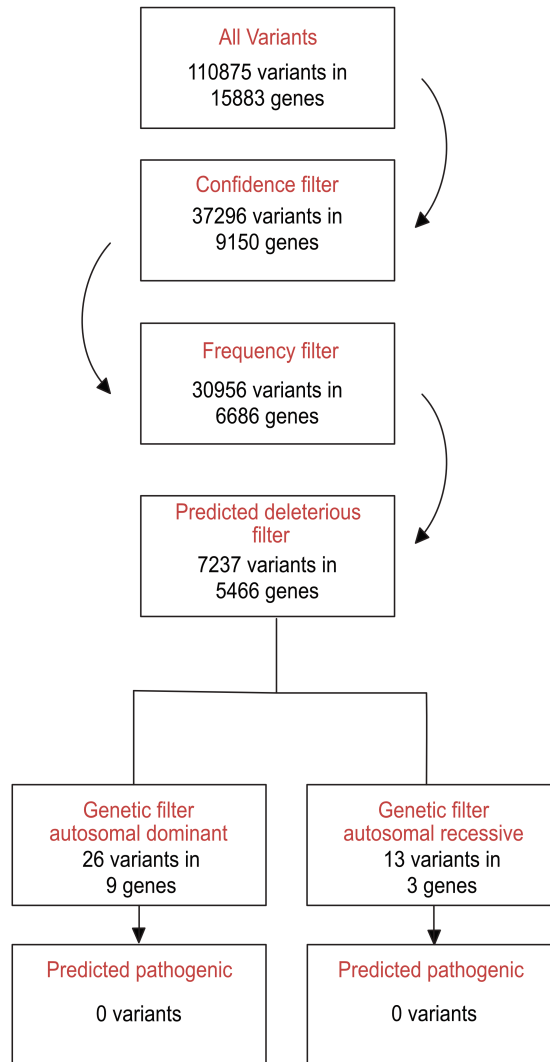


Figure 4.9. Hypothesis 4 variant filtering workflow. All variants were iteratively filtered using defined criteria as discussed above to attempt to identify rare, deleterious variants shared by at least 3 of 4 Spanish sporadic cases.

4.3.3 Mitochondrial variants mediating disease risk

An alternative mechanism by which the m.1555A>G variant may be associated with hearing loss in these individuals is through the co-association of a separate mtDNA variant acting with m.1555A>G in a synergistic or additive manner. In this instance it is also possible that the m.1555A>G variant is simply an ‘innocent bystander’, and the phenotype is dependent on the other mtDNA variant (Swalwell, Blakely et al. 2008). We deemed that this possibility was however unlikely, as patients were selected from 2 international collaborators that had screened for mitochondrial causes of deafness within their respective clinical laboratories. In both cases whole mitochondrial genome sequencing was performed, and m.1555A>G considered the only candidate for causing hearing loss (personal communication, Professor Julio Montoya and Professor Kari Majamaa).

Table 4.20. mtDNA haplogroups of all exome sequenced individuals as determined by MITOMASTER and Phylotree analysis. SNP = single nucleotide polymorphism.

Individual	Haplogroup	Haplogroup defining SNP
Finnish family		
II-8	J1c	m.295C>T, m.12612A>G, m.14798T>C
III-6	J1c	m.295C>T, m.12612A>G, m.14798T>C
III-9	J1c	m.295C>T, m.12612A>G, m.14798T>C
IV-2	J1c	m.295C>T, m.12612A>G, m.14798T>C
Spanish cohort		
DF95	H1b	m.12705T>C, m.14766T>C, m.10454 T>C
DF178	U5b	m.12308A>G, m.7768A>G
DF40	H3q	m.12705T>C, m.14766T>C, m.12236G>A
DF39	U8a	m.12308A>G, m.282T>C, m.6392T>C

In order to determine whether the mtDNA haplogroup background may modify disease risk caused by the m.1555A>G variant, we used ‘off target’ mtDNA reads from each exome sequenced individual to assign the appropriate haplogroups using the MITOMASTER bioinformatic tool manually cross-referenced by Phylotree (www.phylotree.org) (Brandon, Ruiz-Pesini et al. 2009, van Oven and Kayser 2009). This confirmed all individuals were from European mtDNA haplogroups (**Table 4.20**). The Spanish cases were assigned to either Haplogroup H or U, haplogroups commonly found in the Iberian peninsula (Torroni, Huoponen et al. 1996). The Finnish family were

assigned to Haplogroup J1c, a haplogroup that has previously been suggested to modify the disease penetrance of the LHON mutation m.14484A>G (Hudson, Carelli et al. 2007). Although an interesting finding, given the haplogroup is shared between affected and unaffected family members it cannot be a causative factor in the variable penetrance of the phenotype in our patients.

4.4 Discussion

By exome sequencing of 5 individuals in a multi-generational Finnish family that transmitted the m.1555A>G variant along the maternal lineage but manifested a variable penetrance of hearing loss, we identified the heterozygous variant c.3G>A *SSBPI*. Exome sequencing results were confirmed by Sanger sequencing in each of these individuals and a further segregation analysis in the family determined the variant was correctly attributed to the phenotype in 28 of 29 individuals. *SSBPI* encodes a mitochondrial protein; single stranded binding protein (SSBP1) that forms a core component of the mtDNA replisome machinery. Given the important role of SSBP1 in mitochondrial metabolism as discussed in **Section 1.8.2.3** it was considered as the primary candidate to take forward for further analysis (presented in **Chapter 5**).

Given that 28 individuals were found to segregate the *SSBPI* variant with the phenotype, the odds that this mutation segregates with disease by chance are therefore $<1 \times 10^{-6}$ (binomial test). Additionally, 10/15 of the children of III-6 and III-10 carry the *SSBPI* variant without the m.1555A>G variant and have normal hearing. Together, this evidence adds substantial weight to the conclusion that the *SSBPI* variant is a strong candidate for a nuclear genetic modifier of the phenotype associated with the m.1555A>G variant but in isolation is not pathogenic.

Incidentally, the c.2207C>T variant in *MGAM* was also found to segregate with the phenotype in the Finnish family. This gene encodes maltase-glucoamylase, a brush border membrane enzyme that functions in the digestion of starch (Sim, Quezada-Calvillo et al. 2008). In keeping with its biological function, the protein is primarily expressed in the small intestine with low expression in the central nervous system (Genecards 2017). To date there are no reports in the literature linking *MGAM* variants and hearing loss, nor is it possible to envisage a potential mechanism whereby *MGAM* variants could cause hearing loss or modulate mitochondrial function. Given that *SSBPI* and *MGAM* are separated by

297 Kb on chromosome 7, it is likely that the *MGAM* variant is a non-pathogenic SNP in linkage disequilibrium with the *SSBPI* variant and that the two are inherited together within the family. Taken together, this evidence strongly suggests the *SSBPI* variant is the more likely candidate modifier gene within the family.

There was one individual, II-8, in whom the *SSBPI* variant was found incorrectly attributed to the phenotype (II-8 is affected by hearing loss but carries the wild-type allele). However, in this individual, hearing loss was not diagnosed until 42 years of age and significantly, this individual was known to have experienced recurrent childhood ear infections (personal communication, Dr Sanna Hakli, Oulu University, Finland). While we accept that heterogeneity exists in mitochondrial deafness (Uimonen, Moilanen et al. 2001), the significant difference in the age of onset of hearing loss in this individual compared to the rest of the family combined with the history of infections raises enough doubt that we consider alternative forms of deafness to be highly likely in this woman who was therefore removed from further analysis. This highlights the importance of ‘deep phenotyping’, the practice of precisely defining phenotypes to minimise the confounding effect of phenotypic heterogeneity in genetic studies to (Robinson 2012).

A number of factors may account for the inability of our experimental strategy to identify causes of the hearing loss in the Spanish sporadic cases. Importantly, it is possible that there is no genetic cause to be found in the Spanish individuals whose hearing loss may be environmentally determined. Specifically, aminoglycosides are a recognised cause of hearing loss in carriers of m.1555A>G and remain widely used in Spain (Fernandez-Martinez, Miro et al. 2015). We were unable to ascertain whether any of the Spanish cohort had been exposed to aminoglycosides and therefore we could not eliminate this as a potential confounding factor.

Initially, we felt it important to exclude potential monogenic cases of hearing loss that may confound the lack of observed replication in the Spanish cases. Using established clinical gene lists we found no evidence that any individual in the Spanish cohort was likely to have an alternative, established genetically mediated form of deafness. However, we cannot exclude the possibility that the hearing loss in these individuals resulted from variants in hitherto uncharacterised genes physiologically linked to hearing.

Similarly, we aimed to identify whether a conserved pathological mechanism underpinned the hearing loss in both the Finnish and Spanish individuals. To this effect, we screened known genes coding for mtDNA replication proteins; however, we were unable to identify rare, deleterious shared variants in these genes. With this established, we aimed to detect the presence of causative variants in novel genes with only 4 samples, limited by power and reliant on a ‘founder mutation’. This was not the case.

The c.3G>A *SSBPI* variant is found in 4/120610 sequenced alleles in the ExAC database (3/6610 Finnish, 1/66404 European non-Finnish and 0/47596 non-European alleles) possibly indicating a founder effect within the Finnish population. Hence, given its rarity in the general population, it is unsurprising that the variant was specific to the Finnish family and we were therefore unable to detect this variant in the Spanish cohort. Given that the Spanish individuals are derived from a more genetically diverse population than the Finnish family, it is less likely that founder mutations will be identified in selected unrelated individuals as in our cohort. The identification of recurring alleles in an outbred population would therefore require a far larger sample size.

Exome sequencing has a number of technical limitations to be considered in the context of the failure to identify a cause for the hearing loss in the Spanish cohort. Firstly, by definition, exome sequencing interrogates only the exonic component of the genome, and hence only covers ~ 2% of the genome (64 million / 3 billion bases) (Ng, Turner et al. 2009). Although the vast majority of variants causing Mendelian disease are found in protein-coding sequences (Stenson, Mort et al. 2017), non-coding variants and epigenetic modifications are now realised to be causative for a number of diseases and hence may account for the hearing loss in some or all of the Spanish individuals (Spielmann and Mundlos 2016).

Secondly, as only 1-2% of the human genome is comprised of protein coding sequences, exon-targeting capture is a necessary step in exome sequencing. The exon-capture probes are designed based on sequences in gene annotation databases. This creates an inherent bias, as exons which anneal well to capture probes are often easy to sequence in comparison to those with poor probe specificity, leading to the possibility of false negative variant calls. Thirdly, there is heterogeneity in the coverage of sequenced exons due to differences in base composition, for example GC-poor and GC-rich sequences may show biased PCR amplification compromising genome assembly (Chen, Liu et al. 2013). It is

therefore possible that causative variants lie within regions that are not adequately covered by our exome sequencing. Additionally, we are unable to exclude the possibility that structural variation including copy number variations (CNVs) or chromosomal rearrangements may account for the hearing loss in a proportion of Spanish individuals. This class of genomic alterations has recently been shown to be causative for some forms of non-syndromic hearing loss (Shearer, Kolbe et al. 2014); however, detection of these changes by exome sequencing remains technically challenging (Hong, Singh et al. 2016).

There are also a number of factors that may confound the analysis and filtering of exome data leading to the exclusion of causative variants. Firstly, disease-causing variants may have been incorrectly filtered, as pathogenic mutations are known to be included in public databases such as 1000 genomes, dbSNP and ExAC (Arthur, Cheung et al. 2015). Secondly, prediction of variant pathogenicity is reliant on the use of computational algorithms. There are numerous reports of the successful utilisation of *in silico* prediction programs to isolate causative pathogenic variants (Macia, Halbritter et al. 2017, Srour, Shimokawa et al. 2017); but their results also frequently disagree due to differences in their underlying algorithms (Leong, Stuckey et al. 2015). It is therefore recommended that pathogenicity prediction results should always be interpreted cautiously (Walters-Sen, Hashimoto et al. 2015). Interestingly, the c.3G>A variant in *SSBPI* identified segregating in the Finnish family was defined as ‘pathogenic’ by SIFT but ‘benign’ by PolyPhen2. Further analysis of this variant using the alternate *in silico* prediction tools, MutationTaster (Schwarz, Rodelsperger et al. 2010) and LRT (Chun and Fay 2009), both suggested this variant was indeed pathogenic. This disparity between prediction tools is important as it highlights the converse possibility that causative variants may have been discarded in our analysis based on incorrect assignment as benign.

Causative variants may also have been excluded if they occurred at a MAF above our cut-off threshold. Setting a higher MAF threshold increases the number of variants remaining after iterative filtering, often producing an unmanageably large list of variants that cannot be further analysed and ultimately which must be classified variants of unknown significance. The setting of a MAF threshold is arbitrary, hence, MAFs may vary between databases (Manolio, Collins et al. 2009). This can lead to potential difficulties filtering variants predicated on a defined MAF threshold.

Another possibility is that each discrete Spanish individual carries a different disease causing nuclear variant, analogous to focussing our analysis on a single member of the Finnish family without the ability to perform segregation analysis. Furthermore, assigning pathogenicity to variants isolated in singleton cases is fraught with difficulty considering it has been estimated that the average healthy individual carries >400 damaging variants (Xue, Chen et al. 2012).

It is possible that the individuals in the Spanish cohort carry different pathological variants in the same gene, a so-called ‘genetic burden’. However, obtaining the statistical power to ascertain whether there is an enrichment of causative variants in certain genes in cases versus controls requires large cohorts of carriers. As the cost of NGS technologies decreases it becomes increasingly feasible to construct large genetically and phenotypically characterised patient databases. One such database, The NIHR Bioresource (<https://bioresource.nihr.ac.uk/>) could potentially be used to find carriers of m.1555A>G both with and without hearing loss. Analysis of the exomes and whole genomes of these patients could potentially provide a powerful approach to define novel genetic modifier genes.

In conclusion, the work presented in this chapter has demonstrated that exome sequencing coupled with segregation analysis is a powerful technique to identify nuclear genetic modifiers of mitochondrial diseases. Through our analysis we established the c.3G>A variant in *SSBP1*, that encodes a core component of the mitochondrial DNA replisome machinery, as a strong candidate accounting for the variable penetrance of hearing loss in the Finnish family. However, we were not able to demonstrate a conserved mechanism of hearing loss in the Spanish sporadic cases implying divergent mechanisms account for hearing loss in m.1555A>G carriers. The functional characterisation of the *SSBP1* variant constitutes the body of work presented in **Chapter 5**.

Chapter 5

Characterising the functional effect of the *SSBPI* variant

5.1 Introduction

The work presented in **Chapter 4** detailed the use of exome sequencing in familial and sporadic carriers of the m.1555A>G variant in the 12S rRNA gene, *MT-RNR1*. This approach addressed the hypothesis that a nuclear genetic modifier accounted for the variable manifestation of hearing loss in carriers of this mtDNA variant. Our strategy identified the heterozygous variant c.3G>A in *SSBPI* that segregated with hearing loss in a multi-generational Finnish family. To further elucidate the underlying pathological mechanism we studied primary and immortalised fibroblasts derived from (i) two individuals from the Finnish family carrying both the *SSBPI* and m.1555A>G variants, (ii) a patient carrying m.1555A>G without any known nuclear genetic modifier of m.1555A>G and (iii) established laboratory controls from non-hearing impaired patients who do not carry the m.1555A>G variant. Our investigations centred on the determining whether the *SSBPI* and m.1555A>G variants compromised their primary biological functions, specifically mtDNA maintenance and mitochondrial translation respectively.

We also characterised the effect on mitochondrial respiration (OXPHOS), mitochondrial dynamics, oxidative stress and mitochondrial retrograde signalling pathways in our model, attempting to further clarify the downstream consequences of these variants. Additionally, we studied myoblasts and skeletal muscle biopsies derived from familial cases and age matched controls to gain insight into the mechanisms underpinning the tissue specific disease observations in our patients.

5.2 Materials and methods

5.2.1 Cell lines and skeletal muscle

Primary fibroblast cell lines were established from (i) two individuals from the Finnish family (III-6, P1 and III-5, P2) carrying the c.3G>A *SSBPI* and m.1555A>G variants, (ii) an unrelated individual carrying m.1555A>G alone (P3) identified from the Newcastle

Academic Health Partners Bioresource (Newcastle University, UK) (**Table 5.1**) and (iii) three control lines (C1–C3) (**Table 5.2**). Primary myoblast cell lines were established from III-6, (P1m) and III-5, (P2m). Immortalised fibroblast cell lines were established from III-6 (P1i) and III-5 (P2i), P3 (P3i) and from C1 and C2 (C1i, C2i) as described in **Section 2.1.5 (Table 5.1 and Table 5.2)**. Skeletal muscle biopsies from individuals III-10 (P4) and III-8 (P5) were collected by Professor Kari Majamaa (Oulu University, Finland) (**Table 5.3**).

When presenting the results of the following experiments the term ‘patients’ refers to a group consisting of P1, P2 and P3. The results of individual cell lines are specified using the nomenclature presented in **Table 5.1** and **Table 5.2**.

For clarity, ‘*SSBPI*’ used in the text as an identifier refers to grouped P1 and P2 fibroblasts/myoblasts or P4 and P5 skeletal muscle tissue, although it should be noted that these cells also carry the m.1555A>G variant. When appropriate, ‘m.1555A>G’ used as an identifier refers to P3 fibroblasts.

Table 5.1. Clinical and genetic features of the patient derived fibroblast cell lines. I.D. = identifier P = profound pan-frequency hearing loss, HF = high frequency hearing loss, N = normal hearing.

Primary fibroblast I.D	Immortalised fibroblast I.D	Pedigree code	Age (years)	Sex (M/F)	Clinical features	Variants
P1	P1i	III-6	37	M	P	m.1555A>G <i>SSBPI</i> c.3G>A
P2	P2i	III-5	36	F	HF	m.1555A>G <i>SSBPI</i> c.3G>A
P3	P3i	n.a	28	M	N	m.1555A>G

Table 5.2. Details of the control fibroblasts. ID. = identifier. Laboratory I.D denotes identifiers of established cell lines used in Professor Chinnery’s group; n.a = not applicable, -= unknown.

Primary fibroblast I.D	Laboratory I.D	Immortalised fibroblast I.D	Age (years)	Sex (M/F)
C1	F253	C1i	-	-
C2	F153	C2i	23	F
C3	F152	n.a	27	F

Table 5.3. Clinical and genetic details of skeletal muscle biopsies. P = profound pan-frequency hearing loss, HF = high frequency hearing loss.

Patient ID.	Pedigree code	Age (years)	Sex (M/F)	Clinical features	Variant
P4	III-10	38	M	P	m.1555A>G <i>SSBPI</i> c.3G>A
P5	III-8	41	F	HF	m.1555A>G <i>SSBPI</i> c.3G>A

5.2.2 Genomic DNA extraction and Sanger sequencing

Total genomic DNA was extracted from cultured fibroblasts, myoblast cells or skeletal muscle using the DNeasy® Blood & Tissue Kit (Qiagen) as described in **Sections 2.3.1 and 2.3.2**. Sequencing of the c.3G>A *SSBPI* variant was performed as described in **Section 2.3.7** using primer pairs as shown in **Table 4.11**. Further bioinformatic analysis was undertaken using NCBI ORF Finder and Clustal Omega as described in **Section 2.3.14.2**. Confirmation of the m.1555 A>G variant was performed by Sanger sequencing as described in **Section 2.3.7**. The primer pairs are detailed in **Table 5.4**. The sequencing results were analysed using SeqScape v2.6 comparing against the rCRS reference sequence (NCBI accession number NC_012920).

Table 5.4. Primer sequences, annealing temperatures and mtDNA nucleotide position for targeted analysis of m.1555

mtDNA Fragment	Primer direction	Primer Sequence 5'-3'	Anneal temp (°C)	mtDNA position
2	Forward	TGTAACAAACGACGGCCAGTTTAAACTCA AAGGACCTGGC	60	1157-1177
2	Reverse	CAGGAAACAGCTATGACCCTGGTAGTAA GGTGGAGTGGG	60	1709-1689

5.2.3 Protein analysis

Western blot analysis was performed on 40 µg protein from total cell lysate extracted from harvested fibroblasts as described in **Section 2.4.5**. Specific proteins were detected using primary and secondary antibodies as detailed in **Table 2.6**. Normalisation of the densitometric quantification of a protein of interest was performed using GAPDH as

described in **Section 2.4.5**. Analysis of phosphorylated and total proteins by Western blot was undertaken by first probing with the antibody to the phosphorylated protein, stripping the membrane as described in **Section 2.4.5**, and then re-probing with the antibody specific to the total protein. Intra-mitochondrial *de novo* protein synthesis was measured by the *in vivo* mitochondrial translation assay as described in **Section 2.4.9**. The AMPK alpha SimpleStep ELISA and Phospho-AMPK-pT172 ELISA Kit were used to quantify total AMPK-A and phosphorylated AMPK-pT172 respectively as described in **Sections 2.4.6** and **2.4.7**. These results were used to generate a ratio of Phospho-AMPK-pT172: total AMPK-A (AMPK-P:AMPK-A) as a marker of AMPK signalling activity.

5.2.4 Skeletal muscle analysis

Biopsy samples were snap frozen in liquid nitrogen and maintained at -80°C. Tissue preparation, sectioning and staining for (i) H&E and (ii) combined COX/SDH was performed as detailed in **Section 2.2.1**. Age matched control skeletal muscle biopsy samples were obtained from the Cambridge BioResource, Cambridge, UK.

5.2.5 Long range polymerase chain reaction

For the investigation of mtDNA deletions a fragment of approximately 16 kB (see **Table 2.1** for PCR product sizes) that encompasses almost the entire mitochondrial genome was amplified by long range PCR and visualised by agarose gel electrophoresis as described in **Section 2.3.5**.

5.2.6 Analysis of mitochondrial 7S DNA

Total cellular DNA was extracted by two sequential phenol-chloroform extractions with subsequent precipitation from fibroblast cell lines as described in **Section 2.3.12.1**. Five µg of total DNA was restricted using PvuII and run on a 0.6% agarose gel. Southern blotting using specific radiolabelled probes to 7S DNA (Probe A) and 28S was performed as described in **Section 2.3.12.5**.

5.2.7 Mitochondrial repopulation assay

The mitochondrial repopulation assay was undertaken as described in **Section 2.3.13.1**. Genomic DNA was isolated from individual fibroblast pellets as described in **Section 2.3.1**. The mtDNA copy number was determined by performing the *MT-*

ND1/B2M qPCR assay as described in **Section 2.3.9**. RLs were calculated as described in **Section 2.3.13.2**. The repopulation rate of each cell line was calculated by taking the gradient of a linear regression line of mtDNA copy number ratio treated:untreated (RL) in the repopulation phase.

5.2.8 Quantitative real time polymerase chain reaction

Relative mtDNA copy number was determined using the CFX96 C1000 Touch Thermocycler using either *MT-ND1* (mitochondrial reference gene) and *B2M* (nuclear reference gene) or *MT-CO3* (mitochondrial reference gene) and *RNaseP* (nuclear reference gene) as described in **Section 2.3.9**. Quantification of the expression of specific genes was carried out with qPCR using the TaqMan gene Expression Assay using cDNA synthesised from RNA extracted from primary fibroblasts as described in **Section 2.3.10**. Details of the Taqman Gene Expression Assays used in qPCR for gene expression analysis are shown in **Tables 2.2** and **2.3**.

5.2.9 Analysis of mitochondrial bioenergetics and oxidative stress

Cellular ROS were measured using the fluorescent cell permeant dye H₂DCFDA. The Oxiselect™ Oxidative DNA Damage kit was used to measure 8-OHdG DNA modifications. Oxyblot™ Protein Oxidation Detection Kit was used to detect oxidative modification of the cellular proteome. Cellular respiration was assessed with the Seahorse XF96^e extracellular flux analyser. Detailed methodology for these assays is described in **Section 2.6**. Cell growth was assessed by growing fibroblast cells with high glucose medium vs glucose-free medium supplemented with 5mM galactose using IncuCyte® Live Cell imager as described in **Section 2.1.6**. Cell doubling times were calculated by nonlinear regression using an exponential growth equation in Graphpad v7 (Graphpad statistical software).

5.2.10 Mitochondrial network and nucleoid analysis

The mitochondrial network was analysed using live cell imaging as described in **Section 2.5.1**. Images were processed with Image J and further morphological analysis was undertaken with Huygens Essentials software as described in **Section 2.5.2**. Mitochondrial nucleoids were analysed by immunocytochemistry and confocal microscopy as described in **Section 2.5.5**

5.2.11 Heat shock response assay

For the heat shock response assay primary fibroblasts were either maintained at 37°C or treated with heat shock at 42°C for 1 hour and allowed to recover at 37°C for 4 hours. Western blot analysis was then performed using antibodies to HSP60, HSP70 and BiP as described in **Section 2.4.8**. The densitometric quantification of HSP60, HSP70 and BiP at steady state (pS) and after heat shock (pHS) was used to calculate a protein induction fold change defined as pS:pHS.

5.3 Results

5.3.1 Confirmatory Sanger sequencing of *SSBP1* and m.1555A>G variants

Sanger sequencing of DNA extracted from primary and immortalised fibroblasts from P1 and P2 confirmed the presence of the heterozygous c.3G>A *SSBP1* and m.1555A>G variants which were absent in control cells (**Figure 5.1**). Sanger sequencing of DNA extracted from primary and immortalised fibroblasts from P3 confirmed the presence of m.1555A>G and wild type *SSBP1* (**Figure 5.1**).

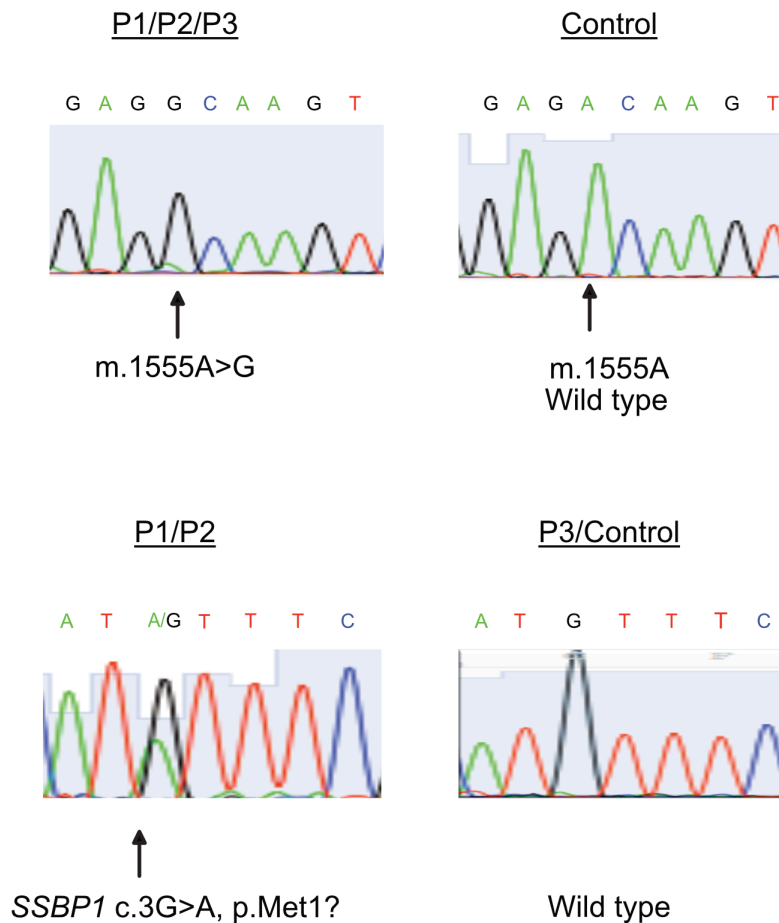
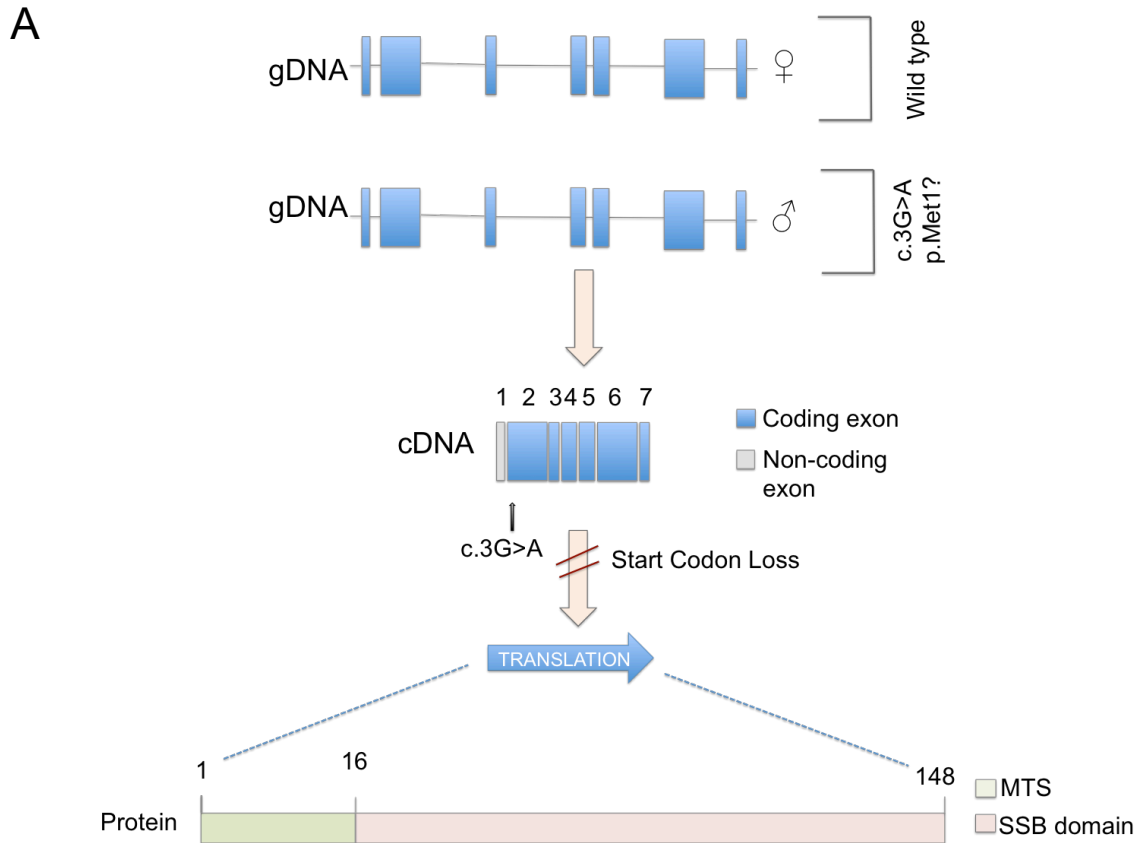


Figure 5.1. Confirmatory Sanger sequencing electropherograms of m.1555A>G and *SSBP1* variants. Sequencing traces are representative of results from DNA extracted from primary and immortalised patient and control fibroblasts.

5.3.2 Genetic effect of the c.3G>A *SSBP1* variant

The c.3G>A variant is situated in the first coding exon (exon 2) of the *SSBP1* gene. The variant is predicted to cause a loss of the third base of the primary start codon ATG coding for methionine and result in the loss of protein translation from one allele (**Figure 5.2 A**). Consistent with the critical role the start site methionine plays in translation initiation, an evolutionary analysis demonstrated complete invariance of the residue across species (**Figure 5.2 B**). Using the NCBI ORF Finder tool, a single alternative out of frame translation start site is found downstream of the canonical start site at codon 16. Activation of this downstream start codon creates a new reading frame and introduces a stop codon at codon 30. This is predicted to produce a truncated protein of 14 amino acids lacking the mitochondrial targeting sequence (MTS).



B

H_sapiens	1	MFRRPVLQVLRQFVRHESETTISLVLERSL--
M_mulata	1	MFRRPVLQVLRQFVRHESETSTISLVLERSL--
P_abelii	1	MFRRPVLQVLRQFVRHESETASSLVLERSL--
B_taurus	1	MFRRPVQVLRQFVRHESEVASSLVLERSL--
R_norvegicus	1	MFRRPVLQVLRQFVRQESEVASSLVLERSL--
M_musculus	1	MFRRPVLQVLRQFVRHESEVASSLVLERSL--
X_laevis	1	MFRPALQVLRQFARCS--TDSVILERSLTK

Figure 5.2. Genomic structure of *SSBP1* gene and multiple sequence alignment of the *SSBP1* protein. (A) *SSBP1* exons marked 1–7, exon 1 is a non-coding exon. Location of c.3G>A variant in exon 2 causing translation start loss mutation marked and resulting in an effective null allele. The wild-type allele (represented as the maternal allele) is unaffected and produces a normal protein product. MTS = mitochondrial targeting sequence, SSB domain = single stranded binding domain. (B) Multiple sequence alignment of *SSBP1* across evolutionarily diverse species generated using Clustal Omega. Conserved methionine residue altered by c.3G>A *SSBP1* is boxed in red.

5.3.3 SSBP1 protein expression in fibroblasts

On the basis on the evidence presented in **Section 5.3.2** we evaluated the effect of the *SSBP1* variant on SSBP1 protein expression by Western blot analysis in primary and immortalised fibroblasts from patient and control fibroblasts. This revealed the SSBP1 protein was reduced to approximately 20% of control levels in P1 and P2 fibroblasts whereas there was no significant difference in the expression of SSBP1 between P3 and controls (**Figure 5.3**).

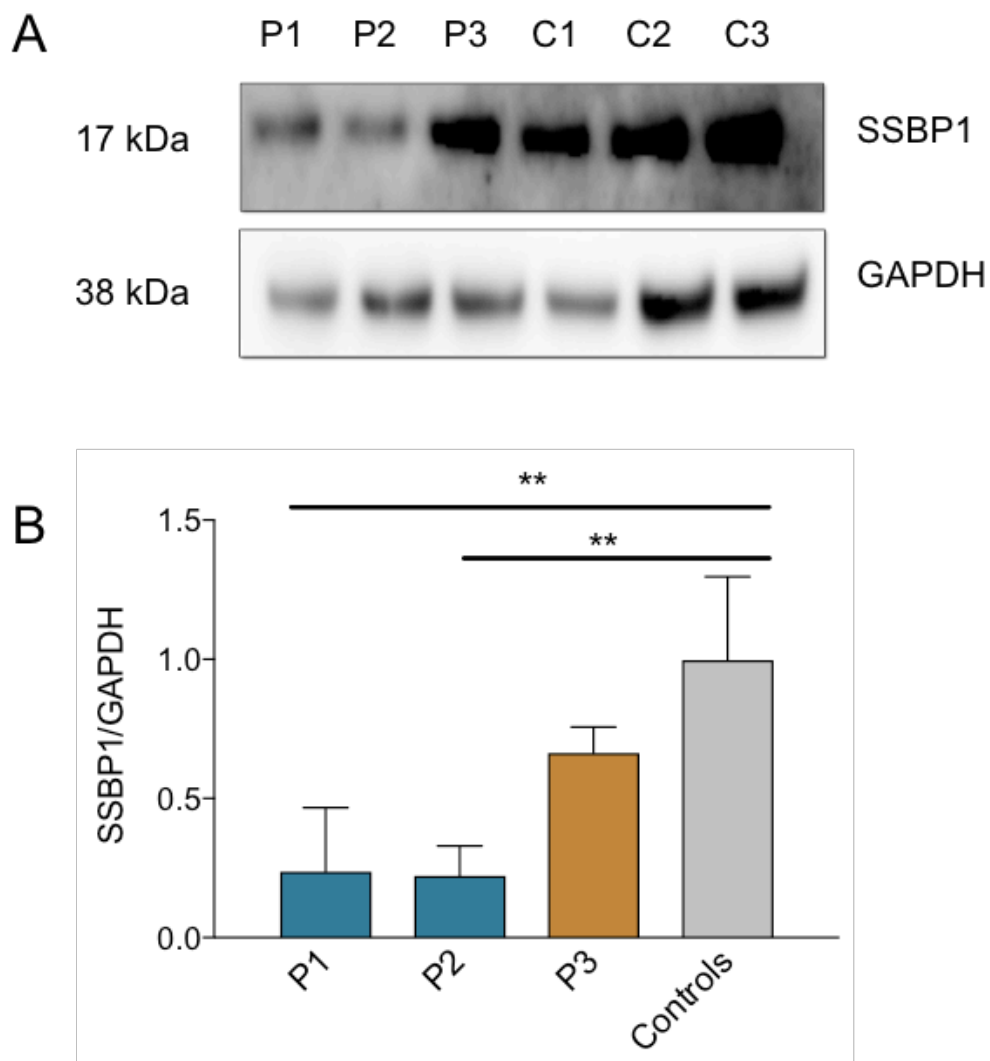


Figure 5.3. SSBP1 protein analysis in patient and control fibroblasts. (A) Western blot analysis of SSBP1 in primary patient (P1–P3) and control fibroblast cell lines (C1–3). Image representative of 3 independent experiments. Western blot analysis results were comparable in immortalised fibroblasts. (B) Densitometric quantification of SSBP1 normalised to GAPDH for primary fibroblasts. P1=0.24±0.23, P2=0.22±0.1, P3=0.66±0.09, Controls=1.0±0.30. Data represents mean normalised SSBP1±SD of 3 independent experiments, **p<0.01 (one way ANOVA with post hoc Tukey test).

5.3.4 *SSBP1* gene expression in fibroblasts

To determine whether the *SSBP1* variant affected gene transcription, the levels of mRNA expression of *SSBP1* in patient (P1–P3) and control (C1–C3) primary fibroblasts was measured using the Taqman® Gene Expression Assay, observing no significant difference between patient and control cells (**Figure 5.4**).

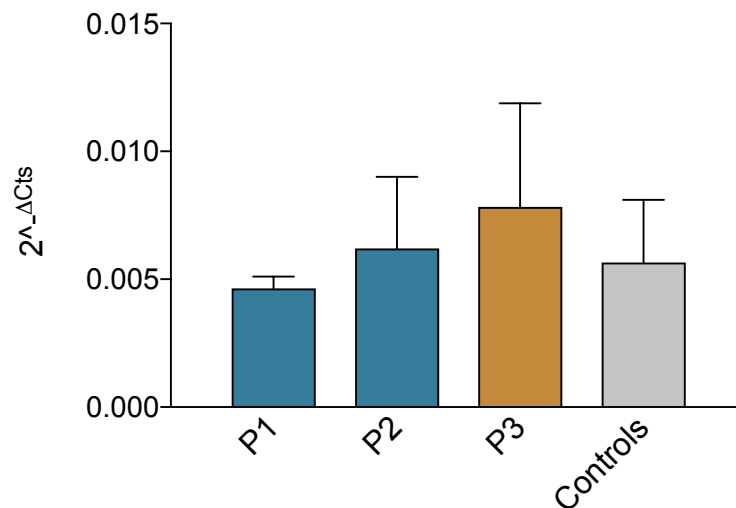


Figure 5.4. *SSBP1* mRNA expression in patient and control fibroblasts. mRNA expression of *SSBP1* in patient (P1–P3) and control (C1–C3) primary fibroblasts measured by the Taqman® Gene Expression Assay. For data normalisation *GAPDH* was used as an endogenous housekeeping gene. Normalisation of Ct values and determination of gene expression was calculated using the $2^{-\Delta Ct}$ ($2^{-\Delta Ct}$) method. P1=0.005±0.0005, P2=0.006±0.003, P3=0.008±0.004, Controls=0.006±0.002. Data represents mean $2^{-\Delta Ct}$ ±SD of 3 biological replicates. No results were significantly different (one way ANOVA).

5.3.5 Analysis of *SSBP1* skeletal muscle biopsy

5.3.5.1 Muscle Histochemistry

Mutations in mtDNA or nuclear genes encoding mitochondrial proteins often present with deficiencies of the respiratory chain (Gorman, Chinnery et al. 2016). Mitochondrial histochemistry provides a reliable method to detect the resulting OXPHOS dysfunction in tissue biopsies (Section 2.2.1) (Taylor, Schaefer et al. 2004). H&E staining of skeletal muscle sections from P5 were unremarkable with no evidence of necrosis, centralised nuclei or inflammatory infiltrates. Sequential COX/SDH staining, however, revealed evidence of a respiratory chain deficiency with a low number of COX-negative and COX intermediate fibres estimated at 5/174 fibres (3.4%, Figure 5.5).

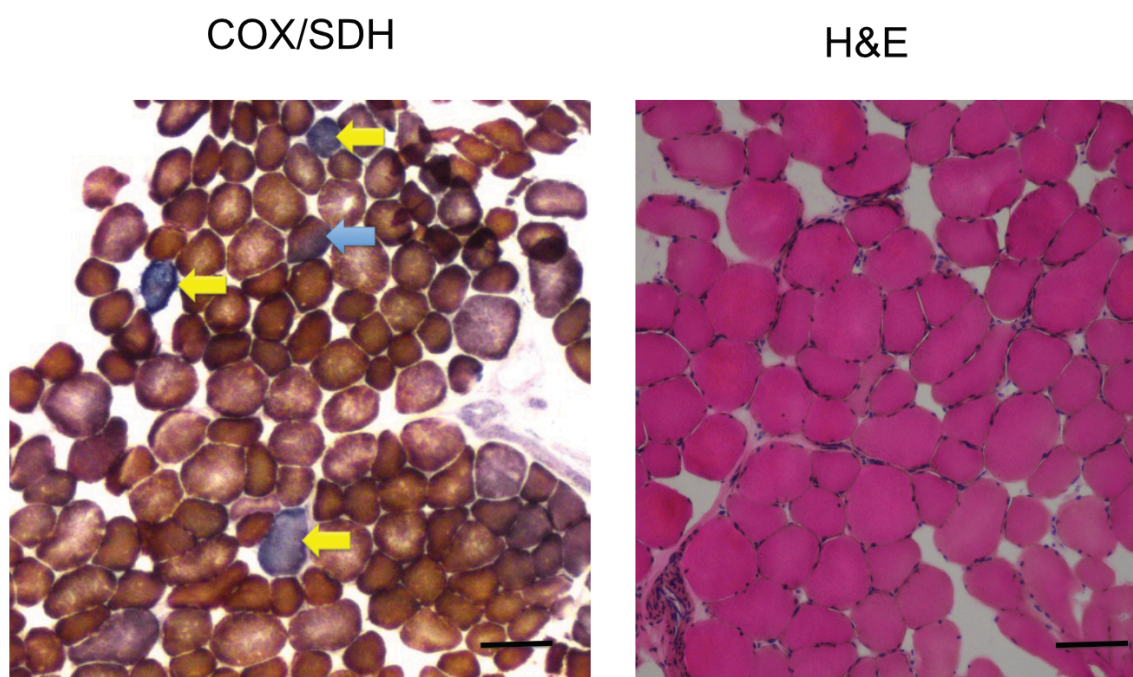


Figure 5.5. Mitochondrial histochemistry of *SSBP1* skeletal muscle biopsy (patient P5). Sequential COX/SDH staining reveals the presence of COX negative fibres (blue fibres marked by yellow arrows) and COX intermediate fibres (partially blue fibre marked by blue arrow). H&E staining reveals fibre size variation within normal limits. Scale bars=100 μ m.

5.3.5.2 Long-range PCR analysis *SSBP1* skeletal muscle DNA

Mutations in mtDNA maintenance genes are typically associated with mtDNA deletions and copy number depletion (Viscomi and Zeviani 2017). Long-range PCR amplification of total genomic DNA obtained from *SSBP1* skeletal muscle homogenate revealed the presence of mtDNA deletions that were not present in an age-matched control (**Figure 5.6**).

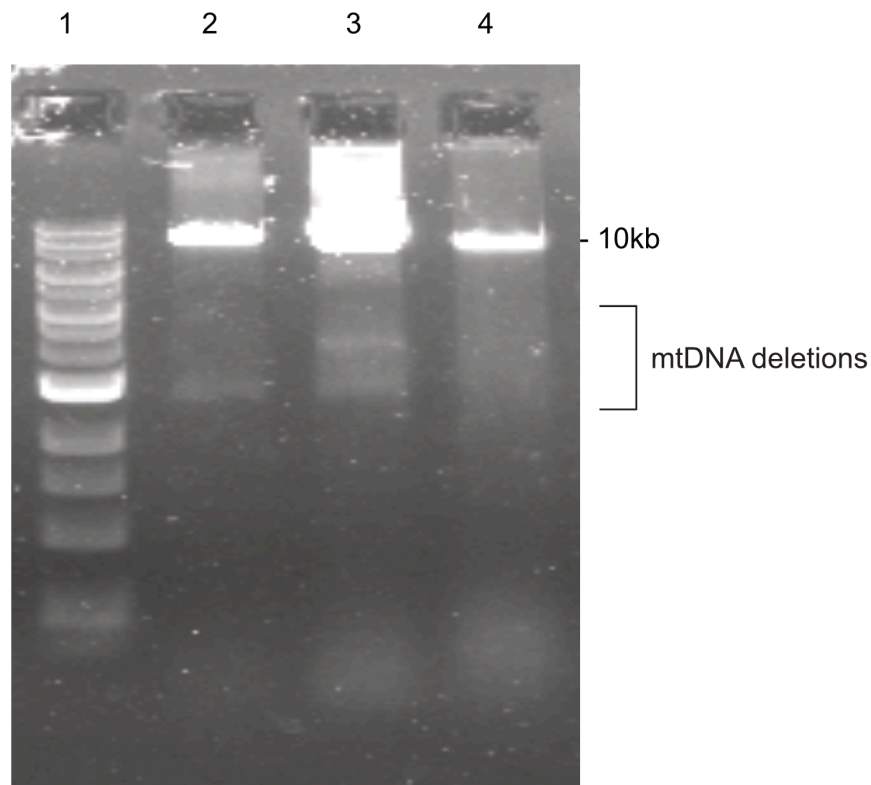


Figure 5.6. Long-range PCR analysis for mtDNA deletions in *SSBP1* and control skeletal muscle biopsies. Agarose gel (0.7%) revealing mtDNA deletions in total genomic DNA isolated from skeletal muscle homogenate of P4 and P5. Lane 1 = GeneRuler 1Kb DNA Ladder, Lane 2 = P4, Lane 3 = P5, Lane 4 = age-matched control.

5.3.5.3 Analysis of mtDNA copy number in *SSBP1* muscle DNA

Given the critical role of *SSBP1* in mtDNA replication, we determined mtDNA copy number from *SSBP1* and control skeletal muscle DNA using real time PCR Taqman® assays targeting *MT-CO3* and *RNaseP*. This revealed muscle mtDNA copy number was reduced in P4 and P5 to approximately 40% of age-matched control level (**Figure 5.7**).

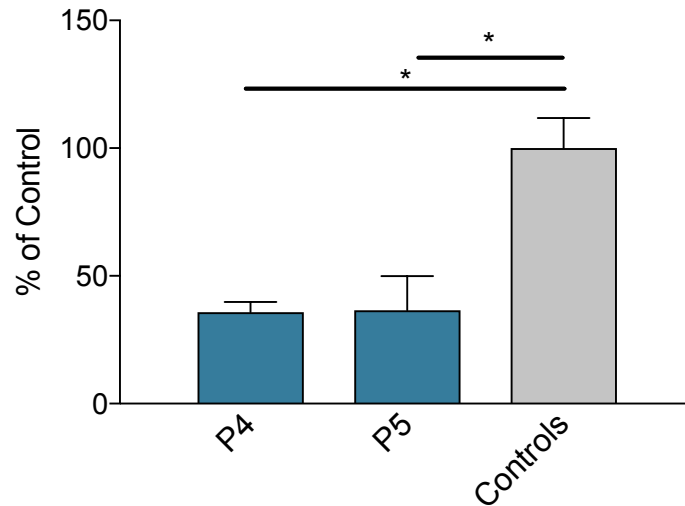


Figure 5.7. mtDNA copy number analysis in *SSBP1* and control skeletal muscle. mtDNA copy number as determined by qPCR targeting *MT-CO3* and *RNaseP* in P4, P5 and controls. P4=35.8±4, P5=36.5±13.3 % of age-matched controls (n=2). Data represents mean mtDNA copy number±SD of 2 independent determinations, *p <0.05 (one way ANOVA with post hoc Tukey test).

5.3.6 Analysis of mtDNA copy number analysis in fibroblasts

The mtDNA copy number was determined from patient (P1–P3) and control (C1–C3) primary fibroblast cell DNA using real time PCR Taqman® assays targeting *MT-ND1* and *B2M*. This revealed no significant difference between any of the cell lines (**Figure 5.8 A**). Western blot analysis of patient (P1–P3) and control (C1–C3) fibroblasts revealed no difference in steady state TFAM expression, consistent with the lack of difference in the mtDNA copy number as detected by the qPCR analysis (**Figure 5.8 B**).

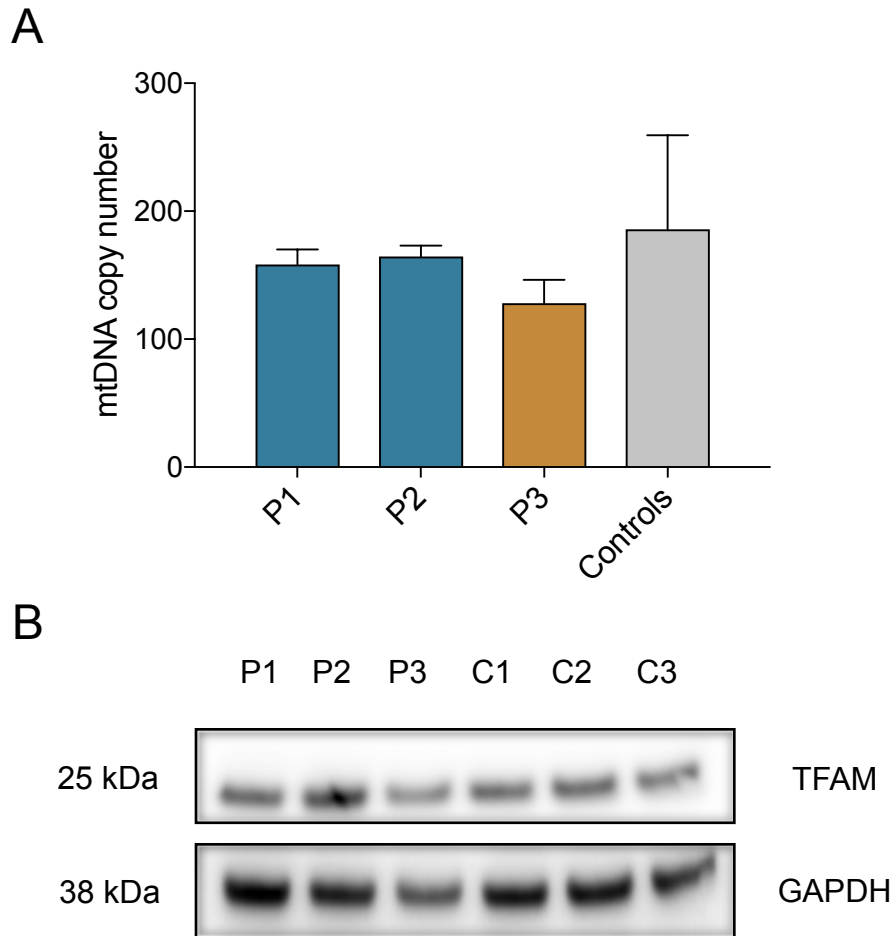


Figure 5.8. mtDNA copy number analysis in patient and control fibroblasts. (A) Total mtDNA copy number of patient (P1–P3) and control (C1–C3) primary fibroblasts analysed by MT-*ND1/B2M* singleplex Taqman real time PCR. P1=158.3±11.9, P2=164.7±8.5, P3=128±18.3, Controls=185.8±73.6 Data represents mean mtDNA copy number±SD of 3 biological replicates. No results were significantly different (one way ANOVA). (B) Western blot analysis of TFAM in primary fibroblasts shows no difference in patients (P1–P3) and controls (C1–C3). Image representative of 2 independent experiments.

5.3.7 Analysis of mtDNA copy number analysis in blood

The mtDNA copy number was determined from total blood DNA in individuals carrying the *SSBP1* variant (n=8) and wild type *SSBP1* (n=9) from the Finnish family, using real time PCR Taqman® assays targeting *MT-ND1* and *B2M*. This revealed no significant difference between the two groups (**Figure 5.9**).

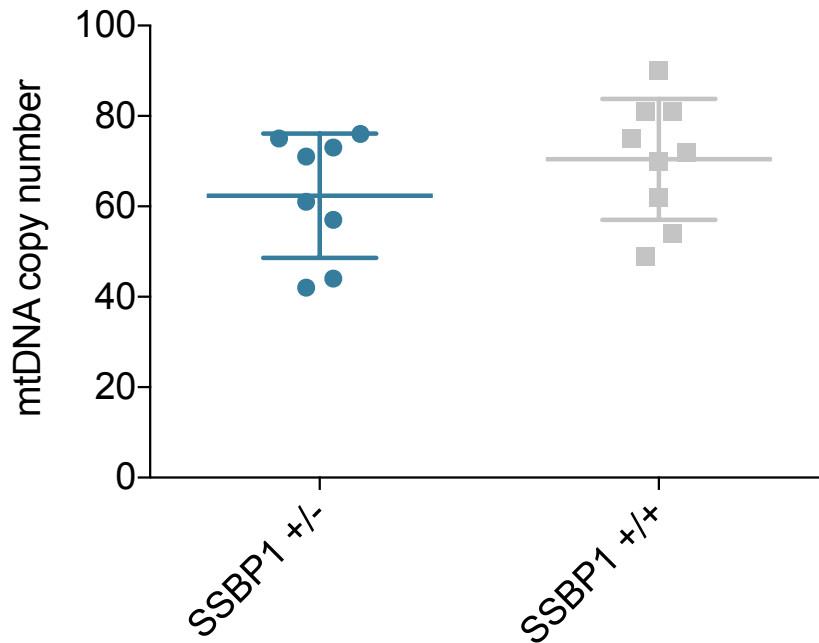


Figure 5.9. mtDNA copy number analysis in blood from individuals in the Finnish family. Carriers of *SSBP1* variant (*SSBP1*^{+/-}) and carriers of wild type *SSBP1* (*SSBP1*^{+/+}) are compared. *SSBP1*^{+/-}=62.4±13.7, *SSBP1*^{+/+}=70.4±13.4. Data represents mean mtDNA copy number±SD with each data point representing a single individual. No significant difference detected between groups, (independent t-test).

5.3.8 Long-range PCR analysis of myoblast and fibroblast DNA

Long-range PCR amplification of total genomic DNA revealed no mtDNA deletions in patient myoblasts (P1m, P2m) or fibroblasts (P1–P3) (**Figure 5.10**).

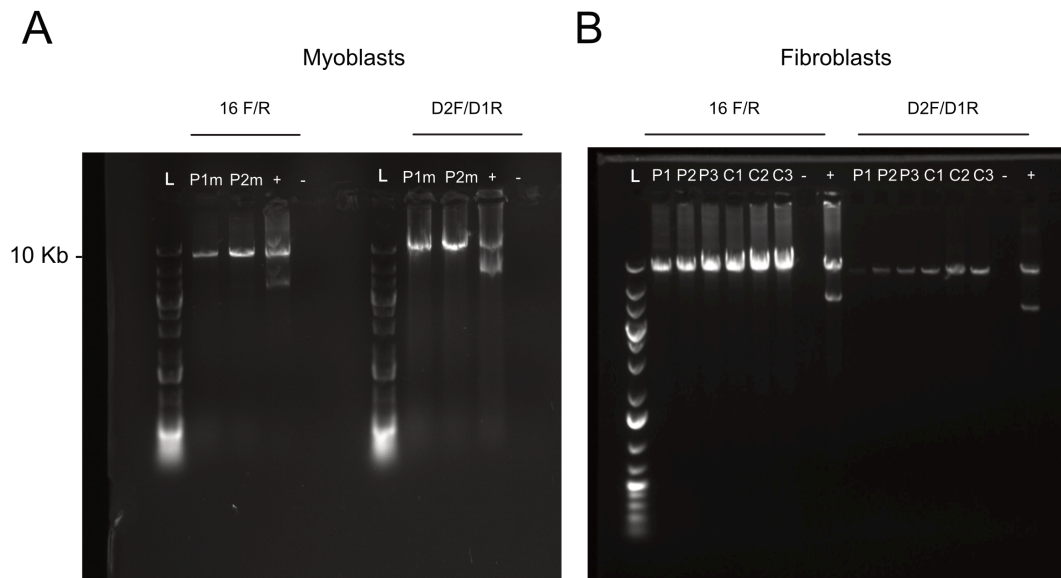


Figure 5.10. Agarose gel of long-range PCR amplified total genomic DNA from myoblasts and fibroblasts. (A) Myoblasts from patients (P1m, P2m) and a (+) positive deletion control. (B) Fibroblasts from patients (P1–P3) and controls (C1–C3) and a (+) positive deletion control. In both gels (-) represents a negative DNA control and L represents GeneRuler 1 Kb ladder. No evidence of mtDNA deletions in patients or controls was detected in either cell type. Primer pairs as indicated: 16F and 16R, D2F and D1R.

5.3.9 Analysis of 7S DNA in fibroblasts

Given the role of SSBP1 in the synthesis and regulation of the mitochondrial D-loop, we investigated the effect of the *SSBP1* variant on the abundance of the D-loop third strand, 7S DNA, using Southern blotting in immortalised patient (P1i–P3i) and control (C1i) fibroblasts (Takamatsu, Umeda et al. 2002). A radiolabeled probe was used that detected both a 6.4 kb fragment of mtDNA including the complete NCR and 7S DNA (**Figure 5.11**). 7S DNA levels normalised to full-length mtDNA were significantly reduced in P1i and P2i compared to P3i and control. There was no difference in the level of full-length mtDNA relative to nuclear 28S DNA, indicating a lack of difference in mtDNA copy number in P1i, P2i and P3i fibroblasts compared to controls (**Figure 5.12**).

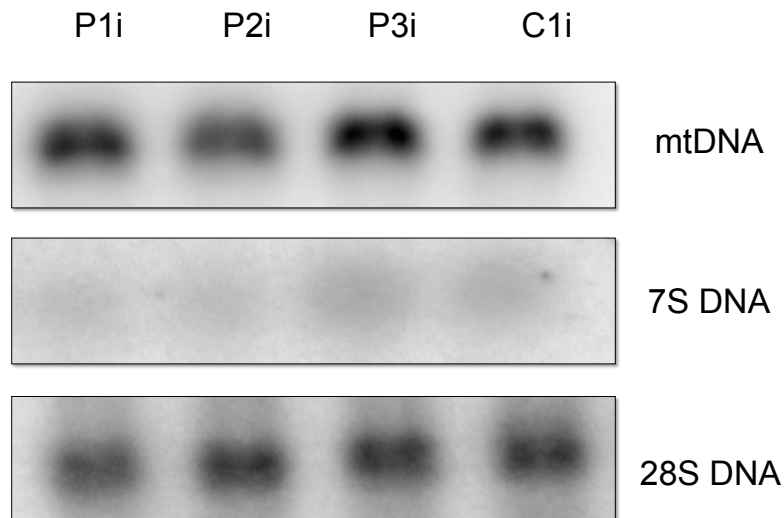


Figure 5.11. Southern blot analysis of 7S and total mtDNA in patient and control fibroblasts. 3 μ g total DNA from patient (P1i–P3i) and control (C1i) fibroblasts was digested with PvuII and analysed by one dimensional Southern blot. Hybridisation was performed with Probe A which detects both genomic mtDNA and 7S DNA. Hybridisation of probe to the 28S DNA was used as a loading control. Image representative of 3 independent experiments.

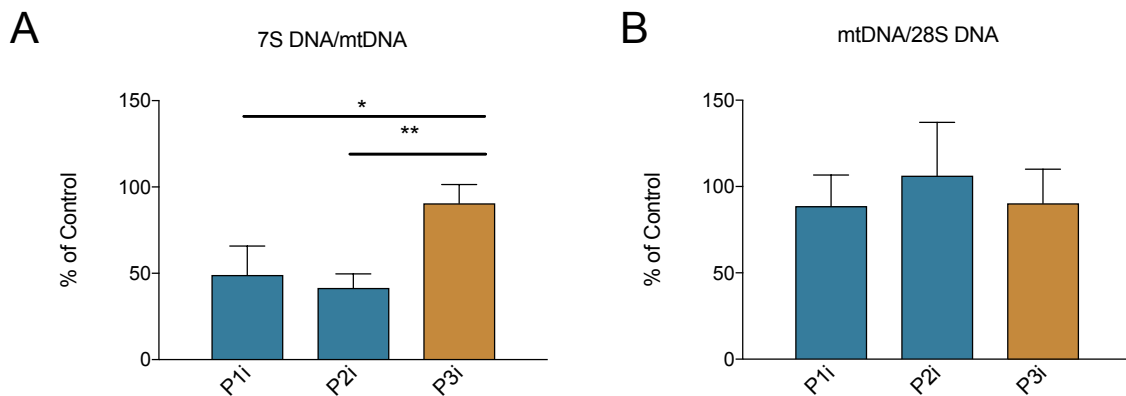


Figure 5.12. Quantification of 7S and total mtDNA in patient and control fibroblasts. (A) 7S DNA levels normalised to genomic mtDNA levels, P1=49.1 \pm 16.7, P2=41.6 \pm 8.1, P3=90.6 \pm 10.8. Data represents mean % of control \pm SD of 3 independent experiments * p <0.05, ** p <0.01 (one way ANOVA with post hoc Tukey test) (B) Full length mtDNA normalized to 28S DNA levels. mtDNA levels P1=88.72 \pm 18, P2=106.3.6 \pm 30.8, P3=90.3 \pm 19.7. Data represents mean % of control \pm SD of 3 independent experiments, no significant difference detected between groups (one way ANOVA).

5.3.10 Mitochondrial repopulation assay

A mitochondrial repopulation assay was undertaken in order to determine the effect of the *SSBP1* and m.1555A>G variants on the efficiency of mtDNA replication. Fibroblasts from patients (P1–P3) and controls (C1, C2) were depleted of mtDNA using EtBr and then

allowed to repopulate their mtDNA copy number by removal of EtBr from the culture medium. EtBr has been shown to interfere with mtDNA replication reducing superhelical density as well as inhibiting mitochondrial protein and RNA synthesis without affecting nuclear DNA (Leibowitz 1971). The effect of EtBr is reversible and hence on removal of the compound, mtDNA replication reactivates and copy number increases. The rate of mtDNA copy number repopulation is thus an indicator of mtDNA replication efficiency. In parallel, each cell line was also cultured in medium without EtBr to control for fluctuations in copy number during cell culture.

5.3.10.1 *Optimisation of protocol for mitochondrial repopulation assay*

Optimisation of the mitochondrial repopulation assay was undertaken to determine (i) the duration of EtBr exposure required by fibroblasts to depopulate mtDNA copy number and (ii) to gain further insight into the subsequent repopulation kinetics. The mtDNA depletion and repopulation curves are constructed from the RLs calculated at each time point (**Figure 5.13**). After commencing treatment with EtBr (day 0) there was a decrease in mtDNA copy number in all fibroblast cell lines by Day 6. EtBr was then withdrawn from the medium at day 15. Following this, mtDNA copy number remained depleted in all cell lines until day 29. Continued repopulation was only seen in P1 cell line at day 36, with all other cell lines showing a decrease in mtDNA copy number. It was noticed that addition of EtBr to the medium progressively decreased cell viability over the course of depopulation phase and hence continuation of the experiment after day 36 was not possible.

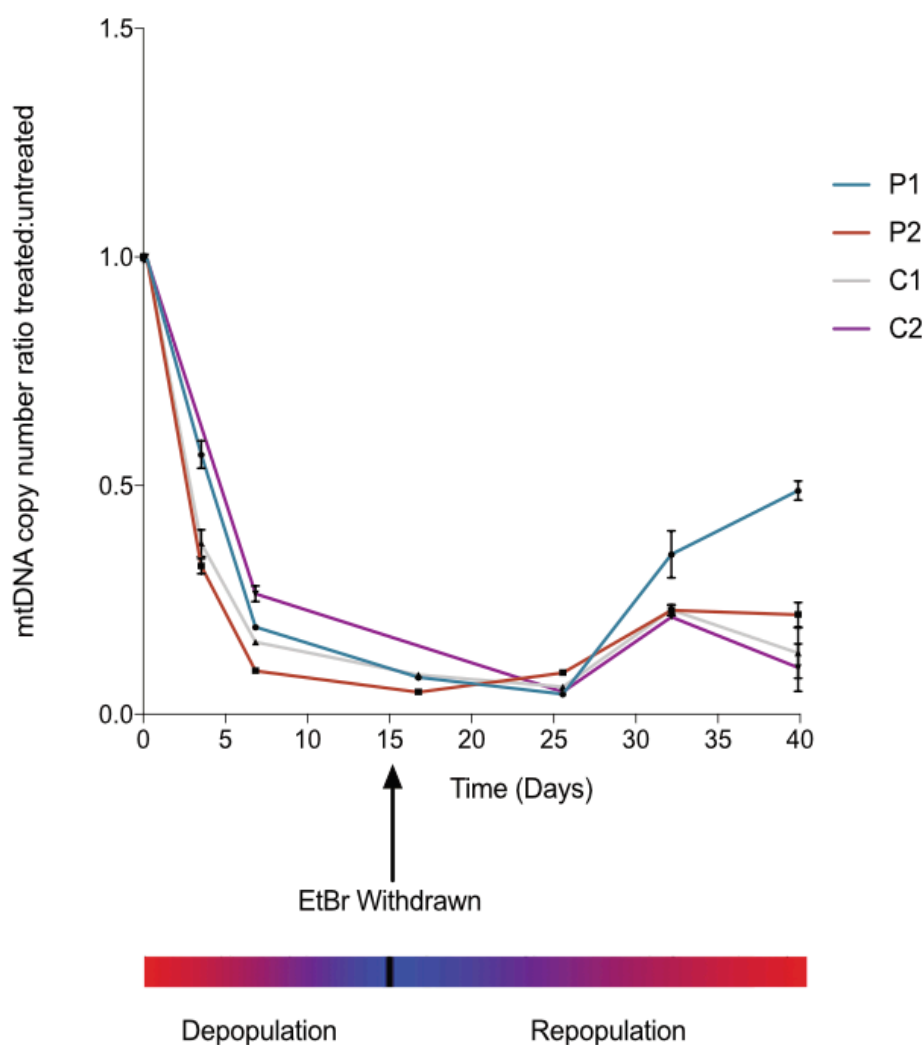


Figure 5.13. Optimisation of mitochondrial repopulation assay. Fibroblasts from patient (P1, P2) and control (C1, C2) were grown in supplemented high glucose DMEM medium and were depleted of mtDNA by treatment with EtBr for 15 days then allowed to repopulate. Each data point represents the mtDNA copy number treated:untreated from the single optimisation experiment. Error bars represent SDs of triplicate qPCR measurement. RLs for each time point are presented in **Appendix 2**.

5.3.10.2 Modified protocol for mitochondrial repopulation assay

Given that 15 days' of exposure to EtBr reduced cell viability, it was not possible to observe sustained mtDNA repopulation in any of the cell lines. Therefore, we employed a modified protocol using 4 days' exposure to EtBr followed by a 6-day period of repopulation. The mtDNA repopulation curves of the individual cell lines are presented in **Figure 5.14**. Each individual cell line was then compared to control cell lines (mean of C1, C2), presented in **Figure 5.15**, **Figure 5.16** and **Figure 5.17**.

This revealed patient cells (P1–P3) had a trend towards higher RLs at each time point in the repopulation phase, although this difference only reached statistical significant at day 8 in P1 and P3. A closer analysis was performed by calculation of a repopulation rate defined as the gradient of a regression line of RLs plotted against time in the repopulation phase (day 6 to day 10). This revealed that repopulation rate of P1 and P2 was approximately double that of P3 and controls (**Figure 5.18**).

Attempting to perform the modified protocol using glucose-free medium supplemented with 5 mM galactose resulted in massive cell death of P1 and P2 cell lines and less marked death of P3 and control cells. Given the reduction in cell viability under these conditions it was not possible to continue with this experimental paradigm.

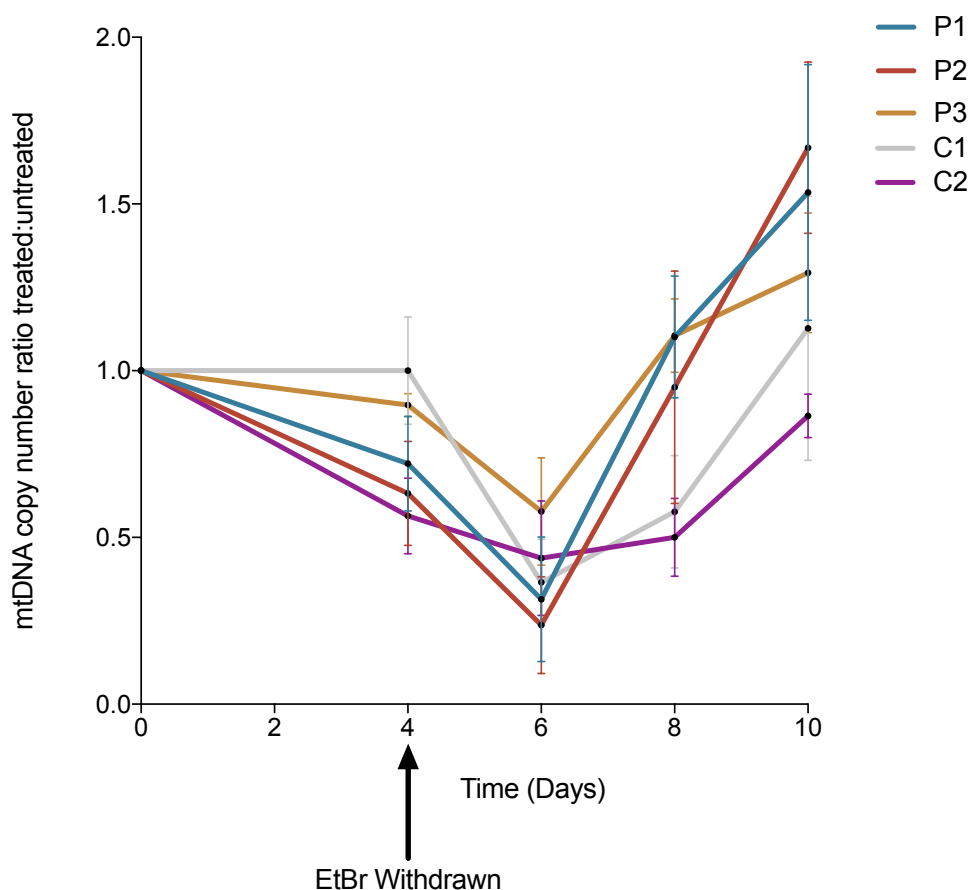


Figure 5.14. Modified mitochondrial repopulation assay. mtDNA repopulation curves for individual patient (P1 –P3) and control lines (C1, C2). Data points represent the mean mtDNA copy number treated:untreated (RL) \pm SD from 3 independent experiments. The RLs of individual cell lines are presented in **Appendix 2**.

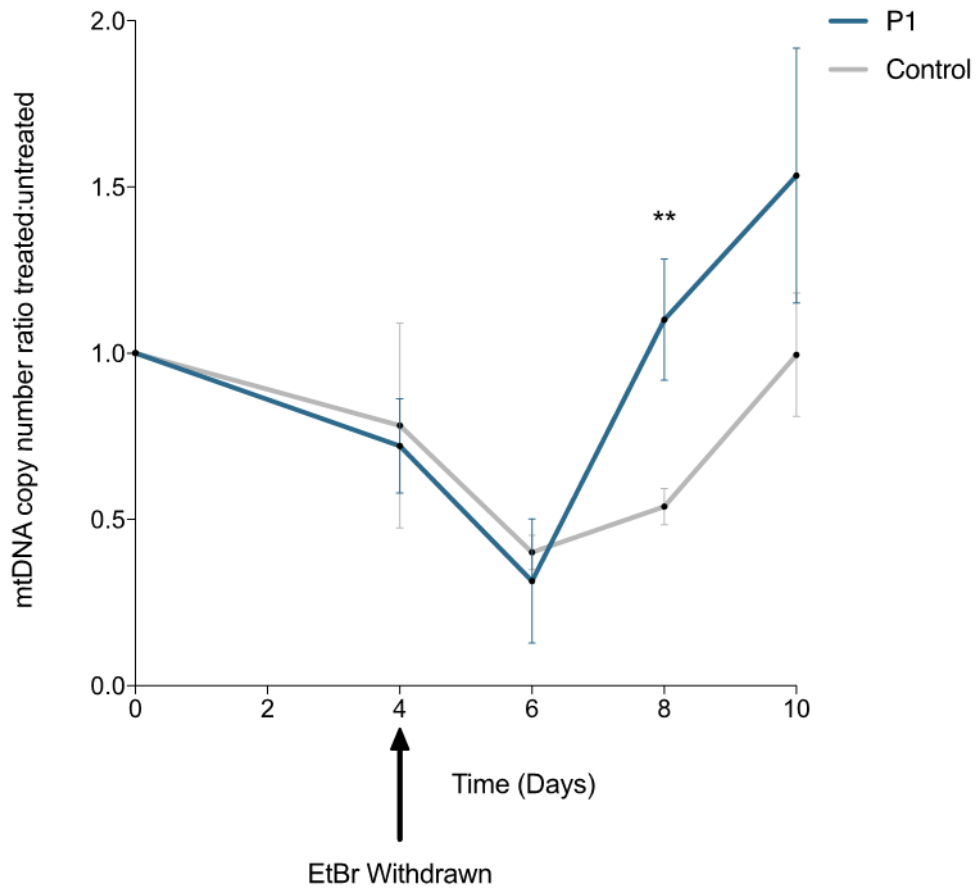


Figure 5.15. mtDNA repopulation curve for P1 and control. The data points represent the mean mtDNA copy number treated:untreated (RL)±SD from 3 independent experiments. No difference was detected between P1 and control at any time point except day 8, day 8 RL P1=1.11±0.03 vs Control= 0.538±0.05 $p < 0.01$ (unpaired t-test, p-value uncorrected). The RLs of individual cell lines are presented in **Appendix 2**.

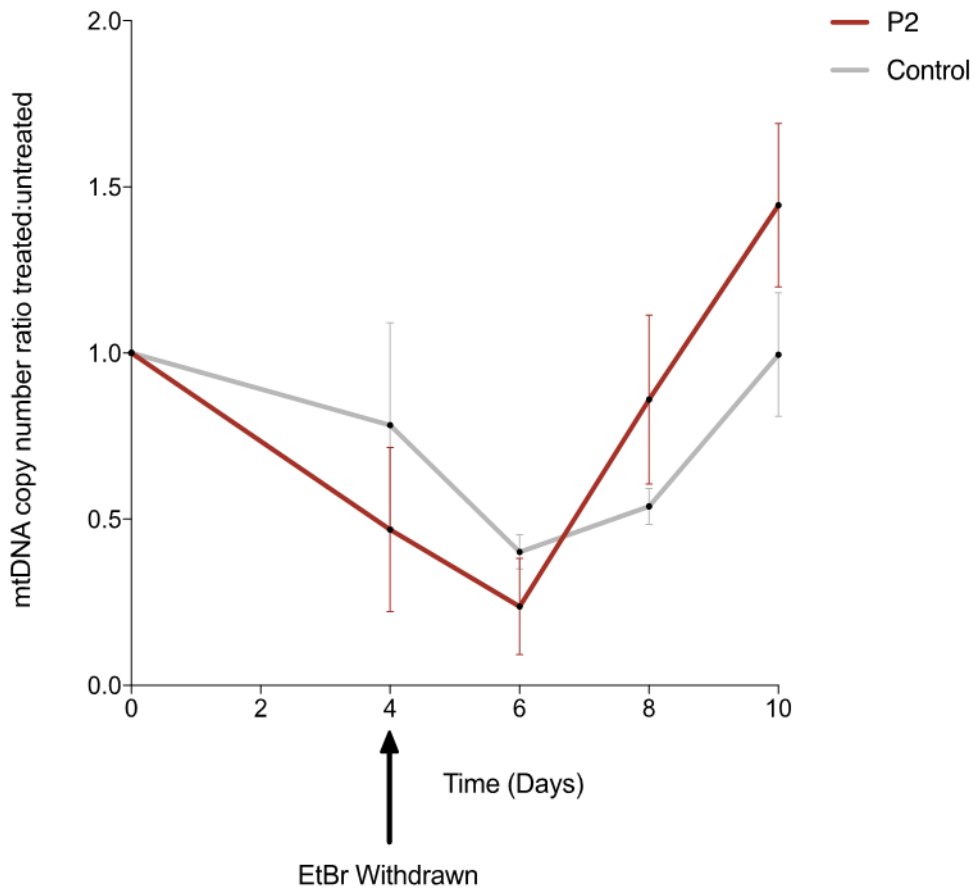


Figure 5.16. mtDNA repopulation curve for P2 and control. The data points represent the mean copy number treated:untreated (RL) \pm SD from 3 independent experiments. The difference between P2 and control was not significant at any time point (unpaired t-tests). The RLs of individual cell lines are presented in **Appendix 2**.

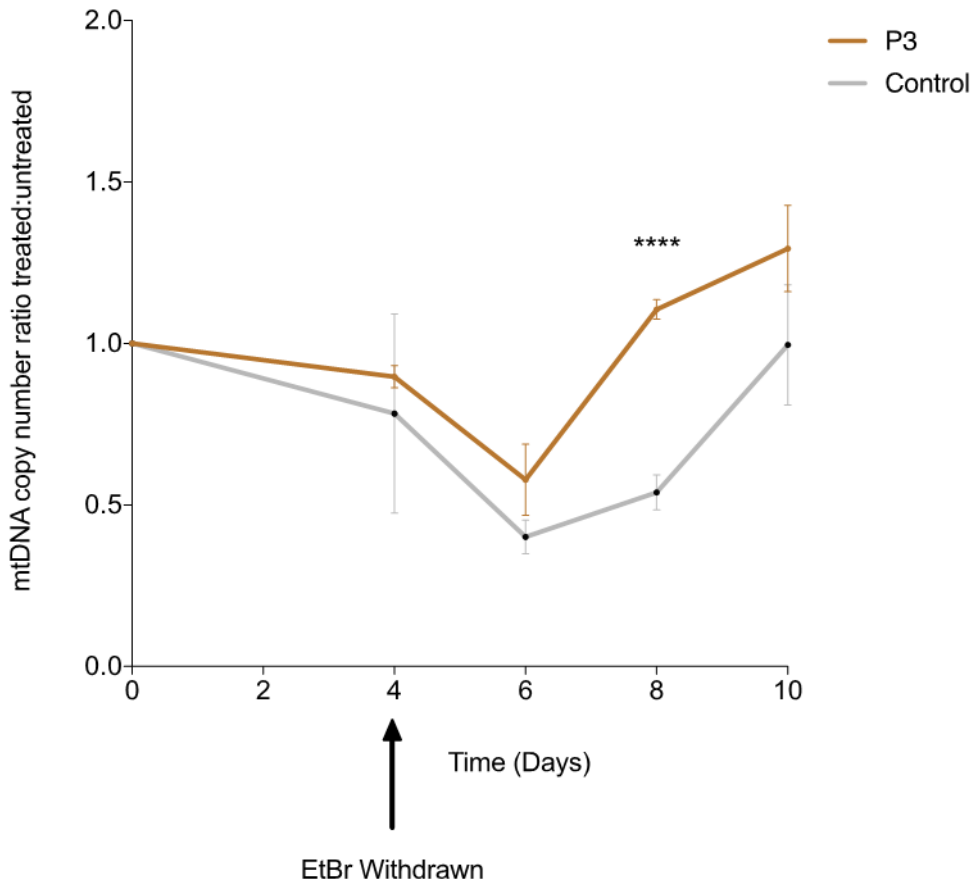
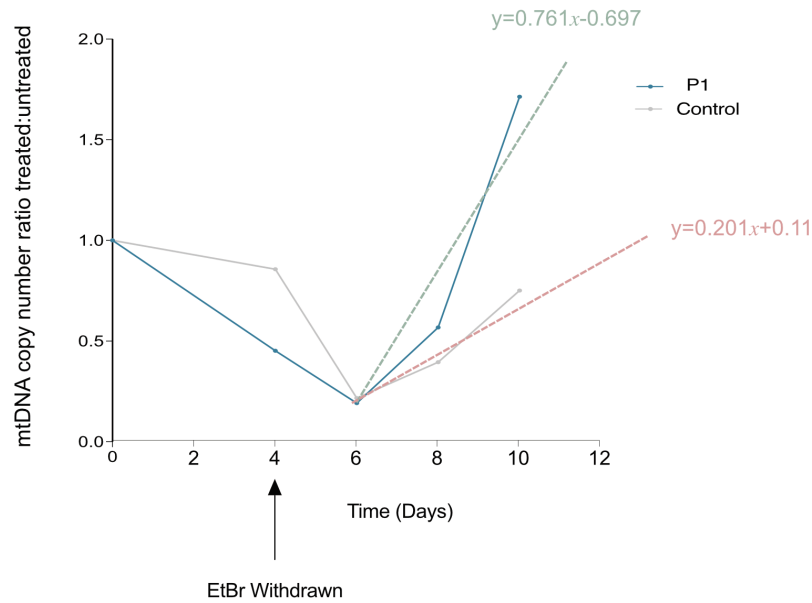


Figure 5.17. mtDNA repopulation curve for P3 and control. The data points represent the mean copy number treated:untreated (RL) \pm SD from 3 independent experiments. The difference between P3 and control was not significant at any time point except day 8; day 8 RL P3=1.106 \pm 0.113 vs Control= 0.538 \pm 0.05, $p < 0.0001$ (unpaired t-test, p-value uncorrected). The RLs of individual cell lines are presented in **Appendix 2**.

A



B

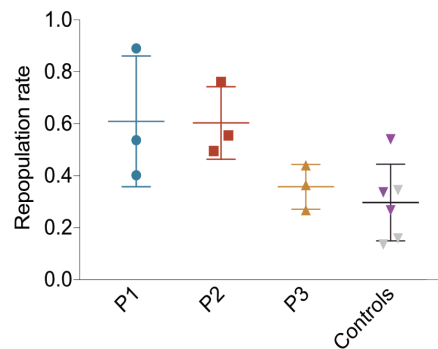


Figure 5.18. Calculation of mtDNA repopulation rate. (A) Representative analysis of the mtDNA repopulation rate. The repopulation rate was calculated by taking the gradient of regression line of mtDNA copy number ratio treated:untreated (RL) in the repopulation phase (day 6 to day 10). (B) Repopulation rates of patient (P1–P3) and control cell lines (purple symbols represent C1, grey symbols represent C2). Each data point represents the calculated repopulation rate from 1 of 3 independent experiments. Data reveal a trend towards an increased repopulation rate of P1 and P2 compared to P3 and controls, $P1=2.06\pm 0.09$, $P2=2.34\pm 1.29$, $P3=1.37\pm 0.72$, fold change of mean repopulation rate \pm SD vs control from 3 independent experiments. Difference between groups not significant (one way ANOVA).

5.3.11 Analysis of mitochondrial respiration in fibroblasts

It was next important to determine whether the *SSBP1* and m.1555A>G variants compromised the mitochondrial respiratory chain function in fibroblasts concordant with their effect in skeletal muscle. To this effect, the OCR was measured in patient (P1–P3) and control (C1–C3) primary fibroblasts using the Seahorse XF^e 96 Extracellular Flux

Analyzer (**Figure 5.19**). OCR was determined at basal state and after the addition of mitochondrial inhibitors enabling the determination of (i) endogenous respiration (ii) maximal respiration and (iii) proton leak respiration. There was no significant difference in these parameters between patient cells and control cells, however patient fibroblasts showed a trend towards decreased maximal respiration, although this did not reach statistical significance (**Figure 5.20**).

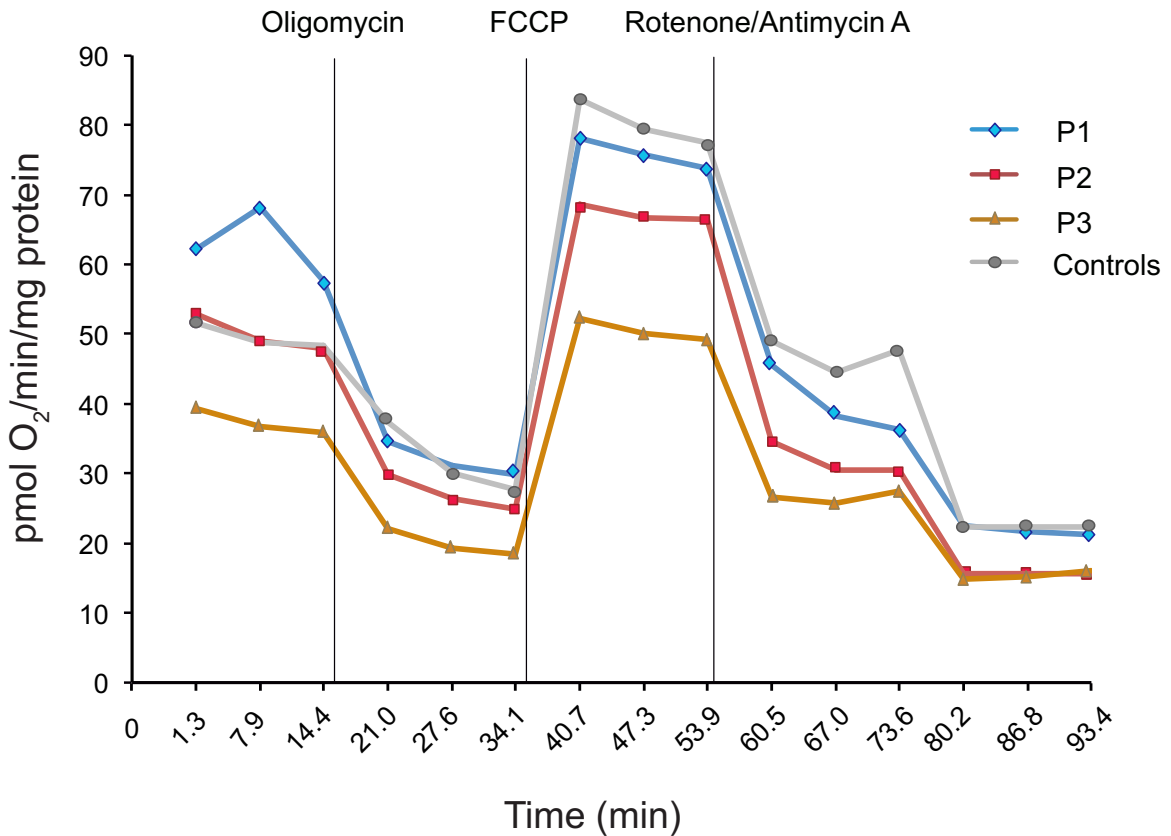


Figure 5.19. Example of Seahorse analysis of mitochondrial respiration in patient and control fibroblasts. Mitochondrial respiration was assayed in fibroblasts from patients (P1–P3) and controls (C1–C3, mean of 3 controls shown) by measuring OCR (pmol O₂/min/mg protein) against time after the addition of oligomycin, FCCP and rotenone/antimycin A at the time points indicated.

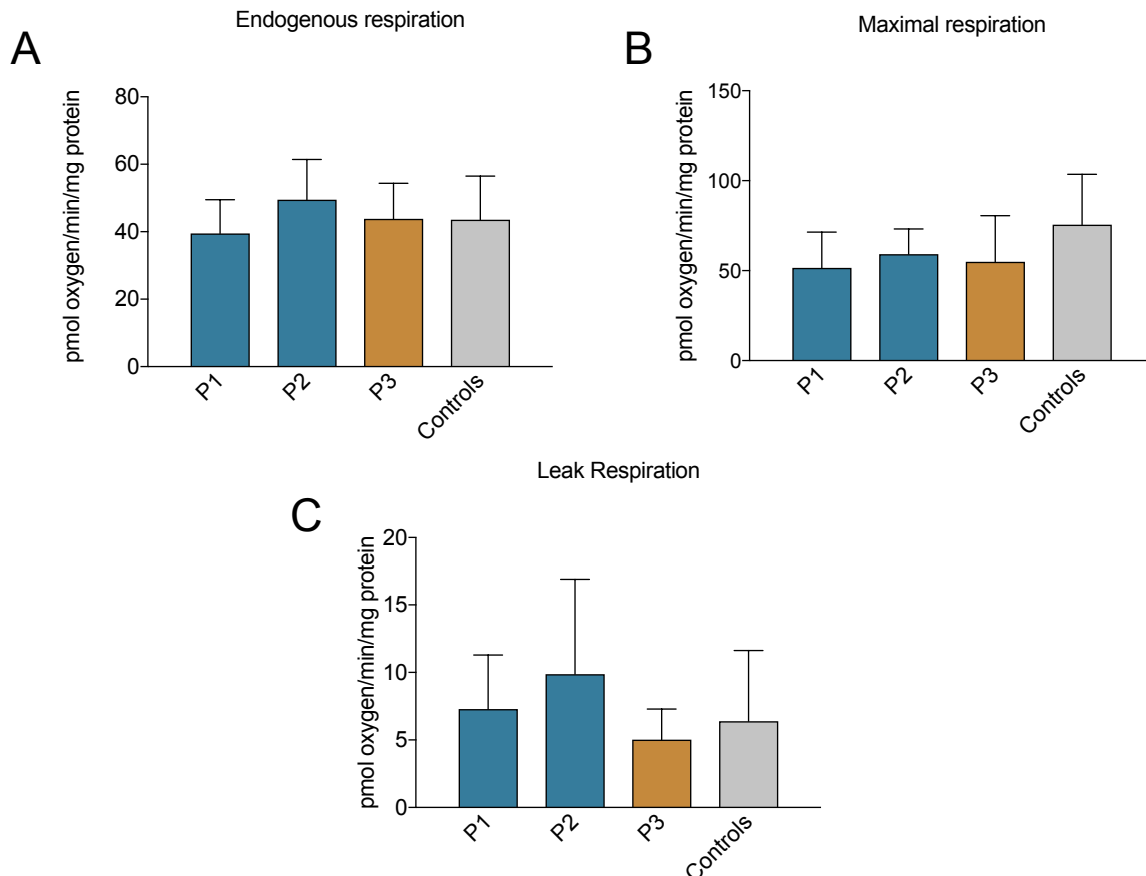


Figure 5.20. Determination of key parameters of mitochondrial respiration in patient and control fibroblasts by Seahorse analysis. Different aspects of mitochondrial respiration were measured using the Seahorse XF96^e extracellular flux analyser by determination of the OCR after sequential addition of metabolic inhibitors. (A) *Endogenous respiration* = basal OCR – non mitochondrial OCR P1=39.5±10.0, P2=49.5±11.9, P3=43.8±10.5, Controls=43.5±13.0 (B) *Maximal respiration* = maximal OCR – non mitochondrial OCR P1=51.6±19.9, P2=59.2±13.9, P3=54.9±25.6, Controls=75.6±28.0. (C) *Proton leak respiration* = post oligomycin OCR – non mitochondrial respiration P1=7.3±4.0, P2=9.9±7.0, P3=5.0±2.3, Controls=6.4±5.2. Data represents mean pmol oxygen/min/mg protein±SD of 4 independent experiments. There was no statistical difference in any aspect of mitochondrial respiration between the groups (one-way ANOVA).

5.3.12 Analysis of fibroblast cell growth

A functioning mitochondrial respiratory chain is a prerequisite for efficient cellular proliferation (Birsoy, Wang et al. 2015). Cellular growth rates were therefore determined in immortalised fibroblasts from patients (P1i-Pi3) and controls (C1i and C2i) grown in glucose and glucose-free medium supplemented with 5 mM galactose. Culture medium containing galactose as the major carbon source does not facilitate anaerobic glycolysis and hence forces cells to use OXPHOS for energy generation (Robinson, Petrova-Benedict

et al. 1992). Under these conditions of enhanced mitochondrial metabolism, P1i, P2i and P3i cells had significantly greater doubling times than controls (**Figure 5.21** and **Figure 5.22**).

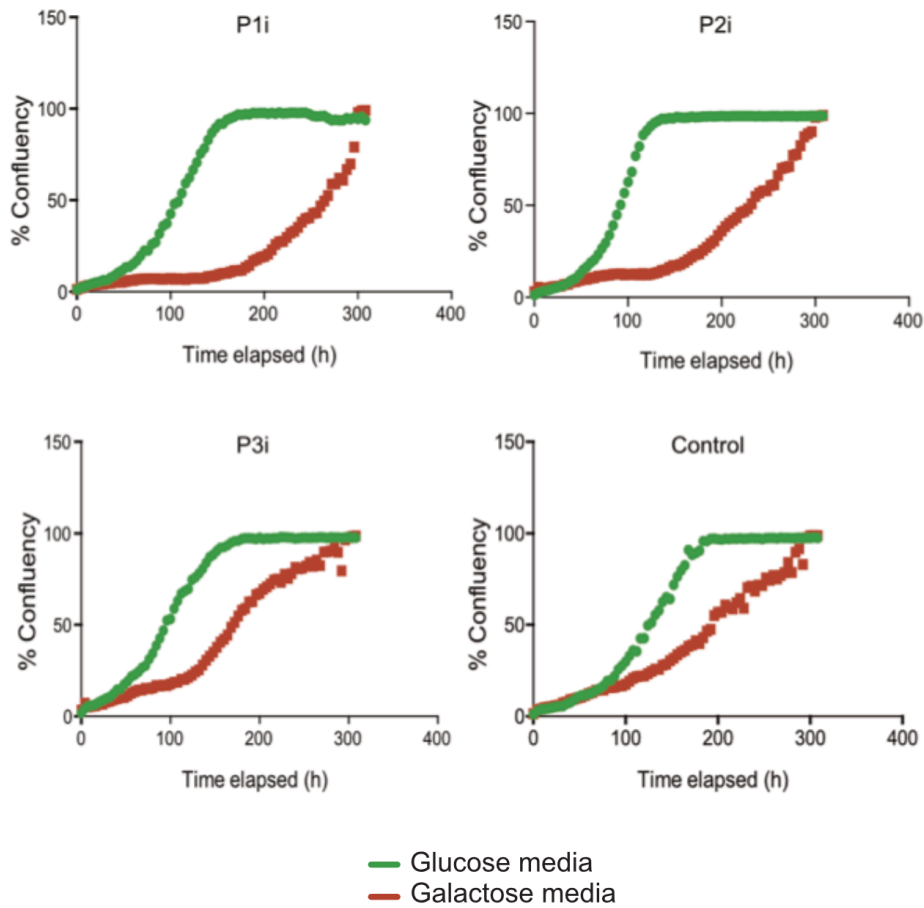


Figure 5.21. Cellular growth curve analysis of patient and control immortalised fibroblasts. Cellular growth curves of patient (P1i–P3i) and control fibroblasts (C1i and C2i; C1i shown as representative of both control lines) on glucose (green line) and glucose free medium supplemented with 5 mM galactose (red line). Graphs represent cell confluency (%) vs time (hours). Data representative of 3 independent experiments.

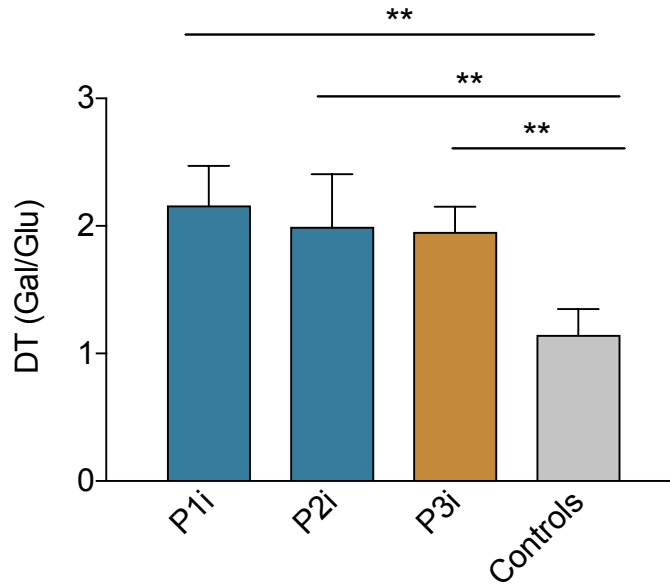


Figure 5.22. Quantification of doubling time (DT) of patient and control immortalised fibroblasts. DT of patient (P1i–P3i) and controls (C1i and C2i) in galactose medium normalized to growth on glucose medium. P1i=2.16±0.31, P2i=1.99±0.41, P3i=1.95±0.199, Controls=1.15±0.2, mean DT±SD of 3 independent experiments, **p<0.01 (one way ANOVA with post hoc Tukey test).

5.3.13 Analysis of intra-mitochondrial translation in fibroblasts

The m.1555A>G variant is predicted to cause mitochondrial mRNA misreading leading to a reduction in translation efficiency (Hobbie, Bruell et al. 2008). To determine whether the m.1555A>G variant affected *de novo* mitochondrial protein synthesis, and whether this effect was compounded by the *SSBP1* variant, an intra-mitochondrial translation assay was performed by the incorporation of ³⁵S radiolabelled methionine. This revealed markedly reduced global mitochondrial protein synthesis in fibroblasts from patients (P1–P3) compared to controls (C1, C2) (**Figure 5.23**).

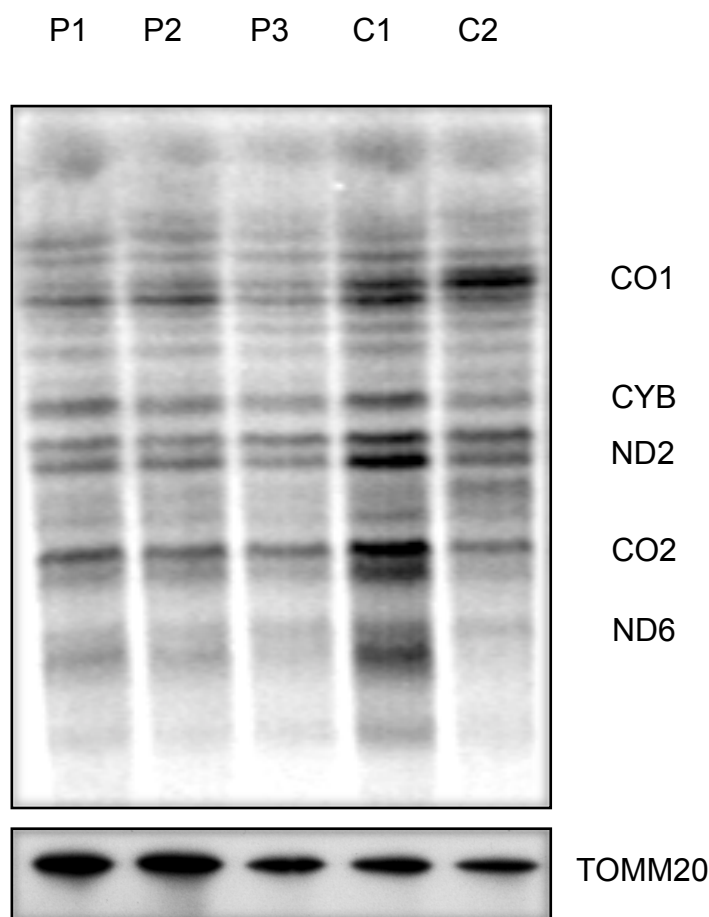


Figure 5.23. Mitochondrial protein translation analysis in patient and control fibroblasts. Mitochondrial protein translation measured by incorporation of ^{35}S methionine reveals a clear reduction of mitochondrial protein synthesis in patient fibroblasts (P1–P3) compared to controls (C1, C2). The characteristic bands of mitochondrially encoded proteins are annotated (ND2, ND6: NADH dehydrogenase subunit 2,6; CO1, CO2: mitochondrially encoded cytochrome c oxidase, I, II; CYB: mitochondrially encoded cytochrome b). Loading determined by TOMM20 Western blot. Image representative of 2 independent experiments.

5.3.14 Analysis of steady state mitochondrially encoded proteins in fibroblasts

Given the reduction in *de novo* protein synthesis, Western blot analysis of primary fibroblasts from patients (P1–P3) and controls (C1–C3) was used to determine the effect of the *SSBP1* and m.1555A>G variants on the steady state expression of the mitochondrially encoded complex IV proteins, MT-CO1 and MT-CO2. There was a statistically significant reduction in MT-CO2 expression in P1, P2 and P3 compared to controls. Similarly, there was a trend towards a reduction in MT-CO1 expression in P1, P2 compared to P3 and controls, however this did not reach statistical significance (**Figure 5.24**).

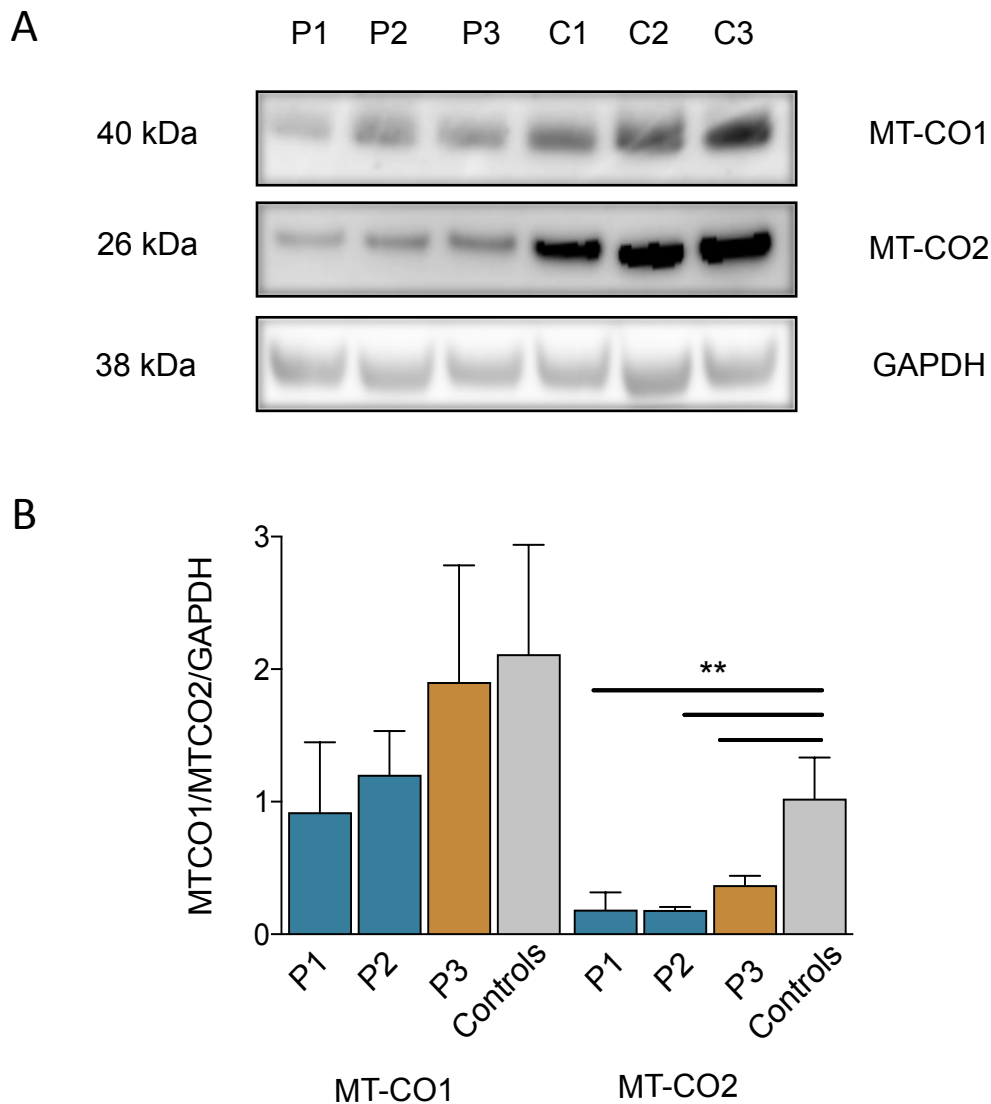


Figure 5.24. Western blot analysis of mitochondrial encoded proteins in patient and control fibroblasts. (A) Western blot analysis of mitochondrial encoded MT-CO1 and MT-CO2 proteins in primary fibroblasts from patients (P1–P3) and controls (C1–C3). Images representative of 3 independent experiments (B) Densitometric quantification of MT-CO1 and MT-CO2 normalised to GAPDH. MT-CO2 (P1=0.19±0.13, P2=0.18±0.02, P3=0.37±0.07, Controls=1.02±0.31, MT-CO1 (P1=0.92±0.53, P2=1.2±0.33, P3=1.9±0.9, Controls=2.1±0.82). Data represents mean normalised MT-CO1 or MT-CO2 levels±SD of 3 independent experiments, **p<0.01 (one way ANOVA with post hoc Tukey test).

5.3.15 Analysis of steady state nuclear encoded mitochondrial proteins in fibroblasts

Western blot analysis of primary fibroblasts from patients (P1–P3) and controls (C1–C3) was used to determine the effect of the *SSBP1* and m.1555A>G variants on the steady state expression of nuclear encoded mitochondrial proteins. This revealed no statistically significant difference in the expression of ATP5A (F₁F₀ ATP synthase, Complex V

subunit) or SDHA (succinate dehydrogenase, Complex II subunit) in P1, P2 and P3 compared to controls (**Figure 5.25**).

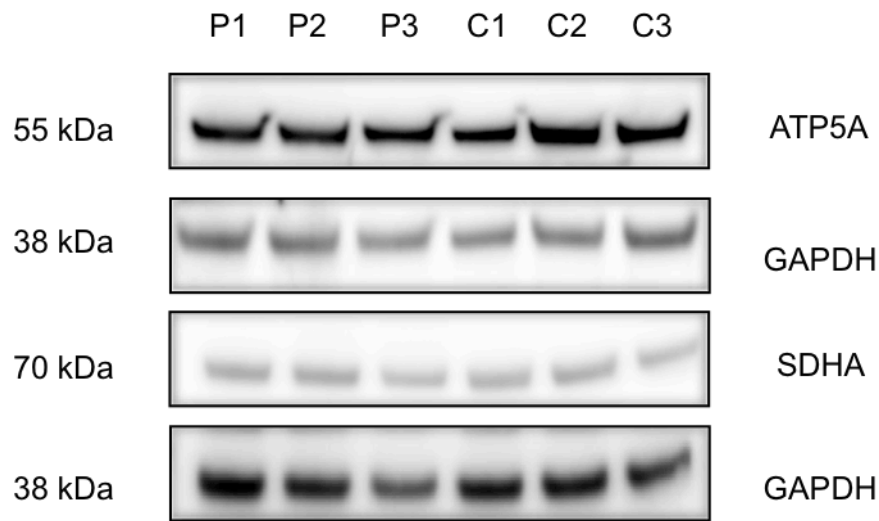


Figure 5.25. Western blot analysis of nuclear encoded mitochondrial proteins in patient and control fibroblasts. (A) Western blot analysis of nuclear encoded ATP5A and SDHA proteins shows no significant difference in primary fibroblasts from patients (P1–P3) and controls (C1–C3). Images representative of 3 independent experiments.

5.3.16 Analysis of mitochondrial gene expression in fibroblasts

We next set out to determine whether the reduction in steady state levels of mitochondrial proteins could result from a reduction in mitochondrial transcription in addition to the demonstrated defect in mitochondrial translation. Therefore, the mRNA expression of the mitochondrial gene *MT-CYB* was measured in patient (P1–P3) and control (C1–C3) fibroblasts using TaqMan® Gene Expression Assay. This revealed no significant difference between groups (**Figure 5.26**).

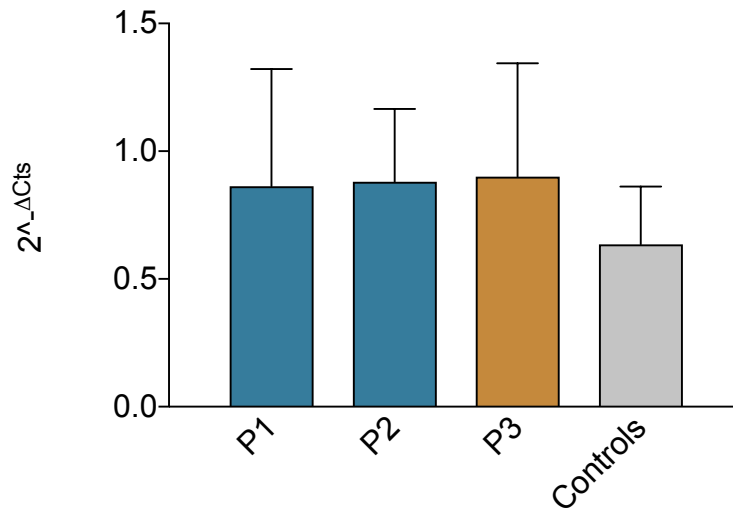


Figure 5.26. Analysis of mitochondrial gene expression in patient and control fibroblasts. Expression of *MT-CYB* was measured in patient (P1–P3) and control (C1–C3) primary fibroblasts. For data normalisation *GAPDH* was used as an endogenous housekeeping gene. Normalisation of Ct values and determination of gene expression was calculated using the $2^{-\Delta Ct}$ method. P1=0.86±0.46, P2=0.88±0.29, P3=0.9±0.44, Controls=0.64±0.22. Data represents mean $2^{-\Delta Ct} \pm SD$ of 3 biological replicates. No results were significantly different (one-way ANOVA).

5.3.17 Analysis of the mitochondrial network in fibroblasts

Mitochondria exist in highly dynamic reticular networks that both drive and respond to changes in cellular conditions by morphological alterations (Picard, Wallace et al. 2016). Maintenance of these networks is critical for both mitochondrial and cellular function (Lackner 2014, Hoitzing, Johnston et al. 2015). The effect of the and *SSBP1* and m.1555A>G variants on mitochondrial network morphology was investigated using Huygens Essential Software to quantify the average mitochondrial fragment length and average number of fragments within 3D-reconstructions of the mitochondrial networks in patient (P1–P3) and control (C1, C2) fibroblasts (**Figure 5.27**). The average length of mitochondrial fragments in P1 was significantly lower than in controls (**Figure 5.28 A**). Similarly, the total number of mitochondrial fragments was significantly increased in P1 compared to controls (**Figure 5.28 B**).

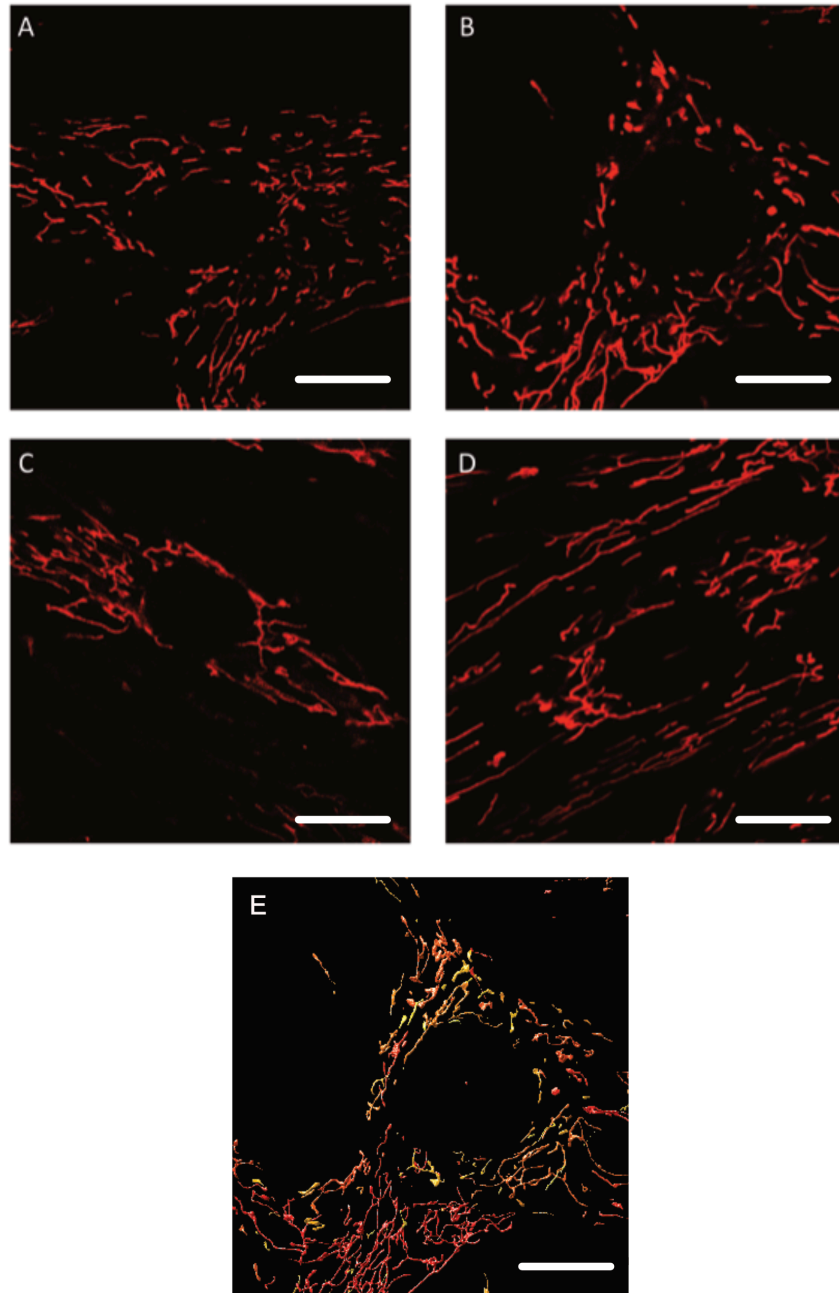


Figure 5.27. Mitochondrial networks in patient and control fibroblasts. Representative images of mitochondrial networks in primary fibroblasts from patient and controls. (A) P1 (B) P2 (C) P3 (D) Control (C1 and C2; C2 shown as representative of both control lines) (E) Example of 3D reconstructed mitochondrial networks analysed by Huygens Essential Software (C2, control shown). Scale bars = 20 μm

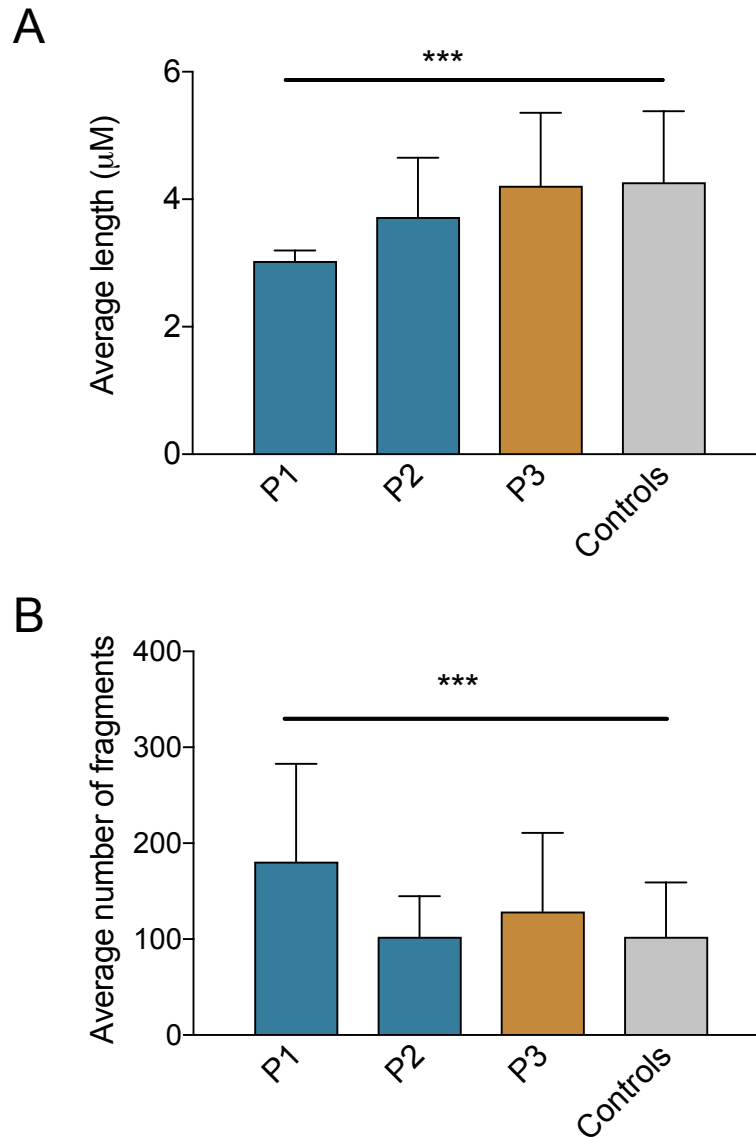


Figure 5.28. The average length and average number of mitochondrial fragments in patient and control fibroblasts. (A) The average length of mitochondrial fragments in patient (P1–P3) and control (C1, C2) primary fibroblasts. P1=3.03±0.17 (n=26 cells), P2=3.72± 0.93 (n=16 cells), P3=4.21± 1.15 (n=18 cells) and Controls=4.27±1.1(C1, C2, n=63 cells). (B) The average number of fragments in patient (P1–P3) and control (C1, C2) primary fibroblasts. P1=180.8±101.9 (n=26 cells), P2=102.4± 42.5 (n=16 cells), P3=128.7±82.1 (n=18 cells) Controls=102.5±56.6 (C1, C2, n=63 cells). Data are mean length (μm)±SD n= ≥16 *** p=<0.0001 (two tailed unpaired t test).

The distribution of mitochondrial fragment lengths within the mitochondrial network of patient fibroblasts (P1–P3) and controls (C1, C2) was also assessed. Adapting the methodology of *Bannwarth et al* a frequency distribution of mitochondrial fragment length was created by sorting individual fragments into bins of <1μm, 1 to 2μm, 2 to 5μm, 5 to 10μm and >10μm (Bannwarth, Ait-El-Mkadem et al. 2014). This revealed that both P1

and P2 had a significantly higher frequency of smaller fragment mitochondria (fragment length ≤ 1 to 5 μm) with significantly reduced larger fragments (fragment length 5 to >10 μm) compared to controls although this was more markedly apparent in P1, corresponding with the significantly decreased average mitochondrial fragment length (**Figure 5.29 A** and **Figure 5.29 B**). Fragment length distribution was more comparable to control in P3 although again there was a significant increase in smaller mitochondrial fragments (fragment length 1 to 2 μm) and a significant decrease in larger fragments (fragment length 5 to 10 μm) (**Figure 5.29 C**).

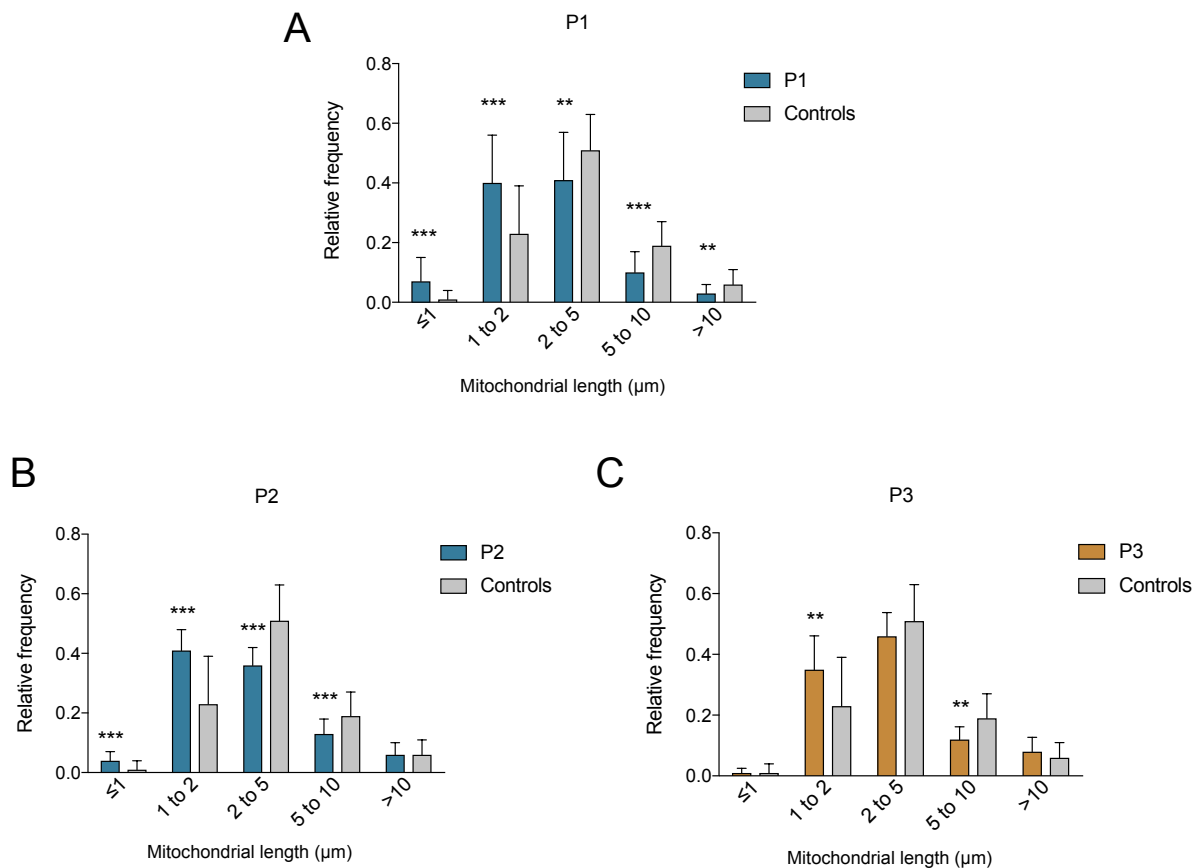


Figure 5.29. Distribution of mitochondrial fragment lengths. (A) P1 (B) P2 (C) P3 compared to control fibroblasts (mean of C1,C2). Data are relative frequency \pm SD $n = \geq 16$ ** $p < 0.01$ *** $p < 0.0001$ (two tailed unpaired t test) (see **Appendix 1** for relative frequency distributions in each cell line).

5.3.18 Analysis of mitochondrial dynamics proteins in fibroblasts

Western blot analysis of patient (P1–P3) and control (C1–C3) fibroblasts was undertaken to determine whether the observed changes in mitochondrial morphology were mediated

by changes in steady state levels of proteins known to control mitochondrial dynamics. This demonstrated a trend towards increased steady state levels of the OPA1 in P1 and P2 fibroblasts compared to P3 and controls. Conversely, there were no significant differences in the mitochondrial fission proteins MFN2 and DRP1 between patients and controls (Figure 5.30 and Figure 5.31).

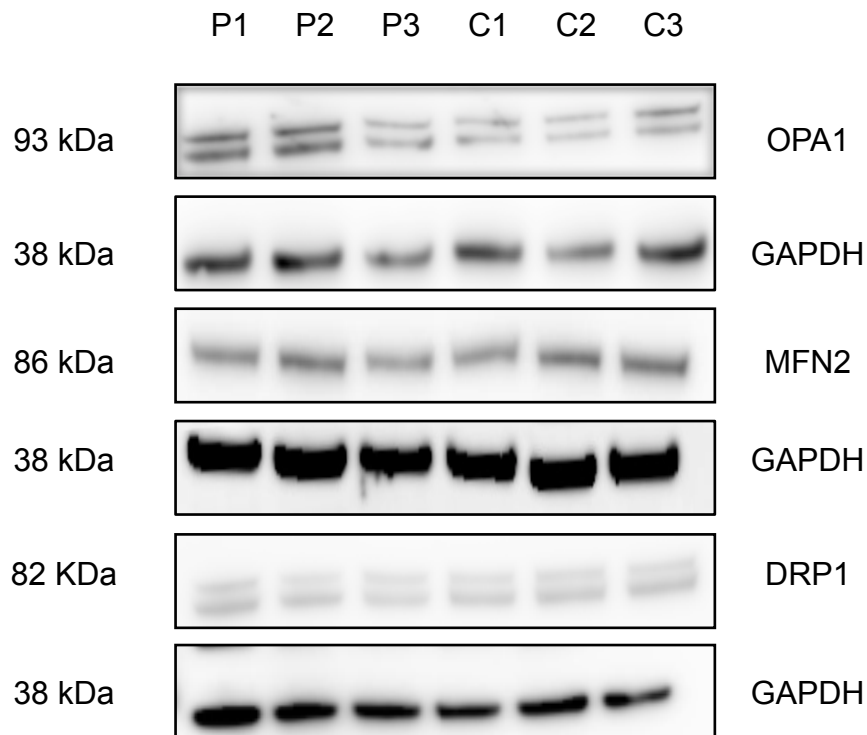


Figure 5.30. Western blot analysis of mitochondrial dynamics proteins in patient and control fibroblasts. Western blot of OPA1, MFN2 and DRP1 in patient (P1–P3) and control (C1–C3) fibroblasts. Images representative of 3 (OPA1) or 2 (MFN2, DRP1) independent experiments.

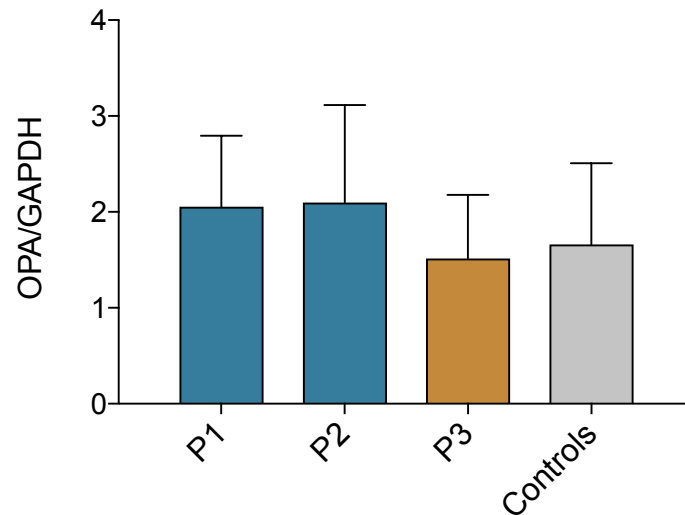


Figure 5.31. Quantification of OPA1 levels in patient and control fibroblasts. Densitometric quantification of OPA1 normalised to GAPDH P1=2.06±0.73, P2=2.10±1.01, P3=1.51±0.7, Controls=1.66±0.84. Data represents mean normalised OPA1±SD of 3 independent experiments. No significant difference detected between groups (one way ANOVA).

5.3.19 Analysis of mitochondrial nucleoids in fibroblasts

SSBP1 is a core component of mitochondrial nucleoids, the DNA-protein assemblies that package the mtDNA (Gilkerson, Bravo et al. 2013). To profile the effect of the *SSBP1* variant on the organisation of mitochondrial nucleoids, patient (P1–P3) and control (C1, C2) fibroblasts were investigated by immunocytochemical staining of mtDNA with anti-DNA and the mitochondrial network with anti-TOMM20. This revealed that mitochondrial nucleoids were dispersed throughout the mitochondrial network in all cell lines as evidenced by co-localisation of anti-DNA and TOMM20 staining in merged images. There was no gross alteration in nucleoid content or nucleoid morphology comparing the patient and control cell lines (**Figure 5.32**).

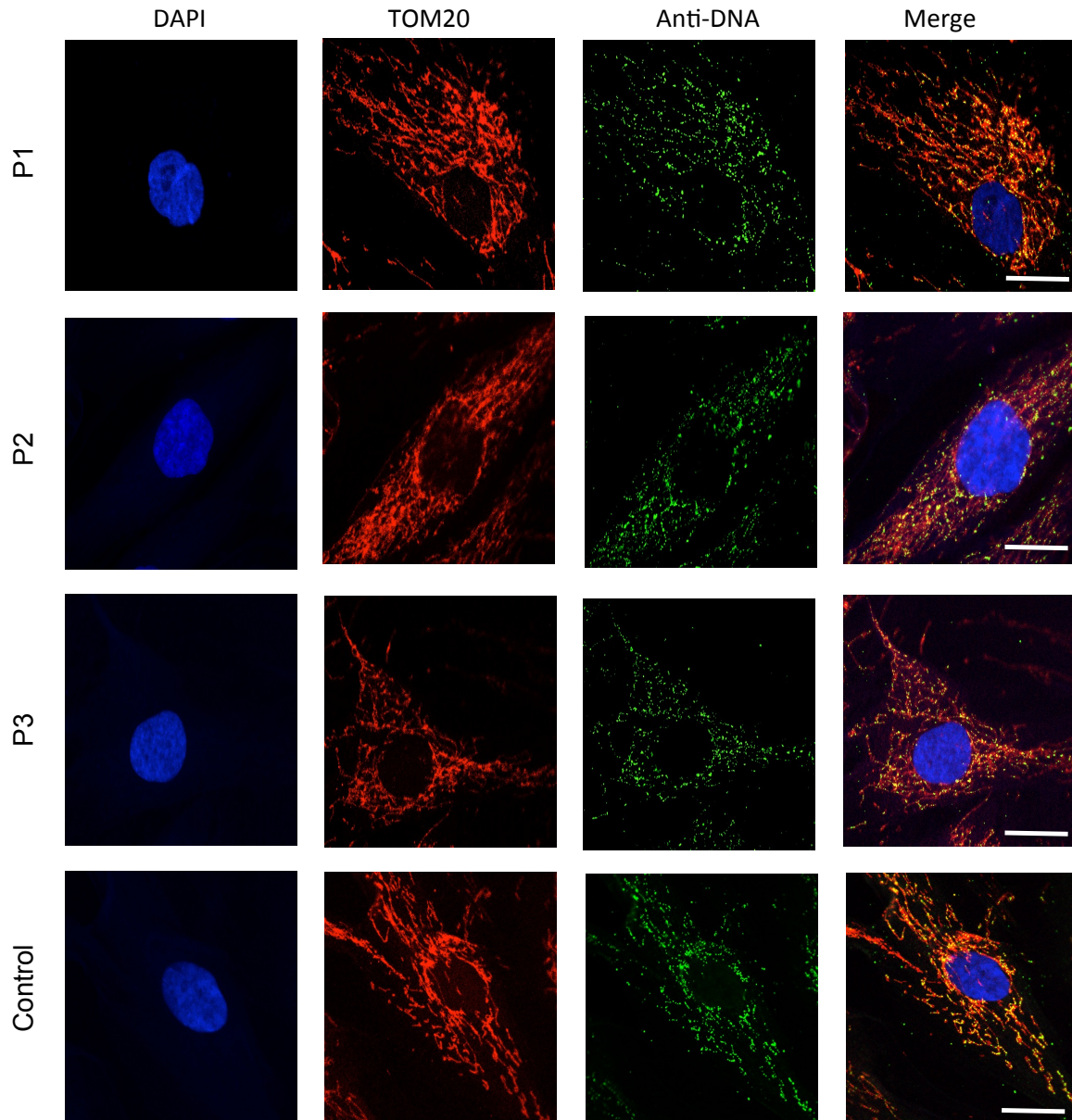


Figure 5.32. Analysis of mitochondrial nucleoids in patient and control fibroblasts. Representative confocal microscopy images of patient (P1–P3) and control (C1 shown as representative of C1 and C2) displaying DAPI staining for the nucleus (first column, blue), Anti-TOM20 for the mitochondrial network (second column, red), Anti-DNA for mitochondrial DNA (third column, green) and a merge image produced by overlaying the nuclear, mitochondrial network and mtDNA images. Approximately 10 cells per cell line were examined in 2 independent experiments. Scale bars=10 μ m.

5.3.20 Analysis of oxidative stress

Mitochondria are the major source of intracellular ROS, important cell signalling molecules that in excess result in oxidative stress (Murphy 2009). Dysfunctional OXPHOS is known to cause the leakage of electrons from the respiratory chain thereby increasing

cellular ROS levels (Hayashi and Cortopassi 2015). Moreover, ROS have previously been implicated as an important mediator in m.1555A>G pathogenesis (**Section 1.13.4**) (Raimundo, Song et al. 2012). We therefore determined oxidative stress levels in patient and control fibroblasts by assaying cellular ROS levels in conjunction with biomarkers of DNA and protein damage (Stark 2005, Jena 2012).

5.3.20.1 Analysis of ROS levels in fibroblasts

Cellular ROS levels were measured in fibroblasts from patients (P1–P3) and controls (C1, C2) using the cell permeant dye H₂DCFDA that fluoresces when oxidized, functioning as a marker of generalised oxidative stress. No significant difference was detected between patient and control cell lines (**Figure 5.33**).

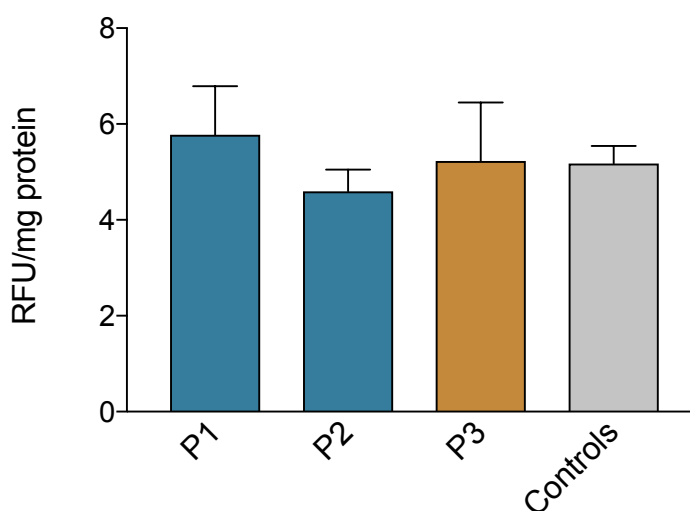


Figure 5.33. Measurement of cellular ROS levels in patient and control fibroblasts. ROS levels in patient (P1–P3) and control (C1, C2) fibroblasts were assessed using the H₂DCFDA assay, (P1=5.78±1.01, P2=4.5±0.45 P3=5.23±1.22, Controls=5.18±0.36) Data represents mean RFU/mg protein±SD of three independent experiments. No significant difference between groups was detected (one-way ANOVA).

5.3.20.2 8-OHdG DNA Damage ELISA in fibroblasts

DNA is considered a major target of oxidative damage within the cell and the formation of 8-hydroxydeoxyguanosine (8-OHdG) is a common marker of oxidative stress. The formation of 8-OHDG DNA adducts levels were quantified by 8-OHdG ELISA, however, no significant difference in 8-OHDG DNA adduct levels was detected between patient (P1–P3) and control (C1–C3) cell lines (**Figure 5.34**).

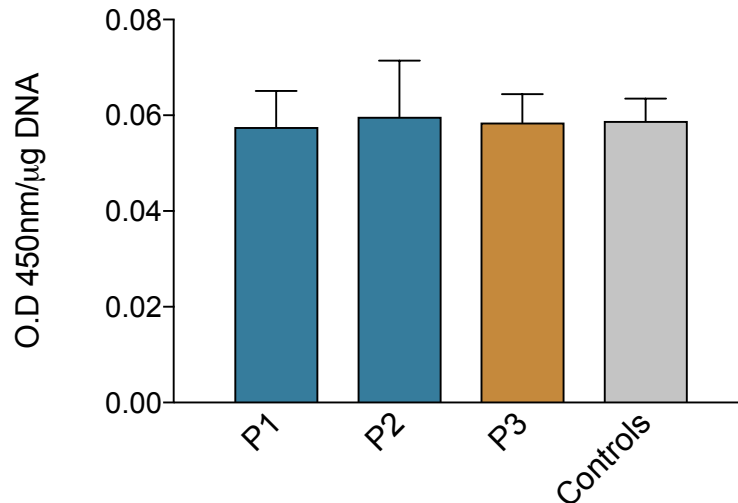


Figure 5.34. Quantification of 8-hydroxydeoxyguanosine in patient and control fibroblast DNA. 8-OHdG levels as quantified by 8-OHdG ELISA in patient (P1–P3) and control cells (C1–C3), P1=0.057±0.007, P2=0.059±0.01, P3=0.058±0.006, Controls=0.059±0.004. Data represents mean OD 450nm/μg DNA±SD of 2 independent experiments. No significant difference between groups was detected (one-way ANOVA).

5.3.20.3 Analysis of steady state glutathione peroxidase in fibroblasts

To further investigate the cellular oxidative stress response, the steady state level of the antioxidant glutathione peroxidase 1 (GPx1) was analysed by Western blot. There was a trend towards decreased GPx1 levels in patient (P1–P3) cells compared to controls, although the decrease was not statistically significant (**Figure 5.35**).

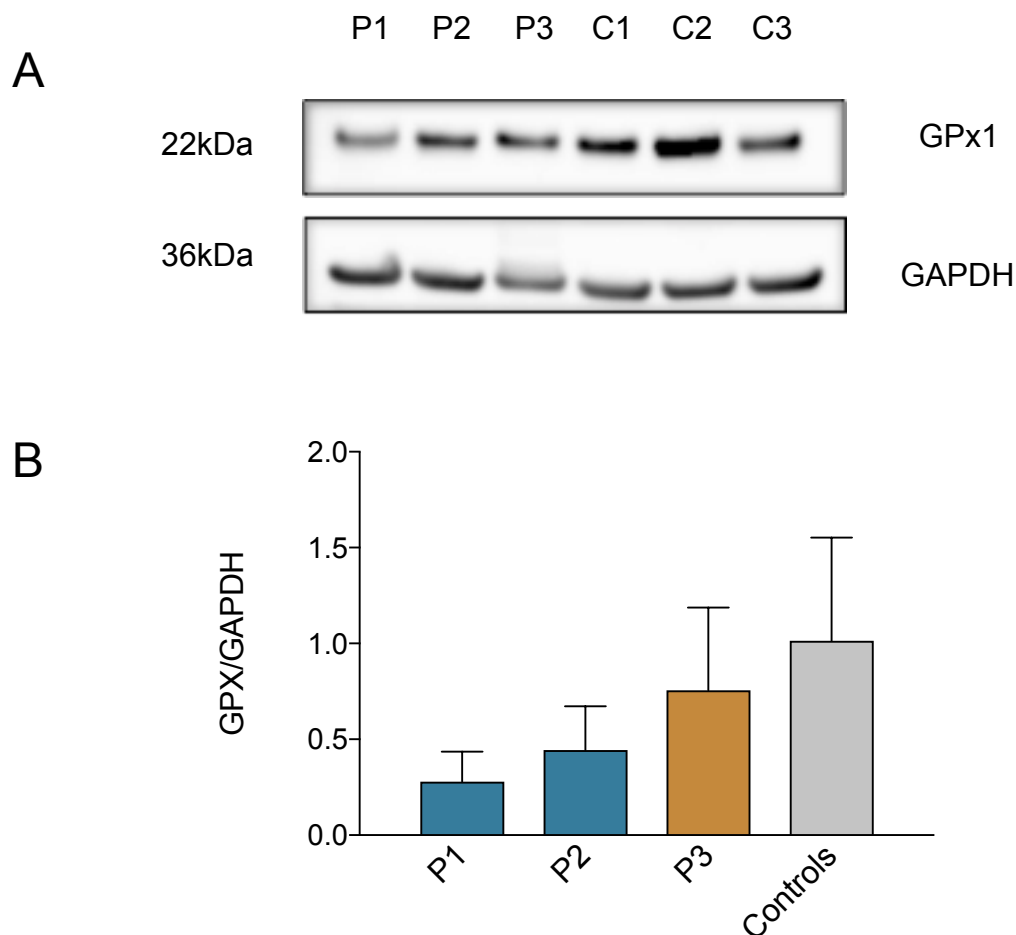


Figure 5.35. Western blot analysis of glutathione peroxidase 1 in fibroblasts. (A) Western blot analysis of cellular antioxidant proteins GPx1 in patient (P1–P3) and control (C1–C3) fibroblasts. Images representative of 3 independent experiments. (B) Densitometric quantification of GPx1 normalised to GAPDH P1=0.28±0.16, P2=0.44±0.22, P3=0.76±0.43, Controls=1.01±0.53. Data represents mean normalised GPx1±SD of 3 independent experiments. No significant difference between groups detected as determined (one-way ANOVA).

5.3.20.4 Analysis of protein carbonylation in fibroblasts

Oxidative modification of protein caused by the reaction of ROS with amino acids is a major source of post-translational protein modification and has been associated with loss of protein function (Cai and Yan 2013). The Oxyblot™ Protein Oxidation Detection Kit was used to investigate carbonylation of proteins across the whole proteome as a marker of generalised oxidative stress in fibroblasts from patient (P1–P3) and controls (C1–C3). The assay detects the derivate product 2,4-dinitrophenylhydrazone. The use of the derivatization control solution allows for comparison of proteins that have not been modified by oxidation. As such, bands that are present in the treated reaction but absent in the negative control can be considered to have undergone oxidative modification. The

overall optical density of the bands correlates with the amount of protein oxidation and hence provides a semi-quantitative assessment of oxidative stress. However, there was no gross difference in total protein carbonylation in patient compared to control cell lines (Figure 5.36).

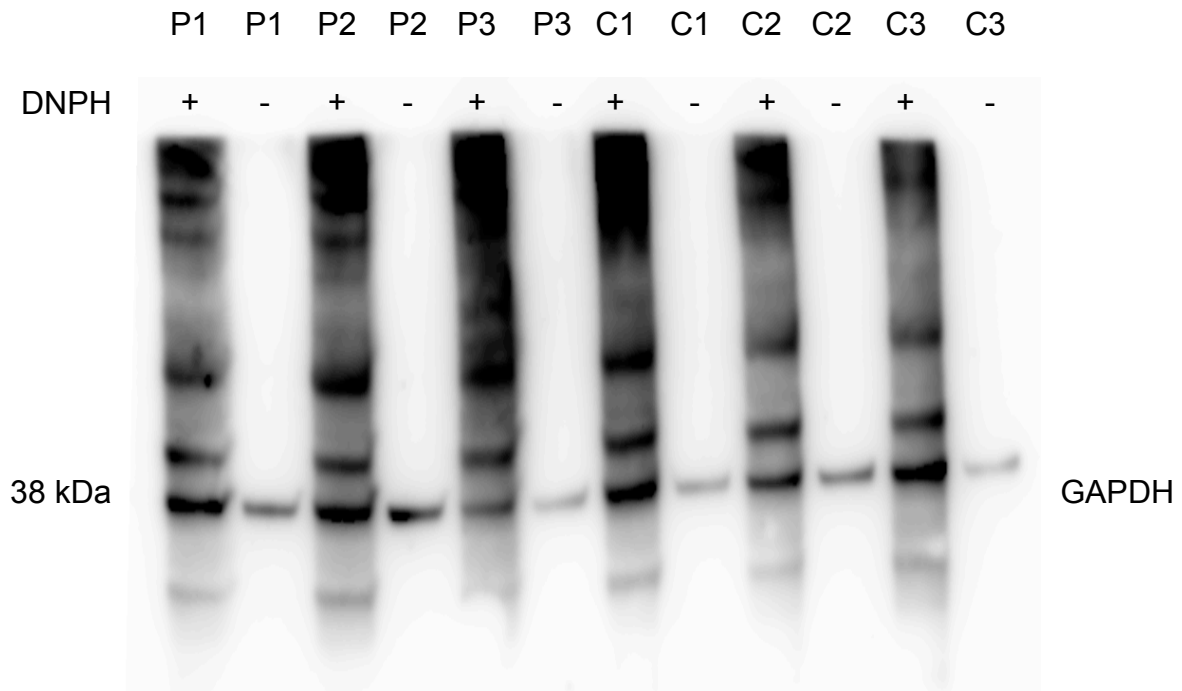


Figure 5.36 Analysis of protein carbonylation in patient and control fibroblasts. Oxyblot analysis of cellular lysates from patient (P1–P3) and controls (C1-3). DNP was added for derivatization of carbonyl groups as indicated. Immunoblotting for GAPDH was undertaken to control lanes for loading control. Image representative of 3 independent experiments.

5.3.21 Analysis of retrograde mitonuclear signalling

Previous work has suggested that activation of the AMPK pathway is an important contributor to m.1555A>G pathogenesis (Section 1.13.4) (Raimundo, Song et al. 2012). To determine the effect of the *SSBP1* and m.1555A>G variants on the AMPK signalling pathway we determined the ratio of activated AMPK (phosphorylated at threonine 172, pT172, AMPK-P) to total cellular AMPK-Alpha (AMPK-A) from patients (P1–P3) and control (C1–C3) fibroblasts. This was undertaken by (i) ELISA and (ii) Western blot analysis using the same cellular lysates in each assay to allow direct comparison between the two methodologies.

5.3.21.1 Total AMPK-A and AMPK pT172 ELISAs

Total AMPK-A was quantified using the AMPK–alpha 1 *in vitro* SimpleStep ELISA. No significant difference was detected between patient and control cell lines (**Figure 5.37 A**). There was also no difference in AMPK-P, quantified by the AMPK pT172 Phospho-ELISA Kit between patients and controls (**Figure 5.37 B**). It followed that there was no significant difference in the AMPK-P:AMPK-A ratio between any of the groups (**Figure 5.37 C**).

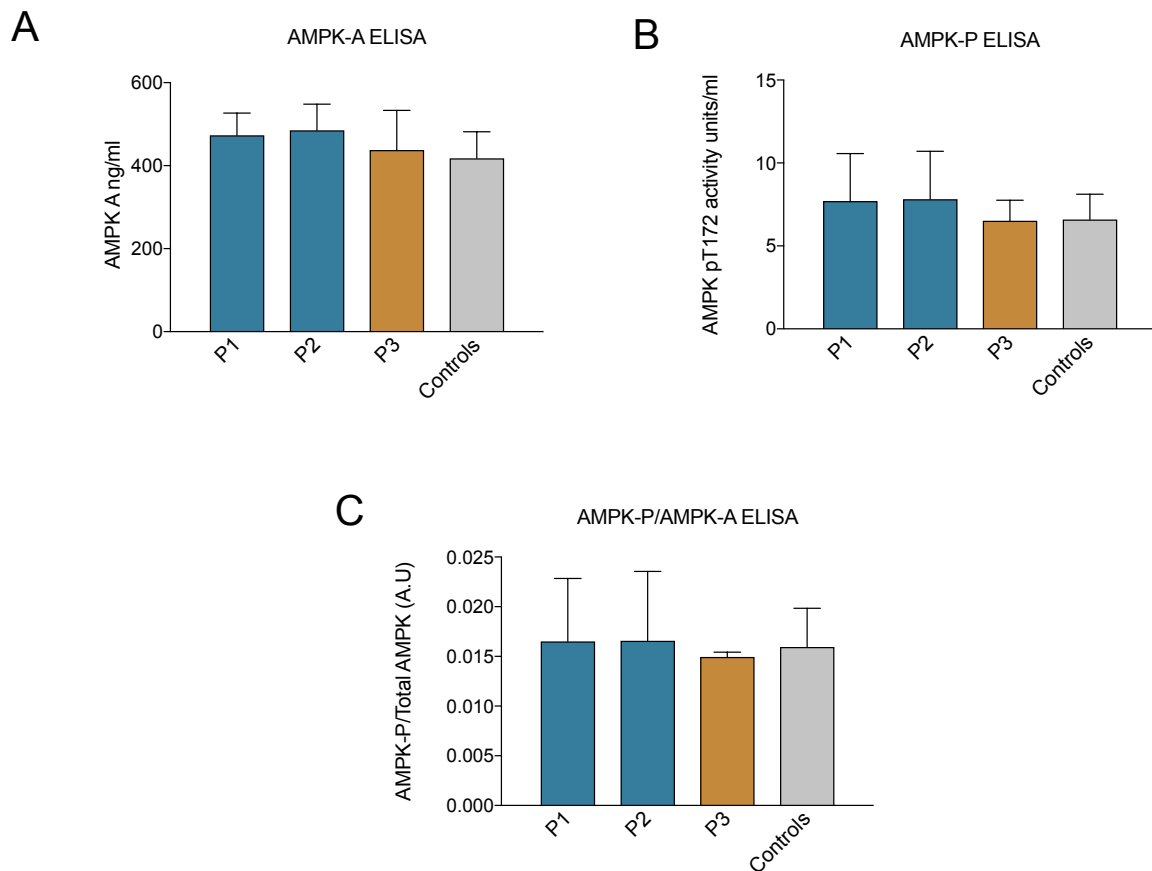


Figure 5.37. Analysis of cellular AMPK activity in patient and control fibroblasts by ELISA (A) Total AMPK-A as quantified by AMPK–alpha 1 *in vitro* SimpleStep ELISA in patient (P1–P3) and control cells (C1–C3) P1=473.5±53.2, P2=485.3±63.0 P3=437.8±95.3, Controls=417.9±64.1. Data represents mean AMPK alpha ng/ml±SD of 3 independent experiments. (B) AMPK-P as quantified by AMPK pT172 Phospho-ELISA Kit P1=7.70±2.9 P2=7.81± 2.9, P3=6.51± 1.24, Controls=6.59±1.53 Data represents mean AMPK pT172 activity units/ml±SD of 3 independent experiments. (C) Ratio of AMPK-P:AMPK-A as quantified by ELISA in (A) and (B) P1=0.017±0.006, P2=0.0166±0.007 P3=0.05±0.00004, Controls=0.016±0.004. Data represents mean AMPK alpha ng/ml / mean AMPK pT172 activity units/ml±SD of 3 independent experiments. The statistical analysis of data represented in (A), (B) and (C) reveal no significant difference between patient and control lines (one way ANOVA).

5.3.21.2 Western blot analysis of total AMPK and AMPK-pT172

Western blot analysis was then performed with the same lysates as used in the ELISAs presented in **Section 5.3.21.1**. Although there was an apparent increase in AMPK-pT172 signal in *SSBP1* fibroblasts compared to controls, normalisation by AMPK-A reduced this difference. However, there remained a trend towards increased AMPK pT172:AMPK-A in P1 cells, although this did not reach statistical significance (**Figure 5.38**).

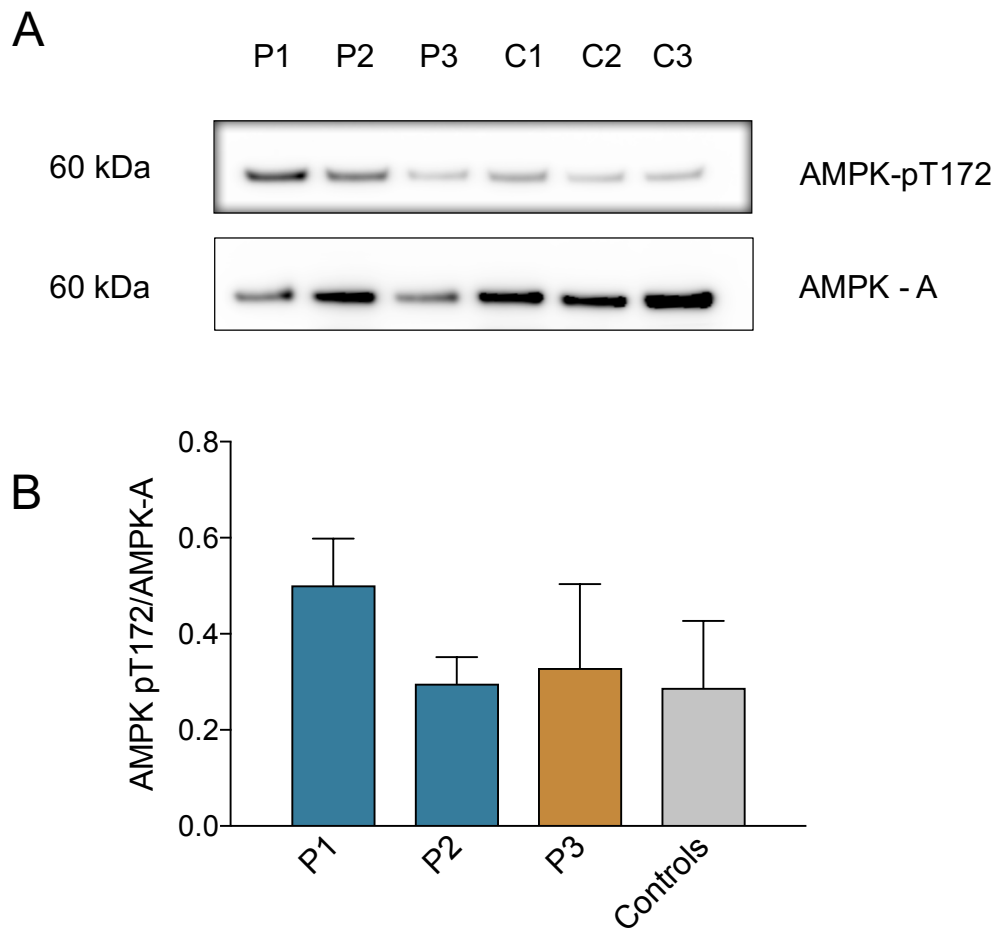


Figure 5.38 Western blot analysis of cellular AMPK activity. (A) Western blot of AMPK-pT172 and AMPK-A in primary patient (P1–P3) and control fibroblast cell lines (C1-3). Image representative of 3 independent experiments. (B) Densitometric quantification of AMPK-pT172 normalised to AMPK-A. P1=0.50±0.097, P2=0.297±0.06, P3=0.328±0.174, Controls=0.29±0.139. Data represents mean normalised AMPK-P:AMPK-A±SD of 3 independent experiments. No significant difference between groups detected as determined (one-way ANOVA).

5.3.21.3 Western blot analysis of total S6K and pS6K-Thr 389

The phosphorylation of ribosomal protein S6 kinase (p70-S6 kinase) is regarded as a hallmark of mTOR signalling activation. The AMPK signalling pathway acts to inhibit mTOR and thereby control protein synthesis, cell growth, and metabolism (Inoki, Kim et al. 2012). To determine whether the *SSBP1* and m.1555A>G variants modulated the signalling pathways downstream of AMPK, Western blot analysis of total S6K and activated S6K (phosphorylated at threonine 389, pT389) was undertaken in patient (P1–P3) and control (C1–C3) fibroblasts and used to calculate S6K-pT389: total S6K as an indicator of S6K activity. There was a trend towards an increase in S6K activity in patient fibroblasts however this did not reach statistical significance (**Figure 5.39**).

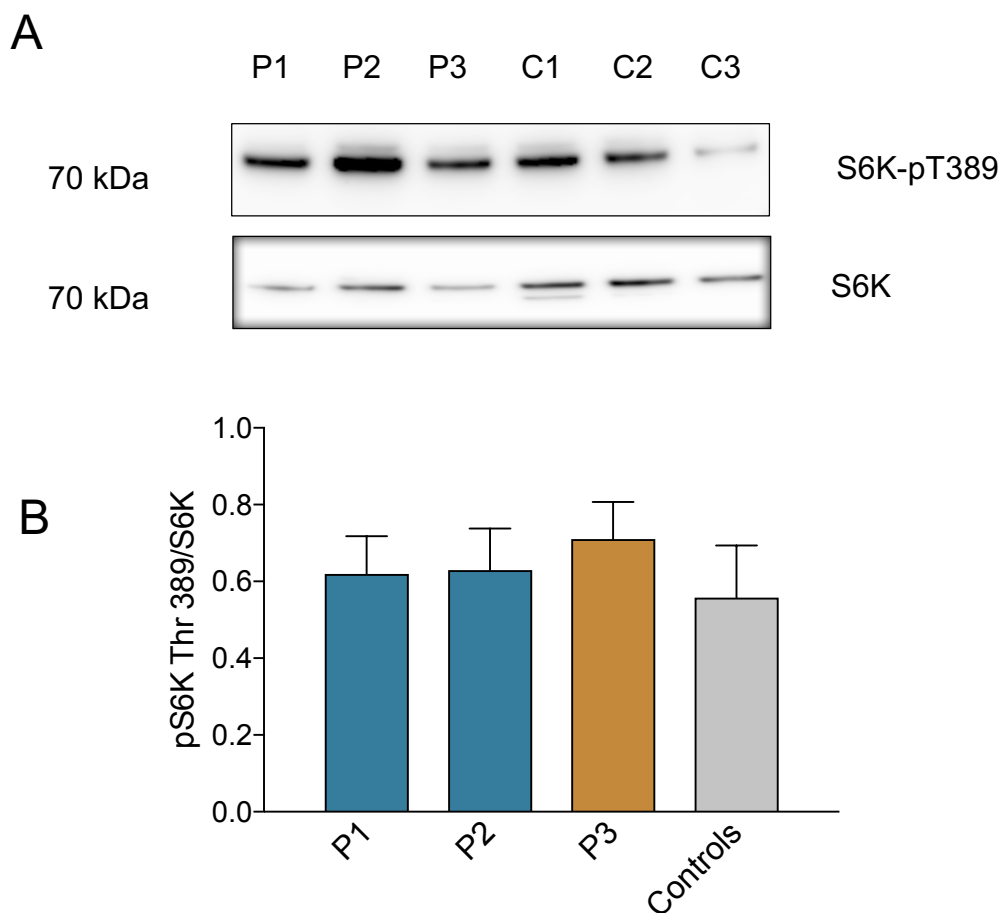


Figure 5.39. Western blot analysis of total S6K and S6K-pT389. (A) Western blot of S6K-pT389 and S6K in primary patient (P1–P3) and control fibroblast cell lines (C1-3). Image representative of 3 independent experiments. (B) Densitometric quantification of S6K-pT389 normalised to total S6K. P1=0.619±0.098, P2=0.629±0.108, P3=0.719±0.096, Controls=0.557±0.136. Data represents mean normalised S6K-pT389: S6K±SD of 3 independent experiments. No significant difference between groups detected (one-way ANOVA).

5.3.21.4 Analysis of the effect of heat shock in patient fibroblasts

SSBP1 has recently been demonstrated to play a critical role in the modulation of the cellular heat shock response, specifically by increasing the expression of cytoplasmic chaperones including HSP90, HSP40 and HSP70 and mitochondrial chaperones HSP10 and HSP60, both at the gene and protein level (Tan, Fujimoto et al. 2015). We hypothesised that the protein expression induction of HSP70 and HSP60 after heat treatment in P1 and P2 fibroblasts would be compromised compared to heat-treated P3 fibroblasts and controls. We also evaluated endoplasmic reticulum (ER) homeostasis by examining the protein levels of BiP, an ER chaperone important in the ER stress response (**Figure 5.40**).

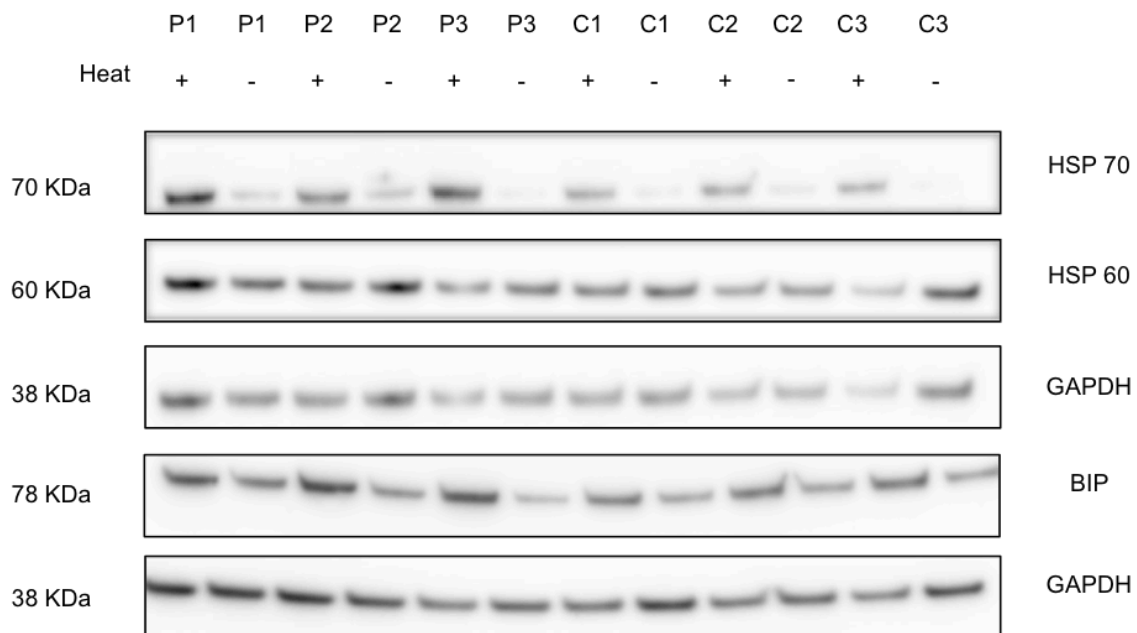


Figure 5.40. Analysis of heat shock in fibroblasts. Western blot of analysis of HSP70, HSP60 and BiP in primary patient (P1–P3) and control fibroblast cell lines (C1-3) at steady state and after heat shock at 42°C for 1 hour and a 4 hour recovery at 37°C. Images representative of 2 independent experiments.

There was no statistical difference between the steady state protein expression levels of HSP60, HSP70 or BiP between SSBP1 cell lines compared to P3 and control cells (**Figure 5.41 B (i)**). Heat treatment robustly induced HSP70 in all cell lines; however, the induction of HSP60 expression was noticeably more modest (**Figure 5.41B (ii)**). Importantly, the induction of HSP60 and HSP70 by heat shock, as quantified by the fold change in protein expression between the heat treated and steady state, was not different between *SSBP1*

cells and those carrying the wild type variant (P3 and controls). Similarly, there was no difference in the induction of BiP between the groups (**Figure 5.40 B (ii)**).

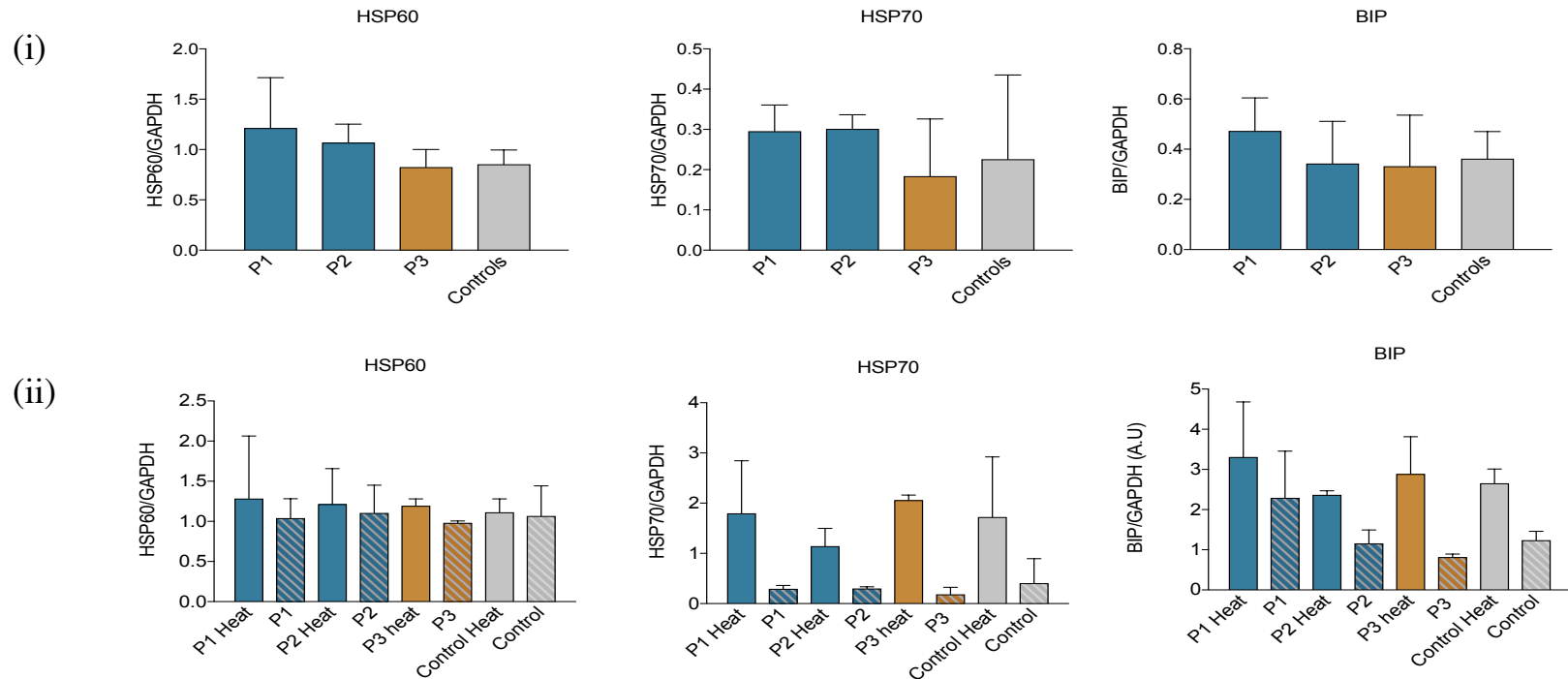


Figure 5.41. Analysis of heat shock response in patient and control fibroblasts. Densitometric quantification of HSP60, HSP70 and BiP in patient (P1–P3) and control cell lines (C1–C3) at steady state. No significant difference was detected between patient and control lines (one way ANOVA). The quantification data for the assays is presented in **Appendix 3**. (B) The densitometric quantification of HSP60, HSP70 and BiP in patient (P1–P3) and control cell lines (C1–C3) was used to calculate a protein induction fold change (pS:pHS); HSP70 (P1 Heat vs P1 fold change=5.8±2.24, P2 Heat vs P2 fold change=3.89±1.62, P3 Heat vs P3 fold change=15.7±11.6 Control Heat vs Control fold change=4.6±1.54). BiP (P1 Heat vs P1 fold change=1.48±0.15, P2 Heat vs P2 fold change=2.13±0.69, P3 Heat vs P3 fold change=3.49±0.80, Control Heat vs Control fold change=2.17±0.28). HSP60 (P1 Heat vs P1 fold change=1.17±0.47, P2 Heat vs P2 fold change=1.08±0.06, P3 Heat vs P3 fold change=1.22±0.05 Control Heat vs Control fold change=1.29±1.04). Data represents pS:pHS±SD of 2 independent experiments. Fold changes of HSP60, HSP70 and BiP were not significantly different between the groups (one way ANOVA).

5.4 Discussion

The data presented in this chapter, including genetic, protein and biochemical analyses provide compelling evidence of an interaction between the c.3G>A *SSBP1* and m.1555A>G variants. Our findings strongly suggest that together these variants act to significantly compromise cellular physiology through a combined effect on mtDNA maintenance and mtDNA translation manifesting as a tissue specific phenotype. This is both the first report of a likely pathological mutation in the core mitochondrial replisome protein SSBP1 and the first evidence of a variant in an mtDNA replication gene modifying the phenotype of m.1555A>G.

The c.3G>A *SSBP1* variant is predicted to cause the loss of the canonical protein translation start site, abolishing a core component of the conserved Kozak sequence (gccRccAUGG) required for the ribosome to initiate protein translation (Zur and Tuller 2013). A number of studies have highlighted start-loss mutations as important contributors to human disease, and to date, over 400 pathogenic single base substitutions within the ATG (AUG at the mRNA level) of the translation initiation codon (TIC) have been reported (Wolf, Caliebe et al. 2011). Loss of the *SSBP1* TIC may lead to the activation of an alternate reading frame coding for an N-terminal truncated protein. Translation in this predicted reading frame generates a 14 amino acid protein lacking the mitochondrial targeting sequence (Omura 1998). This likely mis-targets the truncated protein resulting in degradation by cytosolic proteostatic quality control mechanisms (Chen, Retzlaff et al. 2011, Wrobel, Topf et al. 2015).

Western blot analysis of *SSBP1*, m.1555A>G and control fibroblasts confirmed the *SSBP1* variant reduced SSBP1 protein levels to approximately 20% of control levels. Furthermore, the lack of any detectable SSBP1 isoforms shorter than the annotated protein is consistent with the predicted truncated protein being degraded in the cytosol (Kazak, Reyes et al. 2013). However, it should be noted that the SSBP1 antibody used in this study is polyclonal, hence it is not possible to determine whether specific shorter forms of the protein would be robustly detectable.

The magnitude of the reduction in SSBP1 protein levels in *SSBP1* fibroblasts is surprising since an effective null allele, as predicted to result from the *SSBP1* variant, would be expected to reduce protein levels by a maximum of 50% (Voet 2011). SSBP1 exists within

the cell as a homotetramer, thus it is conceivable that the reduction in subunit availability caused by the loss of SSBP1 protein translation reduces the efficiency of tetramer formation which then triggers enhanced degradation of the remaining free SSBP1 subunits (Goldberg 2003). It would be possible to further test this hypothesis by determining whether treatment of *SSBP1* fibroblasts with an inhibitor of proteasomal degradation, such as MG-132, ameliorated the reduction in steady state protein levels (Kisselev, van der Linden et al. 2012). Alternatively, there may be an inherent allelic imbalance of *SSBP1* gene expression with the c.3G>A variant directly impacting an allele that is responsible for more than 50% of the encoded protein. This process may be accounted for by genomic imprinting, that could be further investigated using bisulfite Pyrosequencing methodology to determine differential methylated regions within the *SSBP1* gene (Barlow and Bartolomei 2014, McKeown, Fort et al. 2014).

The observed reduction of steady state SSBP1 protein levels strongly suggests that the *SSBP1* variant causes dysfunction in SSBP1 translation. However, more definitive evidence of this pathological mechanism could be obtained by creating expression vectors containing either fluorescently tagged wild type or mutant c.3G>A *SSBP1*. These vectors could then be transfected into a control cell line with the expectation that the mutant *SSBP1* would abolish specific immunofluorescence indicative of dysfunctional protein expression (Jinda, Pongvarin et al. 2016). Further validation of this mechanism could be obtained by performing *in vitro* translation of mutant and wild type RNA using a rabbit reticulocyte lysate system containing radiolabelled methionine (Jackson and Hunt 1983).

Additionally, and in agreement with previous work characterising the effect of start-loss mutations, we found there was no significant difference in the mRNA expression levels of *SSBP1* between *SSBP1*, m.1555A>G and control fibroblasts (Sargiannidou, Kim et al. 2015). This finding is consistent with the *SSBP1* variant solely compromising SSBP1 protein translation without an effect on mRNA expression.

Mitochondrial histochemical investigation of III-8, P5, an individual from the Finnish family carrying the *SSBP1* c.3G>A and m.1555A>G variants, revealed the presence of a low number of COX-negative fibres (estimated at 3.4%). COX-negative fibres have been identified in a range of mitochondrial diseases and generally are only present in healthy individuals over the age of 60 years (Brierley, Johnson et al. 1998, Taylor, Schaefer et al. 2004). Given that III-8 was aged 38 years at the time of biopsy, these changes can be

considered to be pathological. It must however be recognised that we were unable to obtain a muscle biopsy from P3 who carries m.1555A>G without c.3G>A *SSBPI* or from the *SSBPI* variant carrying children of III-6 and III-10 that are wild type at m.1555. We therefore are unable to infer whether each variant could cause this effect in isolation. Importantly, a previous study examining skeletal muscle from an m.1555A>G carrier detected no overt histochemical evidence of mitochondrial dysfunction although the presence of mitochondrial deletions was not assessed (Santorelli, Tanji et al. 1999). Incidentally, the presence of muscle ‘minicores’ was noted but given that the subject also presented with cardiomyopathy, a second nuclear mutation is likely to account for the histological findings in this individual (Santorelli, Tanji et al. 1999, Jungbluth 2007).

Further analysis of III-10, P4 and III-8, P5 skeletal muscle revealed the presence of mtDNA deletions and a reduction in mtDNA copy number to 40% of control levels, clearly suggesting the *SSBPI* variant causes dysfunction of mtDNA maintenance. Consistent with these results, mtDNA deletions are also detectable in skeletal muscle from carriers of mutations in other mtDNA maintenance genes such as *MGME1* (mitochondrial genome maintenance exonuclease 1), *MPV17* and *RNASEH1* (Blakely, Butterworth et al. 2012, Kornblum, Nicholls et al. 2013, Reyes, Melchionda et al. 2015).

The absence of mtDNA deletions in *SSBPI* fibroblasts is consistent with a well-recognised phenomenon in carriers of mutations in mtDNA maintenance genes, including *POLG* and *RNASEH1* (Stewart, Schoeler et al. 2011, Reyes, Melchionda et al. 2015). It has been proposed that the deletions are lost in these rapidly dividing cells (Moraes, Ciacci et al. 1993, Weber, Wilson et al. 1997).

Interestingly, in contrast to the findings in skeletal muscle, the mtDNA copy number of *SSBPI* fibroblasts was confirmed by qPCR and Southern blot analysis to be no different to m.1555A>G and control fibroblasts. Moreover, there was no observable difference in blood mtDNA copy number between carriers of the *SSBPI* variant and wild type individuals from the family. This is in agreement with a previous study where reduction of *SSBPI* expression by RNAi did not alter mtDNA copy number in mouse C2C12 cells (Arakaki, Nishihama et al. 2006). Contrastingly, reduction of *SSBPI* expression in HeLa cells has been shown to cause an reduction in mtDNA copy number to 60% of control levels (Ruhanen, Borrie et al. 2010). Taken together, these findings strongly suggest that there are cell and, potentially, tissue specific differences in the requirement for *SSBPI* to

maintain mtDNA copy number. This hypothesis is consistent with the finding that tissue specific compensatory mechanisms maintain normal mtDNA copy number in fibroblasts harbouring mutations in the mtDNA maintenance genes, *POLG2* and *TK2* (Frangini, Rampazzo et al. 2009, Stewart, Schoeler et al. 2011).

The cellular mechanism by which the *SSBP1* variant causes mtDNA deletions in skeletal muscle has not been resolved by this study, however, it is known that patients with defects in *POLG*, a critical mtDNA maintenance gene that encodes the mitochondrial DNA polymerase, $\text{poly}\gamma$, are thought to accumulate mtDNA deletions by replication stalling at homopolymeric tracts (Kunkel and Soni 1988, Hudson and Chinnery 2006). It has been proposed that SSBP1 reduces arrests within these tracts, and thus suppresses mtDNA deletion formation (Mikhailov and Bogenhagen 1996). SSBP1 also acts to reduce replication stalling by stimulating the activity of $\text{poly}\gamma$ thereby increasing the processivity of the $\text{poly}\gamma$ /Twinkle complex (Korhonen, Pham et al. 2004). Moreover, currently unpublished work from the laboratory of Maria Falkenberg (University of Gothenburg, Sweden) has demonstrated that SSBP1 abolishes mtDNA deletion formation in an *in vitro* replication model by decreasing $\text{poly}\gamma$ slippage during L-strand synthesis. This is in concordance with the observation that excessive pausing leads to the accumulation of multiple deleted species by a process of DNA breakage or recombination (Bailey, Cluett et al. 2009).

According to the strand displacement model, SSBP1 coats the H-strand whilst single-stranded during mtDNA replication (Clayton 1982). Therefore, low SSBP1 levels in the carriers of the *SSBP1* variant may increase mtDNA replication stalling and non-specific replication initiation by the non-specific polymerase POLRMT (Miralles Fuste, Shi et al. 2014). This hypothesis could be further investigated by performing 2D-AGE to delineate mitochondrial replication intermediates (mtRIs). An accumulation of mtRIs would signify a replication stalling phenotype as seen in fibroblasts carrying pathogenic mutations in other mtDNA maintenance genes including *TWINK*, *MGME1*, *RNASEH1* and *POLG* (Wanrooij, Goffart et al. 2007, Goffart, Cooper et al. 2009, Kornblum, Nicholls et al. 2013, Reyes, Melchionda et al. 2015) Alternatively, the increased levels of unprotected single stranded DNA may lead to degradation by cellular endonucleases precipitating mtDNA deletions (Richard, Bolderson et al. 2008).

Reduction in SSBP1 has also been demonstrated to enhance mtDNA supercoiling, evidenced by loss of staining by PicoGreen, a fluorochrome that exclusively binds double

stranded DNA but cannot bind to tightly packed genomes (Di Re, Sembongi et al. 2009). It is therefore possible that the altered structure of the mtDNA in *SSBPI* cells may modulate the binding of proteins involved in mtDNA replication leading to the observed reduction of mtDNA copy number in skeletal muscle.

Collectively, these dysregulated processes may combine to ultimately compromise replication fidelity leading to tissue-specific mtDNA deletions and mtDNA copy number depletion (Miralles Fuste, Shi et al. 2014).

Mammalian mtDNA molecules contain a triple-stranded region found in the NCR of many mitochondrial genomes, formed by the stable incorporation of a third, short DNA strand known as 7S DNA. The exact function of 7S DNA is unknown, however, it has been proposed to play a role in mtDNA replication as an intermediate of prematurely terminated H-strand synthesis. Furthermore, perturbations in the steady state levels of 7S DNA have been observed in mtDNA maintenance disorders resulting from mutations in *RNASEH1* and *MGME1* (Kornblum, Nicholls et al. 2013, Nicholls and Minczuk 2014, Reyes, Melchionda et al. 2015). Given the evidence of dysfunctional mtDNA metabolism observed in patient skeletal muscle we further analysed the steady state levels of 7S DNA in patient and control fibroblasts. The reduction in the abundance of 7S DNA relative to genome length mtDNA molecules in *SSBPI* fibroblasts compared to m.1555A>G and control fibroblasts was consistent with previous work demonstrating SSBP1 is required for the regulation of the mtDNA D-loop by modulating the synthesis of 7S DNA (Ruhanen, Borrie et al. 2010). This result provided definitive evidence of mtDNA dysmetabolism in *SSBPI* fibroblasts.

To further clarify the effect of the *SSBPI* and m.1555A>G variants on mtDNA replication we undertook a mitochondrial repopulation assay. We employed the experimental paradigm used by *Stewart et al.* Although, as expected 15 days' of EtBr depletion resulted in depletion of mtDNA copy number, this was accompanied by a profound reduction in cell viability that was not experienced by the original authors (Stewart, Schoeler et al. 2011). It is likely this was a result of a chronic reduction in mtDNA copy number leading to respiratory compromise and triggering cell death. The reasons for the increased sensitivity of our fibroblasts to mtDNA depletion are unclear although this discrepancy may be specific to the cells used in our assay or dependent on cell culture conditions.

We therefore used a modified assay consisting of a shorter, 4-day period of depopulation followed by 6 days' of repopulation. This revealed a consistent trend for higher repopulation levels in all patients compared to control cells. This is in agreement with the increased mtDNA replication efficiency in carriers of the LHON mutation, m.11778A>G (Giordano, Iommarini et al. 2014). It is possible therefore that these homoplasmic mitochondrial variants produce a compensatory nuclear signal to increase mtDNA replication efficiency. To further test this hypothesis qPCR analysis would determine whether the m.1555A>G variant causes upregulation of genes associated with mtDNA replication even in steady state conditions.

A closer analysis of the repopulation kinetics revealed the repopulation rate in *SSBP1* cells was double that of 1555A>G and control cells. This poses the intriguing possibility that the reduction in 7S DNA abundance is directly causative of the higher mtDNA repopulation rate in *SSBP1* fibroblasts. As previously discussed, the function of 7S DNA has not yet been fully resolved, although recently it has been suggested that it may act to control mtDNA replication by inhibiting the assembly of the replisome at LSP as well as replication fork progression (Nicholls and Minczuk 2014). The reduction of 7S DNA in *SSBP1* fibroblasts therefore may remove this control mechanism and facilitate faster mtDNA replication. Consistent with this hypothesis, fibroblasts carrying *MGME1* and *RNASEH1* mutations demonstrate increased 7S DNA levels in conjunction with a reduction in mtDNA repopulation rates (Kornblum, Nicholls et al. 2013, Reyes, Melchionda et al. 2015). A reduction in 7S DNA abundance would, however, be envisaged to only affect a minority of mtDNA molecules, given that only approximately 10% of mtDNAs contain a 7S DNA strand (Brown, Shine et al. 1978). On the other hand, it is important to recognise that only a proportion of mtDNAs are able to replicate, therefore the reduction in 7S DNA may be specific to this subset of mtDNA molecules (unpublished observations, Dr Aurelio Reyes, Mitochondrial Biology Unit, Cambridge, UK).

Alternatively, the reduction in *SSBP1* levels may permit faster mtDNA replication by speeding the progression of the replication fork, no longer limited by needing to remove *SSBP1* from single stranded DNA undergoing replication. This hypothesis could be tested by measuring active mtDNA replication rates by incorporation of bromodeoxyuridine (BrdU) in fibroblasts where nuclear replication has been inhibited by aphidicolin (Lentz, Edwards et al. 2010).

It must also be noted that SSBP1 is only predicted to coat the H-strand according to the strand displacement model of mtDNA replication (Clayton 1982). Therefore, *SSBP1* cells may replicate mtDNA using the strand coupled or RITOLS replication models that require limited quantities of SSBP1 (Holt, Lorimer et al. 2000, Reyes, Kazak et al. 2013). Furthermore, cultured cells depleted of mtDNA by EtBr have been shown to predominantly use strand-coupled replication in the ensuing repopulation phase (Yasukawa, Yang et al. 2005). The forced requirement to switch replication modes in the m.1555A>G and control cells may account for the difference in repopulation rates compared to the *SSBP1* cells that are already adapted to using strand coupled replication.

In order to dissect the mechanistic link between reduced 7S DNA levels and enhanced mtDNA replication, wild type *SSBP1* could be expressed in *SSBP1* cells with the expectation that this would increase 7S DNA levels and result in a reduced mtDNA repopulation rate. Besides SSBP1, studies have demonstrated 7S DNA synthesis is promoted by a number of other factors, including, TFAM and Twinkle helicase (Gensler, Weber et al. 2001, Milenkovic, Matic et al. 2013). Overexpression of either of these factors in *SSBP1* cells would similarly be expected to increase 7S DNA levels and subsequently reduce the mtDNA repopulation rate. Potentially this strategy would distinguish whether the repopulation rate depends on 7S DNA *per se* or whether it is contingent on another function of SSBP1. It should be considered, however, that overexpression of these factors may also dysregulate other cellular processes, confounding the results of the analysis.

It is tempting to speculate that the faster mtDNA replication coupled with increased single stranded regions of DNA that are liable to undergo oxidative damage in *SSBP1* cells may lead to an increase in replication errors by poly γ . This would be expected to result in the accumulation of point mutations. This hypothesis could be further investigated by undertaking ultra-deep sequencing, using NGS technology, to examine for low level heteroplasmic mutations in *SSBP1* fibroblasts (McElhoe, Holland et al. 2014). Further, the distribution of the mutations within the mitochondrial genome may reflect the non-linear distribution of SSBP1 occupancy across mtDNA. It has been demonstrated that SSBP1 occupancy is highest at *MT-CYB* and falls to a minimum at *MT-CO1* (Miralles Fuste, Shi et al. 2014). Hence, given that the *MT-CYB* region remains single stranded for longer during replication, it would be expected that this region would be enriched in point mutations (Reyes, Gissi et al. 1998).

The replication and transcription machineries are spatially linked by nature of the DNA and RNA polymerases sharing a common DNA template. There are, therefore, collisions between these machineries, which pose a substantial risk to genomic integrity (Mirkin and Mirkin 2007). Recent work has highlighted the transcription elongation factor, TEFM as a critical molecular switch between the two processes (Agaronyan, Morozov et al. 2015). It has also been suggested that the D-loop triple strand structure plays a regulatory role in this process. By acting to inhibit replication fork progression, the D-loop structure prevents replication fork collisions as well as collisions between the replication and transcription machineries. Therefore, in *SSBP1* cells an increase in these collisions may ultimately be detrimental to genome stability and potentially result in mtDNA deletions and depletion. (Rudolph, Upton et al. 2013, Nicholls and Minczuk 2014).

Interestingly, a common breakpoint for mtDNA deletions occurs immediately downstream of the 3' end of the D-loop (Zeviani, Servidei et al. 1989). This has been explained by demonstrating that the triple stranded D-loop in fact promotes deletion formation by increasing accessibility for strand invasion (Berk and Clayton 1974). Therefore, a reduction in 7S DNA is predicted to decrease the likelihood of forming this specific mtDNA deletion, however regions downstream of this area would still be prone to deletions. Ultimately, the mechanisms linking these phenomena in our patients clearly warrant closer examination.

Given the importance of the 12S rRNA gene in mitochondrial translation we subsequently examined the effect of the variants on *de novo* and steady state levels of mitochondrial proteins. Fibroblasts from all patients carrying the m.1555A>G variant showed reduced intra-mitochondrial protein synthesis and steady state levels of complex IV subunits, MT-CO1 and MT-CO2, compared to controls. These results are in keeping with previous studies demonstrating the m.1555A>G variant causes mitochondrial translation dysfunction and reduces the rate of *de novo* protein synthesis (Guan, Fischel-Ghodsian et al. 1996, Santorelli, Mak et al. 1996, Guan, Fischel-Ghodsian et al. 2000). Similarly, a study using transmitochondrial cybrids harbouring the complementary 12S rRNA variant, m.1494C>T, also demonstrated a significant reduction in mitochondrial steady state protein levels (Yu, Zheng et al. 2014). Additionally, we found no difference in steady state levels of the nuclear encoded mitochondrial proteins, ATP5A and SDHA, or in the

mitochondrial gene *MT-CYB* mRNA expression, indicating this deficit was specific to mitochondrial translation.

Having identified evidence of OXPHOS dysfunction in the *SSBPI* muscle biopsy we further studied the effect of the variants on mitochondrial bioenergetics in primary fibroblasts. To this effect, OXPHOS function was determined by measurement of mitochondrial respiration, cell growth in forced OXPHOS conditions and cellular ROS levels. There was no significant compromise to OXPHOS as determined by Seahorse analysis, however consistent with three previous studies, fibroblasts carrying the m.1555A>G variant displayed a trend towards lower maximal respiration (Guan, Fischel-Ghodsian et al. 1996, Santorelli, Tanji et al. 1999, Meng, Cang et al. 2017). Further analysis of respiratory function could be performed using the Oxygraph-2k respirometer, a technology that has been shown to provide a higher resolution analysis of OXPHOS deficits (Horan, Pichaud et al. 2012).

In vivo cells primarily rely on OXPHOS to generate cellular ATP. In contrast, cells grown in glucose culture medium generate the majority of their ATP via glycolysis, a phenomenon known as the Crabtree effect (Mot, Liddell et al. 2016). To recapitulate *in vivo* conditions in cell culture, it is useful to adapt the cell culture environment such that cells are less glycolytic and are thus forced to rely on OXPHOS to generate cellular ATP (Marroquin, Hynes et al. 2007, Aguer, Gambarotta et al. 2011). This can be achieved by substituting glucose in the culture medium with galactose that is only slowly metabolised to pyruvate by glycolysis (Dott, Mistry et al. 2014). In agreement with previous work, under these conditions all patient cells carrying the m.1555A>G variant had significantly increased doubling times (Guan, Fischel-Ghodsian et al. 1996, Santorelli, Tanji et al. 1999). This finding likely reflects the reduction in maximal respiration, total protein synthesis and steady state levels of the respiratory chain subunits, MT-CO1 and MT-CO2 that is found in these cells.

Together, these findings reveal a primary defect in mitochondrial respiration mediated by m.1555A>G compromising mitochondrial translation that was no more severe in the presence of the *SSBPI* variant.

Mitochondrial generated ROS are a critical component of cellular homeostasis, but in excess ROS play an important role in the pathological mechanism underlying a number of diseases

including neurodegeneration, cancer and hearing loss (Uttara, Singh et al. 2009, Raimundo, Song et al. 2012, Kamogashira, Fujimoto et al. 2015). However, the role of mitochondrial dysfunction in the generation of excessive ROS remains controversial and importantly, there have been a number of mouse models with severe respiratory chain compromise with neither increased levels of cellular ROS nor evidence of oxidative mtDNA damage (Kujoth, Hiona et al. 2005, Trifunovic, Hansson et al. 2005, Murphy, Holmgren et al. 2011).

Given the suggestion by *Raimundo et al* that ROS may directly mediate m.1555A>G pathology, we wished to determine whether the *SSBP1* c.3G>A and m.1555A>G variants resulted in increased ROS levels and oxidative stress in primary fibroblasts (Raimundo, Song et al. 2012). Cellular ROS levels were therefore assessed by the H₂DCFDA assay, but no significant difference was detected between patient or control fibroblast cells. This result however must be considered in the context of the known limitations of the assay. Importantly, DCFH metabolism is complex, requiring peroxidation involving a transition metal catalyst (Zhu, Bannenberg et al. 1994). Additionally, artefactual redox cycling and the ability of DCFH to react with a broad range of one electron oxidizing species have been described as potential confounding factors (Wardman 2007, Kalyanaraman, Darley-Usmar et al. 2012).

Therefore, in line with the recommendations of *Murphy et al*, we attempted to circumvent the limitations of redox sensitive probes by corroborating our findings using orthogonal techniques (Murphy, Holmgren et al. 2011). We therefore set out to determine whether we could detect differences in the downstream effects of ROS between patients and controls. However, in this regard, we detected no difference between patients and controls in the predominant marker of free radical induced oxidative damage to cellular DNA, 8-OHdG. Similarly, no differences in protein carbonylation levels were detected as assessed by Oxyblot analysis. Importantly, it must be considered that the link between the accumulation of an oxidative stress biomarker, such as protein carbonylation, and excessive ROS is indirect (Grimsrud, Xie et al. 2008). For example, the induction of protein mistranslation in *Escherichia coli* by streptomycin treatment results in increased levels of protein carbonylation but without a change in cellular ROS caused by the increased tendency of misfolded proteins to undergo oxidative modification (Dukan, Farewell et al. 2000). Similarly, measurement of 8-OHdG may be confounded by chemical modifications which occur during the DNA extraction process (Halliwell 2000).

Unexpectedly, steady state levels of GPx1, a critical cellular antioxidant, were reduced in patient compared to control fibroblasts, although the significance of this finding is unclear. Further insight into cellular antioxidant metabolism could be gained by assaying glutathione peroxidase activity levels with measurement of the reduced glutathione (GSH) to oxidized glutathione (GSSG) ratio (Townsend, Tew et al. 2003). Together with qPCR of antioxidant genes these assays would provide a comprehensive analysis of the cellular antioxidant status (Sarkar, Mukherjee et al. 2017).

Notwithstanding the limitations of the assays performed in this study, together these findings suggest the c.3G>A *SSBPI* and m.1555A>G variants do not contribute to increased oxidative stress in the primary fibroblasts used in this study and ROS are unlikely to be a major contributory factor in causing disease in our patients. This contrasts with one previous study analysing ROS levels in m.1555A>G fibroblast cells. However, it is noteworthy that although the authors observed a significant difference between m.1555A>G carriers and controls, a closer analysis of their data reveals the difference does not meet their own definition of statistical significance (ROS levels in m.1555A>G carriers vs. controls p=0.053, p<0.05 defined as statistical significant) (Meng, Cang et al. 2017).

Given the evident impairment to the mitochondrial bioenergetic and protein synthesis capacity of the patient cells, we hypothesised that we may detect alteration in mitochondrial morphology either as a response to cellular stress or as a compensatory mechanism to maintain mitochondrial function. We observed that at steady state P1 fibroblasts had a noticeably more fragmented mitochondrial network, a significantly reduced mitochondrial average length and an increased number of mitochondrial fragments per cell compared to controls. On closer analysis, there was a significant increase in shorter mitochondrial fragments (fragment length ≤ 1 to 5 μm) with a reduction in larger fragments (fragment length 5 to >10 μm) in both P1, P2 and to a lesser degree P3, compared to controls.

Examination of the steady state levels of proteins regulating mitochondrial dynamics revealed a trend towards increased levels of OPA1 in P1 and P2 compared to P3 and controls. It is important to recognise that the expression of OPA1 is primarily regulated at the post-transcriptional level and the alternative splicing of *OPA1* mRNA gives rise to 8 distinct protein isoforms that are expressed in a tissue specific manner (Delettre, Griffoin

et al. 2001, Ishihara, Fujita et al. 2006). These isoforms fulfil divergent cellular processes with the short and long forms critical for mitochondrial fusion and fission respectively (Anand, Wai et al. 2014). However, the Western blot analysis performed in this study is unable to distinguish between OPA1 isoforms. This increase in OPA1 levels may therefore signify a compensatory response to the cellular stress caused by the m.1555A>G and *SSBP1* variants, although the definitive mechanism requires further clarification. Alternatively, the increased network fragmentation may be indicative of increased mitophagy, a primary process in mitochondrial quality control that facilitates the removal of dysfunctional mitochondria. Super-resolution structured illuminated microscopy to co-localise the autophagosome marker LC3 (microtubule associated protein 1A/1B light chain 3) protein with the mitochondrial marker TOMM20 could be used to further investigate this process (Wei, Chiang et al. 2017). Additionally, transmission electron microscopy may reveal the presence of mitochondria within autophagosomes and provide direct evidence of mitophagy (Ding and Yin 2012). Although there was no difference in the steady state levels of the pro-fission proteins, DRP1 and MFN2, measurement of post-translational modifications that are known to alter their cellular function and localisation may provide further insight into the molecular mechanism of the increased fragmentation observed in *SSBP1* cells (Harder, Zunino et al. 2004, Ko, Hyun et al. 2016). For example, SUMOylation and phosphorylation levels of DRP1 could be examined by Western blot analysis (Chang and Blackstone 2010, Prudent, Zunino et al. 2015)

The reasons for the increased fragmentation of the mitochondrial network in P1 compared to P2 is currently unclear but may be determined by yet uncharacterised cell specific factors. It is possible that exchanging the cell culture medium for galactose may increase network fragmentation, an effect seen in cells carrying OPA1 mutations, thereby enhancing the difference between *SSBP1* and control cells (Nasca, Rizza et al. 2017). It is an intriguing possibility that increasing cellular dysfunction in *SSBP1* fibroblasts compared to those carrying m.1555A>G alone or controls manifests as a shift of the mitochondrial fragment length distribution towards shorter fragments. Previous work has demonstrated an increase in mitochondrial network fusion in mouse C2C12 cells treated with RNAi to reduce *SSBP1* levels (Arakaki, Nishihama et al. 2006). This may represent the recognised process of ‘stress-induced mitochondrial hyperfusion’, a cellular response to various physiological stressors (Tondera, Grandemange et al. 2009). Alternatively, this may be a feature of an artificially acute reduction in *SSBP1* that does not resemble the

phenotype of our *SSBP1* cells that have chronically reduced SSBP1 levels. It is conceivable that the additional cellular dysfunction caused by the m.1555A>G variant exceeds the limit of compensation permitted by network fusion triggering network fragmentation, and possibly mitophagy as a means to remove dysfunctional mitochondria (Wai and Langer 2016). Consistent with this hypothesis, transmitochondrial cybrids carrying the 12S rRNA mutation m.1494C>T display mitochondrial network fragmentation triggering mitophagy when treated with gentamicin, essentially acting as an additional cellular stressor corresponding to the effect of the *SSBP1* variant. (Yu, Zheng et al. 2014).

Further investigation is required to determine the mechanisms underlying these observations. However, importantly, these results are consistent with previous studies demonstrating that mammalian cells with defects of the respiratory chain have fragmented mitochondria (Koopman, Visch et al. 2005, Sauvanet, Duvezin-Caubet et al. 2010). Additionally, yeast cells with deletions in critical OXPHOS genes display defects in fusion of the IMM, suggesting fragmentation of the mitochondrial network is a conserved effect of mitochondrial dysfunction (Sauvanet, Duvezin-Caubet et al. 2012). It has also been demonstrated that OXPHOS upregulates IMM fusion by enhancing the cleavage of OPA1 by YME1L1. Furthermore, ATP is known to be required for mitochondrial fusion (Meeusen, McCaffery et al. 2004, Mishra, Carelli et al. 2014). Therefore, the compromised OXPHOS function in our patient cells may link to the observed effect on mitochondrial morphology through a defect in cellular ATP production.

Mutations in the mitochondrial fusion genes *OPA1* and *MFN2* cause multi-system phenotypes characterised by the acquisition of multiple mtDNA deletions and depletion in post mitotic tissues (Yu-Wai-Man, Votruba et al. 2016). *OPA1* and *MFN2* patient derived cells also display mitochondrial fragmentation (Spinazzi, Cazzola et al. 2008). Together, these observations strongly suggest that mitochondrial dynamics are a key regulator of mtDNA maintenance (Yu-Wai-Man, Votruba et al. 2016). It is possible that clonal expansion of an mtDNA deletion results from increased mitochondrial fragmentation by impairing the effective complementation of deleted mtDNA species by wild type species. This process could thereby couple the mitochondrial network fragmentation to the presence of mtDNA deletions in our patients (Chen, Vermulst et al. 2010).

SSBP1 is a core component of mitochondrial nucleoids and additionally it has been proposed that the mitochondrial D-loop functions to segregate multiple copies of mtDNA into nucleoids via interaction with the AAA+ ATPase, ATAD3 (Holt, He et al. 2007). Therefore, we examined the mitochondrial nucleoids in patient and control cells using immunochemistry observing no gross morphological or quantitative deficit in *SSBP1* cells compared to m.1555A>G or controls. These results are in agreement with evidence that *SSBP1* RNAi knockdown in HeLa cells does not alter the organisation of mitochondrial nucleoids (Ruhanen, Borrie et al. 2010). Together, this evidence indicates that normal levels of SSBP1 and 7S DNA are not essential for the organisation of mitochondrial nucleoids in fibroblasts.

It has been suggested that the m.1555A>G variant results in the activation of the AMPK pathway by TFB1M mediated hypermethylation of m.1583 and m.1584 (m⁶2A). As such, it has been proposed to play an important role in m.1555A>G pathogenesis (Raimundo, Song et al. 2012). However, no significant difference in AMPK activity was found between patient and control fibroblasts by either Western blot or ELISA. Interestingly, Western blot analysis revealed that P1 had a trend towards increased AMPK activity, however this finding was not replicated by the ELISA methodology. It is possible that this discrepancy may reflect the reported higher sensitivity of Western blotting over ELISA (Porsch-Ozcurumez, Kischel et al. 2004, Beck, Leite et al. 2005). Recently, AMPK has been identified as a regulator of mitochondrial network fission in response to mitochondrial stress by phosphorylating the mitochondrial fission factor, MFF that acts a receptor for DRP1 (Toyama, Herzig et al. 2016). It is an interesting possibility that increased AMPK activity in P1 may drive mitochondrial network fragmentation. Analysis of MFF phosphorylation levels using phosphomotif antibodies recognising phosphorylated Ser172 MFF may provide some insight into these processes (Toyama, Herzig et al. 2016).

Nevertheless, it is important to consider our inability to demonstrate a significant increase in AMPK signalling in the context of two recent studies that have drawn the conclusion of *Raimundo et al* into question (Raimundo, Song et al. 2012). Firstly, *O'Sullivan et al* demonstrated primary lymphocytes and fibroblasts from m.1555A>G carriers and controls display equivalent levels of m⁶2A indicating hypermethylation is not a physiological process (O'Sullivan, Rutland et al. 2015). Secondly, *Lee et al* generated a mouse overexpressing TFB1M on a C57BL/6N background to attempt to recapitulate the findings

of *Raimundo et al*, that TFB1M was overexpressed on a C57BL/6J background caused cochlear cell death and hearing impairment. The mouse of *Lee et al* displayed fully methylated m⁶2A that could not be further methylated *in vivo*. The mouse had hearing comparable with wild type controls, leading the authors to conclude that m⁶2A hypermethylation may in fact be an artefact of experimental conditions employed by the previous authors (Lee, Rose et al. 2015). Furthermore, the model posited by *Raimundo et al* is unable to comprehensively account for the variable penetrance seen in the Finnish family given that in isolation m.1555A>G is clearly not pathological in these individuals. Together this evidence suggests that, in contrast to other fibroblast models of mitochondrial disease, AMPK is not a major contributor to the cellular phenotype in our patient fibroblasts (Wu and Wei 2012, Distelmaier, Valsecchi et al. 2015).

We next evaluated the mTOR pathway, a master regulator of cellular protein synthesis, in our primary fibroblasts by analysing the activity of S6 Kinase. This revealed a trend towards increased S6K phosphorylation suggesting increased activity of mTOR in the patient cells. AMPK is known to inhibit Rheb, the primary activator of mTOR, and therefore this further suggests that AMPK is not hyperactivated in our patient derived primary fibroblasts (Distelmaier, Valsecchi et al. 2015).

Mitochondrial translation dysfunction has been demonstrated to trigger an integrated stress response culminating in the phosphorylation of eukaryotic translation initiation factor 2A (eIF2 α) and a reduction in cytosolic protein translation (Pakos-Zebrucka, Koryga et al. 2016). It is plausible that the increased activity of S6K may represent a compensatory nuclear response to dysfunctional mitochondrial protein synthesis seen in our patient cells. Consistent with these observations, mouse models of mitochondrial disease such as Leigh syndrome and focal-segmental-glomerulosclerosis-like-renal disease have shown increased mTOR signalling (Johnson, Tsai et al. 2000, Peng, Ostrovsky et al. 2015). However, mechanistic insight into the interaction between mitochondrial and cytosolic translation is only recently emerging (Couvillion, Soto et al. 2016, Munch and Harper 2016, D'Amico, Sorrentino et al. 2017).

There was no evidence of ER stress observed in patient fibroblasts by Western blot analysis of the ER chaperone BiP, indicating that in basal conditions the *SSBPI* and m.1555A>G variants do not result in ER stress in primary fibroblast cell lines. Similarly, there was no observable difference in mitochondrial chaperone HSP60 or cytosolic HSP70

suggesting no evidence of elevated mitochondrial or proteostatic stress in patient fibroblast cells. Consistent with these results, the mitochondrial aspartyl-tRNA synthetase (DARS2) knockout mouse also displays compromised protein synthesis, however proteostatic stress signalling is only triggered in cardiomyocytes. Together these findings further highlight tissue specificity as an important feature of mitochondrial disease (discussed further in **Chapter 6**) (Dogan, Pujol et al. 2014).

There was also no significant compromise to the upregulation of HSP60 and HSP70 with heat shock in *SSBP1* fibroblasts as predicted by the work of *Tan et al* (Tan, Fujimoto et al. 2015). This may indicate functional redundancy in the SSBP1 signalling pathway in our fibroblast model or that sufficient SSBP1 is present in the cell to mediate the effect. It is important to consider, however, that due to high levels of endogenous expression of HSP60, it is difficult to detect small changes in protein levels and therefore it may not be a suitable marker of the mitochondrial UPR in cell culture (Seiferling 2015).

In summary, the data presented in this chapter is consistent with an additive effect of the *SSBP1* and m.1555A>G variants, manifesting as tissue specific phenotype primarily caused by a combined effect on mtDNA maintenance and mtDNA translation.

Chapter 6

Concluding discussion

This chapter provides an overview of the primary findings of this thesis in conjunction with a critical evaluation of the strengths and limitations of the principal research strategies. The salient investigations required to extend the implications of these results are also presented.

Man is by nature a social animal, and by restricting interpersonal communication, hearing loss can lead to profound isolation affecting both mental and physical health. Sensorineural hearing loss is a well-recognised feature of mitochondrial disease, and as such a more complete understanding of the underlying cellular and molecular mechanisms has the potential to deliver significant benefits to patients. The work presented in this thesis aimed to address this need. Specifically, this study set out to identify and characterise nuclear genetic variants accounting for the variable penetrance of hearing loss associated with the m.1555A>G variant in the 12S rRNA gene, *MT-RNR1*.

In **Chapter 3** we determined the importance of the m.1555A>G variant as a cause of hearing loss in the UK population by surveying the 5 laboratories in the UK providing either specific genetic testing for m.1555A>G or whole mitochondrial genome sequencing incorporating the *MT-RNR1* gene. We found the variant was not present at a higher frequency than in the background population in a cohort of patients with hearing loss. We therefore concluded that the variant is not a significant cause of hearing loss in the UK population. This finding provided further evidence that in isolation the m.1555A>G variant is not pathogenic.

Aminoglycosides are an important risk factor for hearing loss in m.1555A>G carriers, however, the identification of families segregating the variant that contain hearing-impaired individuals that have not been exposed to aminoglycosides strongly suggested that other genetic factors are required to cause hearing loss. This evidence, together with the findings of our survey, motivated the design of an exome sequencing approach, presented in **Chapter 4**, to isolate nuclear genetic modifiers in familial and sporadic

carriers of the m.1555A>G variant. We addressed the hypothesis that a nuclear variant accounted for the variable penetrance of hearing loss associated with m.1555A>G by performing exome sequencing in selected Finnish familial (n=5) and Spanish sporadic cases (n=4). This strategy identified the heterozygous variant c.3G>A in the *SSBPI* gene, resulting in a start-loss mutation of *SSBPI*, a core component of the mtDNA replisome machinery. The variant was then established to co-segregate with m.1555A>G and hearing loss in a large multi-generational Finnish family.

Our study is the first reported use of WES technology in carriers of m.1555A>G and in isolating the *SSBPI* variant in the Finnish family we provide a demonstration that WES coupled with segregation analysis is a powerful tool for dissecting the cause of mitochondrial disease. Prior to this work, no pathogenic mutations in *SSBPI* had been associated with human mitochondrial disease.

We were unable to identify a cause of hearing loss in any of the Spanish sporadic cases. It remains a possibility that WGS could be used to successfully delineate causative genes in these ‘unsolved’ individuals. When evaluating our experimental strategy, it should be considered that exome sequencing offers definite advantages over WGS: it is significantly less expensive, more easily understood for functional interpretation, faster to analyse, and an easy dataset to manage. However, aside from the additional ability to interrogate non-coding regions of the genome, WGS permits reliable detection of CNVs and improved detection of ‘off target’ mtDNA reads and would thereby maximize the chance of defining a genomic cause for disease in these individuals (Girirajan, Brkanac et al. 2011).

Although a potentially attractive strategy in these individuals, realising the benefits of WGS in discovering novel genetic causes of disease crucially depends on the concurrent development of improved bioinformatic tools to reduce potential false negative and false positive variant calls. This must also be allied with improvements in the prediction and functional annotation of potentially deleterious variants. Nevertheless, it is expected that in the coming years, as costs continue to fall, this technology will come to predominate in both research and clinical settings (Mardis 2017).

The use of WGS in these ‘unsolved’ m.1555A>G carriers would be particularly apposite given the recent discovery that the non-coding part of the genome performs vital functions in controlling gene expression (Gerstein, Kundaje et al. 2012). Expression quantitative trait

loci (eQTLs) are non-coding genetic elements that directly contribute to variation in expression of mRNAs (Nica and Dermitzakis 2013). Thus, the analysis of *SSBP1* expression levels in patient derived fibroblasts or blood, for example by qPCR, coupled with knowledge of genotypic variation ascertained by WGS may identify an eQTL that alters the expression of *SSBP1*. This would constitute an additional mechanism for the nuclear genetic modification of m.1555A>G in these individuals.

The functional data presented in **Chapter 5** provides compelling evidence of an additive effect of the c.3G>A *SSBP1* and m.1555A>G variants, manifesting as a tissue specific phenotype through a combined effect on mtDNA maintenance and mitochondrial translation. The *SSBP1* variant reduced SSBP1 protein levels and decreased 7S DNA in fibroblasts, and was associated with multiple deletions of mtDNA and mtDNA depletion in skeletal muscle. Analysis of the mitochondrial copy number repopulation kinetics after a period of enforced depopulation by treatment with EtBr, revealed *SSBP1* fibroblasts repopulated at double the rate of 1555A>G and control cells. Fibroblasts from these patients also showed reduced mtDNA encoded protein synthesis in keeping with the co-existing m.1555A>G variant, leading to reduced proliferation rates under conditions of forced mitochondrial respiration (Robinson, Petrova-Benedict et al. 1992, Guan, Fischel-Ghodsian et al. 1996). Additionally, *SSBP1* cells displayed a more fragmented mitochondrial network. Whether this alteration in mitochondrial network dynamics represents an epiphenomenon or a primary pathological process, for example, by allowing clonal expansion of deleted mtDNA species, remains to be determined (Gorman, Pfeffer et al. 2015).

The *SSBP1* variant is unlikely to be pathogenic in isolation given that individuals carrying the variant in conjunction with wild type m.1555A have normal hearing (Family D and Family E). This is paralleled by the heterozygous knockout mouse *Ssbp1*^{tm1a(KOMP)Wtsi} that displays hearing levels no different to wild-type littermates (Brown and Moore 2012). This evidence suggests that the *SSBP1* variant likely has a sub-threshold effect that is exacerbated by m.1555A>G resulting in the cellular phenotype. However, definitive demonstration of this would require the functional analysis of cells derived from individuals in Family D and E.

It is of vital importance to determine the mechanistic link between the *SSBP1* and m.1555A>G variants and tissue specific mtDNA deletions and depletion. Our

investigations have highlighted the potential role of 7S DNA in the dysfunctional replication of mtDNA, with the reduced abundance of steady state 7S DNA potentially altering the mtDNA copy number repopulation kinetics. However, further experimental evidence is required to fully define this interaction. It also remains imperative to confirm the changes seen in fibroblasts and skeletal muscle are paralleled with disease processes in the cochleae of affected individuals.

Our research employed *in vitro* cellular models consisting of patient derived skin fibroblasts and myoblasts in addition to the analysis of skeletal muscle biopsies to define the cellular effects of the variants. These tissue types are readily obtainable by outpatient-based procedures that can be undertaken by any suitably trained healthcare professional after appropriate informed consent. Fibroblast cells are robust in culture and easily propagated providing a reliable *in vitro* system to determine disease specific biochemical parameters. However, as a result of the generally slow growth of primary fibroblasts a prolonged period in culture is required to generate sufficient biomaterial for genetic and biochemical assays. This can potentially increase the risk of confounding factors including bacterial contamination and cellular senescence (Hayflick 1965). In this study we attempted to control for these factors by undertaking regular quality control and using fibroblasts at similar passage number when performing experiments. To overcome the limitations of primary fibroblasts we also immortalised these cells. The resulting cells have far shorter doubling times and moreover the effect of cellular aging is negligible (Sprenger, Kuttner et al. 2010). Nevertheless, one must be mindful that these cells have been subjected to a transforming virus and hence display a disparate gene expression and epigenetic profile compared to their primary fibroblast ancestors (Oh, Jin et al. 2007). It must also be considered that the use of a fibroblast cell model cannot control for the nuclear background of the individual cell lines, which has the potential to confound results. To overcome this, transmitochondrial cybrids could be used to study the *SSBPI* and m.1555A>G variants on an otherwise constant nuclear background.

This work therefore highlights some of the inherent difficulties of the use of *in vitro* cellular models in the study of mitochondrial disease. Although these models potentially offer valuable insights into disease mechanisms, their reductive simplicity may permit the over interpretation of results (Fearon, Gaca et al. 2013). Taking this into account, we must be careful when attempting to translate the physiological effects observed in a fibroblast

model to those that exist in the complex tissues such as the cochlea that consists of highly specialized inter-dependent cell types within a unique ionic microenvironment.

With these limitations aside, fibroblasts carrying the c.3G>A *SSBP1* and m.1555A>G variants demonstrated physiological dysfunction consistent with the known biological functions of the *SSBP1* and *MT-RNR1* genes and hence, particularly when taken in the context of the result in skeletal muscle, provide a useful biological model to define molecular mechanisms in these individuals.

Although we have demonstrated significant pathology in our cellular models, a fundamental question still remains – *why do the carriers of the c.3G>A SSBP1/m.1555A>G variants solely present with hearing loss?* The findings presented in **Chapter 5** clearly demonstrate pathological processes that are only apparent in a restricted subset of tissues, a common feature of mitochondrial disease. This phenomenon of tissue specificity is one of, if not the most pertinent unresolved issue in mitochondrial biology (Vafai and Mootha 2012). In addressing this question, it must be considered that although hearing loss was the foremost presenting feature in the *SSBP1* and m.1555A>G variant carriers, our results indicate that these patients may also have a subclinical myopathy typified by the presence of mtDNA deletions and depletion. Hearing thresholds are easily quantifiable by audiological assessment, however diagnosis of other features of mitochondrial disease such as muscle weakness and fatigue may be harder to define, contributing to under-diagnosis and poorer clinical management (Filler, Lyon et al. 2014).

‘Deep phenotyping’, defined as the precise and comprehensive analysis of phenotypic abnormalities, is emerging as an essential partner to modern genomic technologies in advancing the understanding of the pathological mechanisms of disease (Robinson 2012). Our results highlight the importance of fully phenotyping all patients with suspected mitochondrial disease, with a low threshold for requesting specialist testing, for example cardiac MRI and metabolic profiling. These investigations will collectively inform prognosis and could potentially define suitable biomarkers of this mitochondrial disease (Partington, Givertz et al. 2011, Lehtonen, Forsstrom et al. 2016).

To date, there has been limited progress in defining the cellular mechanisms of tissue specificity. For heteroplasmic mutations it has been suggested that inter-tissue heterogeneity in heteroplasmy levels may contribute to differential tissue specific disease burdens.

Although this cannot account for the hearing loss associated with m.1555A>G, that is assumed to be homoplasmic in all tissues (Li, Schroder et al. 2015). Recent work has implicated modulation of one-carbon metabolism as an important process in mitochondrial disease. Specifically, tissue-restricted dysfunction in serine metabolism leads to cystathionine synthesis and activation of mitochondrial stress signalling leading to mtDNA deletions (Bao, Ong et al. 2016, Nikkanen, Forsstrom et al. 2016). Whether this or other metabolic dysfunctions are relevant processes to disease in our patients would require the study of cochlea or neuronal cells. However, these cells, although representing the affected tissue type in our patients, are prohibitively difficult to acquire from living individuals.

To circumvent this, in collaboration with Professor Ludovic Vallier, (Cambridge Stem Cell Institute, Cambridge, UK), we are currently generating induced pluripotent stem cell (iPSC) lines from the two fibroblast cell lines carrying the c.3G>A *SSBPI* and m.1555A>G variants (P1, P2) and from a fibroblast cell line carrying m.1555A>G alone (P3). The ability to generate iPSCs that can subsequently be differentiated down an otic lineage has the potential to be an effective technique in clarifying disease relevant processes. There has been limited success in developing cochlear hair cells from iPSCs (Oshima, Shin et al. 2010), however, recent work has focussed on the use of three-dimensional culture systems to develop inner ear organoids from human pluripotent stem cells that contain nascent hair cells (Koehler, Nie et al. 2017). Alternatively, the development of auditory neurones from human iPSCs may provide a more tractable model to interrogate cell specific pathology (Gunewardene, Crombie et al. 2016). Using this approach, it would be interesting to determine whether cochlear cells or auditory neurones derived from *SSBPI* iPSCs demonstrated the same, or perhaps enhanced dysregulation of mtDNA maintenance and translation detected in our current cellular models.

There is particular hope that this may prove a fruitful strategy given seminal work from the laboratory of Anu Suomalainen (University of Helsinki, Finland). These researchers generated iPSCs carrying the heteroplasmic m.3243A>G MELAS mutation on an isogenic nuclear background with similar mtDNA levels (Hamalainen, Manninen et al. 2013). Neuronal cells and an array of tissue types derived from iPSC induced teratomas displayed distinct abnormalities in respiratory capacity indicating the importance of tissue specific factors in modifying phenotypes in mitochondrial disease.

More broadly, the generation of patient derived cochlear cells has the potential to define the mechanism underpinning the selective vulnerability of cochlear cells to mitochondrial dysfunction. Heart, skeletal muscle and the cochlea are the most affected tissues in patients with mitochondrial disease (Gorman, Chinnery et al. 2016). Hence, it would be fascinating to verify whether, as proposed, cochlear cells accumulate high levels of mtDNA mutations and deletions due to their post mitotic state and low cellular turn over (Fernandez and Hinojosa 1974, Pickrell and Youle 2013). Moreover, comparative transcriptomic and proteomic signatures of cochlear cells derived from patient and control iPSCs may offer novel insight into disease relevant signalling pathways.

Albeit with a number of practical and ethical concerns, the use of an *in vivo* model is another potentially advantageous strategy to broaden the understanding of pathological molecular mechanisms in our patients. Due to their physiological and genetic similarity to humans, mice provide a reliable model of mitochondrial disease (Dunn, Cannon et al. 2012). There presently exist a number of mouse models of nuclear encoded OXPHOS subunit and mitochondrial maintenance genetic diseases (Torraco, Peralta et al. 2015). However, while these models of nuclear mitochondrial disease have led to important insights into mitochondrial biology, the difficulty of manipulating a multi-copy mtDNA genome enclosed within the bilayer mitochondrial membrane has meant there has been far less progress in designing models of mtDNA mutations (Wallace 1999, Khan, Smigrodzki et al. 2007).

Current technology does not permit the creation of a mouse carrying the m.1555A>G variant. In the absence of this specific model, it would be possible to create a mouse carrying a deleterious variant in a nuclear gene encoding a mitochondrial translation protein together with the *SSBPI* variant. Determination of hearing thresholds in this mouse would delineate whether a translation specific effect of the m.1555A>G variant causes hearing loss or whether an ancillary function of 12S rRNA may also be relevant to the disease process. The recent identification of MOTS-c, a mitochondrial derived peptide regulating cellular metabolism that is encoded by a short opening reading frame (sORF) within the *MT-RNR1* gene, makes this a particular interesting hypothesis to explore (Lee, Zeng et al. 2015). The work of *Tan et al* has highlighted additional functions of *SSBPI*, therefore, the phenotype of a mouse carrying combined mutations in nuclear genes encoding mitochondrial translation and mtDNA replication proteins would reveal whether

the abrogation of a non-replication function of *SSBPI* might play a contributory role to the disease process in our patients (Tan, Fujimoto et al. 2015).

Animal models with spontaneous mtDNA mutations can also provide useful insights into the mechanisms of mitochondrial disease (Li, Cuddon et al. 2006). The m.1555A>G variant is known to be the wild type allele in Old World Monkeys and therefore knocking out *SSBPI* or reproducing the human mutation in these animals, for example using CRISPR/Cas9 technology, may provide an interesting *in vivo* model to gain further mechanistic insights into the pathology in the Finnish family (Pacheu-Grau, Gomez-Duran et al. 2011).

Previous studies have indicated genes encoding mitochondrial translation proteins as candidate genetic modifiers of m.1555A>G (Bykhovskaya, Mengesha et al. 2004, Guan, Yan et al. 2006). Our work provides the first evidence of a gene encoding a mitochondrial replication protein as a potential modifier of m.1555A>G. Together, these findings suggest that nuclear genetic variants that modulate the phenotype of m.1555A>G may be found in genes involved in different aspects of mitochondrial biology and in some instances the variants may be private to individual families. Only by improving our understanding of the complex genetic architecture resulting in hearing loss in our patients can we begin to give comprehensive genetic counselling to carriers and their families.

Although we have made concerted efforts to find additional carriers of pathogenic *SSBPI* mutations we have so far been unsuccessful. This is reflected in the small number of patient samples used in the functional analyses presented in **Chapter 5**. The identification of further families carrying deleterious variants in *SSBPI* and m.1555A>G is important, as the identification of these unrelated carriers would be considered the highest level of proof of pathogenicity (MacArthur, Manolio et al. 2014).

Given the *SSBPI* variant is only pathogenic when segregating with m.1555A>G, finding individuals carrying these two rare alleles poses a major obstacle in conclusively validating the pathogenicity of the *SSBPI* variant. The collation of large numbers of genetically and phenotypically characterised patients for example in the NIHR Bioresource may permit the screening of large numbers of patients to seek out carriers of the m.1555A>G variant. Hearing impaired carriers could then be examined for variants in mitochondrial replication genes, that may imply a conserved mechanism underlies the

phenotype in other m.1555A>G carriers and further validate the pathogenicity of the *SSBP1* variant (McClellan and King 2010).

There are no drug-based therapies for sensorineural hearing loss in clinical use and in the majority of cases, the treatment options for patients with mitochondrial associated hearing loss are limited to lifestyle modification and auditory amplification by hearing aids used with or without hearing assistive technology systems. In cases of severe hearing loss cochlear implantation may be indicated and has been used effectively in patients with m.3243A>G, OPA1 related auditory neuropathy, KSS and MNGIE syndrome (Yamaguchi, Himi et al. 1997, Li, Han et al. 2011, Scarpelli, Zappini et al. 2012, Santarelli, Rossi et al. 2015). In the majority of cases cochlear implantation is a safe, well-tolerated procedure delivering substantial improvements in patient quality of life (Klop, Briaire et al. 2007, Mosnier, Bebear et al. 2015). However, cochlear implantation carries with it the associated risks of anaesthesia, as well as the potential for serious complications including damage to the facial nerve and in specific circumstances the possibility of CSF leaks resulting in meningitis (Terry, Kelt et al. 2015, Saeed, Powell et al. 2016). Additionally, cochlear implantation is not appropriate for a proportion of patients with auditory neuropathy (Ji, Li et al. 2015). This procedure has nevertheless proved to be an extraordinarily successful treatment for over 300,000 patients worldwide (Macherey and Carlyon 2014). The primary motivation of the work presented in this thesis was to further the understanding of disease mechanisms in mitochondrial hearing loss to facilitate the design of effective treatments for hearing restoration. However, it must be recognised that the efficacy of any future biological or genetic therapies must exceed that of cochlear implants to make them a viable alternative.

In summary, the results presented in this thesis provide novel and original insights into the mechanisms of mitochondrial hearing loss by the identification and characterisation of a nuclear modifier of the m.1555A>G variant. Using *in vitro* cellular models, this study provides further evidence that trans-acting modifiers contribute to a complex interplay between nucleus and mitochondria. It is hoped that this work will contribute to a fuller understanding of pathological genetic mechanisms in mitochondrial disease. In time, these advances will inform genetic counselling, improve prognostication and lead to the design of more effective therapies for patients suffering from mitochondrial associated hearing loss.

Chapter 7

Summary of Conclusions

7.1 Conclusions

- Our survey of the 5 laboratories in the UK testing the m.1555A>G variant determined it was not a significant cause of hearing loss. This provided further evidence that in isolation the m.1555A>G variant is not pathogenic. This suggested nuclear modifiers may act in concert with the variant to account for the variable hearing phenotype.
- Exome sequencing was employed for the first time in carriers of the m.1555A>G variant. This defined the primary novel finding of the thesis: the identification of the c.3G>A *SSBPI* variant. This is the first pathogenic mutation discovered in this gene, and this work reveals it acts as a nuclear modifier of m.1555A>G and accounts for the variable hearing phenotype in this Finnish family.
- Together these variants act to dysregulate both mtDNA translation and mtDNA maintenance resulting in a tissue specific disease. These findings extend our understanding of mitochondrial-nuclear interactions in human disease.

7.2 Limitations

- The *SSBPI* variant was only found in one family and hence the ultimate proof of pathogenicity would require finding pathological variants in this gene in other m.1555A>G carriers.
- This research employed *in vitro* cellular models consisting of patient fibroblasts, myoblasts and skeletal muscle. Although these tissues display physiological

dysfunction corresponding to the biological role of the m.1555A>G and *SSBP1* variants whether these findings can account for the cochlear dysfunction of our patients has yet to be determined.

7.3 Future work

- Access to larger cohorts of m.1555A>G carriers through large genetically and phenotypically characterised patient databases may enable a powerful approach to finding novel nuclear modifiers.
- Undertaking WGS in additional carriers of m.1555A>G would maximize the chance of defining a genetic cause for hearing loss in these individuals.
- The generation of patient specific iPSCs that could be differentiated down an otic lineage has the potential to be a highly informative technique to further delineate tissue specific mechanisms of mitochondrial disease.

Appendices

Appendix 1 Analysis of mitochondrial network

Table A1.1. Distribution of mitochondrial fragment length in P1

P1 (Relative frequency)				
Mitochondrial length (μm)	Mean	SD	N (cells)	p-value (vs. control)
≤ 1	0.07	0.08	26	<0.0001
1 to 2	0.40	0.16	26	<0.0001
2 to 5	0.41	0.16	26	0.0017
5 to 10	0.10	0.07	26	<0.0001
>10	0.30	0.03	26	0.0055

Table A1.2. Distribution of mitochondrial fragment length in P2

P2 (Relative frequency)				
Mitochondrial length (μm)	Mean	SD	N (cells)	p-value (vs. control)
≤ 1	0.04	0.03	16	0.0006
1 to 2	0.41	0.07	16	<0.0001
2 to 5	0.36	0.06	16	<0.0001
5 to 10	0.13	0.05	16	0.0055
>10	0.06	0.04	16	>0.99

Table A1.3. Distribution of mitochondrial fragment length in P3

P3 (Relative frequency)				
Mitochondrial length (μm)	Mean	SD	N (cells)	p-value (vs. control)
≤ 1	0.01	0.014	18	>0.99
1 to 2	0.35	0.111	18	0.0039
2 to 5	0.46	0.08	18	0.0994
5 to 10	0.12	0.04	18	0.0006
>10	0.08	0.04	18	0.1339

Table A1.4. Distribution of mitochondrial fragment length in controls

Controls (Relative frequency)			
Mitochondrial length (μm)	Mean	SD	N (cells)
≤ 1	0.01	0.03	63
1 to 2	0.23	0.16	63
2 to 5	0.51	0.12	63
5 to 10	0.19	0.08	63
>10	0.06	0.05	63

Appendix 2 Mitochondrial repopulation assay

Table A2.1. Repopulation levels from optimisation experiment. N.D = not determined

	P1	P2	C1	C2
Time (days)	Repopulation level (mtDNA copy number treated:untreated) \pm SD			
0	1	1	1	1
3	0.562 \pm 0.031	0.313 \pm 0.017	0.364 \pm 0.03	N.D
6	0.175 \pm 0.007	0.078 \pm 0.003	0.143 \pm 0.003	0.251 \pm 0.017
15	0.063 \pm 0.004	0.031 \pm 0.002	0.069 \pm 0.008	N.D
23	0.026 \pm 0.001	0.074 \pm 0.002	0.042 \pm 0.004	0.031 \pm 0.004
29	0.338 \pm 0.052	0.215 \pm 0.012	0.215 \pm 0.011	0.199 \pm 0.005
36	0.481 \pm 0.021	0.204 \pm 0.028	0.119 \pm 0.06	0.086 \pm 0.053

Table A2.2. Repopulation levels from modified protocol experiment 1

	P1	P2	P3	C1	C2
Time (days)	Repopulation level (mtDNA copy number treated:untreated)				
0	1	1	1	1	1
4	0.589	0.452	0.872	0.857	0.549
6	0.330	0.192	0.419	0.217	0.529
8	0.897	0.568	1.021	0.396	0.387
10	1.135	1.714	1.383	0.752	0.800

Table A2.3. Repopulation levels from modified protocol experiment 2

	P1	P2	P3	C1	C2
Time (days)	Repopulation level (mtDNA copy number treated:untreated)				
0	1	1	1	1	1
4	0.864	0.725	0.921	1.175	0.686
6	0.493	0.4	0.575	0.418	0.546
8	1.1567	1.034	1.065	0.729	0.494
10	1.567	1.391	1.111	1.089	0.863

Table A2.4. Repopulation levels from modified protocol experiment 3

	P1	P2	P3	C1	C2
Time (days)	Repopulation level (mtDNA copy number treated:untreated)				
0	1	1	1	1	1
4	0.725	0.232	n.r	0.975	0.466
6	0.128	0.128	0.740	0.457	0.248
8	1.251	0.975	1.236	0.606	0.621
10	1.902	1.233	1.472	1.549	0.932

Table A2.5. Mean repopulation of the 3 modified protocol experiments

	P1	P2	P3	C1	C2
Time	Mean repopulation level (mtDNA copy number treated:untreated) \pm SD				
0	1	1	1	1	1
4	0.721 \pm 0.142	0.469 \pm 0.248	0.897 \pm 0.034	0.565 \pm 0.111	1.001 \pm 0.160
6	0.314 \pm 0.186	0.237 \pm 0.145	0.578 \pm 0.161	0.438 \pm 0.167	0.365 \pm 0.129
8	1.101 \pm 0.182	0.861 \pm 0.254	1.106 \pm 0.113	0.501 \pm 0.117	0.577 \pm 0.168
10	1.534 \pm 0.384	1.445 \pm 0.245	1.294 \pm 0.180	0.864 \pm 0.067	1.127 \pm 0.400

Table A2.6. Repopulation rates calculated from the 3 modified protocol experiments

	Repopulation rates				
	P1	P2	P3	C1	C2
Expt 1	0.890	0.555	0.365	0.267	0.136
Expt 2	0.537	0.495	0.268	0.336	0.159
Expt 3	0.402	0.761	0.440	0.540	0.345
Mean \pm SD	0.610 \pm 0.25	0.6037 \pm 0.14	0.3577 \pm 0.09	0.381 \pm 0.14	0.213 \pm 0.11

Appendix 3 Heat shock response assay

Table A3.1. Western blot analysis of BiP basal levels (GAPDH loading control)

Fibroblast cell line	BiP (basal)	SD	Repeats (n=)
P1	0.4729	0.1317	3
P2	0.3429	0.1679	3
P3	0.3321	0.2034	3
Controls	0.3621	0.108	3

Table A3.2. Western blot analysis of HSP60 basal levels (GAPDH loading control)

Fibroblast cell line	HSP60 (basal)	SD	Repeats (n=)
P1	1.214	0.5011	3
P2	1.07	0.1831	3
P3	0.8252	0.1762	3
Controls	0.8542	0.1419	3

Table A3.3. Western blot analysis of HSP70 basal levels (GAPDH loading control)

Fibroblast cell line	HSP70 (basal)	SD	Repeats (n=)
P1	0.2955	0.06518	2
P2	0.3014	0.03491	2
P3	0.1839	0.1422	2
Controls	0.2262	0.2088	2

Table A3.4. Western blot analysis of BiP basal and post heat shock levels (GAPDH loading control)

Fibroblast cell line	BiP (basal)	SD	BiP (Heat)	SD	Repeats (n=)
P1	2.295	1.163	3.309	1.372	2
P2	1.161	0.3316	2.369	0.1001	2
P3	0.8168	0.07647	2.888	0.9276	2
Controls	1.24	0.2221	2.654	0.3574	2

Table A3.5. Western blot analysis of HSP60 basal and post heat shock levels (GAPDH loading control)

Fibroblast cell line	HSP60 (basal)	SD	HSP60 (Heat)	SD	Repeats (n=)
P1	1.041	0.241	1.285	0.7791	2
P2	1.105	0.3453	1.215	0.4428	2
P3	0.9817	0.02442	1.194	0.08633	2
Controls	1.068	0.375	1.113	0.168	2

Table A3.6. Western blot analysis of HSP70 basal and post heat shock levels (GAPDH loading control)

Fibroblast cell line	HSP70 (basal)	SD	HSP70 (Heat)	SD	Repeats (n=)
P1	0.2955	0.06518	1.799	1.045	2
P2	0.3014	0.03491	1.145	0.3546	2
P3	0.1839	0.1422	2.063	0.09938	2
Controls	0.2262	0.2088	1.724	1.198	2

References

- Abe, S., P. M. Kelley, W. J. Kimberling and S. I. Usami (2001). "Connexin 26 gene (GJB2) mutation modulates the severity of hearing loss associated with the 1555A->G mitochondrial mutation." Am J Med Genet **103**(4): 334-338.
- Action on Hearing Loss (2017). "Action on Hearing Loss,."
- Adzhubei, I., D. M. Jordan and S. R. Sunyaev (2013). "Predicting functional effect of human missense mutations using PolyPhen-2." Curr Protoc Hum Genet **Chapter 7**: Unit7 20.
- Adzhubei, I. A., S. Schmidt, L. Peshkin, V. E. Ramensky, A. Gerasimova, P. Bork, A. S. Kondrashov and S. R. Sunyaev (2010). "A method and server for predicting damaging missense mutations." Nat Methods **7**(4): 248-249.
- Agaronyan, K., Y. I. Morozov, M. Anikin and D. Temiakov (2015). "Mitochondrial biology. Replication-transcription switch in human mitochondria." Science **347**(6221): 548-551.
- Aguer, C., D. Gambarotta, R. J. Mailloux, C. Moffat, R. Dent, R. McPherson and M. E. Harper (2011). "Galactose enhances oxidative metabolism and reveals mitochondrial dysfunction in human primary muscle cells." PLoS One **6**(12): e28536.
- Al-Malky, G., R. Suri, T. Sirimanna and S. J. Dawson (2014). "Normal hearing in a child with the m.1555A>G mutation despite repeated exposure to aminoglycosides. Has the penetrance of this pharmacogenetic interaction been overestimated?" Int J Pediatr Otorhinolaryngol **78**(6): 969-973.
- Allen, J. F. (2015). "Why chloroplasts and mitochondria retain their own genomes and genetic systems: Colocation for redox regulation of gene expression." Proc Natl Acad Sci U S A **112**(33): 10231-10238.
- Alston, C. L., J. Lowe, D. M. Turnbull, P. Maddison and R. W. Taylor (2010). "A novel mitochondrial tRNAGlu (MTTE) gene mutation causing chronic progressive

- external ophthalmoplegia at low levels of heteroplasmy in muscle." J Neurol Sci **298**(1-2): 140-144.
- Amunts, A., A. Brown, J. Toots, S. H. Scheres and V. Ramakrishnan (2015). "Ribosome. The structure of the human mitochondrial ribosome." Science **348**(6230): 95-98.
- Anand, R., T. Wai, M. J. Baker, N. Kladt, A. C. Schauss, E. Rugarli and T. Langer (2014). "The i-AAA protease YME1L and OMA1 cleave OPA1 to balance mitochondrial fusion and fission." J Cell Biol **204**(6): 919-929.
- Anderson, S., A. T. Bankier, B. G. Barrell, M. H. de Bruijn, A. R. Coulson, J. Drouin, I. C. Eperon, D. P. Nierlich, B. A. Roe, F. Sanger, P. H. Schreier, A. J. Smith, R. Staden and I. G. Young (1981). "Sequence and organization of the human mitochondrial genome." Nature **290**(5806): 457-465.
- Andersson, S. G., A. Zomorodipour, J. O. Andersson, T. Sicheritz-Ponten, U. C. Alsmark, R. M. Podowski, A. K. Naslund, A. S. Eriksson, H. H. Winkler and C. G. Kurland (1998). "The genome sequence of *Rickettsia prowazekii* and the origin of mitochondria." Nature **396**(6707): 133-140.
- Andrews, R. M., I. Kubacka, P. F. Chinnery, R. N. Lightowlers, D. M. Turnbull and N. Howell (1999). "Reanalysis and revision of the Cambridge reference sequence for human mitochondrial DNA." Nat Genet **23**(2): 147.
- Antes, A., I. Tappin, S. Chung, R. Lim, B. Lu, A. M. Parrott, H. Z. Hill, C. K. Suzuki and C. G. Lee (2010). "Differential regulation of full-length genome and a single-stranded 7S DNA along the cell cycle in human mitochondria." Nucleic Acids Res **38**(19): 6466-6476.
- Antonicka, H., S. C. Leary, G. H. Guercin, J. N. Agar, R. Horvath, N. G. Kennaway, C. O. Harding, M. Jaksch and E. A. Shoubridge (2003). "Mutations in COX10 result in a defect in mitochondrial heme A biosynthesis and account for multiple, early-onset clinical phenotypes associated with isolated COX deficiency." Hum Mol Genet **12**(20): 2693-2702.
- Antonicka, H. and E. A. Shoubridge (2015). "Mitochondrial RNA Granules Are Centers for Posttranscriptional RNA Processing and Ribosome Biogenesis." Cell Rep.

- Arakaki, N., T. Nishihama, A. Kohda, H. Owaki, Y. Kuramoto, R. Abe, T. Kita, M. Suenaga, T. Himeda, M. Kuwajima, H. Shibata and T. Higuti (2006). "Regulation of mitochondrial morphology and cell survival by Mitogenin I and mitochondrial single-stranded DNA binding protein." Biochim Biophys Acta **1760**(9): 1364-1372.
- Archer, S. L. (2013). "Mitochondrial dynamics--mitochondrial fission and fusion in human diseases." N Engl J Med **369**(23): 2236-2251.
- Ariano, R. E., S. A. Zelenitsky and D. A. Kassum (2008). "Aminoglycoside-induced vestibular injury: maintaining a sense of balance." Ann Pharmacother **42**(9): 1282-1289.
- Arnadottir, J. and M. Chalfie (2010). "Eukaryotic mechanosensitive channels." Annu Rev Biophys **39**: 111-137.
- Arthur, J. W., F. S. Cheung and J. K. Reichardt (2015). "Single nucleotide differences (SNDs) continue to contaminate the dbSNP database with consequences for human genomics and health." Hum Mutat **36**(2): 196-199.
- Ashmore, J., P. Avan, W. E. Brownell, P. Dallos, K. Dierkes, R. Fettiplace, K. Grosh, C. M. Hackney, A. J. Hudspeth, F. Julicher, B. Lindner, P. Martin, J. Meaud, C. Petit, J. Santos-Sacchi and B. Canlon (2010). "The remarkable cochlear amplifier." Hear Res **266**(1-2): 1-17.
- Avent, M. L., B. A. Rogers, A. C. Cheng and D. L. Paterson (2011). "Current use of aminoglycosides: indications, pharmacokinetics and monitoring for toxicity." Intern Med J **41**(6): 441-449.
- Avruch, J., X. Long, Y. Lin, S. Ortiz-Vega, J. Rapley, A. Papageorgiou, N. Oshiro and U. Kikkawa (2009). "Activation of mTORC1 in two steps: Rheb-GTP activation of catalytic function and increased binding of substrates to raptor." Biochem Soc Trans **37**(Pt 1): 223-226.
- Bademci, G., J. Foster Ii, N. Mahdieh, M. Bonyadi, D. Duman, F. B. Cengiz, I. Menendez, O. Diaz-Horta, A. Shirkavand, S. Zeinali, A. Subasioglu, S. Tokgoz-Yilmaz, F. Huesca-Hernandez, M. de la Luz Arenas-Sordo, J. Dominguez-Aburto, E.

- Hernandez-Zamora, P. Montenegro, R. Paredes, G. Moreta, R. Vinueza, F. Villegas, S. Mendoza-Benitez, S. Guo, N. Bozan, T. Tos, A. Incesulu, G. Sennaroglu, S. H. Blanton, H. Ozturkmen-Akay, M. Yildirim-Baylan and M. Tekin (2016). "Comprehensive analysis via exome sequencing uncovers genetic etiology in autosomal recessive nonsyndromic deafness in a large multiethnic cohort." Genet Med **18**(4): 364-371.
- Bae, J. W., D. B. Kim, J. Y. Choi, H. J. Park, J. D. Lee, D. G. Hur, S. H. Bae, D. J. Jung, S. H. Lee, U. K. Kim and K. Y. Lee (2012). "Molecular and clinical characterization of the variable phenotype in Korean families with hearing loss associated with the mitochondrial A1555G mutation." PLoS One **7**(8): e42463.
- Bae, J. W., K. Y. Lee, S. Y. Choi, S. H. Lee, H. J. Park and U. K. Kim (2008). "Molecular analysis of mitochondrial gene mutations in Korean patients with nonsyndromic hearing loss." Int J Mol Med **22**(2): 175-180.
- Bai, U., M. D. Seidman, R. Hinojosa and W. S. Quirk (1997). "Mitochondrial DNA deletions associated with aging and possibly presbycusis: a human archival temporal bone study." Am J Otol **18**(4): 449-453.
- Bailey, L. J., T. J. Cluett, A. Reyes, T. A. Prolla, J. Poulton, C. Leeuwenburgh and I. J. Holt (2009). "Mice expressing an error-prone DNA polymerase in mitochondria display elevated replication pausing and chromosomal breakage at fragile sites of mitochondrial DNA." Nucleic Acids Res **37**(7): 2327-2335.
- Ballana, E., J. M. Mercader, N. Fischel-Ghodsian and X. Estivill (2007). "MRPS18CP2 alleles and DEFA3 absence as putative chromosome 8p23.1 modifiers of hearing loss due to mtDNA mutation A1555G in the 12S rRNA gene." BMC Med Genet **8**: 81.
- Bamshad, M. J., S. B. Ng, A. W. Bigham, H. K. Tabor, M. J. Emond, D. A. Nickerson and J. Shendure (2011). "Exome sequencing as a tool for Mendelian disease gene discovery." Nat Rev Genet **12**(11): 745-755.
- Bandelt, H. J., A. Kloss-Brandstatter, M. B. Richards, Y. G. Yao and I. Logan (2014). "The case for the continuing use of the revised Cambridge Reference Sequence

- (rCRS) and the standardization of notation in human mitochondrial DNA studies." J Hum Genet **59**(2): 66-77.
- Bannwarth, S., S. Ait-El-Mkadem, A. Chaussenot, E. C. Genin, S. Lacas-Gervais, K. Fragaki, L. Berg-Alonso, Y. Kageyama, V. Serre, D. G. Moore, A. Verschueren, C. Rouzier, I. Le Ber, G. Auge, C. Cochaud, F. Lespinasse, K. N'Guyen, A. de Septenville, A. Brice, P. Yu-Wai-Man, H. Sesaki, J. Pouget and V. Paquis-Flucklinger (2014). "A mitochondrial origin for frontotemporal dementia and amyotrophic lateral sclerosis through CHCHD10 involvement." Brain **137**(Pt 8): 2329-2345.
- Bao, X. R., S. E. Ong, O. Goldberger, J. Peng, R. Sharma, D. A. Thompson, S. B. Vafai, A. G. Cox, E. Marutani, F. Ichinose, W. Goessling, A. Regev, S. A. Carr, C. B. Clish and V. K. Mootha (2016). "Mitochondrial dysfunction remodels one-carbon metabolism in human cells." Elife **5**.
- Bar-Yaacov, D., I. Frumkin, Y. Yashiro, T. Chujo, Y. Ishigami, Y. Chemla, A. Blumberg, O. Schlesinger, P. Bieri, B. Greber, N. Ban, R. Zarivach, L. Alfonta, Y. Pilpel, T. Suzuki and D. Mishmar (2016). "Mitochondrial 16S rRNA Is Methylated by tRNA Methyltransferase TRMT61B in All Vertebrates." PLoS Biol **14**(9): e1002557.
- Barlow, D. P. and M. S. Bartolomei (2014). "Genomic imprinting in mammals." Cold Spring Harb Perspect Biol **6**(2).
- Bayrhuber, M., T. Meins, M. Habeck, S. Becker, K. Giller, S. Villinger, C. Vonrhein, C. Griesinger, M. Zweckstetter and K. Zeth (2008). "Structure of the human voltage-dependent anion channel." Proc Natl Acad Sci U S A **105**(40): 15370-15375.
- Beck, S. T., O. M. Leite, R. S. Arruda and A. W. Ferreira (2005). "Combined use of Western blot/ELISA to improve the serological diagnosis of human tuberculosis." Braz J Infect Dis **9**(1): 35-43.
- Bender, A., K. J. Krishnan, C. M. Morris, G. A. Taylor, A. K. Reeve, R. H. Perry, E. Jaros, J. S. Hersheson, J. Betts, T. Klopstock, R. W. Taylor and D. M. Turnbull (2006). "High levels of mitochondrial DNA deletions in substantia nigra neurons in aging and Parkinson disease." Nat Genet **38**(5): 515-517.

- Benit, P., D. Chretien, N. Kadhom, P. de Lonlay-Debeney, V. Cormier-Daire, A. Cabral, S. Peudenier, P. Rustin, A. Munnich and A. Rotig (2001). "Large-scale deletion and point mutations of the nuclear NDUFV1 and NDUFS1 genes in mitochondrial complex I deficiency." Am J Hum Genet **68**(6): 1344-1352.
- Benit, P., A. Slama, F. Cartault, I. Giurgea, D. Chretien, S. Lebon, C. Marsac, A. Munnich, A. Rotig and P. Rustin (2004). "Mutant NDUFS3 subunit of mitochondrial complex I causes Leigh syndrome." J Med Genet **41**(1): 14-17.
- Berk, A. J. and D. A. Clayton (1974). "Mechanism of mitochondrial DNA replication in mouse L-cells: asynchronous replication of strands, segregation of circular daughter molecules, aspects of topology and turnover of an initiation sequence." J Mol Biol **86**(4): 801-824.
- Berlin, C. I., L. Hood, T. Morlet, K. Rose and S. Brashears (2003). "Auditory neuropathy/dys-synchrony: diagnosis and management." Ment Retard Dev Disabil Res Rev **9**(4): 225-231.
- Birsoy, K., T. Wang, W. W. Chen, E. Freinkman, M. Abu-Remaileh and D. M. Sabatini (2015). "An Essential Role of the Mitochondrial Electron Transport Chain in Cell Proliferation Is to Enable Aspartate Synthesis." Cell **162**(3): 540-551.
- Bitner-Glindzicz, M., M. Pembrey, A. Duncan, J. Heron, S. M. Ring, A. Hall and S. Rahman (2009). "Prevalence of mitochondrial 1555A-->G mutation in European children." N Engl J Med **360**(6): 640-642.
- Bjorkholm, P., A. M. Ernst, E. Hagstrom and S. G. Andersson (2017). "Why mitochondria need a genome revisited." FEBS Lett **591**(1): 65-75.
- Blakely, E. L., A. Butterworth, R. D. Hadden, I. Bodi, L. He, R. McFarland and R. W. Taylor (2012). "MPV17 mutation causes neuropathy and leukoencephalopathy with multiple mtDNA deletions in muscle." Neuromuscul Disord **22**(7): 587-591.
- Bleier, L. and S. Drose (2013). "Superoxide generation by complex III: from mechanistic rationales to functional consequences." Biochim Biophys Acta **1827**(11-12): 1320-1331.

- Bogenhagen, D. and D. A. Clayton (1977). "Mouse L cell mitochondrial DNA molecules are selected randomly for replication throughout the cell cycle." Cell **11**(4): 719-727.
- Bogenhagen, D. F. (2012). "Mitochondrial DNA nucleoid structure." Biochim Biophys Acta **1819**(9-10): 914-920.
- Bogenhagen, D. F., D. Rousseau and S. Burke (2008). "The layered structure of human mitochondrial DNA nucleoids." J Biol Chem **283**(6): 3665-3675.
- Bohr, V. A. (2002). "Repair of oxidative DNA damage in nuclear and mitochondrial DNA, and some changes with aging in mammalian cells." Free Radic Biol Med **32**(9): 804-812.
- Bonneux, S., E. Fransen, E. Van Eyken, L. Van Laer, J. Huyghe, P. Van de Heyning, A. Voets, M. Gerards, A. P. Stassen, A. T. Hendrickx, H. J. Smeets and G. Van Camp (2011). "Inherited mitochondrial variants are not a major cause of age-related hearing impairment in the European population." Mitochondrion **11**(5): 729-734.
- Bottger, E. C. (2010). "Mutant A1555G mitochondrial 12S rRNA and aminoglycoside susceptibility." Antimicrob Agents Chemother **54**(7): 3073-3074; author reply 3074-3075.
- Bourdon, A., L. Minai, V. Serre, J. P. Jais, E. Sarzi, S. Aubert, D. Chretien, P. de Lonlay, V. Paquis-Flucklinger, H. Arakawa, Y. Nakamura, A. Munnich and A. Rotig (2007). "Mutation of RRM2B, encoding p53-controlled ribonucleotide reductase (p53R2), causes severe mitochondrial DNA depletion." Nat Genet **39**(6): 776-780.
- Bourgeron, T., P. Rustin, D. Chretien, M. Birch-Machin, M. Bourgeois, E. Viegas-Pequignot, A. Munnich and A. Rotig (1995). "Mutation of a nuclear succinate dehydrogenase gene results in mitochondrial respiratory chain deficiency." Nat Genet **11**(2): 144-149.
- Bradford, M. M. (1976). "A rapid and sensitive method for the quantitation of microgram quantities of protein utilizing the principle of protein-dye binding." Anal Biochem **72**: 248-254.

- Brandon, M. C., E. Ruiz-Pesini, D. Mishmar, V. Procaccio, M. T. Lott, K. C. Nguyen, S. Spolim, U. Patil, P. Baldi and D. C. Wallace (2009). "MITOMASTER: a bioinformatics tool for the analysis of mitochondrial DNA sequences." Hum Mutat **30**(1): 1-6.
- Bravo, R., V. Parra, D. Gatica, A. E. Rodriguez, N. Torrealba, F. Paredes, Z. V. Wang, A. Zorzano, J. A. Hill, E. Jaimovich, A. F. Quest and S. Lavandero (2013). "Endoplasmic reticulum and the unfolded protein response: dynamics and metabolic integration." Int Rev Cell Mol Biol **301**: 215-290.
- Brierley, E. J., M. A. Johnson, R. N. Lightowers, O. F. James and D. M. Turnbull (1998). "Role of mitochondrial DNA mutations in human aging: implications for the central nervous system and muscle." Ann Neurol **43**(2): 217-223.
- Brown, S. D., R. E. Hardisty-Hughes and P. Mburu (2008). "Quiet as a mouse: dissecting the molecular and genetic basis of hearing." Nat Rev Genet **9**(4): 277-290.
- Brown, S. D. and M. W. Moore (2012). "The International Mouse Phenotyping Consortium: past and future perspectives on mouse phenotyping." Mamm Genome **23**(9-10): 632-640.
- Brown, T. A., A. N. Tkachuk, G. Shtengel, B. G. Kopek, D. F. Bogenhagen, H. F. Hess and D. A. Clayton (2011). "Superresolution fluorescence imaging of mitochondrial nucleoids reveals their spatial range, limits, and membrane interaction." Mol Cell Biol **31**(24): 4994-5010.
- Brown, W. M., J. Shine and H. M. Goodman (1978). "Human mitochondrial DNA: analysis of 7S DNA from the origin of replication." Proc Natl Acad Sci U S A **75**(2): 735-739.
- Brzezniak, L. K., M. Bijata, R. J. Szczesny and P. P. Stepień (2011). "Involvement of human ELAC2 gene product in 3' end processing of mitochondrial tRNAs." RNA Biol **8**(4): 616-626.
- Bu, X., M. Shohat, L. Jaber and J. I. Rotter (1993). "A form of sensorineural deafness is determined by a mitochondrial and an autosomal locus: evidence from pedigree segregation analysis." Genet Epidemiol **10**(1): 3-15.

- Burte, F., V. Carelli, P. F. Chinnery and P. Yu-Wai-Man (2015). "Disturbed mitochondrial dynamics and neurodegenerative disorders." Nat Rev Neurol **11**(1): 11-24.
- Bykhovskaya, Y., X. Estivill, K. Taylor, T. Hang, M. Hamon, R. A. Casano, H. Yang, J. I. Rotter, M. Shohat and N. Fischel-Ghodsian (2000). "Candidate locus for a nuclear modifier gene for maternally inherited deafness." Am J Hum Genet **66**(6): 1905-1910.
- Bykhovskaya, Y., E. Mengesha, D. Wang, H. Yang, X. Estivill, M. Shohat and N. Fischel-Ghodsian (2004). "Human mitochondrial transcription factor B1 as a modifier gene for hearing loss associated with the mitochondrial A1555G mutation." Mol Genet Metab **82**(1): 27-32.
- Bykhovskaya, Y., E. Mengesha, D. Wang, H. Yang, X. Estivill, M. Shohat and N. Fischel-Ghodsian (2004). "Phenotype of non-syndromic deafness associated with the mitochondrial A1555G mutation is modulated by mitochondrial RNA modifying enzymes MTO1 and GTPBP3." Mol Genet Metab **83**(3): 199-206.
- Bykhovskaya, Y., M. Shohat, K. Ehrenman, D. Johnson, M. Hamon, R. M. Cantor, B. Aouizerat, X. Bu, J. I. Rotter, L. Jaber and N. Fischel-Ghodsian (1998). "Evidence for complex nuclear inheritance in a pedigree with nonsyndromic deafness due to a homoplasmic mitochondrial mutation." Am J Med Genet **77**(5): 421-426.
- Cai, Z. and L. J. Yan (2013). "Protein Oxidative Modifications: Beneficial Roles in Disease and Health." J Biochem Pharmacol Res **1**(1): 15-26.
- Calvo, S. E., K. R. Clauser and V. K. Mootha (2016). "MitoCarta2.0: an updated inventory of mammalian mitochondrial proteins." Nucleic Acids Res **44**(D1): D1251-1257.
- Campbell, G., K. J. Krishnan, M. Deschauer, R. W. Taylor and D. M. Turnbull (2014). "Dissecting the mechanisms underlying the accumulation of mitochondrial DNA deletions in human skeletal muscle." Hum Mol Genet **23**(17): 4612-4620.
- Carelli, V., P. d'Adamo, M. L. Valentino, C. La Morgia, F. N. Ross-Cisneros, L. Caporali, A. Maresca, P. Loguercio Polosa, P. Barboni, A. De Negri, F. Sadun, R. Karanjia, S. R. Salomao, A. Berezovsky, F. Chicani, M. Moraes, M. Moraes Filho, R. Belfort, Jr. and A. A. Sadun (2016). "Parsing the differences in affected with

- LHON: genetic versus environmental triggers of disease conversion." Brain **139**(Pt 3): e17.
- Ceranic, B. and L. M. Luxon (2004). "Progressive auditory neuropathy in patients with Leber's hereditary optic neuropathy." J Neurol Neurosurg Psychiatry **75**(4): 626-630.
- Cerritelli, S. M., E. G. Frolova, C. Feng, A. Grinberg, P. E. Love and R. J. Crouch (2003). "Failure to produce mitochondrial DNA results in embryonic lethality in Rnaseh1 null mice." Mol Cell **11**(3): 807-815.
- Chaliotis, A., P. Vlastaridis, D. Mossialos, M. Ibba, H. D. Becker, C. Stathopoulos and G. D. Amoutzias (2016). "The complex evolutionary history of aminoacyl-tRNA synthetases." Nucleic Acids Res.
- Chan, S. S. and W. C. Copeland (2009). "DNA polymerase gamma and mitochondrial disease: understanding the consequence of POLG mutations." Biochim Biophys Acta **1787**(5): 312-319.
- Chang, C. R. and C. Blackstone (2010). "Dynamic regulation of mitochondrial fission through modification of the dynamin-related protein Drp1." Ann N Y Acad Sci **1201**: 34-39.
- Chen, B., M. Retzlaff, T. Roos and J. Frydman (2011). "Cellular strategies of protein quality control." Cold Spring Harb Perspect Biol **3**(8): a004374.
- Chen, H., M. Vermulst, Y. E. Wang, A. Chomyn, T. A. Prolla, J. M. McCaffery and D. C. Chan (2010). "Mitochondrial fusion is required for mtDNA stability in skeletal muscle and tolerance of mtDNA mutations." Cell **141**(2): 280-289.
- Chen, J. C., T. C. Tsai, C. S. Liu and C. T. Lu (2007). "Acute hearing loss in a patient with mitochondrial myopathy, encephalopathy, lactic acidosis and stroke-like episodes (MELAS)." Acta Neurol Taiwan **16**(3): 168-172.
- Chen, X., R. Prosser, S. Simonetti, J. Sadlock, G. Jagiello and E. A. Schon (1995). "Rearranged mitochondrial genomes are present in human oocytes." Am J Hum Genet **57**(2): 239-247.

- Chen, Y. C., T. Liu, C. H. Yu, T. Y. Chiang and C. C. Hwang (2013). "Effects of GC bias in next-generation-sequencing data on de novo genome assembly." PLoS One **8**(4): e62856.
- Cheng, J., Y. Zhu, S. He, Y. Lu, J. Chen, B. Han, M. Petrillo, K. O. Wrzeszczynski, S. Yang, P. Dai, S. Zhai, D. Han, M. Q. Zhang, W. Li, X. Liu, H. Li, Z. Y. Chen and H. Yuan (2011). "Functional mutation of SMAC/DIABLO, encoding a mitochondrial proapoptotic protein, causes human progressive hearing loss DFNA64." Am J Hum Genet **89**(1): 56-66.
- Cherukuri, P. F., V. Maduro, K. V. Fuentes-Fajardo, K. Lam, N. C. S. Program, D. R. Adams, C. J. Tiffit, J. C. Mullikin, W. A. Gahl and C. F. Boerkoel (2015). "Replicate exome-sequencing in a multiple-generation family: improved interpretation of next-generation sequencing data." BMC Genomics **16**: 998.
- Chilamakuri, C. S., S. Lorenz, M. A. Madoui, D. Vodak, J. Sun, E. Hovig, O. Myklebost and L. A. Meza-Zepeda (2014). "Performance comparison of four exome capture systems for deep sequencing." BMC Genomics **15**: 449.
- Chinnery, P. F., C. Elliott, G. R. Green, A. Rees, A. Coulthard, D. M. Turnbull and T. D. Griffiths (2000). "The spectrum of hearing loss due to mitochondrial DNA defects." Brain **123** (Pt 1): 82-92.
- Chinnery, P. F. and G. Hudson (2013). "Mitochondrial genetics." Br Med Bull **106**: 135-159.
- Chinnery, P. F., P. J. Zwijnenburg, M. Walker, N. Howell, R. W. Taylor, R. N. Lightowlers, L. Bindoff and D. M. Turnbull (1999). "Nonrandom tissue distribution of mutant mtDNA." Am J Med Genet **85**(5): 498-501.
- Choi, H. C., P. Song, Z. Xie, Y. Wu, J. Xu, M. Zhang, Y. Dong, S. Wang, K. Lau and M. H. Zou (2008). "Reactive nitrogen species is required for the activation of the AMP-activated protein kinase by statin in vivo." J Biol Chem **283**(29): 20186-20197.

- Christian, B. E. and L. L. Spremulli (2009). "Evidence for an active role of IF3mt in the initiation of translation in mammalian mitochondria." Biochemistry **48**(15): 3269-3278.
- Christian, B. E. and L. L. Spremulli (2012). "Mechanism of protein biosynthesis in mammalian mitochondria." Biochim Biophys Acta **1819**(9-10): 1035-1054.
- Chun, S. and J. C. Fay (2009). "Identification of deleterious mutations within three human genomes." Genome Res **19**(9): 1553-1561.
- Claros, M. G., J. Perea, Y. Shu, F. A. Samatey, J. L. Popot and C. Jacq (1995). "Limitations to in vivo import of hydrophobic proteins into yeast mitochondria. The case of a cytoplasmically synthesized apocytochrome b." Eur J Biochem **228**(3): 762-771.
- Clay Montier, L. L., J. J. Deng and Y. Bai (2009). "Number matters: control of mammalian mitochondrial DNA copy number." J Genet Genomics **36**(3): 125-131.
- Clayton, D. A. (1982). "Replication of animal mitochondrial DNA." Cell **28**(4): 693-705.
- Connor, T. M., S. Hoer, A. Mallett, D. P. Gale, A. Gomez-Duran, V. Posse, R. Antrobus, P. Moreno, M. Sciacovelli, C. Frezza, J. Duff, N. S. Sheerin, J. A. Sayer, M. Ashcroft, M. S. Wiesener, G. Hudson, C. M. Gustafsson, P. F. Chinnery and P. H. Maxwell (2017). "Mutations in mitochondrial DNA causing tubulointerstitial kidney disease." PLoS Genet **13**(3): e1006620.
- Cotney, J., S. E. McKay and G. S. Shadel (2009). "Elucidation of separate, but collaborative functions of the rRNA methyltransferase-related human mitochondrial transcription factors B1 and B2 in mitochondrial biogenesis reveals new insight into maternally inherited deafness." Hum Mol Genet **18**(14): 2670-2682.
- Cotney, J. and G. S. Shadel (2006). "Evidence for an early gene duplication event in the evolution of the mitochondrial transcription factor B family and maintenance of rRNA methyltransferase activity in human mtTFB1 and mtTFB2." J Mol Evol **63**(5): 707-717.

- Couvillion, M. T., I. C. Soto, G. Shipkovenska and L. S. Churchman (2016). "Synchronized mitochondrial and cytosolic translation programs." Nature **533**(7604): 499-503.
- Crawley, B. K. and E. M. Keithley (2011). "Effects of mitochondrial mutations on hearing and cochlear pathology with age." Hear Res **280**(1-2): 201-208.
- D'Amico, D., V. Sorrentino and J. Auwerx (2017). "Cytosolic Proteostasis Networks of the Mitochondrial Stress Response." Trends Biochem Sci.
- D'Erchia, A. M., A. Atlante, G. Gadaleta, G. Pavesi, M. Chiara, C. De Virgilio, C. Manzari, F. Mastropasqua, G. M. Prazzoli, E. Picardi, C. Gissi, D. Horner, A. Reyes, E. Sbisà, A. Tullo and G. Pesole (2015). "Tissue-specific mtDNA abundance from exome data and its correlation with mitochondrial transcription, mass and respiratory activity." Mitochondrion **20**: 13-21.
- Dai, P., Y. Yuan, D. Huang, Y. Qian, X. Liu, D. Han, H. Yuan, X. Wang, W. Y. Young and M. X. Guan (2006). "Extremely low penetrance of deafness associated with the mitochondrial 12S rRNA T1095C mutation in three Chinese families." Biochem Biophys Res Commun **348**(1): 200-205.
- Dallos, P., M. C. Billone, J. D. Durrant, C. Wang and S. Raynor (1972). "Cochlear inner and outer hair cells: functional differences." Science **177**(4046): 356-358.
- del Castillo, F. J., M. Rodriguez-Ballesteros, Y. Martin, B. Arellano, J. Gallo-Teran, C. Morales-Angulo, R. Ramirez-Camacho, M. Cruz Tapia, J. Solanellas, A. Martinez-Conde, M. Villamar, M. A. Moreno-Pelayo, F. Moreno and I. del Castillo (2003). "Heteroplasmy for the 1555A>G mutation in the mitochondrial 12S rRNA gene in six Spanish families with non-syndromic hearing loss." J Med Genet **40**(8): 632-636.
- Delettre, C., J. M. Griffoin, J. Kaplan, H. Dollfus, B. Lorenz, L. Faivre, G. Lenaers, P. Belenguer and C. P. Hamel (2001). "Mutation spectrum and splicing variants in the OPA1 gene." Hum Genet **109**(6): 584-591.
- DePristo, M. A., E. Banks, R. Poplin, K. V. Garimella, J. R. Maguire, C. Hartl, A. A. Philippakis, G. del Angel, M. A. Rivas, M. Hanna, A. McKenna, T. J. Fennell, A.

- M. Kernytsky, A. Y. Sivachenko, K. Cibulskis, S. B. Gabriel, D. Altshuler and M. J. Daly (2011). "A framework for variation discovery and genotyping using next-generation DNA sequencing data." Nat Genet **43**(5): 491-498.
- Di Re, M., H. Sembongi, J. He, A. Reyes, T. Yasukawa, P. Martinsson, L. J. Bailey, S. Goffart, J. D. Boyd-Kirkup, T. S. Wong, A. R. Fersht, J. N. Spelbrink and I. J. Holt (2009). "The accessory subunit of mitochondrial DNA polymerase gamma determines the DNA content of mitochondrial nucleoids in human cultured cells." Nucleic Acids Res **37**(17): 5701-5713.
- Ding, W. X. and X. M. Yin (2012). "Mitophagy: mechanisms, pathophysiological roles, and analysis." Biol Chem **393**(7): 547-564.
- Distelmaier, F., F. Valsecchi, D. C. Liemburg-Apers, M. Lebieczinska, R. J. Rodenburg, S. Heil, J. Keijer, J. Fransen, H. Imamura, K. Danhauser, A. Seibt, B. Viollet, F. N. Gellerich, J. A. Smeitink, M. R. Wieckowski, P. H. Willems and W. J. Koopman (2015). "Mitochondrial dysfunction in primary human fibroblasts triggers an adaptive cell survival program that requires AMPK-alpha." Biochim Biophys Acta **1852**(3): 529-540.
- Doda, J. N., C. T. Wright and D. A. Clayton (1981). "Elongation of displacement-loop strands in human and mouse mitochondrial DNA is arrested near specific template sequences." Proc Natl Acad Sci U S A **78**(10): 6116-6120.
- Dogan, S. A., C. Pujol, P. Maiti, A. Kukat, S. Wang, S. Hermans, K. Senft, R. Wibom, E. I. Rugarli and A. Trifunovic (2014). "Tissue-specific loss of DARS2 activates stress responses independently of respiratory chain deficiency in the heart." Cell Metab **19**(3): 458-469.
- Dott, W., P. Mistry, J. Wright, K. Cain and K. E. Herbert (2014). "Modulation of mitochondrial bioenergetics in a skeletal muscle cell line model of mitochondrial toxicity." Redox Biol **2**: 224-233.
- Dror, A. A. and K. B. Avraham (2009). "Hearing loss: mechanisms revealed by genetics and cell biology." Annu Rev Genet **43**: 411-437.

- Dukan, S., A. Farewell, M. Ballesteros, F. Taddei, M. Radman and T. Nystrom (2000). "Protein oxidation in response to increased transcriptional or translational errors." Proc Natl Acad Sci U S A **97**(11): 5746-5749.
- Dunn, D. A., M. V. Cannon, M. H. Irwin and C. A. Pinkert (2012). "Animal models of human mitochondrial DNA mutations." Biochim Biophys Acta **1820**(5): 601-607.
- Edmonds, J. L., D. J. Kirse, D. Kearns, R. Deutsch, L. Spruijt and R. K. Naviaux (2002). "The otolaryngological manifestations of mitochondrial disease and the risk of neurodegeneration with infection." Arch Otolaryngol Head Neck Surg **128**(4): 355-362.
- Edvardson, S., C. Jalas, A. Shaag, S. Zenvirt, C. Landau, I. Lerer and O. Elpeleg (2011). "A deleterious mutation in the LOXHD1 gene causes autosomal recessive hearing loss in Ashkenazi Jews." Am J Med Genet A **155A**(5): 1170-1172.
- Ekstrand, M. I., M. Falkenberg, A. Rantanen, C. B. Park, M. Gaspari, K. Hultenby, P. Rustin, C. M. Gustafsson and N. G. Larsson (2004). "Mitochondrial transcription factor A regulates mtDNA copy number in mammals." Hum Mol Genet **13**(9): 935-944.
- Elliott, H. R., D. C. Samuels, J. A. Eden, C. L. Relton and P. F. Chinnery (2008). "Pathogenic mitochondrial DNA mutations are common in the general population." Am J Hum Genet **83**(2): 254-260.
- Elpeleg, O. (2003). "Inherited mitochondrial DNA depletion." Pediatr Res **54**(2): 153-159.
- Elson, J. L., D. C. Samuels, D. M. Turnbull and P. F. Chinnery (2001). "Random intracellular drift explains the clonal expansion of mitochondrial DNA mutations with age." Am J Hum Genet **68**(3): 802-806.
- Emelyanov, V. V. (2001). "Evolutionary relationship of Rickettsiae and mitochondria." FEBS Lett **501**(1): 11-18.
- Emperador, S., D. Pacheu-Grau, M. P. Bayona-Bafaluy, N. Garrido-Perez, A. Martin-Navarro, M. J. Lopez-Perez, J. Montoya and E. Ruiz-Pesini (2014). "An MRPS12

mutation modifies aminoglycoside sensitivity caused by 12S rRNA mutations." Front Genet **5**: 469.

Estivill, X., N. Govea, E. Barcelo, C. Badenas, E. Romero, L. Moral, R. Scozzri, L. D'Urbano, M. Zeviani and A. Torroni (1998). "Familial progressive sensorineural deafness is mainly due to the mtDNA A1555G mutation and is enhanced by treatment of aminoglycosides." Am J Hum Genet **62**(1): 27-35.

Falkenberg, M., M. Gaspari, A. Rantanen, A. Trifunovic, N. G. Larsson and C. M. Gustafsson (2002). "Mitochondrial transcription factors B1 and B2 activate transcription of human mtDNA." Nat Genet **31**(3): 289-294.

Falkenberg, M., N. G. Larsson and C. M. Gustafsson (2007). "DNA replication and transcription in mammalian mitochondria." Annu Rev Biochem **76**: 679-699.

Farr, C. L., Y. Matsushima, A. T. Lagina, 3rd, N. Luo and L. S. Kaguni (2004). "Physiological and biochemical defects in functional interactions of mitochondrial DNA polymerase and DNA-binding mutants of single-stranded DNA-binding protein." J Biol Chem **279**(17): 17047-17053.

Farwell, K. D., L. Shahmirzadi, D. El-Khechen, Z. Powis, E. C. Chao, B. Tippin Davis, R. M. Baxter, W. Zeng, C. Mroske, M. C. Parra, S. K. Gandomi, I. Lu, X. Li, H. Lu, H. M. Lu, D. Salvador, D. Ruble, M. Lao, S. Fischbach, J. Wen, S. Lee, A. Elliott, C. L. Dunlop and S. Tang (2015). "Enhanced utility of family-centered diagnostic exome sequencing with inheritance model-based analysis: results from 500 unselected families with undiagnosed genetic conditions." Genet Med **17**(7): 578-586.

Faul, F., E. Erdfelder, A. Buchner and A. G. Lang (2009). "Statistical power analyses using G*Power 3.1: tests for correlation and regression analyses." Behav Res Methods **41**(4): 1149-1160.

Fearon, I. M., M. D. Gaca and B. K. Nordskog (2013). "In vitro models for assessing the potential cardiovascular disease risk associated with cigarette smoking." Toxicol In Vitro **27**(1): 513-522.

- Fernandez, C. and R. Hinojosa (1974). "Postnatal development of endocochlear potential and stria vascularis in the cat." Acta Otolaryngol **78**(3-4): 173-186.
- Fernandez-Martinez, M., E. Miro, A. Ortega, G. Bou, J. J. Gonzalez-Lopez, A. Oliver, A. Pascual, E. Cercenado, J. Oteo, L. Martinez-Martinez, F. Navarro and D. Spanish Network for the Research in Infectious (2015). "Molecular identification of aminoglycoside-modifying enzymes in clinical isolates of Escherichia coli resistant to amoxicillin/clavulanic acid isolated in Spain." Int J Antimicrob Agents **46**(2): 157-163.
- Fernandez-Vizarra, E., M. Bugiani, P. Goffrini, F. Carrara, L. Farina, E. Procopio, A. Donati, G. Uziel, I. Ferrero and M. Zeviani (2007). "Impaired complex III assembly associated with BCS1L gene mutations in isolated mitochondrial encephalopathy." Hum Mol Genet **16**(10): 1241-1252.
- Filler, K., D. Lyon, J. Bennett, N. McCain, R. Elswick, N. Lukkahatai and L. N. Saligan (2014). "Association of Mitochondrial Dysfunction and Fatigue: A Review of the Literature." BBA Clin **1**: 12-23.
- Finnila, S. and K. Majamaa (2003). "Lack of a modulative factor in locus 8p23 in a Finnish family with nonsyndromic sensorineural hearing loss associated with the 1555A>G mitochondrial DNA mutation." Eur J Hum Genet **11**(9): 652-658.
- Fischel-Ghodsian, N., M. C. Bohlman, T. R. Prezant, J. M. Graham, Jr., S. D. Cederbaum and M. J. Edwards (1992). "Deletion in blood mitochondrial DNA in Kearns-Sayre syndrome." Pediatr Res **31**(6): 557-560.
- Frangini, M., C. Rampazzo, E. Franzolin, M. C. Lara, M. R. Vila, R. Marti and V. Bianchi (2009). "Unchanged thymidine triphosphate pools and thymidine metabolism in two lines of thymidine kinase 2-mutated fibroblasts." FEBS J **276**(4): 1104-1113.
- Frey, T. G. and C. A. Mannella (2000). "The internal structure of mitochondria." Trends Biochem Sci **25**(7): 319-324.
- Fu, Q., H. Li, P. Moorjani, F. Jay, S. M. Slepchenko, A. A. Bondarev, P. L. Johnson, A. Aximu-Petri, K. Prufer, C. de Filippo, M. Meyer, N. Zwyns, D. C. Salazar-Garcia, Y. V. Kuzmin, S. G. Keates, P. A. Kosintsev, D. I. Razhev, M. P. Richards, N. V.

- Peristov, M. Lachmann, K. Douka, T. F. Higham, M. Slatkin, J. J. Hublin, D. Reich, J. Kelso, T. B. Viola and S. Paabo (2014). "Genome sequence of a 45,000-year-old modern human from western Siberia." Nature **514**(7523): 445-449.
- Fukui, H. and C. T. Moraes (2009). "Mechanisms of formation and accumulation of mitochondrial DNA deletions in aging neurons." Hum Mol Genet **18**(6): 1028-1036.
- Fukuoh, A., G. Cannino, M. Gerards, S. Buckley, S. Kazancioglu, F. Scialo, E. Lihavainen, A. Ribeiro, E. Dufour and H. T. Jacobs (2014). "Screen for mitochondrial DNA copy number maintenance genes reveals essential role for ATP synthase." Mol Syst Biol **10**: 734.
- Gale, J. E., W. Marcotti, H. J. Kennedy, C. J. Kros and G. P. Richardson (2001). "FM1-43 dye behaves as a permeant blocker of the hair-cell mechanotransducer channel." J Neurosci **21**(18): 7013-7025.
- Gao, L., K. Laude and H. Cai (2008). "Mitochondrial pathophysiology, reactive oxygen species, and cardiovascular diseases." Vet Clin North Am Small Anim Pract **38**(1): 137-155, vi.
- Genecards (2017). <http://www.genecards.org/cgi-bin/carddisp.pl?gene=MGAM>
- Genomes Project, C., A. Auton, L. D. Brooks, R. M. Durbin, E. P. Garrison, H. M. Kang, J. O. Korbel, J. L. Marchini, S. McCarthy, G. A. McVean and G. R. Abecasis (2015). "A global reference for human genetic variation." Nature **526**(7571): 68-74.
- Gensler, S., K. Weber, W. E. Schmitt, A. Perez-Martos, J. A. Enriquez, J. Montoya and R. J. Wiesner (2001). "Mechanism of mammalian mitochondrial DNA replication: import of mitochondrial transcription factor A into isolated mitochondria stimulates 7S DNA synthesis." Nucleic Acids Res **29**(17): 3657-3663.
- Gerstein, M. B., A. Kundaje, M. Hariharan, S. G. Landt, K. K. Yan, C. Cheng, X. J. Mu, E. Khurana, J. Rozowsky, R. Alexander, R. Min, P. Alves, A. Abyzov, N. Addleman, N. Bhardwaj, A. P. Boyle, P. Cayting, A. Charos, D. Z. Chen, Y. Cheng, D. Clarke, C. Eastman, G. Euskirchen, S. Fietze, Y. Fu, J. Gertz, F. Grubert, A. Harmanci, P. Jain, M. Kasowski, P. Lacroute, J. Leng, J. Lian, H.

- Monahan, H. O'Geen, Z. Ouyang, E. C. Partridge, D. Patacsil, F. Pauli, D. Raha, L. Ramirez, T. E. Reddy, B. Reed, M. Shi, T. Slifer, J. Wang, L. Wu, X. Yang, K. Y. Yip, G. Zilberman-Schapira, S. Batzoglou, A. Sidow, P. J. Farnham, R. M. Myers, S. M. Weissman and M. Snyder (2012). "Architecture of the human regulatory network derived from ENCODE data." Nature **489**(7414): 91-100.
- Ghezzi, D. and M. Zeviani (2012). "Assembly factors of human mitochondrial respiratory chain complexes: physiology and pathophysiology." Adv Exp Med Biol **748**: 65-106.
- Gilissen, C., A. Hoischen, H. G. Brunner and J. A. Veltman (2012). "Disease gene identification strategies for exome sequencing." Eur J Hum Genet **20**(5): 490-497.
- Gilkerson, R., L. Bravo, I. Garcia, N. Gaytan, A. Herrera, A. Maldonado and B. Quintanilla (2013). "The mitochondrial nucleoid: integrating mitochondrial DNA into cellular homeostasis." Cold Spring Harb Perspect Biol **5**(5): a011080.
- Giordano, C., L. Iommarini, L. Giordano, A. Maresca, A. Pisano, M. L. Valentino, L. Caporali, R. Liguori, S. Deceglie, M. Roberti, F. Fanelli, F. Fracasso, F. N. Ross-Cisneros, P. D'Adamo, G. Hudson, A. Pyle, P. Yu-Wai-Man, P. F. Chinnery, M. Zeviani, S. R. Salomao, A. Berezovsky, R. Belfort, Jr., D. F. Ventura, M. Moraes, M. Moraes Filho, P. Barboni, F. Sadun, A. De Negri, A. A. Sadun, A. Tancredi, M. Mancini, G. d'Amati, P. Loguercio Polosa, P. Cantatore and V. Carelli (2014). "Efficient mitochondrial biogenesis drives incomplete penetrance in Leber's hereditary optic neuropathy." Brain **137**(Pt 2): 335-353.
- Girirajan, S., Z. Brkanac, B. P. Coe, C. Baker, L. Vives, T. H. Vu, N. Shafer, R. Bernier, G. B. Ferrero, M. Silengo, S. T. Warren, C. S. Moreno, M. Fichera, C. Romano, W. H. Raskind and E. E. Eichler (2011). "Relative burden of large CNVs on a range of neurodevelopmental phenotypes." PLoS Genet **7**(11): e1002334.
- Gitschlag, B. L., C. S. Kirby, D. C. Samuels, R. D. Gangula, S. A. Mallal and M. R. Patel (2016). "Homeostatic Responses Regulate Selfish Mitochondrial Genome Dynamics in *C. elegans*." Cell Metab **24**(1): 91-103.

- Go, Y. M., J. D. Chandler and D. P. Jones (2015). "The cysteine proteome." Free Radic Biol Med **84**: 227-245.
- Goffart, S., H. M. Cooper, H. Tyynismaa, S. Wanrooij, A. Suomalainen and J. N. Spelbrink (2009). "Twinkle mutations associated with autosomal dominant progressive external ophthalmoplegia lead to impaired helicase function and in vivo mtDNA replication stalling." Hum Mol Genet **18**(2): 328-340.
- Goldberg, A. L. (2003). "Protein degradation and protection against misfolded or damaged proteins." Nature **426**(6968): 895-899.
- Gomez-Duran, A., D. Pacheu-Grau, E. Lopez-Gallardo, C. Diez-Sanchez, J. Montoya, M. J. Lopez-Perez and E. Ruiz-Pesini (2010). "Unmasking the causes of multifactorial disorders: OXPHOS differences between mitochondrial haplogroups." Hum Mol Genet **19**(17): 3343-3353.
- Goodwin, S., J. D. McPherson and W. R. McCombie (2016). "Coming of age: ten years of next-generation sequencing technologies." Nat Rev Genet **17**(6): 333-351.
- Gorman, G. S., P. F. Chinnery, S. DiMauro, M. Hirano, Y. Koga, R. McFarland, A. Suomalainen, D. R. Thorburn, M. Zeviani and D. M. Turnbull (2016). "Mitochondrial diseases." Nat Rev Dis Primers **2**: 16080.
- Gorman, G. S., G. Pfeffer, H. Griffin, E. L. Blakely, M. Kurzawa-Akanbi, J. Gabriel, K. Sitarz, M. Roberts, B. Schoser, A. Pyle, A. M. Schaefer, R. McFarland, D. M. Turnbull, R. Horvath, P. F. Chinnery and R. W. Taylor (2015). "Clonal expansion of secondary mitochondrial DNA deletions associated with spinocerebellar ataxia type 28." JAMA Neurol **72**(1): 106-111.
- Gorman, G. S., A. M. Schaefer, Y. Ng, N. Gomez, E. L. Blakely, C. L. Alston, C. Feeney, R. Horvath, P. Yu-Wai-Man, P. F. Chinnery, R. W. Taylor, D. M. Turnbull and R. McFarland (2015). "Prevalence of nuclear and mitochondrial DNA mutations related to adult mitochondrial disease." Ann Neurol **77**(5): 753-759.
- Gowans, G. J. and D. G. Hardie (2014). "AMPK: a cellular energy sensor primarily regulated by AMP." Biochem Soc Trans **42**(1): 71-75.

- Graham, J. (2008). Pediatric ENT, Springer.
- Gray, M. W. (2012). "Mitochondrial evolution." Cold Spring Harb Perspect Biol **4**(9): a011403.
- Greber, B. J., P. Bieri, M. Leibundgut, A. Leitner, R. Aebersold, D. Boehringer and N. Ban (2015). "Ribosome. The complete structure of the 55S mammalian mitochondrial ribosome." Science **348**(6232): 303-308.
- Grillet, N., M. Schwander, M. S. Hildebrand, A. Sczaniecka, A. Kolatkar, J. Velasco, J. A. Webster, K. Kahrizi, H. Najmabadi, W. J. Kimberling, D. Stephan, M. Bahlo, T. Wiltshire, L. M. Tarantino, P. Kuhn, R. J. Smith and U. Muller (2009). "Mutations in LOXHD1, an evolutionarily conserved stereociliary protein, disrupt hair cell function in mice and cause progressive hearing loss in humans." Am J Hum Genet **85**(3): 328-337.
- Grimsrud, P. A., H. Xie, T. J. Griffin and D. A. Bernlohr (2008). "Oxidative stress and covalent modification of protein with bioactive aldehydes." J Biol Chem **283**(32): 21837-21841.
- Guan, M. X. (2011). "Mitochondrial 12S rRNA mutations associated with aminoglycoside ototoxicity." Mitochondrion **11**(2): 237-245.
- Guan, M. X., N. Fischel-Ghodsian and G. Attardi (1996). "Biochemical evidence for nuclear gene involvement in phenotype of non-syndromic deafness associated with mitochondrial 12S rRNA mutation." Hum Mol Genet **5**(7): 963-971.
- Guan, M. X., N. Fischel-Ghodsian and G. Attardi (2000). "A biochemical basis for the inherited susceptibility to aminoglycoside ototoxicity." Hum Mol Genet **9**(12): 1787-1793.
- Guan, M. X., N. Fischel-Ghodsian and G. Attardi (2001). "Nuclear background determines biochemical phenotype in the deafness-associated mitochondrial 12S rRNA mutation." Hum Mol Genet **10**(6): 573-580.
- Guan, M. X., Q. Yan, X. Li, Y. Bykhovskaya, J. Gallo-Teran, P. Hajek, N. Umeda, H. Zhao, G. Garrido, E. Mengesha, T. Suzuki, I. del Castillo, J. L. Peters, R. Li, Y.

- Qian, X. Wang, E. Ballana, M. Shohat, J. Lu, X. Estivill, K. Watanabe and N. Fischel-Ghodsian (2006). "Mutation in TRMU related to transfer RNA modification modulates the phenotypic expression of the deafness-associated mitochondrial 12S ribosomal RNA mutations." Am J Hum Genet **79**(2): 291-302.
- Gunewardene, N., D. Crombie, M. Dottori and B. A. Nayagam (2016). "Innervation of Cochlear Hair Cells by Human Induced Pluripotent Stem Cell-Derived Neurons In Vitro." Stem Cells Int **2016**: 1781202.
- Guo, X. W. and C. A. Mannella (1993). "Conformational change in the mitochondrial channel, VDAC, detected by electron cryo-microscopy." Biophys J **64**(2): 545-549.
- Hakli, S., M. Luotonen, M. Sorri and K. Majamaa (2013). "Audiological follow-up of children with the m.1555A>G mutation in mitochondrial DNA." Audiol Neurootol **18**(1): 23-30.
- Halliwel, B. (2000). "Why and how should we measure oxidative DNA damage in nutritional studies? How far have we come?" Am J Clin Nutr **72**(5): 1082-1087.
- Hamalainen, R. H., T. Manninen, H. Koivumaki, M. Kislin, T. Otonkoski and A. Suomalainen (2013). "Tissue- and cell-type-specific manifestations of heteroplasmic mtDNA 3243A>G mutation in human induced pluripotent stem cell-derived disease model." Proc Natl Acad Sci U S A **110**(38): E3622-3630.
- Harder, Z., R. Zunino and H. McBride (2004). "Sumo1 conjugates mitochondrial substrates and participates in mitochondrial fission." Curr Biol **14**(4): 340-345.
- Hardie, D. G., F. A. Ross and S. A. Hawley (2012). "AMPK: a nutrient and energy sensor that maintains energy homeostasis." Nat Rev Mol Cell Biol **13**(4): 251-262.
- Hardie, D. G., B. E. Schaffer and A. Brunet (2016). "AMPK: An Energy-Sensing Pathway with Multiple Inputs and Outputs." Trends Cell Biol **26**(3): 190-201.
- Haut, S., M. Brivet, G. Touati, P. Rustin, S. Lebon, A. Garcia-Cazorla, J. M. Saudubray, A. Boutron, A. Legrand and A. Slama (2003). "A deletion in the human QP-C gene causes a complex III deficiency resulting in hypoglycaemia and lactic acidosis." Hum Genet **113**(2): 118-122.

- Hawley, S. A., J. Boudeau, J. L. Reid, K. J. Mustard, L. Udd, T. P. Makela, D. R. Alessi and D. G. Hardie (2003). "Complexes between the LKB1 tumor suppressor, STRAD alpha/beta and MO25 alpha/beta are upstream kinases in the AMP-activated protein kinase cascade." J Biol **2**(4): 28.
- Hayashi, G. and G. Cortopassi (2015). "Oxidative stress in inherited mitochondrial diseases." Free Radic Biol Med **88**(Pt A): 10-17.
- Hayashi, J., S. Ohta, A. Kikuchi, M. Takemitsu, Y. Goto and I. Nonaka (1991). "Introduction of disease-related mitochondrial DNA deletions into HeLa cells lacking mitochondrial DNA results in mitochondrial dysfunction." Proc Natl Acad Sci U S A **88**(23): 10614-10618.
- Hayflick, L. (1965). "The Limited in Vitro Lifetime of Human Diploid Cell Strains." Exp Cell Res **37**: 614-636.
- Haynes, C. M. and D. Ron (2010). "The mitochondrial UPR - protecting organelle protein homeostasis." J Cell Sci **123**(Pt 22): 3849-3855.
- Hazkani-Covo, E., R. M. Zeller and W. Martin (2010). "Molecular poltergeists: mitochondrial DNA copies (numts) in sequenced nuclear genomes." PLoS Genet **6**(2): e1000834.
- He, J., C. C. Mao, A. Reyes, H. Sembongi, M. Di Re, C. Granycome, A. B. Clippingdale, I. M. Fearnley, M. Harbour, A. J. Robinson, S. Reichelt, J. N. Spelbrink, J. E. Walker and I. J. Holt (2007). "The AAA+ protein ATAD3 has displacement loop binding properties and is involved in mitochondrial nucleoid organization." J Cell Biol **176**(2): 141-146.
- Henderson, D., E. C. Bielefeld, K. C. Harris and B. H. Hu (2006). "The role of oxidative stress in noise-induced hearing loss." Ear Hear **27**(1): 1-19.
- Hetz, C., E. Chevet and S. A. Oakes (2015). "Proteostasis control by the unfolded protein response." Nat Cell Biol **17**(7): 829-838.
- Hobbie, S. N., S. Akshay, S. K. Kalapala, C. M. Bruell, D. Shcherbakov and E. C. Bottger (2008). "Genetic analysis of interactions with eukaryotic rRNA identify the

- mitoribosome as target in aminoglycoside ototoxicity." Proc Natl Acad Sci U S A **105**(52): 20888-20893.
- Hobbie, S. N., C. M. Bruell, S. Akshay, S. K. Kalapala, D. Shcherbakov and E. C. Bottger (2008). "Mitochondrial deafness alleles confer misreading of the genetic code." Proc Natl Acad Sci U S A **105**(9): 3244-3249.
- Hoitzing, H., I. G. Johnston and N. S. Jones (2015). "What is the function of mitochondrial networks? A theoretical assessment of hypotheses and proposal for future research." Bioessays **37**(6): 687-700.
- Holt, I. J., A. E. Harding, R. K. Petty and J. A. Morgan-Hughes (1990). "A new mitochondrial disease associated with mitochondrial DNA heteroplasmy." Am J Hum Genet **46**(3): 428-433.
- Holt, I. J., J. He, C. C. Mao, J. D. Boyd-Kirkup, P. Martinsson, H. Sembongi, A. Reyes and J. N. Spelbrink (2007). "Mammalian mitochondrial nucleoids: organizing an independently minded genome." Mitochondrion **7**(5): 311-321.
- Holt, I. J., H. E. Lorimer and H. T. Jacobs (2000). "Coupled leading- and lagging-strand synthesis of mammalian mitochondrial DNA." Cell **100**(5): 515-524.
- Holt, I. J. and A. Reyes (2012). "Human mitochondrial DNA replication." Cold Spring Harb Perspect Biol **4**(12).
- Hong, C. S., L. N. Singh, J. C. Mullikin and L. G. Biesecker (2016). "Assessing the reproducibility of exome copy number variations predictions." Genome Med **8**(1): 82.
- Horan, M. P., N. Pichaud and J. W. Ballard (2012). "Review: quantifying mitochondrial dysfunction in complex diseases of aging." J Gerontol A Biol Sci Med Sci **67**(10): 1022-1035.
- Hudson, G., V. Carelli, L. Spruijt, M. Gerards, C. Mowbray, A. Achilli, A. Pyle, J. Elson, N. Howell, C. La Morgia, M. L. Valentino, K. Huoponen, M. L. Savontaus, E. Nikoskelainen, A. A. Sadun, S. R. Salomao, R. Belfort, Jr., P. Griffiths, P. Yu-Wai-Man, R. F. de Coo, R. Horvath, M. Zeviani, H. J. Smeets, A. Torroni and P. F.

- Chinnery (2007). "Clinical expression of Leber hereditary optic neuropathy is affected by the mitochondrial DNA-haplogroup background." Am J Hum Genet **81**(2): 228-233.
- Hudson, G. and P. F. Chinnery (2006). "Mitochondrial DNA polymerase-gamma and human disease." Hum Mol Genet **15 Spec No 2**: R244-252.
- Hudson, G., A. Gomez-Duran, I. J. Wilson and P. F. Chinnery (2014). "Recent mitochondrial DNA mutations increase the risk of developing common late-onset human diseases." PLoS Genet **10**(5): e1004369.
- Hudson, G., S. Keers, P. Yu-Wai-Man, P. Griffiths, K. Huoponen, M. L. Savontaus, E. Nikoskelainen, M. Zeviani, F. Carrara, R. Horvath, V. Karcagi, L. Spruijt, I. F. de Coo, H. J. Smeets and P. F. Chinnery (2005). "Identification of an X-chromosomal locus and haplotype modulating the phenotype of a mitochondrial DNA disorder." Am J Hum Genet **77**(6): 1086-1091.
- Hudson, G., P. Yu-Wai-Man and P. F. Chinnery (2008). "Leber hereditary optic neuropathy." Expert Opin Med Diagn **2**(7): 789-799.
- Hutchin, T., I. Haworth, K. Higashi, N. Fischel-Ghodsian, M. Stoneking, N. Saha, C. Arnos and G. Cortopassi (1993). "A molecular basis for human hypersensitivity to aminoglycoside antibiotics." Nucleic Acids Res **21**(18): 4174-4179.
- Hutchison, C. A., 3rd, J. E. Newbold, S. S. Potter and M. H. Edgell (1974). "Maternal inheritance of mammalian mitochondrial DNA." Nature **251**(5475): 536-538.
- Huth, M. E., A. J. Ricci and A. G. Cheng (2011). "Mechanisms of aminoglycoside ototoxicity and targets of hair cell protection." Int J Otolaryngol **2011**: 937861.
- Huynen, M. A., I. Duarte and R. Szklarczyk (2013). "Loss, replacement and gain of proteins at the origin of the mitochondria." Biochim Biophys Acta **1827**(2): 224-231.
- Ikeda, M., T. Ide, T. Fujino, S. Arai, K. Saku, T. Kakino, H. Tynismaa, T. Yamasaki, K. Yamada, D. Kang, A. Suomalainen and K. Sunagawa (2015). "Overexpression of TFAM or twinkle increases mtDNA copy number and facilitates cardioprotection

associated with limited mitochondrial oxidative stress." PLoS One **10**(3): e0119687.

Illumina. (2016). "An Introduction to Next Generation Sequencing Technology ", from https://http://www.illumina.com/content/dam/illumina-marketing/documents/products/illumina_sequencing_introduction.pdf.

Inoki, K., J. Kim and K. L. Guan (2012). "AMPK and mTOR in cellular energy homeostasis and drug targets." Annu Rev Pharmacol Toxicol **52**: 381-400.

Integrated Mitochondrial Protein Index (2016).

Ishihara, N., Y. Fujita, T. Oka and K. Mihara (2006). "Regulation of mitochondrial morphology through proteolytic cleavage of OPA1." EMBO J **25**(13): 2966-2977.

Iwata, S., J. W. Lee, K. Okada, J. K. Lee, M. Iwata, B. Rasmussen, T. A. Link, S. Ramaswamy and B. K. Jap (1998). "Complete structure of the 11-subunit bovine mitochondrial cytochrome bc1 complex." Science **281**(5373): 64-71.

Jackson, R. J. and T. Hunt (1983). "Preparation and use of nuclease-treated rabbit reticulocyte lysates for the translation of eukaryotic messenger RNA." Methods Enzymol **96**: 50-74.

Jacobs, H. T., T. P. Hutchin, T. Kappi, G. Gillies, K. Minkkinen, J. Walker, K. Thompson, A. T. Rovio, M. Carella, S. Melchionda, L. Zelante, P. Gasparini, I. Pyykko, Z. H. Shah, M. Zeviani and R. F. Mueller (2005). "Mitochondrial DNA mutations in patients with postlingual, nonsyndromic hearing impairment." Eur J Hum Genet **13**(1): 26-33.

Jemt, E., O. Persson, Y. Shi, M. Mehmedovic, J. P. Uhler, M. Davila Lopez, C. Freyer, C. M. Gustafsson, T. Samuelsson and M. Falkenberg (2015). "Regulation of DNA replication at the end of the mitochondrial D-loop involves the helicase TWINKLE and a conserved sequence element." Nucleic Acids Res **43**(19): 9262-9275.

Jena, N. R. (2012). "DNA damage by reactive species: Mechanisms, mutation and repair." J Biosci **37**(3): 503-517.

- Ji, F., J. Li, M. Hong, A. Chen, Q. Jiao, L. Sun, S. Liang and S. Yang (2015). "Determination of benefits of cochlear implantation in children with auditory neuropathy." PLoS One **10**(5): e0127566.
- Jiang, P., X. Jin, Y. Peng, M. Wang, H. Liu, X. Liu, Z. Zhang, Y. Ji, J. Zhang, M. Liang, F. Zhao, Y. H. Sun, M. Zhang, X. Zhou, Y. Chen, J. Q. Mo, T. Huang, J. Qu and M. X. Guan (2016). "The exome sequencing identified the mutation in YARS2 encoding the mitochondrial tyrosyl-tRNA synthetase as a nuclear modifier for the phenotypic manifestation of Leber's hereditary optic neuropathy-associated mitochondrial DNA mutation." Hum Mol Genet **25**(3): 584-596.
- Jinda, W., N. Pongvarin, T. D. Taylor, Y. Suzuki, W. Thongnoppakhun, C. Limwongse, P. Lertrit, P. Suriyaphol and L. O. Atchaneeyasakul (2016). "A novel start codon mutation of the MERTK gene in a patient with retinitis pigmentosa." Mol Vis **22**: 342-351.
- Johnson, A. A., Y. Tsai, S. W. Graves and K. A. Johnson (2000). "Human mitochondrial DNA polymerase holoenzyme: reconstitution and characterization." Biochemistry **39**(7): 1702-1708.
- Jonckheere, A. I., J. A. Smeitink and R. J. Rodenburg (2012). "Mitochondrial ATP synthase: architecture, function and pathology." J Inherit Metab Dis **35**(2): 211-225.
- Jourdain, A. A., M. Koppen, C. D. Rodley, K. Maundrell, N. Gueguen, P. Reynier, A. M. Guaras, J. A. Enriquez, P. Anderson, M. Simarro and J. C. Martinou (2015). "A mitochondria-specific isoform of FASTK is present in mitochondrial RNA granules and regulates gene expression and function." Cell Rep **10**(7): 1110-1121.
- Jung, J., J. S. Lee, K. J. Cho, S. Yu, J. H. Yoon, H. Yung Gee and J. Y. Choi (2017). "Genetic Predisposition to Sporadic Congenital Hearing Loss in a Pediatric Population." Sci Rep **7**: 45973.
- Jungbluth, H. (2007). "Multi-minicore Disease." Orphanet J Rare Dis **2**: 31.
- Kadenbach, B. (2012). "Introduction to mitochondrial oxidative phosphorylation." Adv Exp Med Biol **748**: 1-11.

- Kalyanaraman, B., V. Darley-Usmar, K. J. Davies, P. A. Dennery, H. J. Forman, M. B. Grisham, G. E. Mann, K. Moore, L. J. Roberts, 2nd and H. Ischiropoulos (2012). "Measuring reactive oxygen and nitrogen species with fluorescent probes: challenges and limitations." Free Radic Biol Med **52**(1): 1-6.
- Kamogashira, T., C. Fujimoto and T. Yamasoba (2015). "Reactive oxygen species, apoptosis, and mitochondrial dysfunction in hearing loss." Biomed Res Int **2015**: 617207.
- Kang, D., K. Miyako, Y. Kai, T. Irie and K. Takeshige (1997). "In vivo determination of replication origins of human mitochondrial DNA by ligation-mediated polymerase chain reaction." J Biol Chem **272**(24): 15275-15279.
- Karnes, H. E., P. N. Scaletty and D. Durham (2010). "Histochemical and fluorescent analyses of mitochondrial integrity in chick auditory neurons following deafferentation." J Am Acad Audiol **21**(3): 204-218.
- Karnkowska, A., V. Vacek, Z. Zubacova, S. C. Treitli, R. Petrzekova, L. Eme, L. Novak, V. Zarsky, L. D. Barlow, E. K. Herman, P. Soukal, M. Hroudova, P. Dolezal, C. W. Stairs, A. J. Roger, M. Elias, J. B. Dacks, C. Vlcek and V. Hampl (2016). "A Eukaryote without a Mitochondrial Organelle." Curr Biol **26**(10): 1274-1284.
- Kasiviswanathan, R., T. R. Collins and W. C. Copeland (2012). "The interface of transcription and DNA replication in the mitochondria." Biochim Biophys Acta **1819**(9-10): 970-978.
- Kaufman, B. A., N. Durisic, J. M. Mativetsky, S. Costantino, M. A. Hancock, P. Grutter and E. A. Shoubridge (2007). "The mitochondrial transcription factor TFAM coordinates the assembly of multiple DNA molecules into nucleoid-like structures." Mol Biol Cell **18**(9): 3225-3236.
- Kaukonen, J., J. K. Juselius, V. Tiranti, A. Kytala, M. Zeviani, G. P. Comi, S. Keranen, L. Peltonen and A. Suomalainen (2000). "Role of adenine nucleotide translocator 1 in mtDNA maintenance." Science **289**(5480): 782-785.

- Kazak, L., A. Reyes, J. He, S. R. Wood, G. Brea-Calvo, T. T. Holen and I. J. Holt (2013). "A cryptic targeting signal creates a mitochondrial FEN1 isoform with tailed R-Loop binding properties." PLoS One **8**(5): e62340.
- Kellis, M., B. Wold, M. P. Snyder, B. E. Bernstein, A. Kundaje, G. K. Marinov, L. D. Ward, E. Birney, G. E. Crawford, J. Dekker, I. Dunham, L. L. Elnitski, P. J. Farnham, E. A. Feingold, M. Gerstein, M. C. Giddings, D. M. Gilbert, T. R. Gingeras, E. D. Green, R. Guigo, T. Hubbard, J. Kent, J. D. Lieb, R. M. Myers, M. J. Pazin, B. Ren, J. A. Stamatoyannopoulos, Z. Weng, K. P. White and R. C. Hardison (2014). "Defining functional DNA elements in the human genome." Proc Natl Acad Sci U S A **111**(17): 6131-6138.
- Kemp, D. T. (1978). "Stimulated acoustic emissions from within the human auditory system." J Acoust Soc Am **64**(5): 1386-1391.
- Keogh, M. J. and P. F. Chinnery (2015). "Mitochondrial DNA mutations in neurodegeneration." Biochim Biophys Acta **1847**(11): 1401-1411.
- Khan, S. M., R. M. Smigrodzki and R. H. Swerdlow (2007). "Cell and animal models of mtDNA biology: progress and prospects." Am J Physiol Cell Physiol **292**(2): C658-669.
- Kim, H. J., O. Khalimonchuk, P. M. Smith and D. R. Winge (2012). "Structure, function, and assembly of heme centers in mitochondrial respiratory complexes." Biochim Biophys Acta **1823**(9): 1604-1616.
- Kirino, Y., T. Yasukawa, S. Ohta, S. Akira, K. Ishihara, K. Watanabe and T. Suzuki (2004). "Codon-specific translational defect caused by a wobble modification deficiency in mutant tRNA from a human mitochondrial disease." Proc Natl Acad Sci U S A **101**(42): 15070-15075.
- Kisselev, A. F., W. A. van der Linden and H. S. Overkleeft (2012). "Proteasome inhibitors: an expanding army attacking a unique target." Chem Biol **19**(1): 99-115.
- Klop, W. M., J. J. Briaire, A. M. Stiggelbout and J. H. Frijns (2007). "Cochlear implant outcomes and quality of life in adults with prelingual deafness." Laryngoscope **117**(11): 1982-1987.

- Ko, A. R., H. W. Hyun, S. J. Min and J. E. Kim (2016). "The Differential DRP1 Phosphorylation and Mitochondrial Dynamics in the Regional Specific Astroglial Death Induced by Status Epilepticus." Front Cell Neurosci **10**: 124.
- Koehler, K. R., J. Nie, E. Longworth-Mills, X. P. Liu, J. Lee, J. R. Holt and E. Hashino (2017). "Generation of inner ear organoids containing functional hair cells from human pluripotent stem cells." Nat Biotechnol **35**(6): 583-589.
- Kokotas, H., M. B. Petersen and P. J. Willems (2007). "Mitochondrial deafness." Clin Genet **71**(5): 379-391.
- Koopman, W. J., H. J. Visch, S. Verkaart, L. W. van den Heuvel, J. A. Smeitink and P. H. Willems (2005). "Mitochondrial network complexity and pathological decrease in complex I activity are tightly correlated in isolated human complex I deficiency." Am J Physiol Cell Physiol **289**(4): C881-890.
- Korhonen, J. A., M. Gaspari and M. Falkenberg (2003). "TWINKLE Has 5' -> 3' DNA helicase activity and is specifically stimulated by mitochondrial single-stranded DNA-binding protein." J Biol Chem **278**(49): 48627-48632.
- Korhonen, J. A., X. H. Pham, M. Pellegrini and M. Falkenberg (2004). "Reconstitution of a minimal mtDNA replisome in vitro." EMBO J **23**(12): 2423-2429.
- Kornberg, R. D. (1974). "Chromatin structure: a repeating unit of histones and DNA." Science **184**(4139): 868-871.
- Kornblum, C., T. J. Nicholls, T. B. Haack, S. Scholer, V. Peeva, K. Danhauser, K. Hallmann, G. Zsurka, J. Rorbach, A. Iuso, T. Wieland, M. Sciacco, D. Ronchi, G. P. Comi, M. Moggio, C. M. Quinzii, S. DiMauro, S. E. Calvo, V. K. Mootha, T. Klopstock, T. M. Strom, T. Meitinger, M. Minczuk, W. S. Kunz and H. Prokisch (2013). "Loss-of-function mutations in MGME1 impair mtDNA replication and cause multisystemic mitochondrial disease." Nat Genet **45**(2): 214-219.
- Krishnan, K. J., A. K. Reeve, D. C. Samuels, P. F. Chinnery, J. K. Blackwood, R. W. Taylor, S. Wanrooij, J. N. Spelbrink, R. N. Lightowlers and D. M. Turnbull (2008). "What causes mitochondrial DNA deletions in human cells?" Nat Genet **40**(3): 275-279.

- Kruger, V., M. Deckers, M. Hildenbeutel, M. van der Laan, M. Hellmers, C. Dreker, M. Preuss, J. M. Herrmann, P. Rehling, R. Wagner and M. Meinecke (2012). "The mitochondrial oxidase assembly protein1 (Oxa1) insertase forms a membrane pore in lipid bilayers." J Biol Chem **287**(40): 33314-33326.
- Kujoth, G. C., A. Hiona, T. D. Pugh, S. Someya, K. Panzer, S. E. Wohlgemuth, T. Hofer, A. Y. Seo, R. Sullivan, W. A. Jobling, J. D. Morrow, H. Van Remmen, J. M. Sedivy, T. Yamasoba, M. Tanokura, R. Weindruch, C. Leeuwenburgh and T. A. Prolla (2005). "Mitochondrial DNA mutations, oxidative stress, and apoptosis in mammalian aging." Science **309**(5733): 481-484.
- Kukat, C., K. M. Davies, C. A. Wurm, H. Spahr, N. A. Bonekamp, I. Kuhl, F. Joos, P. L. Polosa, C. B. Park, V. Posse, M. Falkenberg, S. Jakobs, W. Kuhlbrandt and N. G. Larsson (2015). "Cross-strand binding of TFAM to a single mtDNA molecule forms the mitochondrial nucleoid." Proc Natl Acad Sci U S A **112**(36): 11288-11293.
- Kukat, C., C. A. Wurm, H. Spahr, M. Falkenberg, N. G. Larsson and S. Jakobs (2011). "Super-resolution microscopy reveals that mammalian mitochondrial nucleoids have a uniform size and frequently contain a single copy of mtDNA." Proc Natl Acad Sci U S A **108**(33): 13534-13539.
- Kullar, P., C. L. Alston, S. Ball, E. L. Blakely, A. M. Differ, C. Fratter, M. G. Sweeney, R. W. Taylor and P. F. Chinnery (2016). "The frequency of the m.1555A>G (MTRNR1) variant in UK patients with suspected mitochondrial deafness." Hearing Balance Commun **14**(2): 101-102.
- Kumar, P., S. Henikoff and P. C. Ng (2009). "Predicting the effects of coding non-synonymous variants on protein function using the SIFT algorithm." Nat Protoc **4**(7): 1073-1081.
- Kunkel, T. A. and A. Soni (1988). "Exonucleolytic proofreading enhances the fidelity of DNA synthesis by chick embryo DNA polymerase-gamma." J Biol Chem **263**(9): 4450-4459.

- Kuzmenko, A., G. C. Atkinson, S. Levitskii, N. Zenkin, T. Tenson, V. Hauryliuk and P. Kamenski (2014). "Mitochondrial translation initiation machinery: conservation and diversification." Biochimie **100**: 132-140.
- Lackner, L. L. (2014). "Shaping the dynamic mitochondrial network." BMC Biol **12**: 35.
- Lagouge, M. and N. G. Larsson (2013). "The role of mitochondrial DNA mutations and free radicals in disease and ageing." J Intern Med **273**(6): 529-543.
- Lambert, T. (2012). "Antibiotics that affect the ribosome." Rev Sci Tech **31**(1): 57-64.
- Lane, N. and W. Martin (2010). "The energetics of genome complexity." Nature **467**(7318): 929-934.
- Laplante, M. and D. M. Sabatini (2012). "mTOR signaling in growth control and disease." Cell **149**(2): 274-293.
- Larsson, N. G., A. Oldfors, J. D. Garman, G. S. Barsh and D. A. Clayton (1997). "Down-regulation of mitochondrial transcription factor A during spermatogenesis in humans." Hum Mol Genet **6**(2): 185-191.
- Le Prell, C. G., D. Yamashita, S. B. Minami, T. Yamasoba and J. M. Miller (2007). "Mechanisms of noise-induced hearing loss indicate multiple methods of prevention." Hear Res **226**(1-2): 22-43.
- Lee, C., J. Zeng, B. G. Drew, T. Sallam, A. Martin-Montalvo, J. Wan, S. J. Kim, H. Mehta, A. L. Hevener, R. de Cabo and P. Cohen (2015). "The mitochondrial-derived peptide MOTS-c promotes metabolic homeostasis and reduces obesity and insulin resistance." Cell Metab **21**(3): 443-454.
- Lee, S., S. Rose, M. D. Metodiev, L. Becker, A. Vernaleken, T. Klopstock, V. Gailus-Durner, H. Fuchs, M. Hrabe De Angelis, S. Douthwaite and N. G. Larsson (2015). "Overexpression of the mitochondrial methyltransferase TFB1M in the mouse does not impact mitoribosomal methylation status or hearing." Hum Mol Genet **24**(25): 7286-7294.

- Lee, S. R., K. S. Yang, J. Kwon, C. Lee, W. Jeong and S. G. Rhee (2002). "Reversible inactivation of the tumor suppressor PTEN by H₂O₂." J Biol Chem **277**(23): 20336-20342.
- Lehtonen, J. M., S. Forsstrom, E. Bottani, C. Viscomi, O. R. Baris, H. Isoniemi, K. Hockerstedt, P. Osterlund, M. Hurme, J. Jylhava, S. Leppa, R. Markkula, T. Helio, G. Mombelli, J. Uusimaa, R. Laaksonen, H. Laaksovirta, M. Auranen, M. Zeviani, J. Smeitink, R. J. Wiesner, K. Nakada, P. Isohanni and A. Suomalainen (2016). "FGF21 is a biomarker for mitochondrial translation and mtDNA maintenance disorders." Neurology **87**(22): 2290-2299.
- Lehtonen, M. S., S. Uimonen, I. E. Hassinen and K. Majamaa (2000). "Frequency of mitochondrial DNA point mutations among patients with familial sensorineural hearing impairment." Eur J Hum Genet **8**(4): 315-318.
- Leibowitz, R. D. (1971). "The effect of ethidium bromide on mitochondrial DNA synthesis and mitochondrial DNA structure in HeLa cells." J Cell Biol **51**(1): 116-122.
- Lek, M., K. J. Karczewski, E. V. Minikel, K. E. Samocha, E. Banks, T. Fennell, A. H. O'Donnell-Luria, J. S. Ware, A. J. Hill, B. B. Cummings, T. Tukiainen, D. P. Birnbaum, J. A. Kosmicki, L. E. Duncan, K. Estrada, F. Zhao, J. Zou, E. Pierce-Hoffman, J. Berghout, D. N. Cooper, N. Deflaux, M. DePristo, R. Do, J. Flannick, M. Fromer, L. Gauthier, J. Goldstein, N. Gupta, D. Howrigan, A. Kiezun, M. I. Kurki, A. L. Moonshine, P. Natarajan, L. Orozco, G. M. Peloso, R. Poplin, M. A. Rivas, V. Ruano-Rubio, S. A. Rose, D. M. Ruderfer, K. Shakir, P. D. Stenson, C. Stevens, B. P. Thomas, G. Tiao, M. T. Tusie-Luna, B. Weisburd, H. H. Won, D. Yu, D. M. Altshuler, D. Ardissino, M. Boehnke, J. Danesh, S. Donnelly, R. Elosua, J. C. Florez, S. B. Gabriel, G. Getz, S. J. Glatt, C. M. Hultman, S. Kathiresan, M. Laakso, S. McCarroll, M. I. McCarthy, D. McGovern, R. McPherson, B. M. Neale, A. Palotie, S. M. Purcell, D. Saleheen, J. M. Scharf, P. Sklar, P. F. Sullivan, J. Tuomilehto, M. T. Tsuang, H. C. Watkins, J. G. Wilson, M. J. Daly, D. G. MacArthur and C. Exome Aggregation (2016). "Analysis of protein-coding genetic variation in 60,706 humans." Nature **536**(7616): 285-291.

- Lentz, S. I., J. L. Edwards, C. Backus, L. L. McLean, K. M. Haines and E. L. Feldman (2010). "Mitochondrial DNA (mtDNA) biogenesis: visualization and dual incorporation of BrdU and EdU into newly synthesized mtDNA in vitro." J Histochem Cytochem **58**(2): 207-218.
- Leong, I. U., A. Stuckey, D. Lai, J. R. Skinner and D. R. Love (2015). "Assessment of the predictive accuracy of five in silico prediction tools, alone or in combination, and two metaservers to classify long QT syndrome gene mutations." BMC Med Genet **16**: 34.
- Li, F. Y., P. A. Cuddon, J. Song, S. L. Wood, J. S. Patterson, G. D. Shelton and I. D. Duncan (2006). "Canine spongiform leukoencephalomyelopathy is associated with a missense mutation in cytochrome b." Neurobiol Dis **21**(1): 35-42.
- Li, H. and R. Durbin (2010). "Fast and accurate long-read alignment with Burrows-Wheeler transform." Bioinformatics **26**(5): 589-595.
- Li, H., B. Handsaker, A. Wysoker, T. Fennell, J. Ruan, N. Homer, G. Marth, G. Abecasis, R. Durbin and S. Genome Project Data Processing (2009). "The Sequence Alignment/Map format and SAMtools." Bioinformatics **25**(16): 2078-2079.
- Li, J. N., D. Y. Han, F. Ji, A. T. Chen, N. Wu, X. Xi, W. D. Shen and S. M. Yang (2011). "Successful cochlear implantation in a patient with MNGIE syndrome." Acta Otolaryngol **131**(9): 1012-1016.
- Li, M., R. Schroder, S. Ni, B. Madea and M. Stoneking (2015). "Extensive tissue-related and allele-related mtDNA heteroplasmy suggests positive selection for somatic mutations." Proc Natl Acad Sci U S A **112**(8): 2491-2496.
- Li, X. and M. X. Guan (2002). "A human mitochondrial GTP binding protein related to tRNA modification may modulate phenotypic expression of the deafness-associated mitochondrial 12S rRNA mutation." Mol Cell Biol **22**(21): 7701-7711.
- Li, X., R. Li, X. Lin and M. X. Guan (2002). "Isolation and characterization of the putative nuclear modifier gene MTO1 involved in the pathogenesis of deafness-associated mitochondrial 12 S rRNA A1555G mutation." J Biol Chem **277**(30): 27256-27264.

- Li, Z., R. Li, J. Chen, Z. Liao, Y. Zhu, Y. Qian, S. Xiong, S. Heman-Ackah, J. Wu, D. I. Choo and M. X. Guan (2005). "Mutational analysis of the mitochondrial 12S rRNA gene in Chinese pediatric subjects with aminoglycoside-induced and non-syndromic hearing loss." Hum Genet **117**(1): 9-15.
- Liesa, M. and O. S. Shirihai (2013). "Mitochondrial dynamics in the regulation of nutrient utilization and energy expenditure." Cell Metab **17**(4): 491-506.
- Lightowers, R. N., P. F. Chinnery, D. M. Turnbull and N. Howell (1997). "Mammalian mitochondrial genetics: heredity, heteroplasmy and disease." Trends Genet **13**(11): 450-455.
- Limongelli, A., J. Schaefer, S. Jackson, F. Invernizzi, Y. Kirino, T. Suzuki, H. Reichmann and M. Zeviani (2004). "Variable penetrance of a familial progressive necrotising encephalopathy due to a novel tRNA(Ile) homoplasmic mutation in the mitochondrial genome." J Med Genet **41**(5): 342-349.
- Lind, C., J. Sund and J. Aqvist (2013). "Codon-reading specificities of mitochondrial release factors and translation termination at non-standard stop codons." Nat Commun **4**: 2940.
- Linder, T., C. B. Park, J. Asin-Cayuela, M. Pellegrini, N. G. Larsson, M. Falkenberg, T. Samuelsson and C. M. Gustafsson (2005). "A family of putative transcription termination factors shared amongst metazoans and plants." Curr Genet **48**(4): 265-269.
- Litonin, D., M. Sologub, Y. Shi, M. Savkina, M. Anikin, M. Falkenberg, C. M. Gustafsson and D. Temiakov (2010). "Human mitochondrial transcription revisited: only TFAM and TFB2M are required for transcription of the mitochondrial genes in vitro." J Biol Chem **285**(24): 18129-18133.
- Liu, P. C. and D. J. Thiele (1999). "Modulation of human heat shock factor trimerization by the linker domain." J Biol Chem **274**(24): 17219-17225.
- Lohman, T. M. and M. E. Ferrari (1994). "Escherichia coli single-stranded DNA-binding protein: multiple DNA-binding modes and cooperativities." Annu Rev Biochem **63**: 527-570.

- Longley, M. J., S. Clark, C. Yu Wai Man, G. Hudson, S. E. Durham, R. W. Taylor, S. Nightingale, D. M. Turnbull, W. C. Copeland and P. F. Chinnery (2006). "Mutant POLG2 disrupts DNA polymerase gamma subunits and causes progressive external ophthalmoplegia." Am J Hum Genet **78**(6): 1026-1034.
- Lu, J., Z. Li, Y. Zhu, A. Yang, R. Li, J. Zheng, Q. Cai, G. Peng, W. Zheng, X. Tang, B. Chen, J. Chen, Z. Liao, L. Yang, Y. Li, J. You, Y. Ding, H. Yu, J. Wang, D. Sun, J. Zhao, L. Xue, J. Wang and M. X. Guan (2010). "Mitochondrial 12S rRNA variants in 1642 Han Chinese pediatric subjects with aminoglycoside-induced and nonsyndromic hearing loss." Mitochondrion **10**(4): 380-390.
- Lu, J., Y. Qian, Z. Li, A. Yang, Y. Zhu, R. Li, L. Yang, X. Tang, B. Chen, Y. Ding, Y. Li, J. You, J. Zheng, Z. Tao, F. Zhao, J. Wang, D. Sun, J. Zhao, Y. Meng and M. X. Guan (2010). "Mitochondrial haplotypes may modulate the phenotypic manifestation of the deafness-associated 12S rRNA 1555A>G mutation." Mitochondrion **10**(1): 69-81.
- Luo, L. F., C. C. Hou and W. X. Yang (2013). "Nuclear factors: roles related to mitochondrial deafness." Gene **520**(2): 79-89.
- MacArthur, D. G., T. A. Manolio, D. P. Dimmock, H. L. Rehm, J. Shendure, G. R. Abecasis, D. R. Adams, R. B. Altman, S. E. Antonarakis, E. A. Ashley, J. C. Barrett, L. G. Biesecker, D. F. Conrad, G. M. Cooper, N. J. Cox, M. J. Daly, M. B. Gerstein, D. B. Goldstein, J. N. Hirschhorn, S. M. Leal, L. A. Pennacchio, J. A. Stamatoyannopoulos, S. R. Sunyaev, D. Valle, B. F. Voight, W. Winckler and C. Gunter (2014). "Guidelines for investigating causality of sequence variants in human disease." Nature **508**(7497): 469-476.
- Macherey, O. and R. P. Carlyon (2014). "Cochlear implants." Curr Biol **24**(18): R878-884.
- Macia, M. S., J. Halbritter, M. Delous, C. Bredrup, A. Gutter, E. Filhol, A. E. Mellgren, S. Leh, A. Bizet, D. A. Braun, H. Y. Gee, F. Silbermann, C. Henry, P. Krug, C. Bole-Feyssot, P. Nitschke, D. Joly, P. Nicoud, A. Paget, H. Haugland, D. Brackmann, N. Ahmet, R. Sandford, N. Cengiz, P. M. Knappskog, H. Boman, B. Linghu, F. Yang, E. J. Oakeley, P. Saint Mezard, A. W. Sailer, S. Johansson, E. Rodahl, S. Saunier,

- F. Hildebrandt and A. Benmerah (2017). "Mutations in MAPKBP1 Cause Juvenile or Late-Onset Cilia-Independent Nephronophthisis." Am J Hum Genet **100**(2): 372.
- Mandel, H., R. Szargel, V. Labay, O. Elpeleg, A. Saada, A. Shalata, Y. Anbinder, D. Berkowitz, C. Hartman, M. Barak, S. Eriksson and N. Cohen (2001). "The deoxyguanosine kinase gene is mutated in individuals with depleted hepatocerebral mitochondrial DNA." Nat Genet **29**(3): 337-341.
- Manley (2010). Active Processes and Otoacoustic Emissions in Hearing, Springer.
- Manolio, T. A., F. S. Collins, N. J. Cox, D. B. Goldstein, L. A. Hindorff, D. J. Hunter, M. I. McCarthy, E. M. Ramos, L. R. Cardon, A. Chakravarti, J. H. Cho, A. E. Guttmacher, A. Kong, L. Kruglyak, E. Mardis, C. N. Rotimi, M. Slatkin, D. Valle, A. S. Whittemore, M. Boehnke, A. G. Clark, E. E. Eichler, G. Gibson, J. L. Haines, T. F. Mackay, S. A. McCarroll and P. M. Visscher (2009). "Finding the missing heritability of complex diseases." Nature **461**(7265): 747-753.
- Marcinko, K. and G. R. Steinberg (2014). "The role of AMPK in controlling metabolism and mitochondrial biogenesis during exercise." Exp Physiol **99**(12): 1581-1585.
- Mardis, E. R. (2017). "DNA sequencing technologies: 2006-2016." Nat Protoc **12**(2): 213-218.
- Margulis, L. (1971). "The origin of plant and animal cells." Am Sci **59**(2): 230-235.
- Marrocco, I., Altieri F, Peluso I (2017). "Measurement and Clinical Significance of Biomarkers of Oxidative Stress in Humans." Oxidative Sci ID: 6501046
- Marroquin, L. D., J. Hynes, J. A. Dykens, J. D. Jamieson and Y. Will (2007). "Circumventing the Crabtree effect: replacing medium glucose with galactose increases susceptibility of HepG2 cells to mitochondrial toxicants." Toxicol Sci **97**(2): 539-547.
- Martin, W. and M. Muller (1998). "The hydrogen hypothesis for the first eukaryote." Nature **392**(6671): 37-41.
- Massa, V., E. Fernandez-Vizarra, S. Alshahwan, E. Bakhsh, P. Goffrini, I. Ferrero, P. Mereghetti, P. D'Adamo, P. Gasparini and M. Zeviani (2008). "Severe infantile

- encephalomyopathy caused by a mutation in COX6B1, a nucleus-encoded subunit of cytochrome c oxidase." Am J Hum Genet **82**(6): 1281-1289.
- Masters, B. S., L. L. Stohl and D. A. Clayton (1987). "Yeast mitochondrial RNA polymerase is homologous to those encoded by bacteriophages T3 and T7." Cell **51**(1): 89-99.
- Matthijs, G., S. Claes, B. Longo-Mbenza and J. J. Cassiman (1996). "Non-syndromic deafness associated with a mutation and a polymorphism in the mitochondrial 12S ribosomal RNA gene in a large Zairean pedigree." Eur J Hum Genet **4**(1): 46-51.
- Mayr, J. A., V. Havlickova, F. Zimmermann, I. Magler, V. Kaplanova, P. Jesina, A. Pecinova, H. Nuskova, J. Koch, W. Sperl and J. Houstek (2010). "Mitochondrial ATP synthase deficiency due to a mutation in the ATP5E gene for the F1 epsilon subunit." Hum Mol Genet **19**(17): 3430-3439.
- McClellan, J. and M. C. King (2010). "Genetic heterogeneity in human disease." Cell **141**(2): 210-217.
- McCubrey, J. A., M. M. Lahair and R. A. Franklin (2006). "Reactive oxygen species-induced activation of the MAP kinase signaling pathways." Antioxid Redox Signal **8**(9-10): 1775-1789.
- McElhoe, J. A., M. M. Holland, K. D. Makova, M. S. Su, I. M. Paul, C. H. Baker, S. A. Faith and B. Young (2014). "Development and assessment of an optimized next-generation DNA sequencing approach for the mtgenome using the Illumina MiSeq." Forensic Sci Int Genet **13**: 20-29.
- McFarland, R., K. M. Clark, A. A. Morris, R. W. Taylor, S. Macphail, R. N. Lightowlers and D. M. Turnbull (2002). "Multiple neonatal deaths due to a homoplasmic mitochondrial DNA mutation." Nat Genet **30**(2): 145-146.
- McKay, S. E., W. Yan, J. Nouws, M. J. Thormann, N. Raimundo, A. Khan, J. Santos-Sacchi, L. Song and G. S. Shadel (2015). "Auditory Pathology in a Transgenic mtTFB1 Mouse Model of Mitochondrial Deafness." Am J Pathol **185**(12): 3132-3140.

- McKeown, P. C., A. Fort and C. Spillane (2014). "Analysis of genomic imprinting by quantitative allele-specific expression by Pyrosequencing((R))." Methods Mol Biol **1112**: 85-104.
- Mears, J. A., L. L. Lackner, S. Fang, E. Ingerman, J. Nunnari and J. E. Hinshaw (2011). "Conformational changes in Dnm1 support a contractile mechanism for mitochondrial fission." Nat Struct Mol Biol **18**(1): 20-26.
- Meeusen, S., J. M. McCaffery and J. Nunnari (2004). "Mitochondrial fusion intermediates revealed in vitro." Science **305**(5691): 1747-1752.
- Meissner, C., P. Bruse, S. A. Mohamed, A. Schulz, H. Warnk, T. Storm and M. Oehmichen (2008). "The 4977 bp deletion of mitochondrial DNA in human skeletal muscle, heart and different areas of the brain: a useful biomarker or more?" Exp Gerontol **43**(7): 645-652.
- Meng, F., X. Cang, Y. Peng, R. Li, Z. Zhang, F. Li, Q. Fan, A. S. Guan, N. Fischel-Ghosian, X. Zhao and M. X. Guan (2017). "Biochemical Evidence for a Nuclear Modifier Allele (A10S) in TRMU (Methylaminomethyl-2-thiouridylate-methyltransferase) Related to Mitochondrial tRNA Modification in the Phenotypic Manifestation of Deafness-associated 12S rRNA Mutation." J Biol Chem **292**(7): 2881-2892.
- Metodiev, M. D., N. Lesko, C. B. Park, Y. Camara, Y. Shi, R. Wibom, K. Hultenby, C. M. Gustafsson and N. G. Larsson (2009). "Methylation of 12S rRNA is necessary for in vivo stability of the small subunit of the mammalian mitochondrial ribosome." Cell Metab **9**(4): 386-397.
- Metzker, M. L. (2010). "Sequencing technologies - the next generation." Nat Rev Genet **11**(1): 31-46.
- Mihaylova, M. M. and R. J. Shaw (2011). "The AMPK signalling pathway coordinates cell growth, autophagy and metabolism." Nat Cell Biol **13**(9): 1016-1023.
- Mikhailov, V. S. and D. F. Bogenhagen (1996). "Termination within oligo(dT) tracts in template DNA by DNA polymerase gamma occurs with formation of a DNA

triplex structure and is relieved by mitochondrial single-stranded DNA-binding protein." J Biol Chem **271**(48): 30774-30780.

Milenkovic, D., S. Matic, I. Kuhl, B. Ruzzenente, C. Freyer, E. Jemt, C. B. Park, M. Falkenberg and N. G. Larsson (2013). "TWINKLE is an essential mitochondrial helicase required for synthesis of nascent D-loop strands and complete mtDNA replication." Hum Mol Genet **22**(10): 1983-1993.

Miller, C., A. Saada, N. Shaul, N. Shabtai, E. Ben-Shalom, A. Shaag, E. HersHKovitz and O. Elpeleg (2004). "Defective mitochondrial translation caused by a ribosomal protein (MRPS16) mutation." Ann Neurol **56**(5): 734-738.

Miller, F. J., F. L. Rosenfeldt, C. Zhang, A. W. Linnane and P. Nagley (2003). "Precise determination of mitochondrial DNA copy number in human skeletal and cardiac muscle by a PCR-based assay: lack of change of copy number with age." Nucleic Acids Res **31**(11): e61.

Mingeot-Leclercq, M. P., Y. Glupczynski and P. M. Tulkens (1999). "Aminoglycosides: activity and resistance." Antimicrob Agents Chemother **43**(4): 727-737.

Miralles Fuste, J., Y. Shi, S. Wanrooij, X. Zhu, E. Jemt, O. Persson, N. Sabouri, C. M. Gustafsson and M. Falkenberg (2014). "In vivo occupancy of mitochondrial single-stranded DNA binding protein supports the strand displacement mode of DNA replication." PLoS Genet **10**(12): e1004832.

Mirkin, E. V. and S. M. Mirkin (2007). "Replication fork stalling at natural impediments." Microbiol Mol Biol Rev **71**(1): 13-35.

Mishra, P., V. Carelli, G. Manfredi and D. C. Chan (2014). "Proteolytic cleavage of Opa1 stimulates mitochondrial inner membrane fusion and couples fusion to oxidative phosphorylation." Cell Metab **19**(4): 630-641.

Mitchell, P. and J. Moyle (1967). "Chemiosmotic hypothesis of oxidative phosphorylation." Nature **213**(5072): 137-139.

Mitomap (2017). <https://www.mitomap.org/MITOMAP>

- Montoya, J., T. Christianson, D. Levens, M. Rabinowitz and G. Attardi (1982). "Identification of initiation sites for heavy-strand and light-strand transcription in human mitochondrial DNA." Proc Natl Acad Sci U S A **79**(23): 7195-7199.
- Moore, J. H. and S. M. Williams (2009). "Epistasis and its implications for personal genetics." Am J Hum Genet **85**(3): 309-320.
- Moraes, C. T., F. Ciacci, E. Bonilla, V. Ionasescu, E. A. Schon and S. DiMauro (1993). "A mitochondrial tRNA anticodon swap associated with a muscle disease." Nat Genet **4**(3): 284-288.
- Mori, K., H. Moteki, Y. Kobayashi, H. Azaiez, K. T. Booth, S. Y. Nishio, H. Sato, R. J. Smith and S. Usami (2015). "Mutations in LOXHD1 gene cause various types and severities of hearing loss." Ann Otol Rhinol Laryngol **124 Suppl 1**: 135S-141S.
- Morton, C. C. and W. E. Nance (2006). "Newborn hearing screening--a silent revolution." N Engl J Med **354**(20): 2151-2164.
- Mosnier, I., J. P. Bebear, M. Marx, B. Fraysse, E. Truy, G. Lina-Granade, M. Mondain, F. Sterkers-Artieres, P. Bordure, A. Robier, B. Godey, B. Meyer, B. Frachet, C. Poncet-Wallet, D. Bouccara and O. Sterkers (2015). "Improvement of cognitive function after cochlear implantation in elderly patients." JAMA Otolaryngol Head Neck Surg **141**(5): 442-450.
- Mot, A. I., J. R. Liddell, A. R. White and P. J. Crouch (2016). "Circumventing the Crabtree Effect: A method to induce lactate consumption and increase oxidative phosphorylation in cell culture." Int J Biochem Cell Biol **79**: 128-138.
- Munch, C. and J. W. Harper (2016). "Mitochondrial unfolded protein response controls matrix pre-RNA processing and translation." Nature **534**(7609): 710-713.
- Murphy, J. L., T. E. Ratnaike, E. Shang, G. Falkous, E. L. Blakely, C. L. Alston, T. Taivassalo, R. G. Haller, R. W. Taylor and D. M. Turnbull (2012). "Cytochrome c oxidase-intermediate fibres: importance in understanding the pathogenesis and treatment of mitochondrial myopathy." Neuromuscul Disord **22**(8): 690-698.

- Murphy, M. P. (2009). "How mitochondria produce reactive oxygen species." Biochem J **417**(1): 1-13.
- Murphy, M. P., A. Holmgren, N. G. Larsson, B. Halliwell, C. J. Chang, B. Kalyanaraman, S. G. Rhee, P. J. Thornalley, L. Partridge, D. Gems, T. Nystrom, V. Belousov, P. T. Schumacker and C. C. Winterbourn (2011). "Unraveling the biological roles of reactive oxygen species." Cell Metab **13**(4): 361-366.
- Naing, A., M. Kenchaiah, B. Krishnan, F. Mir, A. Charnley, C. Egan and G. Bano (2014). "Maternally inherited diabetes and deafness (MIDD): diagnosis and management." J Diabetes Complications **28**(4): 542-546.
- Nakamura, M., S. Nakano, Y. Goto, M. Ozawa, Y. Nagahama, H. Fukuyama, I. Akiguchi, R. Kaji and J. Kimura (1995). "A novel point mutation in the mitochondrial tRNA(Ser(UCN)) gene detected in a family with MERRF/MELAS overlap syndrome." Biochem Biophys Res Commun **214**(1): 86-93.
- Naldini, L., U. Blomer, F. H. Gage, D. Trono and I. M. Verma (1996). "Efficient transfer, integration, and sustained long-term expression of the transgene in adult rat brains injected with a lentiviral vector." Proc Natl Acad Sci U S A **93**(21): 11382-11388.
- Nasca, A., T. Rizza, M. Doimo, A. Legati, A. Ciolfi, D. Diodato, C. Calderan, G. Carrara, E. Lamantea, C. Aiello, M. Di Nottia, M. Niceta, C. Lamperti, A. Ardisson, S. Bianchi-Marzoli, G. Iarossi, E. Bertini, I. Moroni, M. Tartaglia, L. Salviati, R. Carozzo and D. Ghezzi (2017). "Not only dominant, not only optic atrophy: expanding the clinical spectrum associated with OPA1 mutations." Orphanet J Rare Dis **12**(1): 89.
- National Center for Biotechnology Information, N. L. o. M. "Database of Single Nucleotide Polymorphisms (dbSNP)." from <http://www.ncbi.nlm.nih.gov/SNP/>.
- Newman, N. J. (2009). "Leber hereditary optic neuropathy: bad habits, bad vision?" Brain **132**(Pt 9): 2306-2308.
- Ng, S. B., E. H. Turner, P. D. Robertson, S. D. Flygare, A. W. Bigham, C. Lee, T. Shaffer, M. Wong, A. Bhattacharjee, E. E. Eichler, M. Bamshad, D. A. Nickerson and J.

- Shendure (2009). "Targeted capture and massively parallel sequencing of 12 human exomes." Nature **461**(7261): 272-276.
- Nica, A. C. and E. T. Dermitzakis (2013). "Expression quantitative trait loci: present and future." Philos Trans R Soc Lond B Biol Sci **368**(1620): 20120362.
- Nicholls, T. J. and M. Minczuk (2014). "In D-loop: 40 years of mitochondrial 7S DNA." Exp Gerontol **56**: 175-181.
- Nikkanen, J., S. Forsstrom, L. Euro, I. Paetau, R. A. Kohnz, L. Wang, D. Chilov, J. Viinamaki, A. Roivainen, P. Marjamaki, H. Liljenback, S. Ahola, J. Buzkova, M. Terzioglu, N. A. Khan, S. Pirnes-Karhu, A. Paetau, T. Lonqvist, A. Sajantila, P. Isohanni, H. Tyynismaa, D. K. Nomura, B. J. Battersby, V. Velagapudi, C. J. Carroll and A. Suomalainen (2016). "Mitochondrial DNA Replication Defects Disturb Cellular dNTP Pools and Remodel One-Carbon Metabolism." Cell Metab **23**(4): 635-648.
- Nishino, I., A. Spinazzola and M. Hirano (1999). "Thymidine phosphorylase gene mutations in MNGIE, a human mitochondrial disorder." Science **283**(5402): 689-692.
- Noguchi, Y., T. Yashima, T. Ito, T. Sumi, T. Tsuzuku and K. Kitamura (2004). "Audiovestibular findings in patients with mitochondrial A1555G mutation." Laryngoscope **114**(2): 344-348.
- Nordang, L., E. Cestreicher, W. Arnold and M. Anniko (2000). "Glutamate is the afferent neurotransmitter in the human cochlea." Acta Otolaryngol **120**(3): 359-362.
- Nunnari, J. and A. Suomalainen (2012). "Mitochondria: in sickness and in health." Cell **148**(6): 1145-1159.
- Nye, J. S., E. A. Hayes, M. Amendola, D. Vaughn, J. Charrow, D. G. McLone, M. C. Speer, W. E. Nance and A. Pandya (2000). "Myelocystocele-cloacal exstrophy in a pedigree with a mitochondrial 12S rRNA mutation, aminoglycoside-induced deafness, pigmentary disturbances, and spinal anomalies." Teratology **61**(3): 165-171.

- O'Brien, T. W. (1971). "The general occurrence of 55 S ribosomes in mammalian liver mitochondria." J Biol Chem **246**(10): 3409-3417.
- O'Sullivan, M., P. Rutland, D. Lucas, E. Ashton, S. Hendricks, S. Rahman and M. Bitner-Glindzicz (2015). "Mitochondrial m.1584A 12S m62A rRNA methylation in families with m.1555A>G associated hearing loss." Hum Mol Genet **24**(4): 1036-1044.
- Oh, H. Y., X. Jin, J. G. Kim, M. J. Oh, X. Pian, J. M. Kim, M. S. Yoon, C. I. Son, Y. S. Lee, K. C. Hong, H. Kim, Y. J. Choi and K. Y. Whang (2007). "Characteristics of primary and immortalized fibroblast cells derived from the miniature and domestic pigs." BMC Cell Biol **8**: 20.
- Oliveira, M. T. and L. S. Kaguni (2011). "Reduced stimulation of recombinant DNA polymerase gamma and mitochondrial DNA (mtDNA) helicase by variants of mitochondrial single-stranded DNA-binding protein (mtSSB) correlates with defects in mtDNA replication in animal cells." J Biol Chem **286**(47): 40649-40658.
- Omura, T. (1998). "Mitochondria-targeting sequence, a multi-role sorting sequence recognized at all steps of protein import into mitochondria." J Biochem **123**(6): 1010-1016.
- Oshima, K., K. Shin, M. Diensthuber, A. W. Peng, A. J. Ricci and S. Heller (2010). "Mechanosensitive hair cell-like cells from embryonic and induced pluripotent stem cells." Cell **141**(4): 704-716.
- Otaegui, D., H. Irizar, M. Goicoechea, J. Perez-Tur, M. Belar and A. Lopez de Munain (2008). "Molecular characterization of putative modulatory factors in two Spanish families with A1555G deafness." Audiol Neurootol **13**(5): 320-327.
- Ott, M., V. Gogvadze, S. Orrenius and B. Zhivotovsky (2007). "Mitochondria, oxidative stress and cell death." Apoptosis **12**(5): 913-922.
- Ott, M. and J. M. Herrmann (2010). "Co-translational membrane insertion of mitochondrially encoded proteins." Biochim Biophys Acta **1803**(6): 767-775.

- Pacheu-Grau, D., A. Gomez-Duran, E. Lopez-Gallardo, T. Pinos, A. L. Andreu, M. J. Lopez-Perez, J. Montoya and E. Ruiz-Pesini (2011). "'Progress' renders detrimental an ancient mitochondrial DNA genetic variant." Hum Mol Genet **20**(21): 4224-4231.
- Pakos-Zebrucka, K., I. Koryga, K. Mnich, M. Ljujic, A. Samali and A. M. Gorman (2016). "The integrated stress response." EMBO Rep **17**(10): 1374-1395.
- Pandya, A., X. Xia, J. Radnaabazar, J. Batsuuri, B. Dangaansuren, N. Fischel-Ghodsian and W. E. Nance (1997). "Mutation in the mitochondrial 12S rRNA gene in two families from Mongolia with matrilineal aminoglycoside ototoxicity." J Med Genet **34**(2): 169-172.
- Paradies, G., V. Paradies, V. De Benedictis, F. M. Ruggiero and G. Petrosillo (2014). "Functional role of cardiolipin in mitochondrial bioenergetics." Biochim Biophys Acta **1837**(4): 408-417.
- Parikh, S., A. Goldstein, M. K. Koenig, F. Scaglia, G. M. Enns, R. Saneto, I. Anselm, B. H. Cohen, M. J. Falk, C. Greene, A. L. Gropman, R. Haas, M. Hirano, P. Morgan, K. Sims, M. Tarnopolsky, J. L. Van Hove, L. Wolfe and S. DiMauro (2015). "Diagnosis and management of mitochondrial disease: a consensus statement from the Mitochondrial Medicine Society." Genet Med **17**(9): 689-701.
- Partington, S. L., M. M. Givertz, S. Gupta and R. Y. Kwong (2011). "Cardiac magnetic resonance aids in the diagnosis of mitochondrial cardiomyopathy." Circulation **123**(6): e227-229.
- Payne, B. A. and P. F. Chinnery (2015). "Mitochondrial dysfunction in aging: Much progress but many unresolved questions." Biochim Biophys Acta **1847**(11): 1347-1353.
- Peng, M., J. Ostrovsky, Y. J. Kwon, E. Polyak, J. Licata, M. Tsukikawa, E. Marty, J. Thomas, C. A. Felix, R. Xiao, Z. Zhang, D. L. Gasser, Y. Argon and M. J. Falk (2015). "Inhibiting cytosolic translation and autophagy improves health in mitochondrial disease." Hum Mol Genet **24**(17): 4829-4847.

- Pernas, L. and L. Scorrano (2016). "Mito-Morphosis: Mitochondrial Fusion, Fission, and Cristae Remodeling as Key Mediators of Cellular Function." Annu Rev Physiol **78**: 505-531.
- Phasukkijwatana, N., B. Kunhapan, J. Stankovich, W. L. Chuenkongkaew, R. Thomson, T. Thornton, M. Bahlo, T. Mushiroda, Y. Nakamura, S. Mahasirimongkol, A. W. Tun, C. Srisawat, C. Limwongse, C. Peerapittayamongkol, T. Sura, W. Suthammarak and P. Lertrit (2010). "Genome-wide linkage scan and association study of PARL to the expression of LHON families in Thailand." Hum Genet **128**(1): 39-49.
- Phillips, P. C. (2008). "Epistasis--the essential role of gene interactions in the structure and evolution of genetic systems." Nat Rev Genet **9**(11): 855-867.
- Picard, M., D. C. Wallace and Y. Burrelle (2016). "The rise of mitochondria in medicine." Mitochondrion **30**: 105-116.
- Pickrell, A. M. and R. J. Youle (2013). "Mitochondrial disease: mtDNA and protein segregation mysteries in iPSCs." Curr Biol **23**(23): R1052-1054.
- Pohjoismaki, J. L., S. Wanrooij, A. K. Hyvarinen, S. Goffart, I. J. Holt, J. N. Spelbrink and H. T. Jacobs (2006). "Alterations to the expression level of mitochondrial transcription factor A, TFAM, modify the mode of mitochondrial DNA replication in cultured human cells." Nucleic Acids Res **34**(20): 5815-5828.
- Porsch-Ozcurumez, M., N. Kischel, H. Priebe, W. Splettstosser, E. J. Finke and R. Grunow (2004). "Comparison of enzyme-linked immunosorbent assay, Western blotting, microagglutination, indirect immunofluorescence assay, and flow cytometry for serological diagnosis of tularemia." Clin Diagn Lab Immunol **11**(6): 1008-1015.
- Posse, V., S. Shahzad, M. Falkenberg, B. M. Hallberg and C. M. Gustafsson (2015). "TEFM is a potent stimulator of mitochondrial transcription elongation in vitro." Nucleic Acids Res **43**(5): 2615-2624.
- Prezant, T. R., J. V. Agapian, M. C. Bohlman, X. Bu, S. Oztas, W. Q. Qiu, K. S. Arnos, G. A. Cortopassi, L. Jaber, J. I. Rotter and et al. (1993). "Mitochondrial ribosomal

- RNA mutation associated with both antibiotic-induced and non-syndromic deafness." Nat Genet **4**(3): 289-294.
- Priuska, E. M. and J. Schacht (1997). "Mechanism and prevention of aminoglycoside ototoxicity: outer hair cells as targets and tools." Ear Nose Throat J **76**(3): 164-166, 168, 170-161.
- Prudent, J., R. Zunino, A. Sugiura, S. Mattie, G. C. Shore and H. M. McBride (2015). "MAPL SUMOylation of Drp1 Stabilizes an ER/Mitochondrial Platform Required for Cell Death." Mol Cell **59**(6): 941-955.
- Puranam, R. S. and G. Attardi (2001). "The RNase P associated with HeLa cell mitochondria contains an essential RNA component identical in sequence to that of the nuclear RNase P." Mol Cell Biol **21**(2): 548-561.
- Purohit, P. and S. Stern (1994). "Interactions of a small RNA with antibiotic and RNA ligands of the 30S subunit." Nature **370**(6491): 659-662.
- Purves (2008). Neuroscience, Sinauer Associates.
- Pyle, A., G. Hudson, I. J. Wilson, J. Coxhead, T. Smertenko, M. Herbert, M. Santibanez-Koref and P. F. Chinnery (2015). "Extreme-Depth Re-sequencing of Mitochondrial DNA Finds No Evidence of Paternal Transmission in Humans." PLoS Genet **11**(5): e1005040.
- Qian, Y. and M. X. Guan (2009). "Interaction of aminoglycosides with human mitochondrial 12S rRNA carrying the deafness-associated mutation." Antimicrob Agents Chemother **53**(11): 4612-4618.
- Quiros, P. M., A. Mottis and J. Auwerx (2016). "Mitonuclear communication in homeostasis and stress." Nat Rev Mol Cell Biol **17**(4): 213-226.
- Rabbani, B., M. Tekin and N. Mahdieh (2014). "The promise of whole-exome sequencing in medical genetics." J Hum Genet **59**(1): 5-15.
- Rahman, S., R. Ecob, H. Costello, M. G. Sweeney, A. J. Duncan, K. Pearce, D. Strachan, A. Forge, A. Davis and M. Bitner-Glindzicz (2012). "Hearing in 44-45 year olds

with m.1555A>G, a genetic mutation predisposing to aminoglycoside-induced deafness: a population based cohort study." BMJ Open **2**: e000411.

Raimundo, N., L. Song, T. E. Shutt, S. E. McKay, J. Cotney, M. X. Guan, T. C. Gilliland, D. Hohuan, J. Santos-Sacchi and G. S. Shadel (2012). "Mitochondrial stress engages E2F1 apoptotic signaling to cause deafness." Cell **148**(4): 716-726.

Recht, M. I., D. Fourmy, S. C. Blanchard, K. D. Dahlquist and J. D. Puglisi (1996). "RNA sequence determinants for aminoglycoside binding to an A-site rRNA model oligonucleotide." J Mol Biol **262**(4): 421-436.

Reichert, A. S. and W. Neupert (2002). "Contact sites between the outer and inner membrane of mitochondria-role in protein transport." Biochim Biophys Acta **1592**(1): 41-49.

Reyes, A., C. Gissi, G. Pesole and C. Saccone (1998). "Asymmetrical directional mutation pressure in the mitochondrial genome of mammals." Mol Biol Evol **15**(8): 957-966.

Reyes, A., L. Kazak, S. R. Wood, T. Yasukawa, H. T. Jacobs and I. J. Holt (2013). "Mitochondrial DNA replication proceeds via a 'bootlace' mechanism involving the incorporation of processed transcripts." Nucleic Acids Res **41**(11): 5837-5850.

Reyes, A., L. Melchionda, A. Nasca, F. Carrara, E. Lamantea, A. Zanolini, C. Lamperti, M. Fang, J. Zhang, D. Ronchi, S. Bonato, G. Fagiolari, M. Moggio, D. Ghezzi and M. Zeviani (2015). "RNASEH1 Mutations Impair mtDNA Replication and Cause Adult-Onset Mitochondrial Encephalomyopathy." Am J Hum Genet **97**(1): 186-193.

Richard, D. J., E. Bolderson, L. Cubeddu, R. I. Wadsworth, K. Savage, G. G. Sharma, M. L. Nicolette, S. Tsvetanov, M. J. McIlwraith, R. K. Pandita, S. Takeda, R. T. Hay, J. Gautier, S. C. West, T. T. Paull, T. K. Pandita, M. F. White and K. K. Khanna (2008). "Single-stranded DNA-binding protein hSSB1 is critical for genomic stability." Nature **453**(7195): 677-681.

Richardson, G. P. and I. J. Russell (1991). "Cochlear cultures as a model system for studying aminoglycoside induced ototoxicity." Hear Res **53**(2): 293-311.

- Robinson, B. H., R. Petrova-Benedict, J. R. Buncic and D. C. Wallace (1992). "Nonviability of cells with oxidative defects in galactose medium: a screening test for affected patient fibroblasts." Biochem Med Metab Biol **48**(2): 122-126.
- Robinson, P. N. (2012). "Deep phenotyping for precision medicine." Hum Mutat **33**(5): 777-780.
- Ropp, P. A. and W. C. Copeland (1996). "Cloning and characterization of the human mitochondrial DNA polymerase, DNA polymerase gamma." Genomics **36**(3): 449-458.
- Rorbach, J. and M. Minczuk (2012). "The post-transcriptional life of mammalian mitochondrial RNA." Biochem J **444**(3): 357-373.
- Rorbach, J., R. Richter, H. J. Wessels, M. Wydro, M. Pekalski, M. Farhoud, I. Kuhl, M. Gaisne, N. Bonnefoy, J. A. Smeitink, R. N. Lightowers and Z. M. Chrzanowska-Lightowers (2008). "The human mitochondrial ribosome recycling factor is essential for cell viability." Nucleic Acids Res **36**(18): 5787-5799.
- Rubio-Cosials, A., J. F. Sidow, N. Jimenez-Menendez, P. Fernandez-Millan, J. Montoya, H. T. Jacobs, M. Coll, P. Bernado and M. Sola (2011). "Human mitochondrial transcription factor A induces a U-turn structure in the light strand promoter." Nat Struct Mol Biol **18**(11): 1281-1289.
- Rudolph, C. J., A. L. Upton, A. Stockum, C. A. Nieduszynski and R. G. Lloyd (2013). "Avoiding chromosome pathology when replication forks collide." Nature **500**(7464): 608-611.
- Ruhanen, H., S. Borrie, G. Szabadkai, H. Tynismaa, A. W. Jones, D. Kang, J. W. Taanman and T. Yasukawa (2010). "Mitochondrial single-stranded DNA binding protein is required for maintenance of mitochondrial DNA and 7S DNA but is not required for mitochondrial nucleoid organisation." Biochim Biophys Acta **1803**(8): 931-939.
- Saada, A., A. Shaag, S. Arnon, T. Dolfen, C. Miller, D. Fuchs-Telem, A. Lombes and O. Elpeleg (2007). "Antenatal mitochondrial disease caused by mitochondrial ribosomal protein (MRPS22) mutation." J Med Genet **44**(12): 784-786.

- Saeed, H., H. R. Powell and S. R. Saeed (2016). "Cochlear implantation in X-linked deafness - How to manage the surgical challenges." Cochlear Implants Int **17**(4): 178-183.
- Sala, A. J., L. C. Bott and R. I. Morimoto (2017). "Shaping proteostasis at the cellular, tissue, and organismal level." J Cell Biol **216**(5): 1231-1241.
- Samuels, D. C., E. A. Schon and P. F. Chinnery (2004). "Two direct repeats cause most human mtDNA deletions." Trends Genet **20**(9): 393-398.
- Sanger, F., S. Nicklen and A. R. Coulson (1977). "DNA sequencing with chain-terminating inhibitors." Proc Natl Acad Sci U S A **74**(12): 5463-5467.
- Santarelli, R., R. Rossi, P. Scimemi, E. Cama, M. L. Valentino, C. La Morgia, L. Caporali, R. Liguori, V. Magnavita, A. Monteleone, A. Biscaro, E. Arslan and V. Carelli (2015). "OPA1-related auditory neuropathy: site of lesion and outcome of cochlear implantation." Brain **138**(Pt 3): 563-576.
- Santorelli, F. M., S. C. Mak, M. El-Schahawi, C. Casali, S. Shanske, T. Z. Baram, R. E. Madrid and S. DiMauro (1996). "Maternally inherited cardiomyopathy and hearing loss associated with a novel mutation in the mitochondrial tRNA(Lys) gene (G8363A)." Am J Hum Genet **58**(5): 933-939.
- Santorelli, F. M., K. Tanji, P. Manta, C. Casali, S. Krishna, A. P. Hays, D. M. Mancini, S. DiMauro and M. Hirano (1999). "Maternally inherited cardiomyopathy: an atypical presentation of the mtDNA 12S rRNA gene A1555G mutation." Am J Hum Genet **64**(1): 295-300.
- Sargiannidou, I., G. H. Kim, S. Kyriakoudi, B. L. Eun and K. A. Kleopa (2015). "A start codon CMT1X mutation associated with transient encephalomyelitis causes complete loss of Cx32." Neurogenetics **16**(3): 193-200.
- Sarkar, S., S. Mukherjee, A. Chattopadhyay and S. Bhattacharya (2017). "Differential modulation of cellular antioxidant status in zebrafish liver and kidney exposed to low dose arsenic trioxide." Ecotoxicol Environ Saf **135**: 173-182.

- Satoh, M. and T. Kuroiwa (1991). "Organization of multiple nucleoids and DNA molecules in mitochondria of a human cell." Exp Cell Res **196**(1): 137-140.
- Sauvanet, C., S. Duvezin-Caubet, J. P. di Rago and M. Rojo (2010). "Energetic requirements and bioenergetic modulation of mitochondrial morphology and dynamics." Semin Cell Dev Biol **21**(6): 558-565.
- Sauvanet, C., S. Duvezin-Caubet, B. Salin, C. David, A. Massoni-Laporte, J. P. di Rago and M. Rojo (2012). "Mitochondrial DNA mutations provoke dominant inhibition of mitochondrial inner membrane fusion." PLoS One **7**(11): e49639.
- Sbisa, E., F. Tanzariello, A. Reyes, G. Pesole and C. Saccone (1997). "Mammalian mitochondrial D-loop region structural analysis: identification of new conserved sequences and their functional and evolutionary implications." Gene **205**(1-2): 125-140.
- Scarpelli, M., A. Todeschini, F. Rinaldi, S. Rota, A. Padovani and M. Filosto (2014). "Strategies for treating mitochondrial disorders: an update." Mol Genet Metab **113**(4): 253-260.
- Scarpelli, M., F. Zappini, M. Filosto, A. Russignan, P. Tonin and G. Tomelleri (2012). "Mitochondrial Sensorineural Hearing Loss: A Retrospective Study and a Description of Cochlear Implantation in a MELAS Patient." Genet Res Int **2012**: 287432.
- Schaefer, A. M., R. McFarland, E. L. Blakely, L. He, R. G. Whittaker, R. W. Taylor, P. F. Chinnery and D. M. Turnbull (2008). "Prevalence of mitochondrial DNA disease in adults." Ann Neurol **63**(1): 35-39.
- Schoonbroodt, S., V. Ferreira, M. Best-Belpomme, J. R. Boelaert, S. Legrand-Poels, M. Korner and J. Piette (2000). "Crucial role of the amino-terminal tyrosine residue 42 and the carboxyl-terminal PEST domain of I kappa B alpha in NF-kappa B activation by an oxidative stress." J Immunol **164**(8): 4292-4300.
- Schwartz, M. and J. Vissing (2002). "Paternal inheritance of mitochondrial DNA." N Engl J Med **347**(8): 576-580.

- Schwarz, J. M., C. Rodelsperger, M. Schuelke and D. Seelow (2010). "MutationTaster evaluates disease-causing potential of sequence alterations." Nat Methods **7**(8): 575-576.
- Seidel-Rogol, B. L., V. McCulloch and G. S. Shadel (2003). "Human mitochondrial transcription factor B1 methylates ribosomal RNA at a conserved stem-loop." Nat Genet **33**(1): 23-24.
- Seiferling, D. (2015). Regulation of the mammalian mitochondrial unfolded protein response, University of Cologne.
- Sena, L. A. and N. S. Chandel (2012). "Physiological roles of mitochondrial reactive oxygen species." Mol Cell **48**(2): 158-167.
- Seviour, K. B., A. Hatamochi, I. A. Stewart, Y. Bykhovskaya, D. R. Allen-Powell, N. Fischel-Ghodsian and M. A. Maw (1998). "Mitochondrial A7445G mutation in two pedigrees with palmoplantar keratoderma and deafness." Am J Med Genet **75**(2): 179-185.
- Shadel, G. S. (2008). "Expression and maintenance of mitochondrial DNA: new insights into human disease pathology." Am J Pathol **172**(6): 1445-1456.
- Shadel, G. S. and T. L. Horvath (2015). "Mitochondrial ROS signaling in organismal homeostasis." Cell **163**(3): 560-569.
- Shankar, S. P., J. H. Fingert, V. Carelli, M. L. Valentino, T. M. King, S. P. Daiger, S. R. Salomao, A. Berezovsky, R. Belfort, Jr., T. A. Braun, V. C. Sheffield, A. A. Sadun and E. M. Stone (2008). "Evidence for a novel x-linked modifier locus for leber hereditary optic neuropathy." Ophthalmic Genet **29**(1): 17-24.
- Shearer, A. E., R. W. Eppsteiner, K. T. Booth, S. S. Ephraim, J. Gurrola, 2nd, A. Simpson, E. A. Black-Ziegelbein, S. Joshi, H. Ravi, A. C. Giuffre, S. Happe, M. S. Hildebrand, H. Azaiez, Y. A. Bayazit, M. E. Erdal, J. A. Lopez-Escamez, I. Gazquez, M. L. Tamayo, N. Y. Gelvez, G. L. Leal, C. Jalas, J. Ekstein, T. Yang, S. Usami, K. Kahrizi, N. Bazazzadegan, H. Najmabadi, T. E. Scheetz, T. A. Braun, T. L. Casavant, E. M. LeProust and R. J. Smith (2014). "Utilizing ethnic-specific

- differences in minor allele frequency to recategorize reported pathogenic deafness variants." Am J Hum Genet **95**(4): 445-453.
- Shearer, A. E., D. L. Kolbe, H. Azaiez, C. M. Sloan, K. L. Frees, A. E. Weaver, E. T. Clark, C. J. Nishimura, E. A. Black-Ziegelbein and R. J. Smith (2014). "Copy number variants are a common cause of non-syndromic hearing loss." Genome Med **6**(5): 37.
- Shendure, J. and H. Ji (2008). "Next-generation DNA sequencing." Nat Biotechnol **26**(10): 1135-1145.
- Shi, Y., A. Dierckx, P. H. Wanrooij, S. Wanrooij, N. G. Larsson, L. M. Wilhelmsson, M. Falkenberg and C. M. Gustafsson (2012). "Mammalian transcription factor A is a core component of the mitochondrial transcription machinery." Proc Natl Acad Sci U S A **109**(41): 16510-16515.
- Shoffner, J. M., M. T. Lott, A. S. Voljavec, S. A. Soueidan, D. A. Costigan and D. C. Wallace (1989). "Spontaneous Kearns-Sayre/chronic external ophthalmoplegia plus syndrome associated with a mitochondrial DNA deletion: a slip-replication model and metabolic therapy." Proc Natl Acad Sci U S A **86**(20): 7952-7956.
- Showkat, M., M. A. Beigh and K. I. Andrabi (2014). "mTOR Signaling in Protein Translation Regulation: Implications in Cancer Genesis and Therapeutic Interventions." Mol Biol Int **2014**: 686984.
- Sim, L., R. Quezada-Calvillo, E. E. Sterchi, B. L. Nichols and D. R. Rose (2008). "Human intestinal maltase-glucoamylase: crystal structure of the N-terminal catalytic subunit and basis of inhibition and substrate specificity." J Mol Biol **375**(3): 782-792.
- Slatkin, M. (2008). "Linkage disequilibrium--understanding the evolutionary past and mapping the medical future." Nat Rev Genet **9**(6): 477-485.
- Smeitink, J., L. van den Heuvel and S. DiMauro (2001). "The genetics and pathology of oxidative phosphorylation." Nat Rev Genet **2**(5): 342-352.

- Smith, A. C. and A. J. Robinson (2016). "MitoMiner v3.1, an update on the mitochondrial proteomics database." Nucleic Acids Res **44**(D1): D1258-1261.
- Spelbrink, J. N., F. Y. Li, V. Tiranti, K. Nikali, Q. P. Yuan, M. Tariq, S. Wanrooij, N. Garrido, G. Comi, L. Morandi, L. Santoro, A. Toscano, G. M. Fabrizi, H. Somer, R. Croxen, D. Beeson, J. Poulton, A. Suomalainen, H. T. Jacobs, M. Zeviani and C. Larsson (2001). "Human mitochondrial DNA deletions associated with mutations in the gene encoding Twinkle, a phage T7 gene 4-like protein localized in mitochondria." Nat Genet **28**(3): 223-231.
- Spielmann, M. and S. Mundlos (2016). "Looking beyond the genes: the role of non-coding variants in human disease." Hum Mol Genet **25**(R2): R157-R165.
- Spinazzi, M., S. Cazzola, M. Bortolozzi, A. Baracca, E. Loro, A. Casarin, G. Solaini, G. Sgarbi, G. Casalena, G. Cenacchi, A. Malena, C. Frezza, F. Carrara, C. Angelini, L. Scorrano, L. Salviati and L. Vergani (2008). "A novel deletion in the GTPase domain of OPA1 causes defects in mitochondrial morphology and distribution, but not in function." Hum Mol Genet **17**(21): 3291-3302.
- Spinazzola, A., C. Viscomi, E. Fernandez-Vizarra, F. Carrara, P. D'Adamo, S. Calvo, R. M. Marsano, C. Donnini, H. Weiher, P. Strisciuglio, R. Parini, E. Sarzi, A. Chan, S. DiMauro, A. Rotig, P. Gasparini, I. Ferrero, V. K. Mootha, V. Tiranti and M. Zeviani (2006). "MPV17 encodes an inner mitochondrial membrane protein and is mutated in infantile hepatic mitochondrial DNA depletion." Nat Genet **38**(5): 570-575.
- Sprenger, A., V. Kuttner, M. L. Biniossek, C. Gretzmeier, M. Boerries, C. Mack, C. Has, L. Bruckner-Tuderman and J. Dengjel (2010). "Comparative quantitation of proteome alterations induced by aging or immortalization in primary human fibroblasts and keratinocytes for clinical applications." Mol Biosyst **6**(9): 1579-1582.
- Srour, M., N. Shimokawa, F. F. Hamdan, C. Nassif, C. Poulin, L. Al Gazali, J. A. Rosenfeld, N. Koibuchi, G. A. Rouleau, A. Al Shamsi and J. L. Michaud (2017). "Dysfunction of the Cerebral Glucose Transporter SLC45A1 in Individuals with Intellectual Disability and Epilepsy." Am J Hum Genet **100**(5): 824-830.

- Stark, G. (2005). "Functional consequences of oxidative membrane damage." J Membr Biol **205**(1): 1-16.
- Stenson, P. D., M. Mort, E. V. Ball, K. Evans, M. Hayden, S. Heywood, M. Hussain, A. D. Phillips and D. N. Cooper (2017). "The Human Gene Mutation Database: towards a comprehensive repository of inherited mutation data for medical research, genetic diagnosis and next-generation sequencing studies." Hum Genet.
- Stewart, J. B. and P. F. Chinnery (2015). "The dynamics of mitochondrial DNA heteroplasmy: implications for human health and disease." Nat Rev Genet **16**(9): 530-542.
- Stewart, J. D., S. Schoeler, K. S. Sitarz, R. Horvath, K. Hallmann, A. Pyle, P. Yu-Wai-Man, R. W. Taylor, D. C. Samuels, W. S. Kunz and P. F. Chinnery (2011). "POLG mutations cause decreased mitochondrial DNA repopulation rates following induced depletion in human fibroblasts." Biochim Biophys Acta **1812**(3): 321-325.
- Stock, D., C. Gibbons, I. Arechaga, A. G. Leslie and J. E. Walker (2000). "The rotary mechanism of ATP synthase." Curr Opin Struct Biol **10**(6): 672-679.
- Sue, C. M., L. J. Lipsett, D. S. Crimmins, C. S. Tsang, S. C. Boyages, C. M. Presgrave, W. P. Gibson, E. Byrne and J. G. Morris (1998). "Cochlear origin of hearing loss in MELAS syndrome." Ann Neurol **43**(3): 350-359.
- Sukhorukov, V. M., D. Dikov, A. S. Reichert and M. Meyer-Hermann (2012). "Emergence of the mitochondrial reticulum from fission and fusion dynamics." PLoS Comput Biol **8**(10): e1002745.
- Sun, F., X. Huo, Y. Zhai, A. Wang, J. Xu, D. Su, M. Bartlam and Z. Rao (2005). "Crystal structure of mitochondrial respiratory membrane protein complex II." Cell **121**(7): 1043-1057.
- Superti-Furga, A., E. Schoenle, P. Tuchschnid, R. Caduff, V. Sabato, D. DeMattia, R. Gitzelmann and B. Steinmann (1993). "Pearson bone marrow-pancreas syndrome with insulin-dependent diabetes, progressive renal tubulopathy, organic aciduria and elevated fetal haemoglobin caused by deletion and duplication of mitochondrial DNA." Eur J Pediatr **152**(1): 44-50.

- Sutovsky, P., R. D. Moreno, J. Ramalho-Santos, T. Dominko, C. Simerly and G. Schatten (2000). "Ubiquitinated sperm mitochondria, selective proteolysis, and the regulation of mitochondrial inheritance in mammalian embryos." Biol Reprod **63**(2): 582-590.
- Suzuki, T. and T. Suzuki (2014). "A complete landscape of post-transcriptional modifications in mammalian mitochondrial tRNAs." Nucleic Acids Res **42**(11): 7346-7357.
- Swalwell, H., E. L. Blakely, R. Sutton, K. Tonska, M. Elstner, L. He, T. Taivassalo, D. K. Burns, D. M. Turnbull, R. G. Haller, M. M. Davidson and R. W. Taylor (2008). "A homoplasmic mtDNA variant can influence the phenotype of the pathogenic m.7472Cins MTTTS1 mutation: are two mutations better than one?" Eur J Hum Genet **16**(10): 1265-1274.
- Takamatsu, C., S. Umeda, T. Ohsato, T. Ohno, Y. Abe, A. Fukuoh, H. Shinagawa, N. Hamasaki and D. Kang (2002). "Regulation of mitochondrial D-loops by transcription factor A and single-stranded DNA-binding protein." EMBO Rep **3**(5): 451-456.
- Tan, B. G., F. C. Wellesley, N. J. Savery and M. D. Szczelkun (2016). "Length heterogeneity at conserved sequence block 2 in human mitochondrial DNA acts as a rheostat for RNA polymerase POLRMT activity." Nucleic Acids Res **44**(16): 7817-7829.
- Tan, K., M. Fujimoto, R. Takii, E. Takaki, N. Hayashida and A. Nakai (2015). "Mitochondrial SSBP1 protects cells from proteotoxic stresses by potentiating stress-induced HSF1 transcriptional activity." Nat Commun **6**: 6580.
- Taylor, R. W., C. Giordano, M. M. Davidson, G. d'Amati, H. Bain, C. M. Hayes, H. Leonard, M. J. Barron, C. Casali, F. M. Santorelli, M. Hirano, R. N. Lightowers, S. DiMauro and D. M. Turnbull (2003). "A homoplasmic mitochondrial transfer ribonucleic acid mutation as a cause of maternally inherited hypertrophic cardiomyopathy." J Am Coll Cardiol **41**(10): 1786-1796.

- Taylor, R. W., A. M. Schaefer, M. J. Barron, R. McFarland and D. M. Turnbull (2004). "The diagnosis of mitochondrial muscle disease." Neuromuscul Disord **14**(4): 237-245.
- Terry, B., R. E. Kelt and A. Jeyakumar (2015). "Delayed Complications After Cochlear Implantation." JAMA Otolaryngol Head Neck Surg **141**(11): 1012-1017.
- Tiranti, V., P. Corona, M. Greco, J. W. Taanman, F. Carrara, E. Lamantea, L. Nijtmans, G. Uziel and M. Zeviani (2000). "A novel frameshift mutation of the mtDNA COIII gene leads to impaired assembly of cytochrome c oxidase in a patient affected by Leigh-like syndrome." Hum Mol Genet **9**(18): 2733-2742.
- Tiranti, V., E. Rossi, A. Ruiz-Carrillo, G. Rossi, M. Rocchi, S. DiDonato, O. Zuffardi and M. Zeviani (1995). "Chromosomal localization of mitochondrial transcription factor A (TCF6), single-stranded DNA-binding protein (SSBP), and endonuclease G (ENDOG), three human housekeeping genes involved in mitochondrial biogenesis." Genomics **25**(2): 559-564.
- Tiranti, V., A. Savoia, F. Forti, M. F. D'Apolito, M. Centra, M. Rocchi and M. Zeviani (1997). "Identification of the gene encoding the human mitochondrial RNA polymerase (h-mtRPOL) by cyberscreening of the Expressed Sequence Tags database." Hum Mol Genet **6**(4): 615-625.
- Tomecki, R., A. Dmochowska, K. Gewartowski, A. Dziembowski and P. P. Stepień (2004). "Identification of a novel human nuclear-encoded mitochondrial poly(A) polymerase." Nucleic Acids Res **32**(20): 6001-6014.
- Tondera, D., S. Grandemange, A. Jourdain, M. Karbowski, Y. Mattenberger, S. Herzig, S. Da Cruz, P. Clerc, I. Raschke, C. Merkwirth, S. Ehses, F. Krause, D. C. Chan, C. Alexander, C. Bauer, R. Youle, T. Langer and J. C. Martinou (2009). "SLP-2 is required for stress-induced mitochondrial hyperfusion." EMBO J **28**(11): 1589-1600.
- Torraco, A., S. Peralta, L. Iommarini and F. Diaz (2015). "Mitochondrial Diseases Part I: mouse models of OXPHOS deficiencies caused by defects in respiratory complex subunits or assembly factors." Mitochondrion **21**: 76-91.

- Torrioni, A., F. Cruciani, C. Rengo, D. Sellitto, N. Lopez-Bigas, R. Rabionet, N. Govea, A. Lopez De Munain, M. Sarduy, L. Romero, M. Villamar, I. del Castillo, F. Moreno, X. Estivill and R. Scozzari (1999). "The A1555G mutation in the 12S rRNA gene of human mtDNA: recurrent origins and founder events in families affected by sensorineural deafness." Am J Hum Genet **65**(5): 1349-1358.
- Torrioni, A., K. Huoponen, P. Francalacci, M. Petrozzi, L. Morelli, R. Scozzari, D. Obinu, M. L. Savontaus and D. C. Wallace (1996). "Classification of European mtDNAs from an analysis of three European populations." Genetics **144**(4): 1835-1850.
- Townsend, D. M., K. D. Tew and H. Tapiero (2003). "The importance of glutathione in human disease." Biomed Pharmacother **57**(3-4): 145-155.
- Toyama, E. Q., S. Herzig, J. Curchet, T. L. Lewis, Jr., O. C. Loson, K. Hellberg, N. P. Young, H. Chen, F. Polleux, D. C. Chan and R. J. Shaw (2016). "Metabolism. AMP-activated protein kinase mediates mitochondrial fission in response to energy stress." Science **351**(6270): 275-281.
- Trifunovic, A., A. Hansson, A. Wredenberg, A. T. Rovio, E. Dufour, I. Khvorostov, J. N. Spelbrink, R. Wibom, H. T. Jacobs and N. G. Larsson (2005). "Somatic mtDNA mutations cause aging phenotypes without affecting reactive oxygen species production." Proc Natl Acad Sci U S A **102**(50): 17993-17998.
- Trinklein, N. D., W. C. Chen, R. E. Kingston and R. M. Myers (2004). "Transcriptional regulation and binding of heat shock factor 1 and heat shock factor 2 to 32 human heat shock genes during thermal stress and differentiation." Cell Stress Chaperones **9**(1): 21-28.
- Tsao, K., P. A. Aitken and D. R. Johns (1999). "Smoking as an aetiological factor in a pedigree with Leber's hereditary optic neuropathy." Br J Ophthalmol **83**(5): 577-581.
- Tsuboi, M., H. Morita, Y. Nozaki, K. Akama, T. Ueda, K. Ito, K. H. Nierhaus and N. Takeuchi (2009). "EF-G2mt is an exclusive recycling factor in mammalian mitochondrial protein synthesis." Mol Cell **35**(4): 502-510.

- Tsukihara, T., H. Aoyama, E. Yamashita, T. Tomizaki, H. Yamaguchi, K. Shinzawa-Itoh, R. Nakashima, R. Yaono and S. Yoshikawa (1995). "Structures of metal sites of oxidized bovine heart cytochrome c oxidase at 2.8 Å." Science **269**(5227): 1069-1074.
- Tuppen, H. A., E. L. Blakely, D. M. Turnbull and R. W. Taylor (2010). "Mitochondrial DNA mutations and human disease." Biochim Biophys Acta **1797**(2): 113-128.
- Tyynismaa, H., H. Sembongi, M. Bokori-Brown, C. Granycome, N. Ashley, J. Poulton, A. Jalanko, J. N. Spelbrink, I. J. Holt and A. Suomalainen (2004). "Twinkle helicase is essential for mtDNA maintenance and regulates mtDNA copy number." Hum Mol Genet **13**(24): 3219-3227.
- Uimonen, S., J. S. Moilanen, M. Sorri, I. E. Hassinen and K. Majamaa (2001). "Hearing impairment in patients with 3243A-->G mtDNA mutation: phenotype and rate of progression." Hum Genet **108**(4): 284-289.
- Usami, S., S. Abe, J. Akita, A. Namba, H. Shinkawa, M. Ishii, S. Iwasaki, T. Hoshino, J. Ito, K. Doi, T. Kubo, T. Nakagawa, S. Komiyama, T. Tono and S. Komune (2000). "Prevalence of mitochondrial gene mutations among hearing impaired patients." J Med Genet **37**(1): 38-40.
- Uttara, B., A. V. Singh, P. Zamboni and R. T. Mahajan (2009). "Oxidative stress and neurodegenerative diseases: a review of upstream and downstream antioxidant therapeutic options." Curr Neuropharmacol **7**(1): 65-74.
- Vafai, S. B. and V. K. Mootha (2012). "Mitochondrial disorders as windows into an ancient organelle." Nature **491**(7424): 374-383.
- Valente, L., V. Tiranti, R. M. Marsano, E. Malfatti, E. Fernandez-Vizarra, C. Donnini, P. Mereghetti, L. De Gioia, A. Burlina, C. Castellani, G. P. Comi, S. Savasta, I. Ferrero and M. Zeviani (2007). "Infantile encephalopathy and defective mitochondrial DNA translation in patients with mutations of mitochondrial elongation factors EFG1 and EFTu." Am J Hum Genet **80**(1): 44-58.
- van der Bliek, A. M., Q. Shen and S. Kawajiri (2013). "Mechanisms of mitochondrial fission and fusion." Cold Spring Harb Perspect Biol **5**(6).

- Van Dyck, E., F. Foury, B. Stillman and S. J. Brill (1992). "A single-stranded DNA binding protein required for mitochondrial DNA replication in *S. cerevisiae* is homologous to *E. coli* SSB." EMBO J **11**(9): 3421-3430.
- Van Goethem, G., B. Dermaut, A. Lofgren, J. J. Martin and C. Van Broeckhoven (2001). "Mutation of POLG is associated with progressive external ophthalmoplegia characterized by mtDNA deletions." Nat Genet **28**(3): 211-212.
- van Oven, M. and M. Kayser (2009). "Updated comprehensive phylogenetic tree of global human mitochondrial DNA variation." Hum Mutat **30**(2): E386-394.
- Vandebona, H., P. Mitchell, N. Manwaring, K. Griffiths, B. Gopinath, J. J. Wang and C. M. Sue (2009). "Prevalence of mitochondrial 1555A-->G mutation in adults of European descent." N Engl J Med **360**(6): 642-644.
- Veenstra, D. L., J. Harris, R. L. Gibson, M. Rosenfeld, W. Burke and C. Watts (2007). "Pharmacogenomic testing to prevent aminoglycoside-induced hearing loss in cystic fibrosis patients: potential impact on clinical, patient, and economic outcomes." Genet Med **9**(10): 695-704.
- Vielhaber, S., G. Debska-Vielhaber, V. Peeva, S. Schoeler, A. P. Kudin, I. Minin, S. Schreiber, R. Dengler, K. Kollwe, W. Zschratte, C. Kornblum, G. Zsurka and W. S. Kunz (2013). "Mitofusin 2 mutations affect mitochondrial function by mitochondrial DNA depletion." Acta Neuropathol **125**(2): 245-256.
- Viscomi, C. and M. Zeviani (2017). "MtDNA-maintenance defects: syndromes and genes." J Inherit Metab Dis.
- Voet (2011). Biochemistry, John Wiley & Sons.
- Wai, T. and T. Langer (2016). "Mitochondrial Dynamics and Metabolic Regulation." Trends Endocrinol Metab **27**(2): 105-117.
- Wallace, D. C. (1999). "Mitochondrial diseases in man and mouse." Science **283**(5407): 1482-1488.

- Wallace, D. C. (2005). "A mitochondrial paradigm of metabolic and degenerative diseases, aging, and cancer: a dawn for evolutionary medicine." Annu Rev Genet **39**: 359-407.
- Wallace, D. C. (2011). "Bioenergetic origins of complexity and disease." Cold Spring Harb Symp Quant Biol **76**: 1-16.
- Wallace, D. C. and D. Chalkia (2013). "Mitochondrial DNA genetics and the heteroplasmy conundrum in evolution and disease." Cold Spring Harb Perspect Biol **5**(11): a021220.
- Wallace, D. C., W. Fan and V. Procaccio (2010). "Mitochondrial energetics and therapeutics." Annu Rev Pathol **5**: 297-348.
- Walters-Sen, L. C., S. Hashimoto, D. L. Thrush, S. Reshmi, J. M. Gastier-Foster, C. Astbury and R. E. Pyatt (2015). "Variability in pathogenicity prediction programs: impact on clinical diagnostics." Mol Genet Genomic Med **3**(2): 99-110.
- Wang, X., J. Lu, Y. Zhu, A. Yang, L. Yang, R. Li, B. Chen, Y. Qian, X. Tang, J. Wang, X. Zhang and M. X. Guan (2008). "Mitochondrial tRNAThr G15927A mutation may modulate the phenotypic manifestation of ototoxic 12S rRNA A1555G mutation in four Chinese families." Pharmacogenet Genomics **18**(12): 1059-1070.
- Wang, Y., Y. L. Lyu and J. C. Wang (2002). "Dual localization of human DNA topoisomerase IIIalpha to mitochondria and nucleus." Proc Natl Acad Sci U S A **99**(19): 12114-12119.
- Wanrooij, S., S. Goffart, J. L. Pohjoismaki, T. Yasukawa and J. N. Spelbrink (2007). "Expression of catalytic mutants of the mtDNA helicase Twinkle and polymerase POLG causes distinct replication stalling phenotypes." Nucleic Acids Res **35**(10): 3238-3251.
- Wanrooij, S., J. Miralles Fuste, J. B. Stewart, P. H. Wanrooij, T. Samuelsson, N. G. Larsson, C. M. Gustafsson and M. Falkenberg (2012). "In vivo mutagenesis reveals that OriL is essential for mitochondrial DNA replication." EMBO Rep **13**(12): 1130-1137.

- Wardman, P. (2007). "Fluorescent and luminescent probes for measurement of oxidative and nitrosative species in cells and tissues: progress, pitfalls, and prospects." Free Radic Biol Med **43**(7): 995-1022.
- Watson, D. R., R. J. McClelland and D. A. Adams (1996). "Auditory brainstem response screening for hearing loss in high risk neonates." Int J Pediatr Otorhinolaryngol **36**(2): 147-183.
- Weber, K., J. N. Wilson, L. Taylor, E. Brierley, M. A. Johnson, D. M. Turnbull and L. A. Bindoff (1997). "A new mtDNA mutation showing accumulation with time and restriction to skeletal muscle." Am J Hum Genet **60**(2): 373-380.
- Wei, Y., W. C. Chiang, R. Sumpter, Jr., P. Mishra and B. Levine (2017). "Prohibitin 2 Is an Inner Mitochondrial Membrane Mitophagy Receptor." Cell **168**(1-2): 224-238 e210.
- Westermann, B. (2010). "Mitochondrial fusion and fission in cell life and death." Nat Rev Mol Cell Biol **11**(12): 872-884.
- Wolf, A., A. Caliebe, N. S. Thomas, E. V. Ball, M. Mort, P. D. Stenson, M. Krawczak and D. N. Cooper (2011). "Single base-pair substitutions at the translation initiation sites of human genes as a cause of inherited disease." Hum Mutat **32**(10): 1137-1143.
- Wong, A. C. and A. F. Ryan (2015). "Mechanisms of sensorineural cell damage, death and survival in the cochlea." Front Aging Neurosci **7**: 58.
- Woods, C. G., J. Cox, K. Springell, D. J. Hampshire, M. D. Mohamed, M. McKibbin, R. Stern, F. L. Raymond, R. Sandford, S. Malik Sharif, G. Karbani, M. Ahmed, J. Bond, D. Clayton and C. F. Inglehearn (2006). "Quantification of homozygosity in consanguineous individuals with autosomal recessive disease." Am J Hum Genet **78**(5): 889-896.
- Wrobel, L., U. Topf, P. Bragoszewski, S. Wiese, M. E. Sztolsztener, S. Oeljeklaus, A. Varabyova, M. Lirski, P. Chroscicki, S. Mroczek, E. Januszewicz, A. Dziembowski, M. Koblowska, B. Warscheid and A. Chacinska (2015).

- "Mistargeted mitochondrial proteins activate a proteostatic response in the cytosol." Nature **524**(7566): 485-488.
- Wu, C. C., Y. H. Chiu, P. J. Chen and C. J. Hsu (2007). "Prevalence and clinical features of the mitochondrial m.1555A>G mutation in Taiwanese patients with idiopathic sensorineural hearing loss and association of haplogroup F with low penetrance in three families." Ear Hear **28**(3): 332-342.
- Wu, S. B. and Y. H. Wei (2012). "AMPK-mediated increase of glycolysis as an adaptive response to oxidative stress in human cells: implication of the cell survival in mitochondrial diseases." Biochim Biophys Acta **1822**(2): 233-247.
- Xiao, B., M. J. Sanders, E. Underwood, R. Heath, F. V. Mayer, D. Carmena, C. Jing, P. A. Walker, J. F. Eccleston, L. F. Haire, P. Saiu, S. A. Howell, R. Aasland, S. R. Martin, D. Carling and S. J. Gamblin (2011). "Structure of mammalian AMPK and its regulation by ADP." Nature **472**(7342): 230-233.
- Xie, J., A. E. Talaska and J. Schacht (2011). "New developments in aminoglycoside therapy and ototoxicity." Hear Res **281**(1-2): 28-37.
- Xing, G., Z. Chen and X. Cao (2007). "Mitochondrial rRNA and tRNA and hearing function." Cell Res **17**(3): 227-239.
- Xu, J., J. Ji and X. H. Yan (2012). "Cross-talk between AMPK and mTOR in regulating energy balance." Crit Rev Food Sci Nutr **52**(5): 373-381.
- Xue, Y., Y. Chen, Q. Ayub, N. Huang, E. V. Ball, M. Mort, A. D. Phillips, K. Shaw, P. D. Stenson, D. N. Cooper, C. Tyler-Smith and C. Genomes Project (2012). "Deleterious- and disease-allele prevalence in healthy individuals: insights from current predictions, mutation databases, and population-scale resequencing." Am J Hum Genet **91**(6): 1022-1032.
- Yamaguchi, T., T. Himi, Y. Harabuchi, M. Hamamoto and A. Kataura (1997). "Cochlear implantation in a patient with mitochondrial disease--Kearns-Sayre syndrome: a case report." Adv Otorhinolaryngol **52**: 321-323.

- Yan, Q., Y. Bykhovskaya, R. Li, E. Mengesha, M. Shohat, X. Estivill, N. Fischel-Ghodsian and M. X. Guan (2006). "Human TRMU encoding the mitochondrial 5-methylaminomethyl-2-thiouridylate-methyltransferase is a putative nuclear modifier gene for the phenotypic expression of the deafness-associated 12S rRNA mutations." Biochem Biophys Res Commun **342**(4): 1130-1136.
- Yang, C., U. Curth, C. Urbanke and C. Kang (1997). "Crystal structure of human mitochondrial single-stranded DNA binding protein at 2.4 Å resolution." Nat Struct Biol **4**(2): 153-157.
- Yang, Y., D. M. Muzny, J. G. Reid, M. N. Bainbridge, A. Willis, P. A. Ward, A. Braxton, J. Beuten, F. Xia, Z. Niu, M. Hardison, R. Person, M. R. Bekheirnia, M. S. Leduc, A. Kirby, P. Pham, J. Scull, M. Wang, Y. Ding, S. E. Plon, J. R. Lupski, A. L. Beaudet, R. A. Gibbs and C. M. Eng (2013). "Clinical whole-exome sequencing for the diagnosis of mendelian disorders." N Engl J Med **369**(16): 1502-1511.
- Yao, P. and P. L. Fox (2013). "Aminoacyl-tRNA synthetases in medicine and disease." EMBO Mol Med **5**(3): 332-343.
- Yasukawa, T., M. Y. Yang, H. T. Jacobs and I. J. Holt (2005). "A bidirectional origin of replication maps to the major noncoding region of human mitochondrial DNA." Mol Cell **18**(6): 651-662.
- Ye, J., G. Coulouris, I. Zaretskaya, I. Cutcutache, S. Rozen and T. L. Madden (2012). "Primer-BLAST: a tool to design target-specific primers for polymerase chain reaction." BMC Bioinformatics **13**: 134.
- Yu, J., J. Zheng, X. Zhao, J. Liu, Z. Mao, Y. Ling, D. Chen, C. Chen, L. Hui, L. Cui, Y. Chen, P. Jiang and M. X. Guan (2014). "Aminoglycoside stress together with the 12S rRNA 1494C>T mutation leads to mitophagy." PLoS One **9**(12): e114650.
- Yu-Wai-Man, P., P. G. Griffiths, G. S. Gorman, C. M. Lourenco, A. F. Wright, M. Auer-Grumbach, A. Toscano, O. Musumeci, M. L. Valentino, L. Caporali, C. Lamperti, C. M. Tallaksen, P. Duffey, J. Miller, R. G. Whittaker, M. R. Baker, M. J. Jackson, M. P. Clarke, B. Dhillon, B. Czermin, J. D. Stewart, G. Hudson, P. Reynier, D. Bonneau, W. Marques, Jr., G. Lenaers, R. McFarland, R. W. Taylor, D. M.

- Turnbull, M. Votruba, M. Zeviani, V. Carelli, L. A. Bindoff, R. Horvath, P. Amati-Bonneau and P. F. Chinnery (2010). "Multi-system neurological disease is common in patients with OPA1 mutations." Brain **133**(Pt 3): 771-786.
- Yu-Wai-Man, P., M. Votruba, F. Burte, C. La Morgia, P. Barboni and V. Carelli (2016). "A neurodegenerative perspective on mitochondrial optic neuropathies." Acta Neuropathol **132**(6): 789-806.
- Zeviani, M., S. Servidei, C. Gellera, E. Bertini, S. DiMauro and S. DiDonato (1989). "An autosomal dominant disorder with multiple deletions of mitochondrial DNA starting at the D-loop region." Nature **339**(6222): 309-311.
- Zhang, H., L. H. Meng and Y. Pommier (2007). "Mitochondrial topoisomerases and alternative splicing of the human TOP1mt gene." Biochimie **89**(4): 474-481.
- Zhang, L., L. Yu and C. A. Yu (1998). "Generation of superoxide anion by succinate-cytochrome c reductase from bovine heart mitochondria." J Biol Chem **273**(51): 33972-33976.
- Zheng, J., W. Shen, D. Z. He, K. B. Long, L. D. Madison and P. Dallos (2000). "Prestin is the motor protein of cochlear outer hair cells." Nature **405**(6783): 149-155.
- Zheng, K. W., R. Y. Wu, Y. D. He, S. Xiao, J. Y. Zhang, J. Q. Liu, Y. H. Hao and Z. Tan (2014). "A competitive formation of DNA:RNA hybrid G-quadruplex is responsible to the mitochondrial transcription termination at the DNA replication priming site." Nucleic Acids Res **42**(16): 10832-10844.
- Zheng, L. and B. Shen (2011). "Okazaki fragment maturation: nucleases take centre stage." J Mol Cell Biol **3**(1): 23-30.
- Zhu, H., G. L. Bannenberg, P. Moldeus and H. G. Shertzer (1994). "Oxidation pathways for the intracellular probe 2',7'-dichlorofluorescein." Arch Toxicol **68**(9): 582-587.
- Zhu, J., K. R. Vinothkumar and J. Hirst (2016). "Structure of mammalian respiratory complex I." Nature **536**(7616): 354-358.
- Zhu, M. and S. Zhao (2007). "Candidate gene identification approach: progress and challenges." Int J Biol Sci **3**(7): 420-427.

- Zhu, Y., S. Huang, D. Kang, M. Han, G. Wang, Y. Yuan, Y. Su, H. Yuan, S. Zhai and P. Dai (2014). "Analysis of the heteroplasmy level and transmitted features in hearing-loss pedigrees with mitochondrial 12S rRNA A1555G mutation." BMC Genet **15**: 26.
- Zong, W. X., J. D. Rabinowitz and E. White (2016). "Mitochondria and Cancer." Mol Cell **61**(5): 667-676.
- Zorov, D. B., M. Juhaszova and S. J. Sollott (2014). "Mitochondrial reactive oxygen species (ROS) and ROS-induced ROS release." Physiol Rev **94**(3): 909-950.
- Zou, J., Y. Guo, T. Guettouche, D. F. Smith and R. Voellmy (1998). "Repression of heat shock transcription factor HSF1 activation by HSP90 (HSP90 complex) that forms a stress-sensitive complex with HSF1." Cell **94**(4): 471-480.
- Zur, H. and T. Tuller (2013). "New universal rules of eukaryotic translation initiation fidelity." PLoS Comput Biol **9**(7): e1003136.